Investigating ancient metabolic reactions contributing to G0 quiescence survival in fission yeast S. pombe

Investigating ancient metabolic reactions contributing to G0 quiescence survival in fission yeast *S. pombe*

By Caroline Starzynski
Supervisor Prof. Mitsuhiro Yanagida

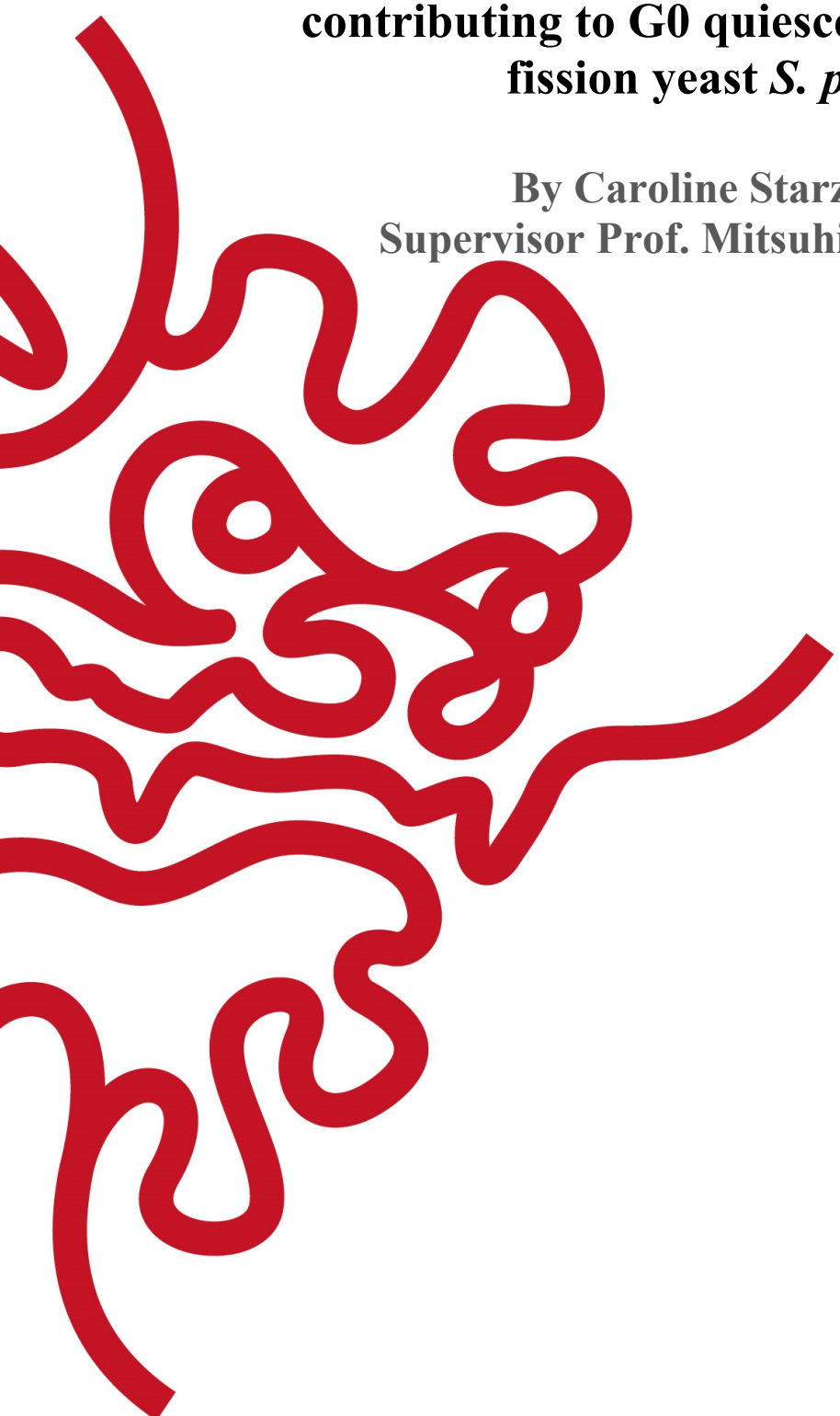

Declaration of Original and Sole Authorship

I, Caroline Starzynski, declare that this thesis entitled 'Investigation on conserved mechanism contributing to quiescence survival' and the data presented in it are original and my own work.

I confirm that:

- No part of this work has previously been submitted for a degree at this or any other university.
- References to the work of others have been clearly acknowledged. Quotations from the work of others have been clearly indicated, and attributed to them.
- In cases where others have contributed to part of this work, such contribution has been clearly acknowledged and distinguished from my own work.
- None of this work has been previously published elsewhere.

Date: December 4th, 2017

Signature:

Acknowledgment

I would like to thank my supervisor Prof. Mitsuhiro Yanagida for accepting me, a rather ‘simple-minded’ student, and introducing to me a more sophisticated view on science. Right at the beginning I was only led by my naïve desire to do science but was completely ignorant of the stony way which comes along. Surely, there were many moments of bitterness and failure from my side but his kind patience and critical comments served as a source of motivation. Prof. Yanagida has a sharp mind of a great scientist. He truly was a wise source of knowledge and inspiration to me, for both work and life. His discussions were very valuable and contributed greatly to the development of my thesis.

I am also very thankful to the researcher of the G0 unit, Dr. Kenichi Sajiki, who guided me loyally throughout my thesis work, by teaching me the ‘core’ of scientific work and analysis. He taught me how to efficiently plan experimental approaches and explained to me the importance of conveying a nice and focused scientific story.

Moreover, I am grateful to the technician of the G0 unit, Ms. Ayaka Mori, who contributed greatly to the experiments presented in this thesis. Also, Yuria Tahara, a technician in the same lab, was always there if I had a question and helped me out with the Delta vision microscope.

Finally, I would like to express words of gratitude to the members of the G0 unit who were very supportive throughout my time as a PhD student in the lab.

List of Abbreviations and acronyms

A list of all relevant abbreviations that were used throughout this thesis is presented below:

- [4Fe-4S], iron-sulfur cluster;
- 2-OG, 2-oxoglutarate;
- AAT, aspartate aminotransferase;
- BCAA, branched-chain amino acids;
- BLAST, Basic Logic Alignment Search Tool;
- BLOSUM, blocks substitution matrix;
- CoQ, ubiquinone;
- DHADH, Dihydroxy-acid dehydratase;
- EMM2, Edingburgh minimal medium No. 2
- EMM2-N, Edingburgh minimal medium No. 2 without added nitrogen source
- ETC, electron transfer chain;
- ETF, electron transferring flavoprotein;
- G0, Gap 0 phase
- GDH, glutamate dehydrogenase;
- GZE, G zero essential;
- HICDH, homoisocitrate dehydrogenase;
- NADH, nicotinamide adenine dinucleotide hydrogen
- OCR, oxygen consumption rate;
- Redox, reduction-oxidation reactions
- SOD, superoxide dismutase;
- VE, vegetative phase;
- YE; yeast extract
- YPD; yeast, polypeptone, *D*-glucose

Abstract

Since all living organism rely on assimilating environmental nitrogen (N) to promote cell divisions, an efficient system to deal with N scarcity is deterministic for survival. For example, the fission yeast *Schizosaccharomyces pombe* (*S. pombe*) withstands long-term N starvation by induction of growth arrest and quiescence entry (G0 phase). In past studies 89 *S. pombe* genes were found to be required for survival upon G0 phase. Because these are involved in diverse intracellular functions, a clear mechanism for quiescence was difficult to assign. Therefore, we developed a BLAST-based approach to generate phylogenetic profiles and characterize evolutionary conserved metabolic reactions by comparative analysis using prokaryotic databases of *Escherichia coli* and *Bacillus subtilis*. We report fourteen proteins fulfilling this study's homology criteria, half of which (7/14) are localized to the mitochondria. Subsequent *in silico* analysis suggests the involvement of two functional response mechanisms which comprise oxygen-consuming and glutamate-metabolic reactions. Among these, *Δsod2* showed abnormally low oxygen consumption upon quiescence and loss of regenerative capability. We report that the conserved mechanisms to survive N starvation comprise enzymes which are associated with the regulation of oxygen and glutamate-oxoglutarate metabolism.

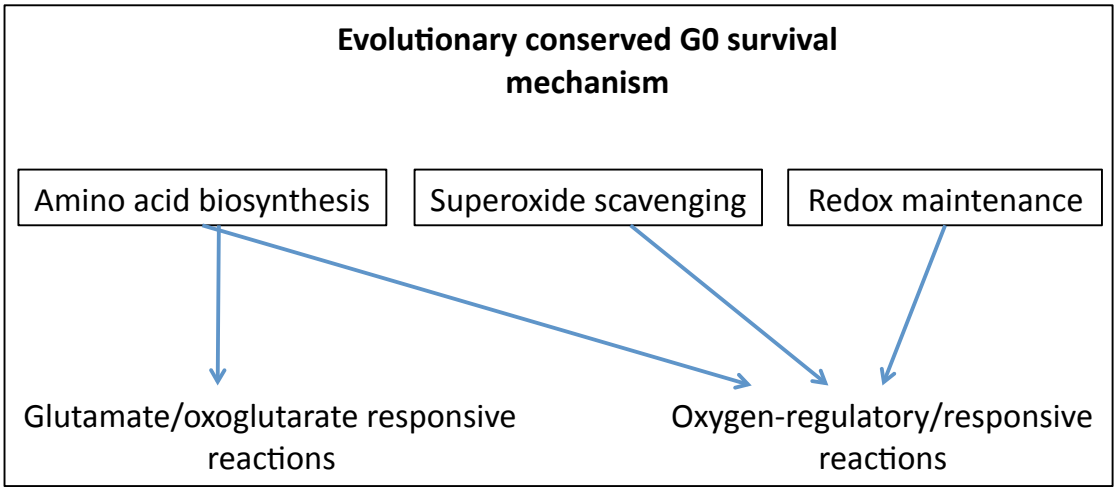

Table of contents

1. Introduction

2. Materials and Methods

3. Results

List of Figures

List of Tables

List of Supplementary Figures (located in the Appendix)

1. Introduction

1.1. An introduction to the cell cycle and quiescence

Cell growth relies on a series of intracellular events occurring in a cyclic pattern, designated as 'the cell cycle'. It is defined by distinct phases comprising DNA replication (S phase), chromosome segregation and subsequent cell division (M phase) yielding two daughter cells. Gap phases, G1 and G2, follow M and S phase, respectively. Progression from one event to the other needs to go through cell cycle check points which control that prerequisites for cell progression are met (Saka et al., 1994, Hartwell and Weinert, 1989). In eukaryotic organisms environmental clues, such as nutritional signals, and growth hormone availability are required for the progression through the cell cycle (MillerNorbury and Nurse, 1989). This makes the regulatory mechanism of the cell cycle progression into a deterministic factor for cell fate and thus, survival (Evans et al., 1983, Murray et al., 1989). The absence of the required proliferative signals is known to abolish cell cycle progression and divert the cell into a resting phase termed quiescence or G0 (Augenlicht and Baserga, 1974, Temin, 1971). The transition from active cell cycle to quiescence phase is reversible upon addition of growth signals (Pardee, 1974, Zetterberg and Larsson, 1985). There are cell types which need to switch between these two states. Adult stem cells, for instance, usually exist in that quiescent mode (**Figure 1.1.**) which is thought to preserve its cellular integrity and thus, supports viability and tissue regenerative properties (Sperka et al., 2012). The ability to transit between these two phases is therefore of great importance to tissue integrity (Sherr, 1996). Since cellular physiology and metabolic organization change upon G0 phase entry, the question arises what genetic regulations are responsible for

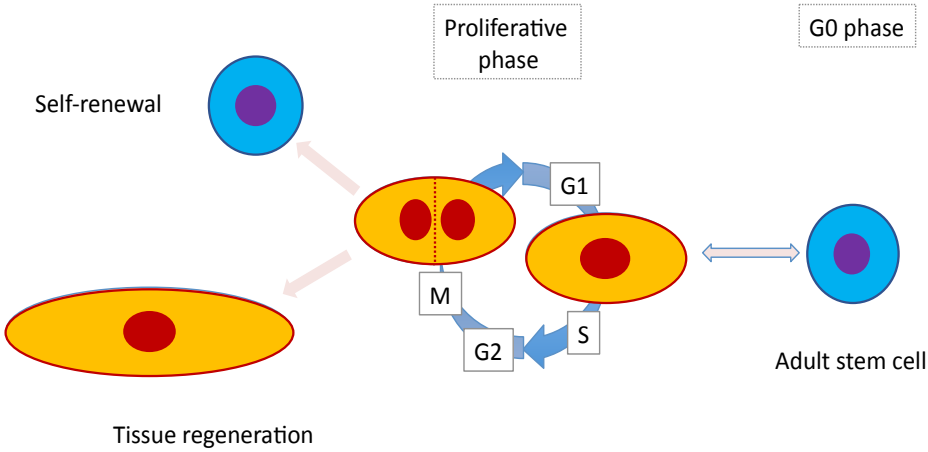

Figure 1.1. Stem cells shuttle between quiescent and proliferative states. Human adult stem cells exist in the non-dividing or resting phase, termed quiescence. To self-renew or contribute to tissue regeneration cells transit into proliferating mode. Surely, stem cells need to enter the cell cycle to produce differentiated daughter cells upon tissue damage, or for self-renewal. But once the proliferative deed is done the stem cell switches back into quiescent mode.

the transition and maintenance of quiescence. Knockdown-studies in mammalian cell systems appear as a rather complicated endeavor (Eisener-Dorman et al., 2009). Nevertheless, the reversible withdrawal from cell growth into the G0 state seems to be an evolutionary ubiquitous mechanism of survival. Besides mammalian systems, fission yeast (Yanagida, 2009), bacteria (Roszak and Colwell, 1987) and parasites (Saldivia et al., 2016) rely on the ability to transit between vegetative and quiescent states. Due to its importance for survival, the regulatory mechanism of quiescence is likely to be conserved. Therefore, employing a simpler eukaryotic organism might serve as an ideal approach to study the basic regulatory machinery of the G0 switch and maintenance.

The unicellular eukaryote fission yeast *Schizosaccharomyces pombe* is a great model to study cell growth and intracellular pathways which are found in humans.

In fact, *S. pombe* shares a number of processes found in human (Hoffman et al., 2016, Aravind et al., 2000). Besides a relatively high amount of conserved proteins, it was reported that around 65% of *S. pombe* protein interactions are conserved in human (Vo et al., 2016). Therefore, the current study relies on *S. pombe* as a model organism to uncover ancient G0 phase survival mechanisms.

1.2. Fission yeast - A crucial model organism for cell cycle studies and beyond

Numerous *S. pombe* studies successfully identified and characterized genes contributing to regulatory mechanisms of the cell cycle (Hagan et al., 2016, Russell and Nurse, 1987), chromosome segregation (Yanagida, 2000), nutritional adaptations (Saitoh and Yanagida, 2014) and quiescence (Takeda and Yanagida, 2010, Sajiki et al., 2009, Su et al., 1996). By the year 2002 its genome had been sequenced (Wood et al., 2002) and 5,054 protein-encoding genes were recorded (Hoffman et al., 2016). Following the completion of *S. pombe* genome sequencing, a PCR-based approach for targeted deletion of non-essential genes was developed (Bahler et al., 1998, Decottignies et al., 2003). This simple technique transformed *S. pombe* into a 'box of bricks' for generating a model with desired genetic features. The general idea behind mutant screenings is to determine gene function via the emerging phenotype differing from the wild type strain. In this way insights into phenotypic changes, gained from mutational experiments, can be used to characterize a specific gene product. A few decades ago first phenotypic studies on gene mutants were successful in characterizing

essential players of the cell cycle control. The initial experimental design relied on mutagenesis treatment which generated strains displaying a temperature sensitive (*ts*) phenotype at restricted temperature (36°C). These isolated ts mutants strains showed unusual physiological features like aberrant cell size and cell cycle progression defects (Nurse et al., 1976). Besides genes behind the cell cycle checkpoint control (Fantes and Nurse, 1978) another deterministic factor influencing the passage through the cycle was reported to be nutrient availability in *S. pombe*. In fact, depletion of nitrogen from the culturing media caused radical cell size reduction coupled with a cell cycle arrest (Fantes and Nurse, 1977, Young and Fantes, 1987) predominantly in the G1 phase prior to the S phase (Costello, 1986, Su et al., 1996). These growth-arrested yeast cells were found to exist in a resting state, distinct from the proliferative mode (Iida and Yahara, 1984).

This contrasts with glucose-starved cells which arrested after DNA synthesis in G2 phase with a higher DNA content (Masuda et al., 2016). Notably, G2-arrested cells do not differ in cell size and shape from vegetative cells (Mochida and Yanagida, 2006). Other features of nitrogen-starved G0 phase active metabolism (Sajiki et al., 2013) and prolonged viability (Su et al., 1996). This is in contrast to glucose-restricted cells in stationary phase whose survival rate is rather reduced to a few days (Roux et al., 2006).

Nitrogen (N) depletion was reported to cause a rapid remodeling of gene expression. Notably, after 20 minutes of N starvation expression of ribosome biogenesis genes significantly decreased and an increase in nucleotide salvage gene expressions was observed (Kristell et al., 2010). Twelve hours following nitrogen starvation the cell volume had decreased by 50% (Marguerat et al., 2012) which is a

consequence of radical reductions in protein levels due to the large-scale protein degradation pathway known as autophagy (Nakashima et al., 2006, Kohda et al., 2007). Besides radical re-adjustments of the proteome, bulk mRNA content decreased at the onset of quiescence by ~80% compared to vegetative state levels. The majority of mRNA transcripts decreased in number, whereas 1-2% of mRNA transcripts were more abundant at quiescence (Marguerat et al., 2012). In the next section past G0 studies in *S. pombe,* which successfully identified the genes behind crucial intracellular pathways such as the cell cycle and quiescence, will be described.

1.3. Past genetic screenings with *S. pombe*

With the rise of the high-throughput analysis era, screening of mutant libraries, spanning thousands of genes, has been increasingly employed. It has proved as an efficient approach for identifying several genetic players of cellular pathways under defined experimental conditions. To answer the above-mentioned question about the regulatory machinery of N-starvation induced G0 survival, a collection of temperature-sensitive mutant strains was screened for growth arrest during G0 conditions. The common technique for G0 induction is nitrogen (N) source (0.5% NH_4Cl) depletion from the *S. pombe* culturing medium Edinburgh minimal medium EMM2 (**Figure 1.2.**). G0 phase can be confirmed by light microscopic method since its shows an easily discernible round morphology in contrast to rod-shaped proliferating cells (Su et al., 1996). Further experimental confirmation involves DNA content measurements of G0 phase cells by fluorescence-activated cell sorting (FACS) since G0 cells are pre-replicative and contain 1C DNA.

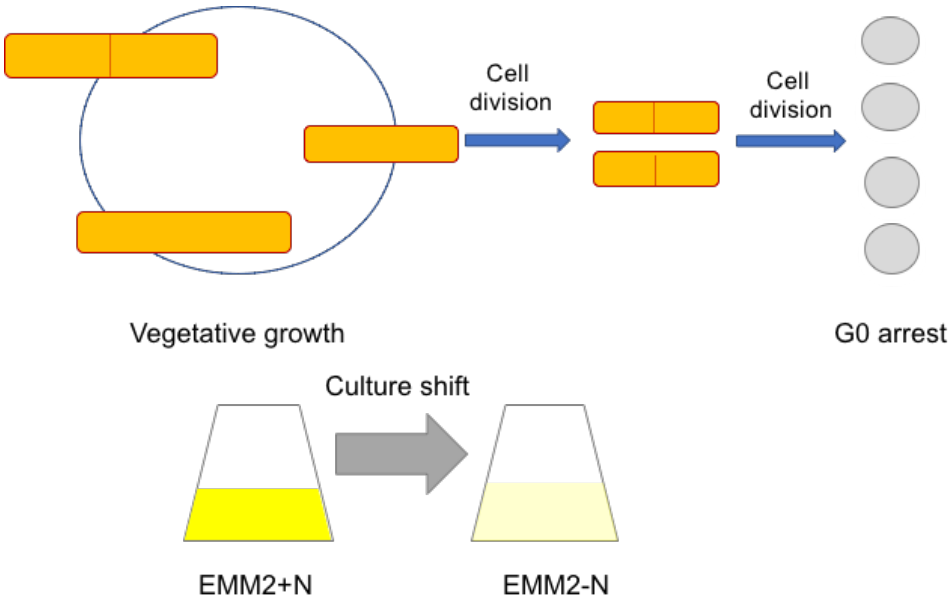

Figure 1.2. Methodology to induce G0 phase in *S. pombe*. The synthetic medium Edinburgh minimal medium 2 (EMM2) is preferentially employed it contains one well-defined N source which is ammonium chloride (red). Leaving out this particular compound is enough for G0 studies.

This contrasts with G2 arrested cells which went through S phase and contain 2C DNA. Past experimental approaches by G0 unit in Okinawa involved screenings of two different types of mutant strains (**Figure 1.3.**): 1) Temperature-sensitive (*ts*) *S. pombe* mutant library, generated by mutagenesis treatment (Hayashi et al., 2004, Hayashi et al., 2007) and 2) non-essential deletion mutant strains (Shimanuki et al., 2007). A previous screening approach used a *ts* mutant library which identified 33 genes to be required during N depleted incubation (Sajiki et al., 2009). Since mutations in these 33 genes caused both, restricted temperature and N starvation sensitivities, the affected

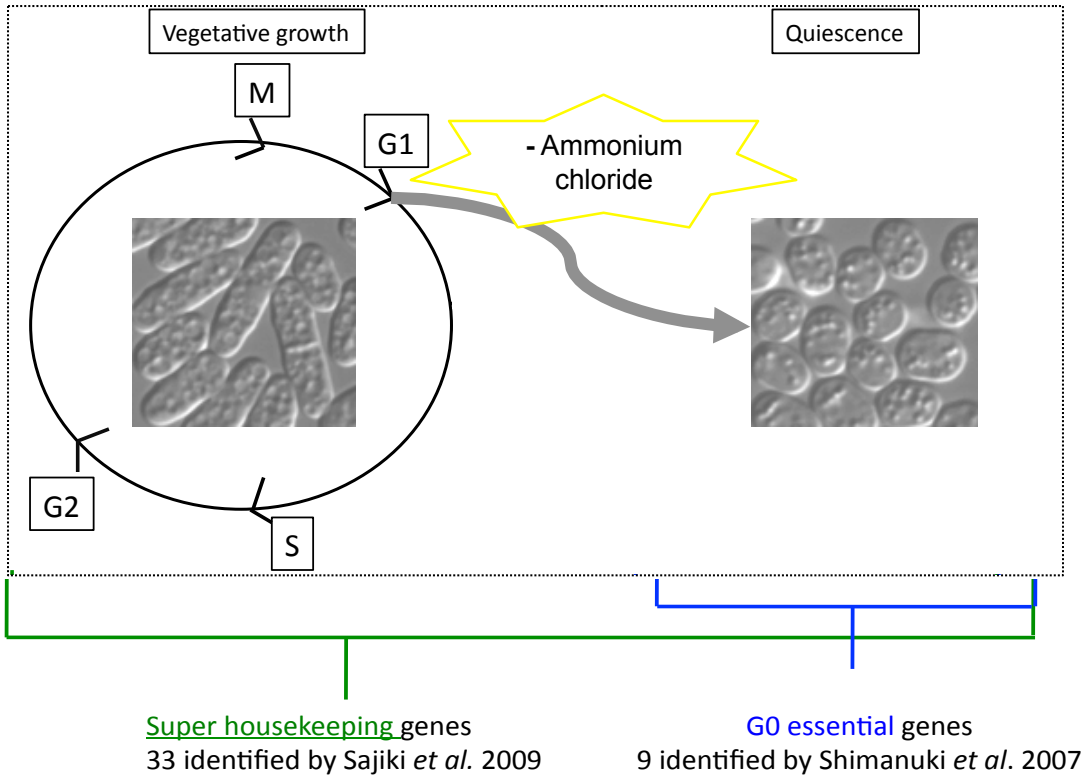

Figure 1.3. Summary of past studies on *S. pombe* quiescence (G0 phase) regulation. Quiescence in *S. pombe* is induced by depletion of ammonium chloride from the culture medium. Two types of mutant libraries were used for nitrogen starvation (–N) screening experiments. Temperature-sensitive mutant strains, affected in cellular house-keeping genes. These were termed 'super housekeeping' (SHK) genes. A different approach used Bioneer whole-gene deletion library. The pilot study identified genes which are specifically required for G0 only. They are therefore G0 essential.

genes are thought to promote survival during vegetative growth and quiescence. These genes are designated as 'super housekeeping' (SHK) genes.

Mutants with impaired stress response pathways, involving MAP kinase cascade proteins and transport were shown to be unable to enter G0 state. This finding suggests that intracellular trafficking and stress response signaling is required for the initial transition period leading into G0. Other mutants are involved in diverse

intracellular processes such as RNA metabolism, protein trafficking, glycolysis ergosterol synthesis and cell wall organization.

Despite their dual importance of SHK genes for survival in both physiological phases, gene products truly essential for G0 survival still need to be characterized.

The next section will deal with past experimental approaches by the G0 unit to characterize this regulatory machinery.

1.4. Previous work on the identification of G0 regulatory players

A direct way to assess the requirement of a certain gene during -N starvation conditions is by depleting the cell out of it and watch the resulting effect. Therefore, viability assessments in N starved media with *S. pombe* mutant strains, lacking the target gene, will give a more precise statement whether the gene is indispensable. In an initial N starvation pilot study, Shimanuki *et al.* investigated genes exclusively essential for G0 survival and found nine genes through screening of 53 deletion mutant strains (**Figure 1.4.**).

These nine deletion strains can proliferate in regular culture medium, but lose viability in G0 phase under N starvation (Shimanuki et al., 2007). From the results, we understood that diverse functions comprising signaling, transcriptional regulation and intracellular transport (**Figure 1.4.**: red boxes) are involved in quiescence. The remaining three genes (*sds23*, *rrd1* and *cbs2*) encode proteins involved in nutrient sensing/signaling via phosphatase-kinase relay (Yanagida, 2009).

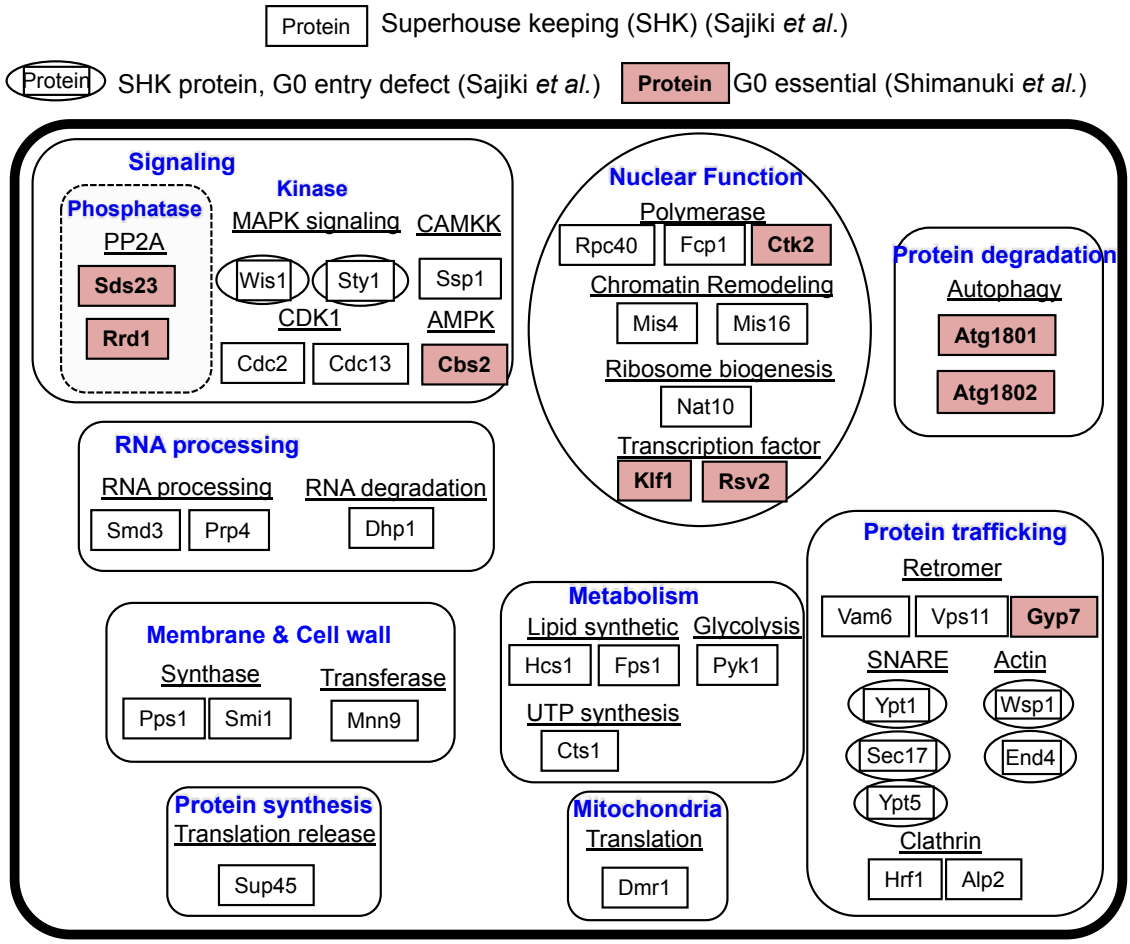

Figure 1.4. Overview of the identified SHK and G0 survival essential genes. Sajiki *et al.*, found gene products which are essential for growth and viability under vegetative state and N-starved G0 phase, termed 'super housekeeping genes' (SHK) (white boxes, black font). Some SHK gene mutants were unable to entry the G0 state upon N starvation (white box encircled). Shimanuki *et* al., tried to identify genes indispensable for G0 survival only. Nine gene products were reported so far to affect G0 viability when depleted (red boxes, black font).

The results of the pilot study gave an initial outlook about the possibilities of mutant library screenings for the identification of G0 essential genes. As a next step, screenings of a larger number of deletion mutants was performed which will be discussed in the next section.

1.5. G0 survival essential genes support viability during N starvation

G zero (G0) survival essential (GZE) genes were investigated by employing the Bioneer haploid deletion mutant library featuring more than 3, 500 strains. The current study will be based on the unpublished results obtained by members of the G0 unit. In contrast to the above-mentioned *ts* mutant libraries, the Bioneer haploid deletion mutant strains thrive under vegetative culture conditions even at restricted temperature. In this way, it was ensured that the screening focus lies truly on identifying GZE genes. The screening consisted of two procedures (**Figure 1.5.**): 1) Spot tests on EMM-N agar plates which found 154 gene deletion strains. These *S. pombe* mutants were unable to grow on the N deprived agar plates (**Figure 1.5.A**). 2) Subsequent long-term viability assessment in liquid EMM2-N media was conducted (**Figure 1.5.B**). In the end 89 GZE genes were found to have impaired viability when transferred from N-starved to N-replenished medium within a four-week-long -N incubation (**Figure 1.6.**). Depending on the gene deletion, diminished viability was observed at varying time points of -N incubation. This observed viability impairment is defined by a reduced ability to regenerate upon N replenishment (Sajiki et al., publication in progress).

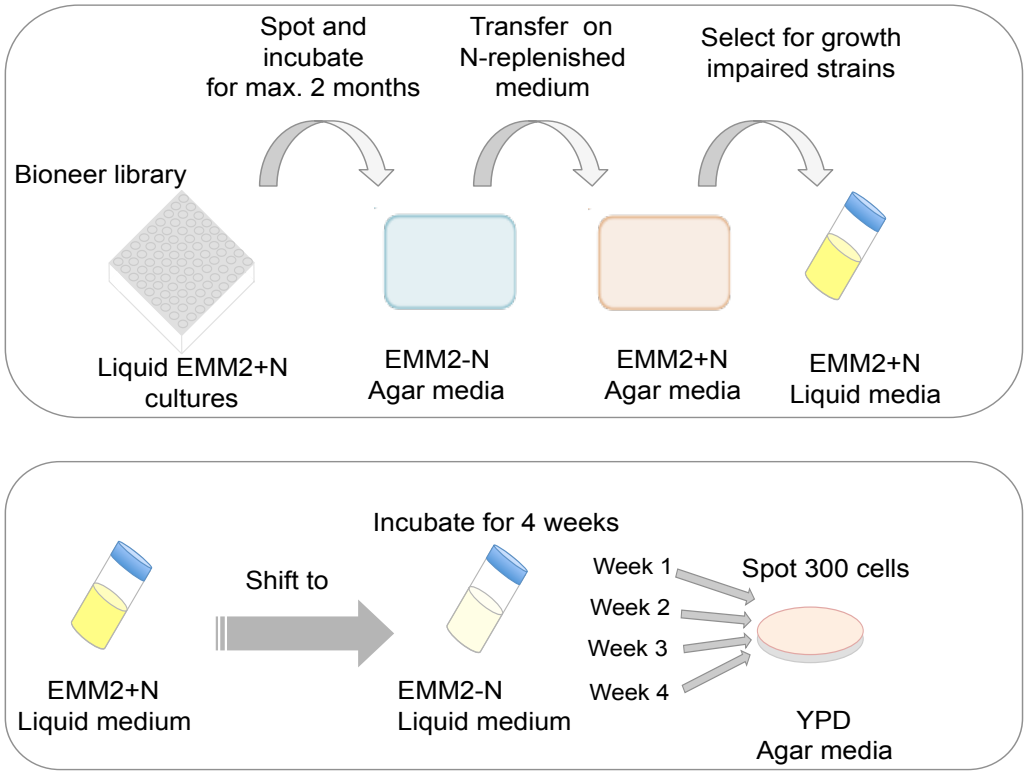

Figure 1.5. Experimental design for GZE gene identification. Sajiki et al., (publication in progress) performed two experimental set-ups: **A)** The first deals with screening of 3,500 gene deletion strains (Bioneer library) by spotting vegetative cells from liquid EMM2+N cultures, on agar plates depleted of the nitrogen source (EMM2-N). After max. 2 months the strains are transferred on N-replenished plates (EMM2+N) **B)** In the second experiment the selected strains are checked for viability after long-term incubation in -N conditions (four weeks). Each week a fixed number of 300 cells were plated on agar plates with rich medium yeast extract, polypeptone and *D*-glucose (YPD). In this way, the ability to regenerate from quiescence was assessed for each of the 154 selected deletion mutants. The results provide an idea about the time of viability loss during -N incubation.

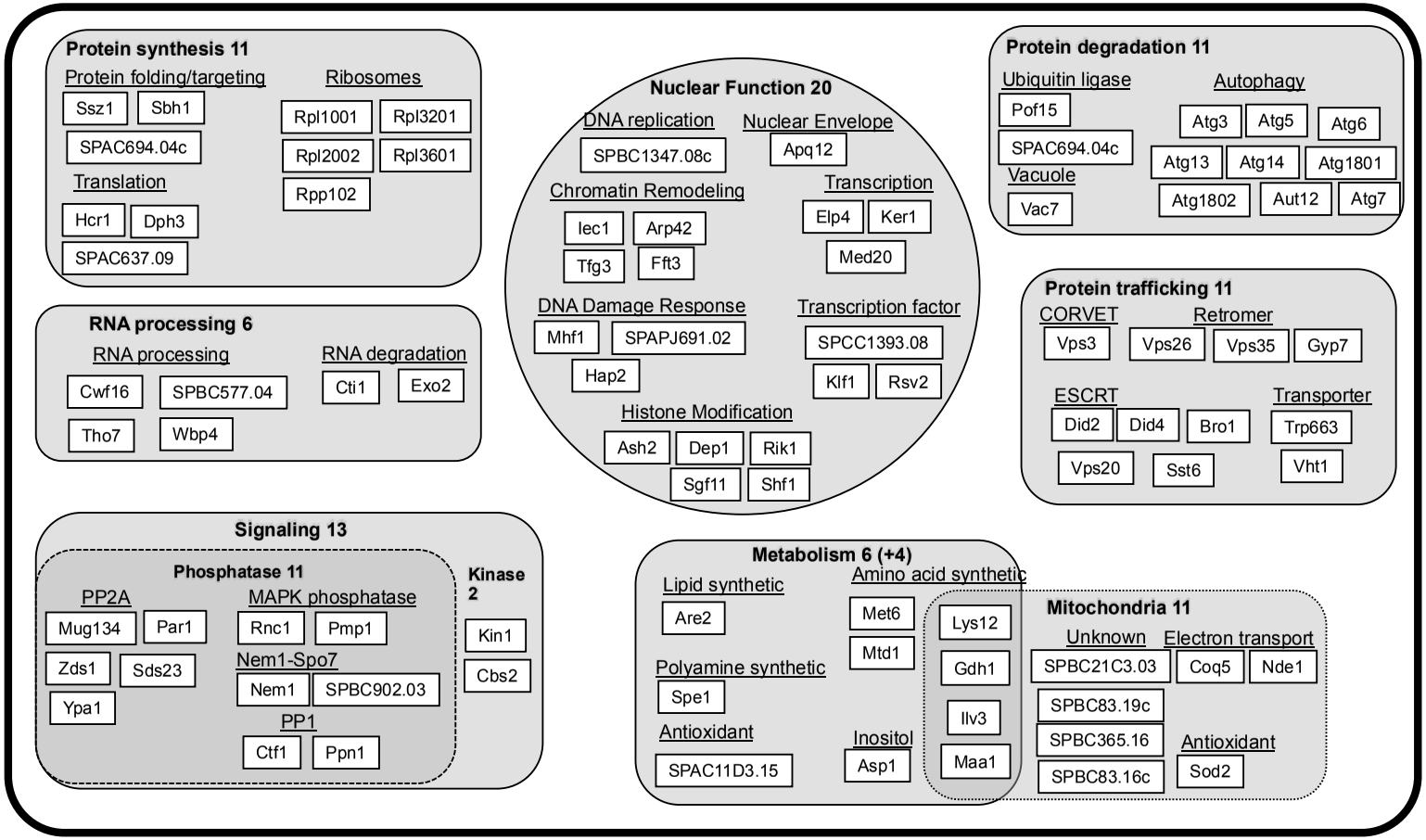

Figure 1.6. Overview of the G0 essential (GZE) genes. Results from viability assessments after incubation in N starvation conditions performed by Sajiki *et al*., publication in progress. The nine GZE gene products identified by Shimanuki *et al., 2007* are included.

It is likely that -N survival involves different stages where protein functions contribute to pathways in a time-dependent mechanism. Sajiki *et al*., reported distinct metabolic responses for 75 metabolic compounds whose abundance changes upon initial N starvation. These included rapid decrease in free amino acids, and compounds of purine biosynthesis within one hour of N starvation. On the other hand, increase in the TCA cycle compounds 2-oxoglutarate (2-OG) and succinate indicate remodeling of carbon (C) metabolism (Sajiki et al., 2013). Especially, 2-OG is a well-known compound associated with both energy and nitrogen metabolic pathways. It was reported to be elevated in response to N starvation under plenty of glucose in many organisms like the bacteria (Shimizu, 2013, Bren et al., 2016) and in plants (Lancien et al., 2000). Since the changes in 2-OG seem to be a ubiquitous response to N level fluctuations, the pressing assumption about a common N starvation survival mechanism arises. It may be that quiescence induction and 2-OG rise upon N starvation likely originate from universal intracellular response mechanisms. We assume that the basic pathway had proven to be the most efficient way throughout evolutionary progress. There this study focuses on the identification of evolutionary conserved enzymes among the 89 GZE protein products which are involved in the ancient N starvation survival reactions and pathways. This kind of 'phylogenetic profiling' as described in (Sun et al., 2005) may provide a clue about function and possible interactions among other GZE proteins.

1.6. Search for common mechanisms shared among bacteria and *S. pombe*

The bacterial survival response to amino acid starvation is the entry into a resting state which is similar to quiescence showing increased carbon storage,

decrease in protein biosynthesis, cell wall thickening and a general increase in resistance towards oxidative stress (Rittershaus et al., 2013). Therefore, the following question arises whether there are conserved proteins among the *S. pombe* (G zero essential) GZE proteins which might be involved in universal mechanisms essential for nitrogen starvation-induced quiescence survival.

The two widely characterized bacterial species *Bacillus subtilis* (strain168) and *Escherichia coli* (strain K12) are employed in the current homology search study. Since their genomes had been completely sequenced by (Blattner et al., 1997) and (Kunst et al., 1997) it is ensured that no homolog is overseen. The commensal *E. coli*, and the non-pathogenic soil bacterium *B. subtilis* differ in their cell wall physiology, a trait easily discernable by the gram stain. They both respond to starvation by protein biosynthetic inhibition and growth halt, known as stringent response (Hauryliuk et al., 2015). Therefore, they appear as ideal study objects for comparative analysis. To support the assumption of a universal nitrogen starvation survival pathway the degree of conservation of GZE proteins to prokaryotes needs to be assessed.

2. Materials and Methods

2.1. Study on mitochondria-localized G0 essential gene products

2.1.1. Protein homology search

The **B**asic **L**ogic **A**lignment **S**earch **T**ool (BLAST)-assisted homology search consisted of two steps: 1) Each GZE protein sequence was compared against *E. coli* K12 and *B. subtilis* 168 protein databases separately. These databases consisted of non-redundant protein sequences (nr). BLOSUM62 was used as a scoring matrix with expect threshold of 10. The word-size for matches was 2 to increase sensitivity for distantly related proteins. The 'best hit' BLASTp approach, with following criteria sequence coverage rate of $\geq 50\%$ (Moreno-Hagelsieb and Latimer, 2008) and E value $\leq$ 1.0E-04 (Sun et al., 2005), was performed. If the highest hit to prokaryotic protein sequences had identical functions, the corresponding GZE and its prokaryotic counterparts were selected for BLAST pairwise alignment against the corresponding query *S. pombe* sequence (Pearson, 2013). The initial criteria for the BLAST pairwise homology confirmation are an E-value cut-off rate $\leq$ 1.0E-05 and a sequence coverage $\geq 50\%$.

2.1.2. Multiple sequence alignments and search for conserved active sites

Multiple alignments against selected GZE *S. pombe* orthologs including human, *E. coli*, and *B. subtilis* sequences were constructed with the Chimera Viewer tool (Pettersen et al., 2004). Protein alignments are obtained by running ClustalW (Larkin et al., 2007) which are then loaded on the Chimera program for functional site identification. The functional sites are included into the sequence alignments by exporting the crystal structures directly from the RSCS (PDB) protein databank (Berman et al., 2000). *S. pombe* protein sequences are obtained from pombase.org database (Wood et al., 2012),

whereas protein sequences for other organisms are obtained from uniprot.com database (The UniProt, 2017). Information on enzymatic functions and biosynthetic pathways are retrieved from the **K**yoto **E**ncyclopedia of **G**enes and **G**enomes (KEGG) pathway database (Kanehisa and Goto, 2000).

2.1.3. Generation of phylogenic trees for Maa1, Gdh1 and Coq5 orthologs

FASTA files are obtained from uniprot.org database (The UniProt, 2017). or GenBank® (Benson et al., 2004, Benson et al., 2005). Sequences are aligned using the ClustalW algorithm (Larkin et al., 2007). The resulting alignments are loaded in the **M**olecular **E**volutionary **G**enetics **A**nalysis (MEGA) version 6 (Tamura et al., 2013) to carry out Maximum likelihood phylogenetic analysis with 1,000 bootstrap replicates. Detailed information on the *in silico* tools is shown in **Table 2.1.**

Table 2.1. Overview of the internet-accessible resources used for this study

Name of *in silico* tool	Purpose	Reference	Address
BLAST	Homology search	Altschul *et al*., 1997	https://blast.ncbi.nlm.nih.gov/Blast.cgi?PAGE=Proteins
CHIMERA	Multiple alignments	Pettersen *et al*., 2014	https://www.cgl.ucsf.edu/chimera
Pombase	Retrieve *S. pombe* sequence and information	Wood *et al.*, 2012	https://www.pombase.org
Uniprot	Retrieve protein sequences, protein information	The UniProt Consortium, 2017	www.uniprot.org
GenBank	Retrieve protein sequences	Benson *et al.*, 2013	https://www.ncbi.nlm.nih.gov/genbank/
KEGG	Study enzymatic reactions	Kanehisa *et al*., 2000	http://www.genome.jp/kegg/pathway.html
PDB	Search for crystal sturcture works	Berman *et al*., 2000	www.rcsb.org
ClustalW	Sequence alignmnets	Larkin *et al.*, 2007	http://www.genome.jp/tools-bin/clustalw
MEGA 6	Phylogeny tree construction	Tamura et al., 2013	http://www.megasoftware.net/

2.1.4. Oxygen consumption measurements

Oxygen consumption rate (OCR) measurements are performed with the Seahorse XF-96 flux analyzer (Bioscience, USA) at 26°C. Preparation and handling are performed according to the manufacturer's protocol. For the OCR pilot study, different cell

concentrations of 972h- wild type at vegetative and G0-arrested state are assayed: $1x10^6$, $2.5x10^6$, $5x10^6$ and $7.5x10^6$ cells per mL. The ideal concentrations are used for the OCR study of deletion strains. Overnight cultures in the synthetic Edinburgh minimal medium with added ammonium chloride (EMM2+N) are set up separately containing deletion strains and 972 h- wild type control. Each strain is divided into VE and G0 samples. Culture shift from EMM2+N into ammonium depleted minimal medium (EMM2-N), by using nitrocellulose membrane filtration method (Shimanuki et al., 2007), was performed to induce G0 and sampled after 24h. The results for measurements of each individual strain type are shown as the mean ± STD. Graphs are plotted with Excel. At least three independent experiments for each deletion strain were performed.

2.1.5. Imaging of GZE deletion mutants

Before shifts from EMM2+N to EMM2-N, cells were incubated overnight at 26°C.
24 hours after transfer into EMM2-N medium and constant incubation at 26°C, G0 cells were used for microscopy. Cells were fixated in glutaraldehyde and observed by Axio Vision 2 (Zeiss) microscope. Cells in vegetative state were used as control.

2.2. Characterization of UbiB family protein SPBC21C3.03

2.2.1. Strains and cell culture conditions

For the sensitivity screening of *S. pombe* ABC1-like kinase family members, following strains were used in the study: Wild type *S. pombe* 972 h-, Δ*SPBC21C3.03*, Δ*SPAC10F6.14c*, Δ*SPBC15C.04*, Δ*coq8* and as controls Δ*sod2*, Δ*nde1*, Δ*rad3* (for UV and hydroxyurea only). Before experimental procedures deletion of all four UbiB family members from Bioneer library was checked by confirmation PCR as described on the Bioneer homepage. For the drug screenings, wild type 972 h- cells and mutants were grown overnight at 26°C in liquid YE [0.5% yeast extract, 2% glucose] and cell number was adjusted prior to spotting on agar plates with added drugs and no drugs. Plates containing drugs were made a few days before spotting.

2.2.2. UbiB protein family sequence alignments

Protein sequence in FASTA format for *E. coli* UbiB protein was obtained from uniprot.org. The *S. pombe* protein sequences for the three UbiB family members were retrieved from pombase.org. Alignments of the protein sequences were performed with the online tool found at Multalin.org.

2.2.3. Microscopy

Imaging by Axio Vision 2 microscope was performed as described in section 2.15. Images of cells at vegetative and G0 states were taken. Wild type and *S. pombe* UbiB family mutants Δ*SPBC21C3.03*, Δ*coq8,* Δ*SPAC10F6.14c* and Δ*SPBC15C.04* were used.

2.2.4. Drug screen by spot test during vegetative state

YE agar plates with and without drug were made usually 3-4 days prior to the spotting experiments. Stock solutions of the drugs were made using either Dimethylsulfoxide (DMSO), water or ethanol as solvent according to the manufacturer's recommendation. The cultured cells were serially diluted and spotted on the prepared agar plates. Then

the plates were incubated at 26°C and 36°C in parallel. After 5 days, pictures of the plates were taken. The following compounds, used for the sensitivity screenings, are shown in **Table 2.2** . Spot tests were performed twice and yielded reproducible results.

Table 2.2. Chemical agents used for the spot test experiment. Overview of the drugs and compounds used for the growth sensitivity tests. Following makes were used Sigma Aldrich (USA) and Wako (Japan). As the solvent either Dimethyl sulfoxide (DMSO), H_2O and ethanol (EtOH) were used. Stock solution concentrations for each drug are indicated.

Name	Maker	Solvent	Stock conc.
Cerulenin	SIGMA	DMSO	1mg / ml
Thiabendazole	Wako	DMSO	100 mM
30% H2O2	Wako	H2O	500 mM
Paraquat dichloride hydrate	SIGMA	H2O	100 mM
Methyl viologen dichloride hydrate	SIGMA	H2O	100 mM
Calcofluor	SIGMA	H2O	10 mg/ml
Amphotericin B from Streptomyces sp.	SIGMA	DMSO	10mg/ml
Tunicamycin from Streptomyces sp.	SIGMA	DMSO	1 mg/ml
Monensin sodium salt	SIGMA	EtOH	10 mg/ml
CuSO4	Wako	H2O	100 mM
CdSO4	SIGMA	H2O	40 mM
Antimycin A from Streptomyces sp.	SIGMA	DMSO	2 mM
tert-Butyl Hydroperoxide solution	SIGMA	H2O	
Hydroxyurea	Wako	H2O	1M
(S)-(+)-Camptothecin	SIGMA	DMSO	10mM
Erythromycin	SIGMA	EtOH	50 mg/ml
Iron(Ⅲ) Chloride Hexahydrate	Wako	H2O	500 mM

2.2.5. Drug screen by spot test during quiescent state

Viability assessment was conducted to investigate the ability of colony formation in the G0-arrested mutant strain Δ*SPBC21C3.03* and wild type 972 h^-. Following 24 hours after cultrue shift from EMM2+N to EMM2-N, 300 cells were spread with glass beads on rich YPD [1% yeast extract, 2% D-glucose, 2% polypeptone] plates. Plates were incubated at 26°C for 3 days and colony number was counted. The drugs used for the viability assessment are H_2O_2, Antimycin A and Cerulenin shown in **Table 2.2.**

3. Results

3.1. Roughly a dozen GZE highly conserved in bacteria

BLAST-based (Basic Local Alignment Search Tool) phylogenetic profiling of the 89 GZE proteins is the subject of this study. The BLAST search consisted of two steps. Firstly, each of the 89 GZE *S. pombe* proteins was run against the three selected databases using BLAST protein-protein (BLASTp) alignment tool. The aim of this study is the generation of phylogenetic profiles for *S. pombe* GZE gene products via bioinformatics approaches. Phylogenetic profiling was claimed to be an efficient method in predicting protein function (Kotaru, 2009) and establishing functional relationships between proteins which happen to be shared among species (Kensche et al., 2008). The criteria for the initial BLASTp homology search, a combination based on two reports, is an E value $\leq$ 1E-04 (Sun et al., 2005) with a coverage rate (CR) $\geq$ 50% (Moreno-Hagelsieb and Latimer, 2008). The E-value stands for the expected number of possible alignments having the same score by mere chance. The smaller the E value the less likely is the chance of having false positives among the homology candidates. Since ancestral N starvation mechanisms are searched for, it is required that the prokaryotic homology candidate has the same function in both bacterial species.

As a side note: The sequence identity value, i.e. percentage of identical residues between two proteins, was not chosen to be a criterion since it was reported to be misleading for BLAST-based searches. Difficulty in homology judgment by sequence identity values was reported, especially in alignments with protein orthologs of farther related organisms, which have a lesser identity percentage due to random mutation events over time, and sequences shorter than 100 amino acids (Pearson, 2013).

Still false negatives may occur. In fact, during this study's homology search, criteria were not met for Met6 in both prokaryotic species despite similar homoserine

acetyltransferase function. It is likely that bacterial homologs to Met6 are more distantly related and were subject to mutational changes throughout evolutionary progress. Therefore, Met6 and its best hits in bacteria were selected for further assessment by BLAST pairwise alignment approach. The obtained results are shown in **Table 3.1**. The sequences fulfilling this study's criteria are marked in green. A striking observation is that the majority of 89 GZE protein (~62%) fulfill homology criteria against human sequences. This makes the mechanism of *S. pombe* N starvation survival to a predominantly eukaryotic, or evolutionary 'modern' process. Nevertheless, around a dozen GZE proteins show high conservation in both prokaryotic species.

There are two occurrences, where the prokaryotic counterpart from one species fulfills criteria but fails in the other. Prokaryotic proteins are not equally conserved to *S. pombe* due to variation in mutational rates which may be due to different environmental conditions. For example, Maa1 alignment to *E. coli* best hit fulfilled the criteria, but not in *B. subtilis*. The ribosomal protein Rpl1001, on the other hand, fulfills the criteria to *B. subtilis* protein but fails in the *E. coli*. Despite not fulfilling this study's criteria the prokaryotic hits show the same function. Nevertheless, prokaryotic homolog pairs where one only species fulfills homology criteria, but the same function in the other bacteria, were selected for further BLAST pairwise alignment.

There is one case, where homology criteria are not met in both bacterial alignments. In fact, best hits to the homoserine acetyltransferase Met6 are proteins with similar functions despite not fulfilling the criteria. Due to the similar function, the bacterial protein may be a homolog with low conservation. It will be treated as an exception in the next step.

Table 3.1. BLASTp results. 89 *S. pombe* GZE sequences were run against *E. coli*, *B. subtilis* and human databases. Results are shown as E value, sequence indentity (ID in %) and sequence coverage rate (CR in %). Green font indicates fulfillment of initial homology criteria being E-04 and CR more than 50%. Protein names are indicated as their official names (if applicable) or GenBank namings (accessible at https://www.ncbi.nlm.nih.gov/genbank/). Unavailabe alignments are expressed as NA in grey.

S. pombe	*E. coli* Protein	E value	ID	CR	*B. subtilis* Protein	E value	ID	CR	Human Protein	E value	ID	CR
Gdh1	GdhA	2.E-137	50	98	RocG	2.E-52	33	83	CAA46995.1	2.00E-24	26	79
Ilv3	ilvD	8.E-116	37	93	IlvD	2.E-152	43	92	NA	NA	NA	NA
Maa1	AspC	9.E-102	40	90	YhdR	4.E-03	25	37	AAA35568.1	2.E-166	56	90
Coq5	UbiE	3.E-66	44	86	MenG	6.E-33	32	80	COQ5	2.E-80	47	84
Sod2	SodA	8.E-55	44	88	SodA	1.E-56	48	86	SOD2	1.E-63	47	97
Lys12	DmlA	2.E-51	33	98	DmlA	9.E-54	32	98	AAA85639.1	1.E-60	37	95
Ssz1	DnaK	4.E-37	27	93	DnaK	2.E-41	27	80	BAB18615.1	4.E-63	29	80
SPBC21C3.03	UbiB	8.E-35	25	64	UbiB	2.E-21	24	68	ADCK2	3.E-75	31	65
Nde1	Ndh	6.E-23	25	57	YumB	3.E-24	28	68	CAH56481.1	7.7	32	12
Vht1	CQR81743.1	2.E-19	25	59	AIY94153.1	0.1	28	16	BAG61995.1	3.4	30	12
Spe1	AAB40485.1	2.E-16	24	74	AAA67473.1	4.E-12	23	78	AAA59966.2	5.E-128	51	83
Mtd1	FolD	3.E-14	24	90	FolD	9.E-21	25	95	MTHFD2L	8.E-14	23	93
Atg7	AAC76966.2	1.E-09	28	26	AIY92453.1	1.E-10	34	13	EAW64093.1	1.E-155	40	98
Fft3	CAS10170.1	1.E-54	28	66	AQR83667.1	1.E-49	28	57	BAH13535.1	6.E-160	42	67
Kin1	AIZ30111.1	4.E-03	27	11	CAA74267.1	2.E-29	32	27	EAW74174.1	2.E-74	34	54
Sst6	AAC75430.2	1.E-02	26	15	AIY92727.1	5.E-02	36	11	EAW68384.1	8.E-01	31	21
Cbs2	OJR82076.1	7.E-02	29	15	AIY91291.1	2.E-02	22	69	AAC50495.1	8.E-59	35	92
Pmp1	AKK12860.1	8.E-02	36	14	AIY91391.1	6.3	41	9	AAH31643.1	6.E-14	38	44
Ker1	AAC73381.1	8.E-02	35	34	AQR83371.1	0.32	44	22	NA	NA	NA	NA
Asp1	AAC73939.1	0.16	23	9	AAA62687.1	2.5	23	10	HISPPD1	2.E-135	33	93
Sbh1	AAC75904.1	0.23	32	73	AIY94038.1	4.6	30	46	BAD97104.1	6.E-10	39	75
SPBC1347.08c	CQR83496.1	0.26	32	22	AIY95153.1	0.19	35	11	BAB13892.1	0.004	41	21
Rpl3601	AAA70368.1	0.27	36	53	AIY92078.1	0.6	33	39	AAH03052.1	9.E-28	59	88
Met6	OJR69203.1	9.00E-12	27	36	CUB57778.1	9.00E-24	27	44	ARHGEF11	1.E+01	33	9
Rpl1001	OWC08492.1	1.6	29	49	CAB11899.1/RplP	1.E-04	28	58	AAH71918.1	3.E-108	69	94
Mhf1	AAC75296.1	0.39	33	68	CAA10883.1/YkuT	6.E-03	41	50	MHF1	3.E-06	30	92
Ctf1	AAC75355.1	0.47	26	17	AIY92654.1	1.4	41	10	BAG62297.1	2.E-20	56	56
Atg5	AAC75531.1	0.53	27	23	AIY93146.1	2	40	15	AAH93011.1	7.E-24	28	89
Atg1801	CAA44853.3	0.55	26	12	AIY92411.1	0.83	27	17	EAW87325.1	2.E-64	38	94
Nem1	AAC75816.2	0.66	36	8	CAA80274.1	2.2	39	6	EAW90237.1	9.E-51	48	36
Ypa1	AAC73969.1	0.67	27	46	CAB12238.1	0.12	27	20	AAH02545.1	1.E-79	42	93
Wbp4	ASS85334.1	0.7	25	29	AIY94900.1	9.E-02	35	21	AAC34811.1	8.E-06	37	23
Vps20	AKK16060.2	0.76	28	39	AQR80884.1	1.2	28	22	AAQ91196.1	1.E-26	34	83
Cti1	CAA50734.1	0.78	46	18	AIY92898.1	0.27	37	28	EAW80418.1	4.E-07	32	57
Atg1802	AKK13594.1	0.8	42	9	AIY93121.1	0.55	19	19	AAH07596.1	1.E-38	28	98
SPBC902.03	AAC73512.1	0.81	23	38	AIY94816.1	2.1	37	35	NA	NA	NA	NA
Gyp7	ACB02625.1	0.83	24	19	AAB80883.1	3.E-03	23	20	EAW97276.1	2.E-59	37	41
Vps35	AAA57974.1	0.85	38	6	AIY94443.1	3.7	37	4	AAF02778.2	3.E-145	36	91
Dph3	AAC75325.2	0.91	34	51	AIY93663.1	0.87	35	43	AAH10181.1	1.E-24	61	78
Are2	AAB18502.1	0.91	24	19	AIY93600.1	2.3	33	6	AAH06263.4	3.E-26	31	51
Bro1	AAC77356.1	0.96	48	5	AIY92381.1	5.E-02	40	7	BAG58674.1	1.E-38	27	83
Vps3	AAC73151.1	1.1	25	11	CAB04776.1	7.E-03	29	7	AAC16903.1	2.E-05	20	55
Rpp102	AAA57948.1	1.1	25	67	AIY95023.1	0.31	37	40	AAA36471.1	3.E-15	47	99

Table 3.1. Table 3.1. BLASTp results (Continued) Results are presented as E value, sequence identiy (ID in %) and coverage rate (CR in %). Protein names are indicated as their official names (if applicable) or GenBank namings (accessible at https://www.ncbi.nlm.nih.gov/genbank/). Unavailabe alignments are displayed as NA in grey.

S. pombe	*E. coli* Protein	E value	ID	CR	*B. subtilis* Protein	E value	ID	CR	Human Protein	E value	ID	CR
Hcr1	AAC77142.1	1.1	28	26	AAA22360.1	1.7	24	27	NA	NA	NA	NA
Atg6	AAC43086.1	1.2	30	14	AIY91960.1	0.019	40	10	AAC68653.1	2.E-55	29	98
Tho7	AAC75375.1	1.2	33	25	AQR80030.1	0.18	24	46	CAG33654.1	0.14	26	65
Arp42	ACR63254.1	1.2	32	15	CAB05381.1	3.7	26	27	AAC94991.1	4.E-77	34	99
Sgf11	AIZ51089.1	1.3	33	35	AIY93733.1	0.64	28	95	EAW51621.1	5.E-04	32	78
Did4	CQR83400.1	1.3	21	38	AAC63530.1	0.95	32	26	AAC00005.1	1.E-37	40	88
Exo2	AAC73381.1	1.3	24	9	AQR80554.1	1.2	32	5	BAG50941.1	7.E-154	40	50
SPCC1393.08	ACY25764.1	1.3	30	15	CAB04797.1	7	26	22	BAG53416.1	6.E-30	50	18
Rnc1	AAA58111.1	1.4	40	8	AIY95550.1	0.37	43	10	AAH12061.1	5.E-38	32	75
Igo1	AAC74033.1	1.4	25	45	AIY93952.1	1.7	40	28	EAX01839.1	6.E-08	36	55
Rpl2002	BAA10915.1	1.5	26	45	AIY95522.1	0.59	25	33	AAC18781.1	2.E-60	54	99
Rsv2	AAC74275.2	1.5	31	9	AIY92694.1	4.6	31	9	AAA61318.1	5.E-04	41	8
Atg14	CQR83331.1	1.6	26	23	AIY93175.1	9.E-02	24	35	EAW77450.1	4.3	20	53
Elp4	ASS85325.1	1.7	26	24	AIY94726.1	1.4	42	9	EAW68237.1	5.E-14	24	92
Vac7	AAC74271.1	1.8	45	8	CAA74536.1	0.71	36	9	EAW48755.1	2.8	39	15
Aut12	BAA00577.1	1.9	36	10	CAB15908.1	5.E-02	30	13	AAH06299.1	5.E-44	29	78
Atg13	ACB03502.1	1.9	28	10	CAB13399.2	0.6	29	14	EAW52326.1	3	33	8
Zds1	CAA40461.1	2.1	21	20	AIY94205.1	7	25	10	CAA40461.1	2	21	20
Klf1	BAA97896.1	2.2	31	7	AAB80869.1	2.0	25	11	AAK15698.1	5.E-11	48	7
Rpl3201	AAC73862.1	2.3	30	28	CAA51609.1	8.E-03	48	21	AAH11514.1	5.E-48	59	96
Tfg3	AAC74157.1	2.3	42	14	AAA68243.1	1.5	34	20	CAC01935.1	3.E-06	29	64
Vps26	AAC74492.1	2.4	46	8	AIY95302.1	0.35	31	18	AAH09747.1	4.E-125	57	98
Cwf16	AMH30284.1	2.4	35	26	AIY91539.1	1.6	49	12	BAB14757.1	8.E-48	48	68
SPBC365.16	AAC73507.1	2.6	26	19	AIY95047.1	0.02	26	46	AAH27478.2	4	33	17
Trp663	AAA24422.1	2.6	33	5	AIY92485.1	0.77	67	3	NA	NA	NA	NA
SPAC11D3.15	AAA58111.1	2.6	26	5	AOA09954.1	1.2	29	3	AAI42673.1	0	51	99
Tho5	AAC74193.1	3	30	38	AIY92908.1	0.67	22	27	EAW59808.1	2.E-11	32	86
SPBC83.16c	BAL40810.1	3.1	28	11	AIY92148.1	0.41	41	6	AAI42986.1	2.E-18	24	95
SPAC694.04c	AAC74323.1	3.2	28	9	AIY91950.1	1	39	11	AAH51871.1	2.E-87	47	96
Iec1	AAA62780.1	3.5	30	23	AIY93808.1	0.099	32	30	CAB59315.1	4.E-17	35	44
Hap2	AAC75201.1	3.5	34	63	CAA75554.1	0.8	29	40	RBP2	1.4	25	68
Apq12	AAC76272.1	3.7	50	27	AIY94732.1	3.6	44	21	BAH14137.1	4.3	37	35
Shf1	AAA67637.1	3.7	33	27	AIY95242.1	4.5	44	9	AAC39598.1	7.5	32	30
Med20	AAC74934.1	3.8	23	59	AIY94249.1	0.44	27	29	AAQ88610.1	5.6	24	40
Sds23	AIZ93721.1	3.9	24	24	AIY92372.1	0.099	29	20	AAKG2	4.E-01	31	17
Ash2	AAC73883.2	4.3	31	8	AIY92472.1	0.88	28	9	AAH15936.1	2.E-41	25	88
Ppn1	AAC73113.1	5.1	24	10	AIY93169.1	0.44	35	5	NA	NA	NA	NA
Did2	AAB02998.1	5.7	37	18	AIY93019.1	0.84	34	33	AAG01448.1	2.E-55	46	98
Par1	AAT48187.1	6	26	12	AIY92223.1	4.E-03	32	12	BAD18542.1	0	55	92
Dep1	AAC74817.1	6.7	25	21	CAB13430.1	2.E-03	23	23	NA	NA	NA	NA
Atg3	AAA51476.1	6.7	26	19	AIY94358.1	1.4	19	27	AAH24221.1	1.E-50	37	95
SPBC83.19c	ACB04131.1	7.3	43	21	AIY95554.1	1.4	25	73	EAW68471.1	1.6	28	51
Pof15	AMH37970.1	8	23	26	AIY95202.1	0.25	38	13	BAE98206.1	1.8	26	26
Rik1	AAB18497.1	9	27	8	AIY92788.1	3.9	25	9	AAA62838.1	2.E-18	19	96
Rex1	NA	NA	NA	NA	AIY92565.1	0.93	25	13	NA	NA	NA	NA
SPAPJ691.02	NA	NA	NA	NA	CAB13896.2	1.5	35	35	EAX00503.1	2.E-18	38	77

For the second step, BLAST pairwise alignment criteria were set to a coverage rate equal to or bigger than 50%, and secondly to an E value ≤ E-05. The GZE protein sequences, which fulfilled the initial BLASTp criteria, were chosen for subsequent BLAST pairwise analysis. This will make the BLAST results comparable with each other even among different species with variable database sizes (Agrawal et al., 2008).

In the end of the BLAST search, around 15 % (14 proteins) of the 89 *S. pombe* protein sequences fulfilled this study's homology search criteria (**Table 3.2.**). BLAST results for human serve as a reference. In fact, most of the human proteins fulfilled homology criteria to *S. pombe* protein sequences except for NADH dehydrogenase (Nde1) and dihydroxy-acid dehydratase (SPAC17G8.06c/Ilv3).

Among the top-conserved sequences to *E. coli*, the highest-ranking protein is glutamate dehydrogenase Gdh1 with striking 50% sequence identity (ID), followed by ubiquinone methyltransferase Coq5 and manganese-binding superoxide dismutase Sod2, both at 45 % ID. *S. pombe* aspartate aminotransferase Maa1 with 42% ID. There are two proteins with IDs between 35-40%: Dihydroxy-acid dehydratase Ilv3 and homoisocitrate dehydrogenase Lys12. On the other hand, the highest-ranking alignment to *B. subtilis* counterpart is manganese-binding superoxide dismutase Sod2 with 49% ID. The second-highest GZE protein is dihydroxy-acid dehydratase SPAC17G8.06c/Ilv3 with 43% ID. There are no alignments within the 35-40% ID range, but several below 35% such as Lys12, Gdh1 and Coq5. Surprisingly, *B. subtilis* alignment to Maa1 situates in the lower half of the ranking with 25% ID.

The best hit for Met6 in *E. coli* did not fulfill the criteria, whereas the alignment against *B. subtilis* counterpart did. The *E. coli* protein may be a distant homolog with

Table 3.2. Fourteen highly conserved GZE proteins. BLAST pairwise alignment results according to following criteria: Sequence converage of alignment equal or bigger than 50% and equal to or less than E vaue E-05. Grey area signifies Met6 alignment which did not fulfill criteria in *E. coli* but is sufficient in *B. subilis*. Met6 may have prokaryotic homologs but is not highly conserved as the other fourteen GZE proteins. The results are ranked according to sequence identity in descending order.

S. pombe **vs.** ***E. coli***

S. pombe	*E. coli*	E value	Identity (%)	Coverage (%)	Function	Human	E value	Identity (%)	Coverage (%)
Gdh1	GdhA	2.00E-142	50	98	Glutamate dehydrogenase	GLUD2	8.00E-30	25	79
Coq5	UbiE	1.00E-71	45	86	Ubiquinol metyltransferase	COQ5	6.00E-86	47	84
Sod2	SodA	5.00E-60	45	88	Superoxide dismutase	SOD2	2.00E-69	47	97
Maa1	AspC	7.00E-109	42	90	Aspartate aminotransferase	GOT2	7.00E-172	56	90
Ilv3	IlvD	2.00E-119	37	93	Dihydroxy-acid dehydratase	NA	NA	NA	NA
Lys12	DmlA	6.00E-59	35	98	Tartrate dehdyrogenase	IDH2	3.00E-66	37	95
Rpl1001	OWC08492.1	2.00E-27	29	63	50S ribosomal protein L16	RPL10	9.00E-105	69	94
Fft3	RapA	1.00E-54	28	66	Snf2 helicase	SMARCA1	3.00E-165	42	67
Ssz1	Dnak	9.00E-41	27	93	Protein chaperone	HSPA8	2.00E-68	29	80
SPBC21C3.03	UbiB	1.00E-39	25	72	UbiB family protein	ADCK2	1.00E-80	31	69
Nde1	Ndh	9.00E-27	25	61	NADH dehdyrogenase	NA	NA	NA	NA
Vht1	CQR81743.1	2.00E-23	25	66	L-rhamnonate transporter	C4orf26	3.3	30	12
Spe1	LysA	2.00E-20	24	78	DAP decarboxylase	OAZ	2.00E-133	51	85
Mtd1	FolD	3.00E-19	24	90	MTHF dehydrogenase	MTHFD1	2.00E-19	23	93
Met6	OJR69203.1	2.00E-18	27	46	Homoserine acetyltransferase	PRKAG1	2.00E-64	34	98

S. pombe **vs.** ***B. subtilis***

S. pombe	*B. subtilis*	E value	Identity (%)	Coverage (%)	Function	Human	E value	Identity (%)	Coverage (%)
Sod2	SodA	1.00E-65	49	87	Superoxide dismutase	SOD2	2.00E-69	47	97
Ilv3	IlvD	5.00E-156	43	92	Dihydroxy-acid dehydratase	NA	NA	NA	NA
Lys12	YcsA	5.00E-67	34	96	Tartrate dehdyrogenase	IDH2	3.00E-66	37	95
Gdh1	RocG	1.00E-56	33	86	Glutamate dehydrogenase	GLUD2	8.00E-30	25	79
Coq5	UbiE	6.00E-40	33	90	Menaquinol metyltransferase	COQ5	6.00E-86	47	84
Vht1	ADM38621.1	2.00E-20	31	50	D-galactonate transporter	C4orf26	3.3	30	12
Fft3	RapA	1.00E-60	30	72	Snf2 helicase	SMARCA1	3.00E-165	42	67
Nde1	YumB	7.00E-28	28	68	NADH dehydrogenase	NA	NA	NA	NA
Rpl1001	CAB11899.1	1.00E-08	28	65	50S ribosomal protein L16	RPL10	9.00E-105	69	94
Ssz1	Dnak	7.00E-45	27	80	Protein chaperone	HSPA8	2.00E-68	29	80
Maa1	YhdR	8.00E-07	25	51	Aspartate aminotransferase	GOT2	7.00E-172	56	90
Mtd1	FolD	2.00E-25	24	91	MTHF dehydrogenase	MTHFD1	2.00E-19	23	93
SPBC21C3.03	UbiB	2.00E-26	23	67	UbiB family protein	ADCK2	1.00E-80	31	69
Spe1	LysA	1.00E-15	23	80	DAP decarboxylase	OAZ	2.00E-133	51	85
Met6	CUB57778.1	9.00E-24	27	68	Homoserine acetyltransferase	LRRFP1	2.00E-04	27	44

low similarity. Therefore, BLASTp results for Met6 are included in the homology results in **Table 3.2.** but are shaded in grey. This study aims for investigating potentially conserved G0 survival promoting interactions between highly conserved GZE proteins based on phylogenetic profiling. In order to make an accurate judgment about ancient interactions, a high degree of conservation, i.e. fulfillment of this study's criteria, is set as a prerequisite in the present investigation.

3.2. The majority of GZE homology candidates acts within the mitochondria

According to pombase.org *S. pombe* has 4,516 ortholog in eukaryotes, whereas only 1,005 in bacteria and only 243 in archaea (Wood et al., 2012). Nevertheless, just about a dozen *S. pombe* protein sequences seem to be highly conserved. The proteins, fulfilling the criteria of sequence homology search, are displayed in **Figure 3.1.**

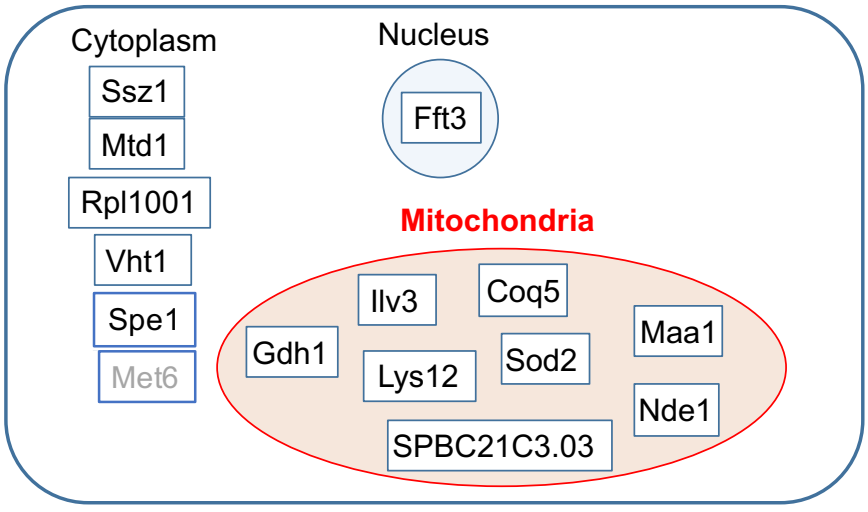

Figure 3.1. The highly conserved GZE proteins. Fourteen GZE proteins show high similarity to prokaryotic sequences. This study's homology search is based on the previously identified G0 survival essential (GZE) gene products by Dr. Kenichi Sajiki (Sajiki *et al.*, publication in progress). Met6 may be a homolog with relatively low

conservation which is derived from its similar function. It is shaded in grey as it is not included in the selection of highly conserved proteins.

Due to the high degree of similarity to bacterial proteins these proteins are designated as 'homology candidates' since their homologies still need to be confirmed in the course of this study.

Alignments of cytoplasmic or nuclear GZE proteins with bacterial sequences produce pairs predominantly within the sequence identity range of 35-23%. It was reported that roughly 90% of alignments with sequence identity of around 35% were found to be true homologs, only 10% of the alignments, displaying an ID of 20%, were true positives (Rost, 1999). Due to this rapid decrease in certainty, a sequence identity range between 20-35% was termed as the 'twilight zone' for homology assignment where false positives are more likely to occur. Therefore, special consideration needs to be given in homology candidates displaying a sequence ID within this range (Pevsner, 2003).

Nevertheless, due to the high conservation among mitochondria-located GZE proteins, focus on the role of mitochondria during N starvation will be laid. Despite being localized to the same intracellular compartment, which is the mitochondria, results from the viability assessment (Sajiki *et al*., publication in progress) found that requirement of the gene products occurs at different time points of N starvation (**Table 3.3.)**. Among the eight GZE gene deletion mutants, the quiescent Δ*sod2* strain suffered the most detrimental and rapid loss in its ability to regenerate following transfer into vegetative state conditions. This contrasts with the remaining seven which are widely viable within the initial quiescence period but suffer from impairment viability by the last half of the four-week-long incubation. Viability impairment is defined by a diminished ability to regenerate N starvation.

Table 3.3. Ability to regenerate from N-starvation induced quiescence. This viability assessment is based on the fact that G0-arrested cells do not divide, viability of quiescent cells cannot be assessed. Therefore, the ability to form colonies upon N replenishment is checked as an indicator of cell viability. Despite being highly conserved and associated with mitochondrial processes, viability upon N replenished conditions in the eight GZE deletion mutants seem to be differentially affected. After spreading 300 G0-arrested cells in N-replenished media (YPD, Yeast extract, polypeptone, glucose), ability to regenerate is derived from the number of colonies formed against the number plated. Based on data obtained from Dr. Kenichi Sajiki.

Gene Name	VE	24h	1 week	2 weeks	3 weeks	4 weeks
Wild type	**104.4**	**97.8**	**87.8**	**103.3**	**90.6**	**90**
Δsod2	76.7	48.3	3.7	0	0	0
Δilv3	103.3	105	78.3	98.3	48.3	0
Δmaa1	108.3	113.3	83.3	86.7	40	2.5
Δlys12	116.7	85	91.7	25	10	20
Δgdh1	88.3	78.3	81.7	26.7	23.3	15
ΔSPBC21C3.03	110	86.7	95	95	63	26.7
Δcoq5	76.7	85	95	86.7	75	40
Δnde1	98.3	91.7	88.3	91.7	58.3	45

Ability to regenerate (colony formation ability in %)

<5%

<30%

<50%

In other words, gene deletion strains, sensitive to -N conditions, showed a colony formation ability of < 50%. Among the eight deletion mutants Δ*sod2* shows a sudden reduction in colony formation by week1, followed by complete viability loss at week 2 of N starvation. By week 4 deletion mutant strains Δ*ilv3,* Δ*maa1,* Δ*lys12,* Δ*gdh1* and Δ*SPBC21C3.03* suffer from diminished ability to regenerate (<30%), whereas Δ*coq5* and Δ*nde1* are affected by moderate viability impairment (<50%).

Also, a functional background with respect to N starvation-induced quiescence will be tried to be deducted. Genetic information as well as, results from homology

searches will be presented. Sequence alignments with bacterial protein homologs are used to understand the conserved cellular function within *S. pombe.*

3.3. The sole superoxide scavenging GZE - Sod2

In *S. pombe* mitochondria-located superoxide dismutase was confirmed to be essential for N starvation survival in *S. pombe*. The gene ***sod2*** encodes the 24 kDa oxidative stress scavenging enzyme manganese superoxide dismutase. The information on the type of reaction catalyzed by Sod2 can be accessed on the KEGG database via the enzyme commission number (EC:1.15.1.1) (Kanehisa & Goto, 2000). Sod2 transforms superoxide radicals into hydrogen peroxide and molecular oxygen (Jeong et al., 2001). In fact, *S. pombe sod2* expression is increased upon oxidative stress and cadmium treatment (Wilhelm et al., 2008).

Sequence alignment with BLAST showed homologs in *E. coli* (44% identity (ID) and *B. subtilis* (48% ID) (**Figure 3.2**.). Since no crystal structure for *S. pombe* Sod2 was resolved, the data for the *E. coli* GdhA bound to hydroxide (crystal structure ID: 1D5N) (Borgstahl et al., 2000) and peroxide (crystal structure ID: 3K95) (Porta et al., 2010) will serve as a references. The structures were found in the PDB database, featuring a collection of crystal structures.

Since both 1D5N and 3K95 show overall identical structural information, only 1D5N is used in the CHIMERA sequence alignment. *E. coli* SodA comprises α -helical N-terminal and a mixed α/β C-terminal domain (Borgstahl et al., 1992) (**Figure 3.3**.). The multiple sequence alignments confirm the conservation of important functional sites in Sod2 to prokaryotic protein sequences.

S. pombe Sod2 vs. *E. coli* SodA

Score	Expect	Method	Identities	Positives	Gaps
174 bits(442)	5e-60	Compositional matrix adjust.	94/209(45%)	128/209(61%)	24/209(11%)

```
Query  27   TLPPLPYAYNALEPALSETIMKLHHDKHHQTYVNNLNAAQEKLAD-PNLDLEGEVA----  81
            TLP LPYAY+ALEP    E  M++HH KHHQTYVNN NAA E L +  NL +E  +
Sbjct  4    TLPSLPYAYDALEPHFDEQTMEIHHTKHHQTYVNNANAALESLPEFANLPVEELITKLDQ  63

Query  82   ----LQAAIKFNGGGHINHSLFWKILAPQKEGGGKPVTSGSLHKAITSKWGSLEDFQKEM  137
                  +  ++ N GGH NHSLFWK L   K+G       G L  AI   +GS+++F+ E
Sbjct  64   LPADKKTVLRNNAGGHANHSLFWKGL---KKG---TTLQGDLKAAIERDFGSVDNFKAEF  117

Query  138  NAALASIQGSGWAWLIVDKDGSLRITTTANQDTIVKSK--------PIIGIDAWEHAYYP  189
              A AS  GSGWAWL++  D  L + +TANQD+ +  +         PI+G+D WEHAYY
Sbjct  118  EKAAASRFGSGWAWLVLKGD-KLAVVSTANQDSPLMGEAISGASGFPILGLDVWEHAYYL  176

Query  190  QYENRKAEYFKAIWNVINWKEAESRYSNR  218
             +++NR+ +Y K  WNV+NW EA +R++ +
Sbjct  177  KFQNRRPDYIKEFWNVVNWDEAAARFATK  205
```

S. pombe Sod2 vs. *B. subtilis* SodA

Score	Expect	Method	Identities	Positives	Gaps
189 bits(480)	1e-65	Compositional matrix adjust.	98/202(49%)	133/202(65%)	16/202(7%)

```
Query  25   KATLPPLPYAYNALEPALSETIMKLHHDKHHQTYVNNLNAAQE---KLADPNLDL-----  76
            K  LP LPYAY+ALEP   +  M +HH KHH TY+ NLNAA E   +LAD +++
Sbjct  3    KHELPKLPYAYDALEPHFDKETMNIHHTKHHNTYITNLNAALEGHAELADKSVEELVANL  62

Query  77   -EGEVALQAAIKFNGGGHINHSLFWKILAPQKEGGGKPVTSGSLHKAITSKWGSLEDFQK  135
             E   A++ A++ NGGGH NH+ FW IL+P   GGG+PV  G L  AI +K+GS + F++
Sbjct  63   NEVPEAIRTAVRNNGGGHANHTFFWTILSPN--GGGQPV--GELATAIEAKFGSFDAFKE  118

Query  136  EMNAALASIQGSGWAWLIVDKDGSLRITTTANQDTIVKS--KPIIGIDAWEHAYYPQYEN  193
             E   A A+  GSGWAWL+V+ +G L +T+T NQD+ +      P+IG+D WEHAYY  Y+N
Sbjct  119  EFAKAGATRFGSGWAWLVVN-NGELEVTSTPNQDSPLTEGKTPVIGLDVWEHAYYLNYQN  177

Query  194  RKAEYFKAIWNVINWKEAESRY  215
            R+ +Y  A WNV++W  AE RY
Sbjct  178  RRPDYIGAFWNVVDWNAAEKRY  199
```

S. pombe Sod2 vs. *Human* SOD2

Score	Expect	Method	Identities	Positives	Gaps
199 bits(506)	2e-69	Compositional matrix adjust.	104/221(47%)	139/221(62%)	13/221(5%)

```
Query  4    FLSKNSVAAIRNVSIARGV---HTKATLPPLPYAYNALEPALSETIMKLHHDKHHQTYVN  60
             LS+       R ++ A G       K +LP LPY Y ALEP ++  IM+LHH KHH  YVN
Sbjct  1    MLSRAVCGTSRQLAPALGYLGSRQKHSLPDLPYDYGALEPHINAQIMQLHHSKHHAAYVN  60

Query  61   NLNAAQEKLADP--NLDLEGEVALQAAIKFNGGGHINHSLFWKILAPQKEGGGKPVTSGS  118
            NLN  +EK  +      D+  ++ALQ A+KFNGGGHINHS+FW  L+P   GGG+P   G
Sbjct  61   NLNVTEEKYQEALAKGDVTAQIALQPALKFNGGGHINHSIFWTNLSPN--GGGEP--KGE  116

Query  119  LHKAITSKWGSLEDFQKEMNAALASIQGSGWAWLIVDKD-GSLRITTTANQDTIVKSK--  175
            L +AI    +GS + F+++ AA    +QGSGW WL  +K+ G L+I     NQD +  +
Sbjct  117  LLEAIKRDFGSFDKFKEKLTAASVGVQGSGWGWLGFNKERGHLQIAACPNQDPLQGTTGL  176

Query  176  -PIIGIDAWEHAYYPQYENRKAEYFKAIWNVINWKEAESRY  215
             P++GID WEHAYY QY+N + +Y KAIWNVINW+    RY
Sbjct  177  IPLLGIDVWEHAYYLQYKNVRPDYLKAIWNVINWENVTERY  217
```

Figure 3.2. BLAST pairwise alignments against Sod2. *S. pombe* sequences were separately run against *E. coli*, *B. subtilis* and human databases.

S. pombe	*E. coli*	E value	Identity (%)	Coverage (%)	Human	E value	Identity (%)	Coverage (%)	*B. subtilis*	E value	Identity (%)	Coverage (%)
Sod2	SodA	5.00E-60	45	88	SOD2	2.00E-69	47	97	SodA	1.00E-65	49	87

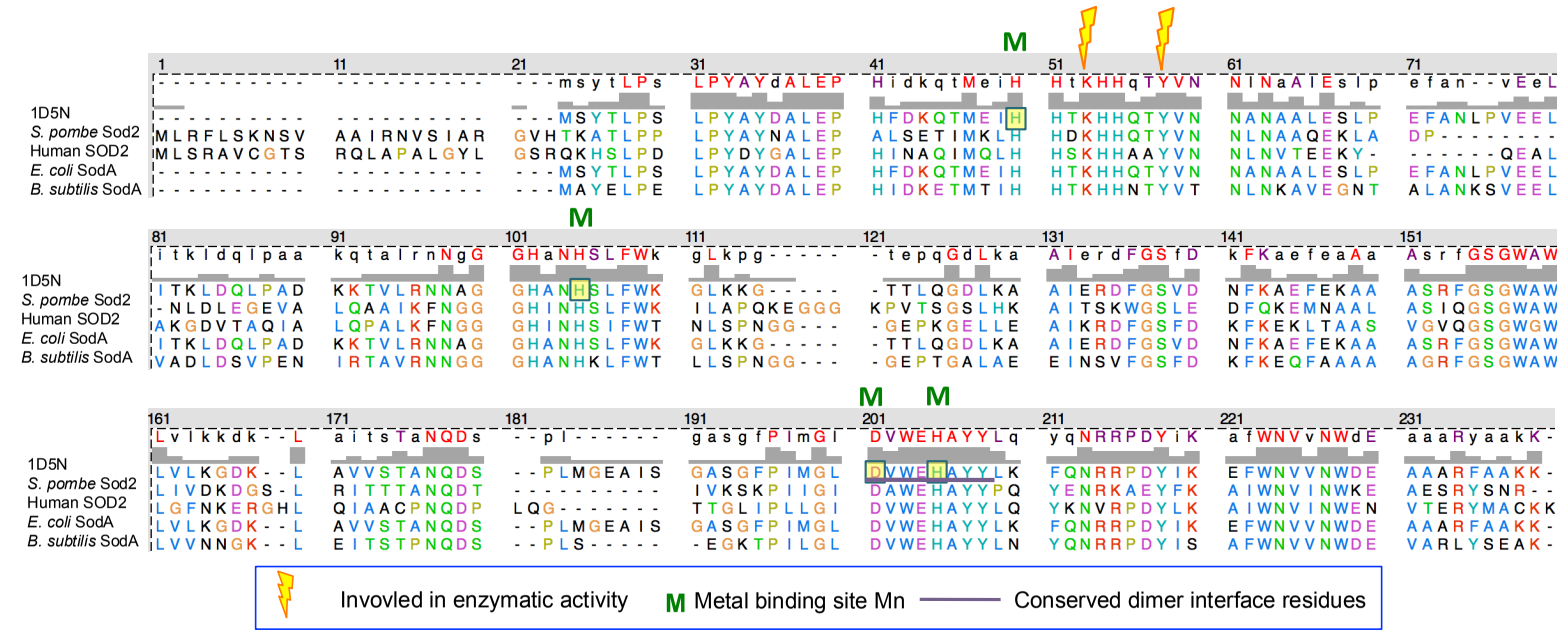

Figure 3.3. Sod2 aligned with its homologs. Functional information inferred from crystal structure of *E. coli SodA* 1D5N (Borgstahl *et al*., 2000). BLASTp results are displayed on the top.Several functional sites are conserved in *E. coli*, *B. subtilis* and human, among these are two sites for enzymatic activity (Y58, K53; yellow bolt) and four manganese binding sites at the active (H50, H105, D201, H205; green arrow) which were shown to interact with peroxide (Porta et al., 2010). In addition, the DXWEHXXYL motif (D201-L209), essential for catalytic function and stability, is shared among the four species. Color scheme is based on ClustalX default setting which differentiates between residue type and frequency of occurence in the same column (consensus residue).

The *S. pombe* genome encodes two SODs; manganese and copper-zinc containing SODs, designated as Mn SOD and Cu-Zn SOD respectively (Takahashi et al., 2011). Notably, only the Mn SOD was shown to be necessary for N starvation survival. In order to understand the evolutionary background of SOD homologs, which may give a reason why Sod2 and not the Fe-binding Sod1 is essential for N starvation survival in *S. pombe*, SOD phylogeny tree was reconstructed using MEGA 6 software (Tamura et al., 2013). The phylogeny tree clarifies about the extent of amino acid changes the individual SOD isoforms obtained throughout the evolutionary process. It therefore is not to measure evolutionary time and does not inform us when the changes had happened, but serves as an information what extent a speciation event happened during evolution which is merely based on amino acid sequence changes (Pavlopoulos et al., 2010). Several protein sequences, spanning species from bacteria through archaea to multicellular eukaryotes, were used as input in the current SOD phylogeny assessment. Also, SODs with other metal binding preferences were included such as copper-zinc (Cu-Zn) SODs, and iron (Fe) SODs. Cu-Zn SODs diverged from Mn and Fe binding SODs.

B. subtilis Mn SOD appears is closer to *S. pombe* Sod2 than *E. coli* SodA which is contained in the same clade as Fe-containing SOD isoforms. The reconstructed SOD phylogeny tree therefore supports the initial BLAST results that bacterial SodA is the orthologue to Sod2 which means that both evolved from on ancestral SOD protein. Sod2 evolved from the same ancestral protein as the other SOD isoforms and thus, homology can be therefore claimed.

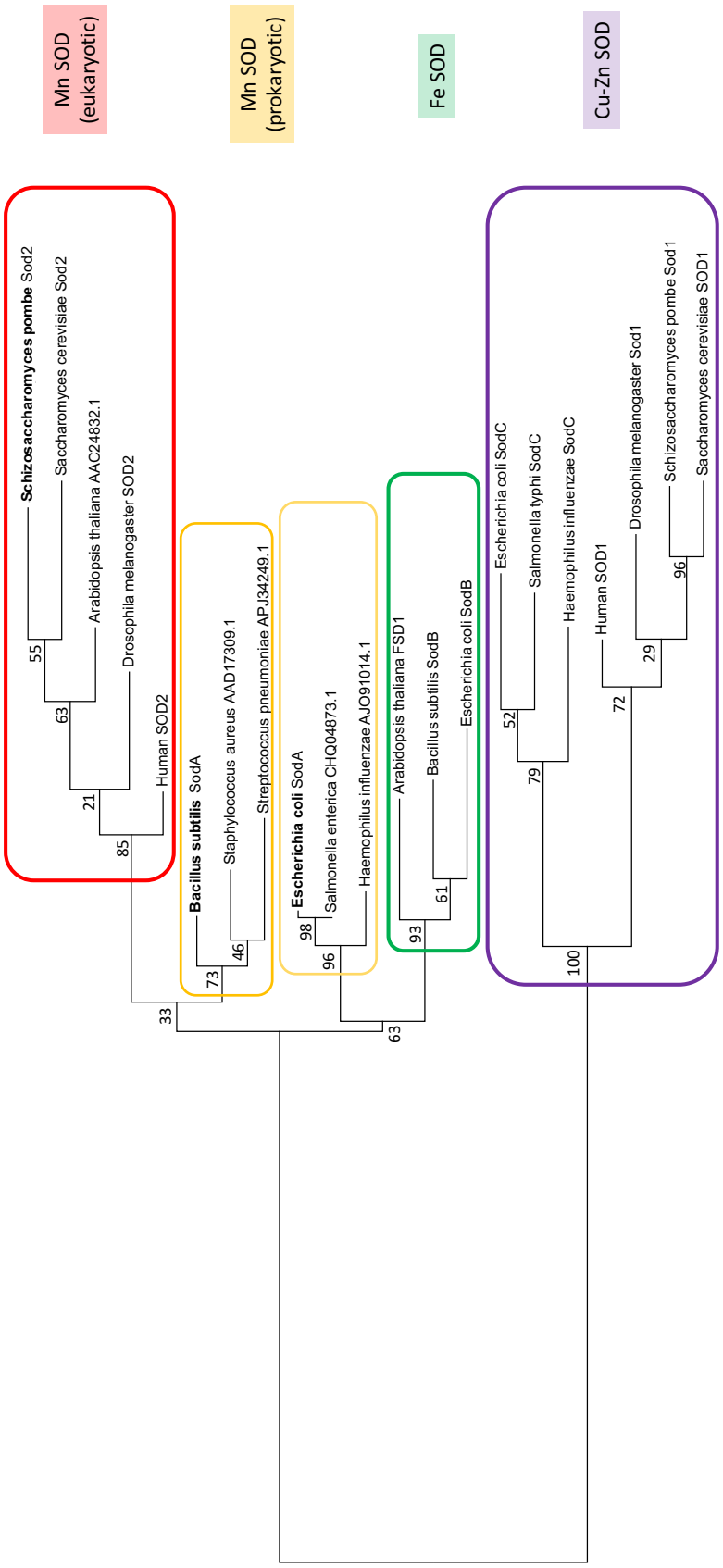

Figure 3.4. SOD phylogeny reconstruction. Maximum likelihood phylogeny tree was computed with MEGA6. Node reliability is expressed with confidence percentage from 1,000 bootstrap repeats. Based on node distribution SOD isoforms can be distiguished based on the type of the bound metal: eukaryotic manganese (Mn) SOD (red), prokaryotic MnSOD, iron (Fe) SOD (green) and copper zinc (Cu-Zn) SOD (purple). Node reliability is considered significant when confidence intervals are higher than 50%.

3.4. Four mitochondrial amino biosynthetic enzymes essential during G0 survival

There are four amino acid metabolic enzymes under the GZE candidates of homology to bacteria. Viability of the four amino acid biosynthetic GZE deletion mutants starts to deteriorate between week 2 and week 3. In the next section, Lys12 and Ilv3, which are involved in multi-step amino acid biosynthetic pathways according to KEGG database (Kanehisa and Goto, 2000), will be introduced first.

3.4.1. GZE Enzymes generating amino acid synthetic precursors – Lys12 and Ilv3

The two GZE enzymes homoisocitrate dehydrogenase Lys12 and dihydroxy-acid dehydratase Ilv3 are situated in amino acid biosynthetic multi-step pathways. In the following paragraphs their conservation to bacteria will be reported.

The homoisocitrate dehydrogenase Lys12 (~39 kDa) converts homoisocitrate to 2-oxoadipate by NAD^+ cofactor conversion (HICDH, EC: 1.1.1.87) which is a step in lysine biosynthetic via the α-aminoadipate (AAA) pathway. The enzyme is found in the cytoplasm (Matsuyama et al., 2006) and the mitochondrion based on information from *S. cerevisiae* homolog (Renvoise et al., 2014).

Lys12 is part of a biosynthetic pathway consisting of ten steps. Nevertheless, only Lys12 was shown to be essential for four-week-long N starvation regeneration. Based on the information on the lysine biosynthetic pathway, retrieved from KEGG database (Kanehisa and Goto, 2000), Lys12 is situated in the middle of the biosynthetic mechanism (**Figure 3.5.)**. To understand why only one enzyme out of a multi-step pathway is essential for G0 phase survival, data on protein abundances for each enzyme at vegetative (VE) and G0 state (Marguerat et al., 2012) was obtained from pombase.org (Wood et al., 2012). When considering protein levels among the

biosynthetic enzymes, Lys12 shows the lowest abundance per cell during the 24-hour-long N starvation period. The varying protein abundances may be a potential reason why deletion mutants of the other lysine biosynthetic enzymes do not affect regenerative ability upon four-week-long N starvation. Therefore, it is likely that lysine biosynthetic mutants, other than Δ*lys12*, may cause viability decrease after a longer incubation (>4 weeks).

Since most bacteria do not rely on the predominantly fungal AAA pathway for lysine biosynthesis, no functional homologs to *E. coli* and *B. subtilis* are found. Also, humans do not synthesize lysine and thus, do not possess any homoisocitrate dehydrogenase isoforms. Nevertheless, BLAST homology search showed up with alignments which fulfilled this study's homology criteria **(Figure 3.6.)** For the bacterial BLASTp top hits tartrate dehydrogenase (TDH) and in human isocitrate dehydrogenase (ICDH) came up. Like Lys12, these proteins belong to the conserved β-decarboxylating dehydrogenase family (Miyazaki et al., 2005) which is known to catalyze substrates with a *D*-malate-based structural backbone (Vorobieva et al., 2014). Despite no homoisocitrate dehydrogenase ortholog is found in *E. coli* and *B. subtilis* it does not mean that there are no HICDHs in bacteria. *Thermus thermophilus*

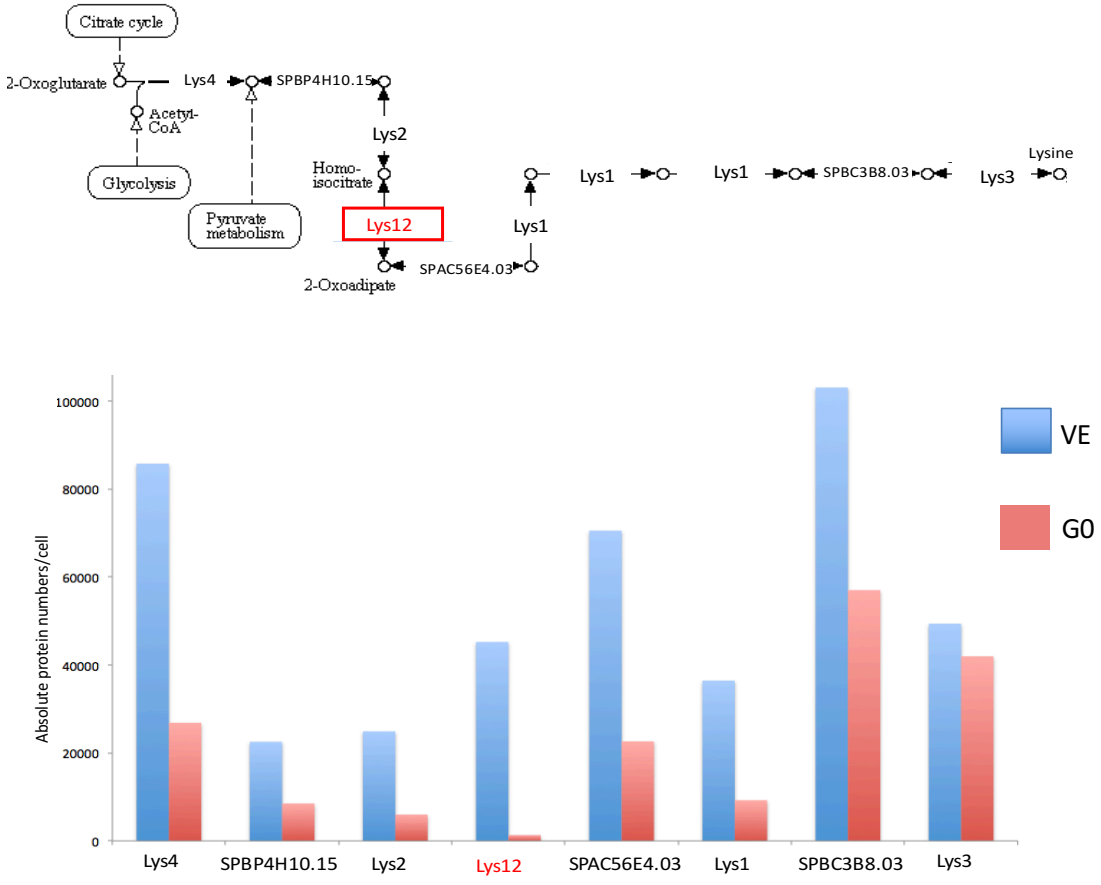

Figure 3.5. Lysine biosynthetic pathway. Fluctuation in protein abundance of lysine biosynthetic proteins during vegetative (VE, blue) and G0 (red) states. Lysine biosynthetic pathway was adapted from KEGG database (Kanehisa & Goto, 2000). Protein abundance per cell is inferred from Marguerat *et al.* 2012. which can be accessed via pombase.org database (Wood *et al.*, 2012).

homoisocitrate dehydrogenase (Hicdh) is included in the alignment. Despite not being functional homologs, BLASTp showed that sequence alignments between Lys12 to *E. coli* and *B. subtilis* proteins are significantly similar. Therefore, *E. coli* DmlA and *B. subtilis* YcsA were included into the CHIMERA alignment (**Figure 3.7.)** with *S. pombe* Lys12 crystal structure 3TY3 as a reference (Bulfer et al., 2012). In fact, despite not being functional homologs *E. coli* DmlA and *B. subtilis* YcsA share many functional sites with *S. pombe* Lys12. Although *T. thermophilus* Hicdh is a functional homolog to

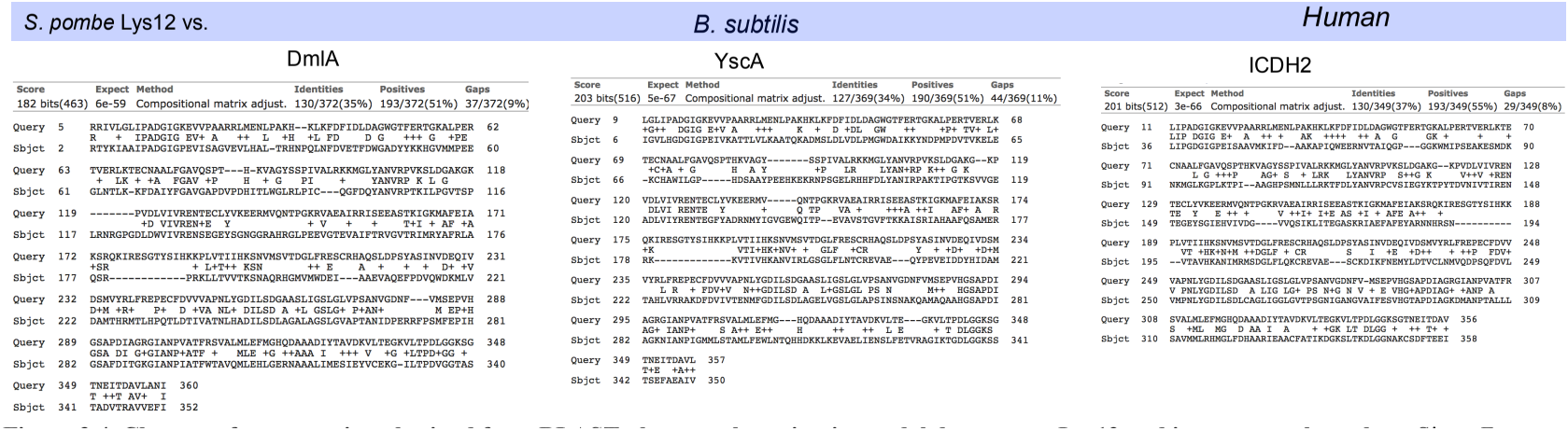

Figure 3.6. BLAST pairwise alignments against Lys12. Since *E coli*, *B. subtilis* and human lack homoisocitrate dehydrogenase orthologs, the closest BLAST hits were used for the alignments. These are bacterial tartrate dehydrogenase and human isocitrate dehydrogenase in human

Lys12, some differences are found in the alignment. This is in accordance to the claim that *T. thermophilus* Hicdh is closer to the ancestral protein. The residue R96 was reported to be essential for substrate specificity in *T. thermophilus*. Once mutated to valine its substrate preference changed from isocitrate to isopropyl malate. The change to valine is assumed to cause an increase in hydrophobicity and therefore repels isocitrate (Miyazaki et al., 2005) (Malik and Viola, 2010). It is not known whether substrate specificity in Lys12 is defined by the same position as in *T. thermophilus*. But at the same position to *T. thermophilus* R96, *S. pombe* Lys12 has a valine residue. It is not known whether this valine residue influences hydrophobicity as reported in bacterial Hicdh.

In fact, BLASTp search yielded hits with tartrate dehydrogenases (TDHs) at the top, however, isopropyl-malate and isocitrate dehydrogenases (IPMDH and ICDH) showed similar degrees of identities to *S. pombe* Lys12. To understand how closely related homoisocitrate with the other family members. Phylogeny for the four types of paralogs from the β-decarboxyl dehydrogenase family (ICDH, IPMDH, TDH and HICDH) was computed with MEGA6 using 1,000 times bootstrapped maximum likelihood method (**Figure 3.8.**). From the phylogenetic tree, one learns that ICDHs diverged early from the rest of the paralogs which means that ICDHs differ the most in amino acid sequence. Despite clear divergence from ICDH, the precursor for HICDH did not diverge significantly (20% confidence) from the shared precursor of TDH and IPMDH. The archaeal HICDH in *Pyrococcus horikoshii* and *Thermococcus kodarensis* do not clearly locate to the HICDH node. In fact, it was reported that there is only one multi-functional HICDH in *P. horikoshii* using isocitrate, homoisocitrate and isopropyl-

S. pombe	*E. coli*	E value	Identity (%)	Coverage (%)	Human	E value	Identity (%)	Coverage (%)	*B. subtilis*	E value	Identity (%)	Coverage (%)
Lys12	DmlA	6.00E-59	35	98	IDH2	3.00E-66	37	95	YcsA	5.00E-67	34	96

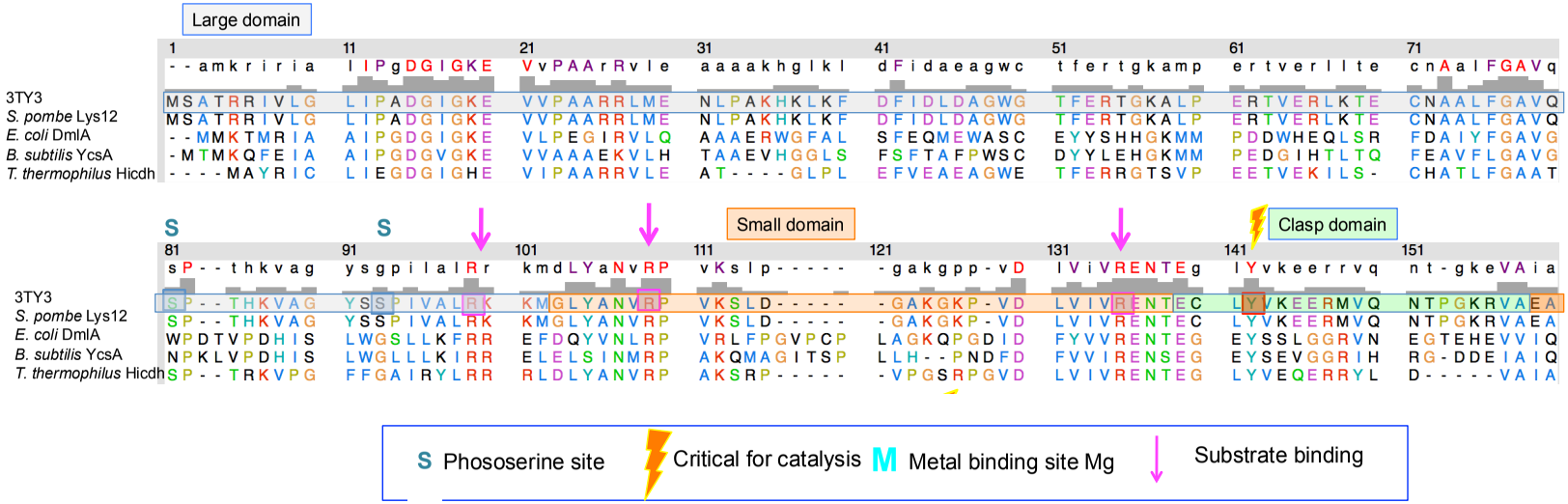

Figure 3.7. Lys12 aligned against its bacterial homologs. No homoisocitrate dehydrogenase (Hicdh) orthologs were found in both bacterial species. Therefore, *T. thermophilus Hicdh* was included in the alignment. Information from the resolved Lys12 crystal structure 3TY3 (Bulfer et al., 2011) was used as a reference. According to 3TY3, two large domains, two small domains and a clasp domain were reported. In fact, despite not being functional homologs *E. coli* DmlA and *B. subtilis* YcsA share many functional sites with *S. pombe* Lys12. The four substrate binding sites (R99, R109, R135, D241; pink arrow)

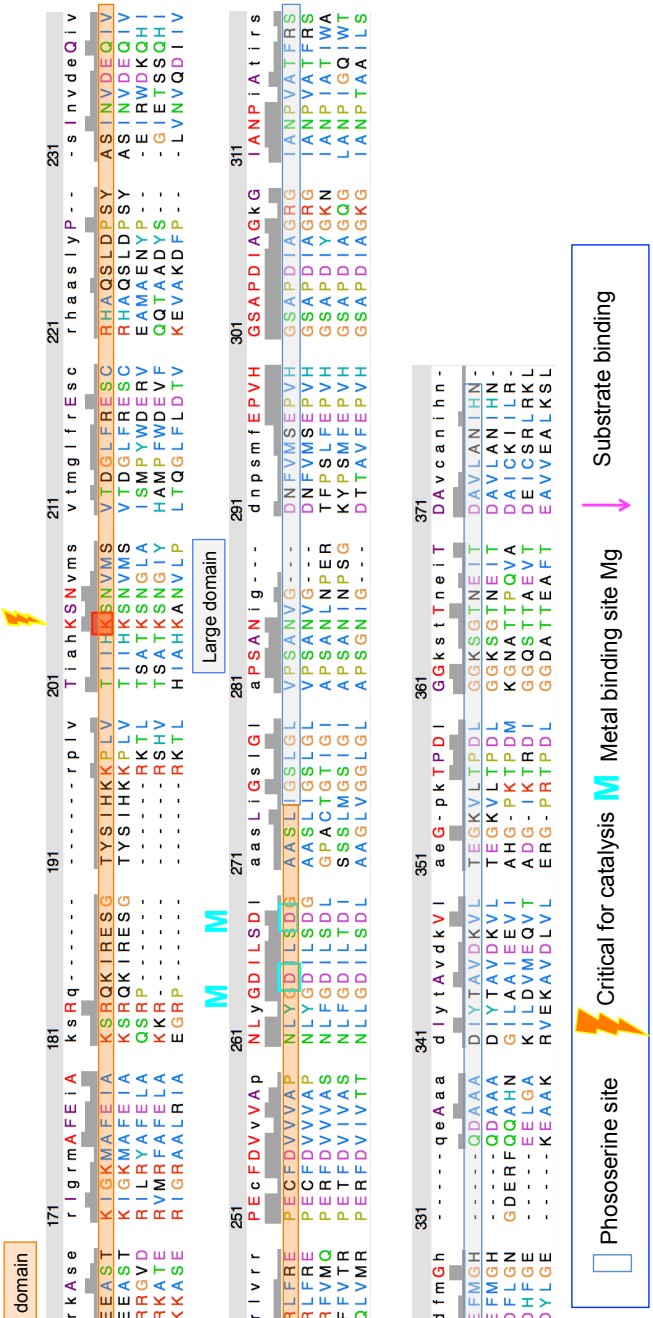

Figure 3.7. Lys12 aligned against its bacterial homologs (continued). Also the magnesium binding sites (D265, D269; blue M) are conserved. In addition, the two sites critical for catalysis (Y142, K205; orange bolt). The two phosphoserine sites (S81, S93; green S) are not conserved in *E. coli* and *B. subtilis*. Color scheme is based on ClustalX default setting which differentiates between residue type and frequency of occurence in the same column (consensus residue).

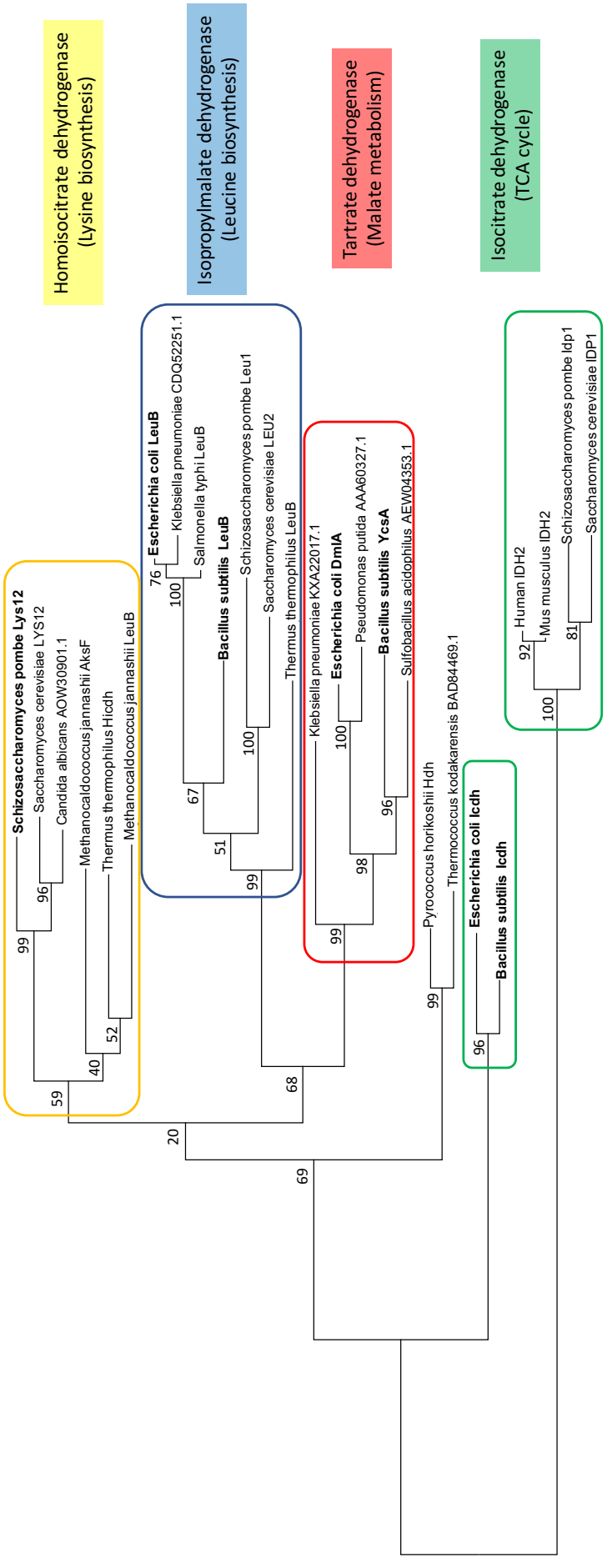

Figure 3.8. Phylogeny of the β-decarboxylating dehydrogenase family. Ancestry of Lys12 and its paralogs were analyzed by running maximum-likelihood with MEGA. 1,000 Bootstrap replicates were computed and the confidence levels are shown.

malate as substrates (Miyazaki, 2005). Finally, IPMDH (blue box) and TDH (red box) split into sub-nodes after diverging from HICDH ancestor. These are highly specialized proteins but nevertheless, 'promiscuous' catalytic behavior of DmlA was reported in *E. coli* where it was shown to complement leucine biosynthetic LeuB (Vorobieva et al., 2014).

Tartare dehydrogenases catalyze either oxidation of tartrate or decarboxylation of malate into pyruvate (Malik and Viola, 2010). *E. coli* DmlA catalyzes reactions with malate and tartrate as substrate. As malate dehydrogenase it generates pyruvate (Lukas et al., 2010). As a summary, one can say that HICDHs are closer to the ancestral isoforms which were able to use both homoisocitrate and isopropyl-malate as substrates. Bacteria, which use a different pathway for lysine biosynthesis seem to possess more specialized IPMDH. In fact, it cannot be denied that several amino acid biosynthetic pathways may have evolved from a general pathway which got specialized over evolutionary time (Fondi et al., 2007). **Figure 3.9**. stresses the possibility that TCA cycle, lysine and leucine biosynthetic reactions, which rely on an identical catalytic reaction pattern may be have diverged from an ancestral pathway. This possibility has been already suggested in previous reports (Jia et al., 2006, Nishida et al., 1999). The information about each pathway was inferred from KEGG database (Kanehisa and Goto, 2000).

In conclusion, Lys12 shares significantly high similarity to its paralogs in bacteria. Phylogenic reconstruction, based on amino acid changes, suggests that Lys12 diverged in a speciation event from the ancestor for both IPMDH and TDH. Therefore, this study's Lys12 BLAST results can be explained based on their evolutionary close

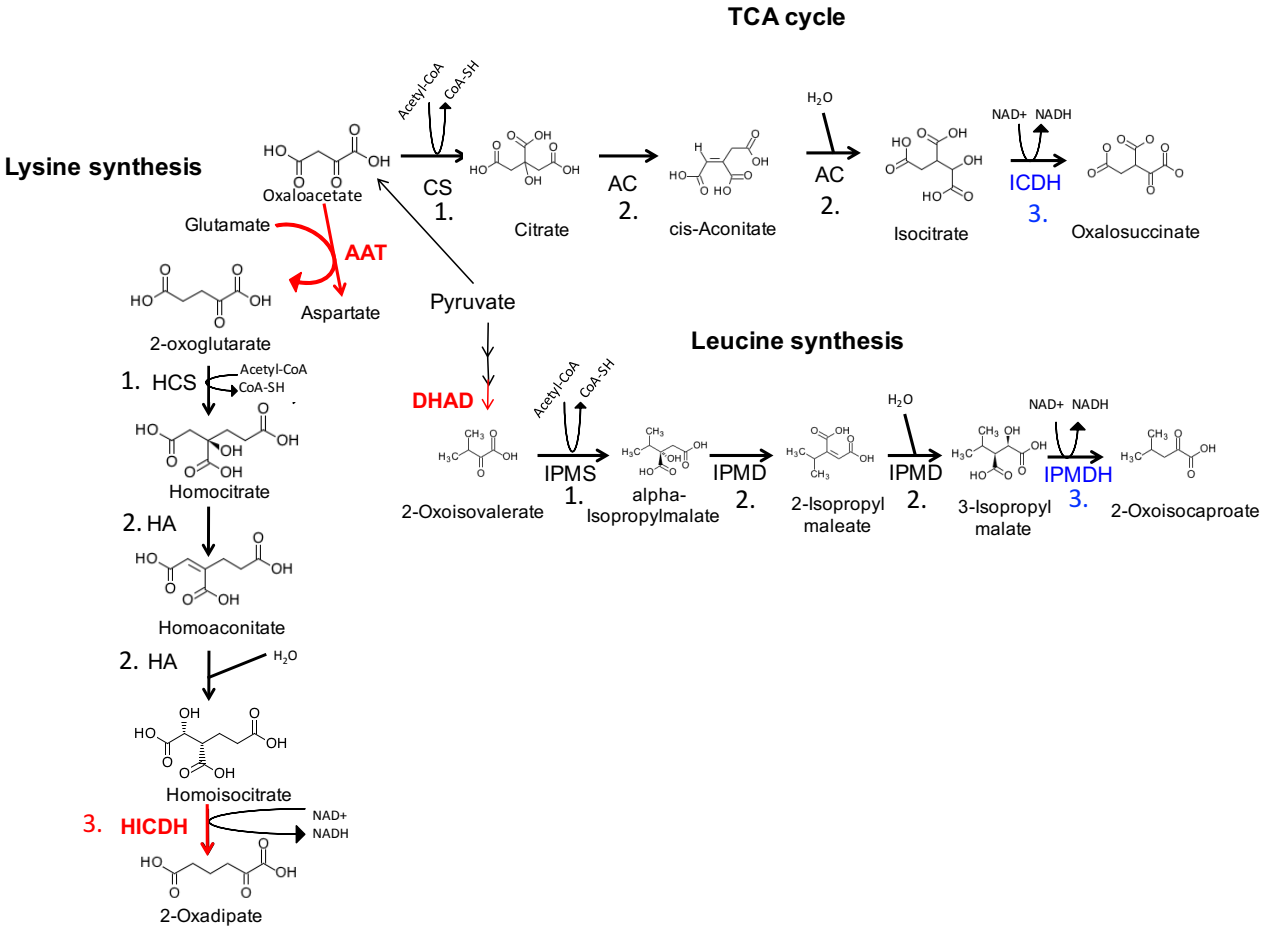

Figure 3.9. Parallel reaction mechanisms. Considering the types of reactions contributing to lysine, leucine and TCA cycle compound synthesis, an identical pattern can be seen. 'Reaction 1' is catalyzed by synthases: HCS (homoisocitrate synthase, EC:2.3.3.14), CS (citrate synthase, EC:2.3.3.1), IPMS (isopropyl-malate synthase, EC:2.3.3.13). There are two steps involving 'Reaction 2' which is performed by HA (homoaconitate hydratase; EC:4.2.1.36), AC (aconitate hydratase, EC:4.2.1.3), IMPD (isopropyl-malate dehydratase, EC:4.2.1.33). β-decarboxylating dehydrogenase family members catalyze homoisocitrate dehydrogenase (HICDH), isopropyl-malate dehdyrogenase (IPMDH, EC:1.1.1.85) and isocitrate dehdyrogenase (ICDH, EC:1.1.1.42). Information and chemical structures adapted from KEGG database (Kanehisa & Goto, 2000). GZE protein (aspartate aminotransferase (AAT), dihydroxy-acid dehydratase (DHAD) and Lys12 are marked in red. Paralogs to Lys12 are marked in blue. Tartrate dehydrogenase (TDH) is not included as it is not part of a biosynthetic pathway.

relationship. In addition, lysine biosynthetic (AAA pathway), part of the TCA cycle and leucine biosynthetic reaction evolved from one ancestral pathway. This

SPAC17G8.06c/ ilv3 (~64 kDa) is predicted to encode dihydroxy-acid dehydratase (DHAD) by homology (Velasco et al., 1993). It is involved in the dehydration reactions of dihydroxy-isovalerate and dihydroxy-3-methyl-butyrate giving 2-keto-isovalerate and 2-keto-3-methylbutyrate, respectively (DHAD, EC: 4.2.1.9). In fact, 2-keto-3-methylbutyrate is used as a precursor for valine and leucine, whereas 2-keto-isovalerate is the substrate for isoleucine synthesis (Kim and Lee, 2006).

Similar to homoisocitrate dehydrogenase Lys12 in lysine biosynthesis, the dihydroxy-acid dehydratase Ilv3 is part of a multi-step biosynthetic pathway generating the branched-chain amino acids (BCAAs): Leucine, isoleucine and valine (**Figure 3.10**.). Judging from protein levels at VE and G0 states (Marguerat et al., 2012), Ilv3 protein abundance is relatively unchanged at VE and G0 phase. Interestingly, the enzyme acetohydroxy-acid reductoisomerase SPBC56F2.12 (EC: 1.1.1.8) is highly abundant in the biosynthetic pathway during vegetative state. It catalyzes the step before dihydroxy-acid dehydratase SPAC17G8.06c/Ilv3. Again, fluctuation in protein levels among the individual enzymes of the BCAA biosynthetic pathway, may account for different outcomes after four-week-long N starvation. Same as for lysine biosynthetic enzymes, one cannot exclude the possibility that the deletion mutants of the other BCAA biosynthetic enzymes may start to show viability impairment beyond the four-week-long -N incubation.

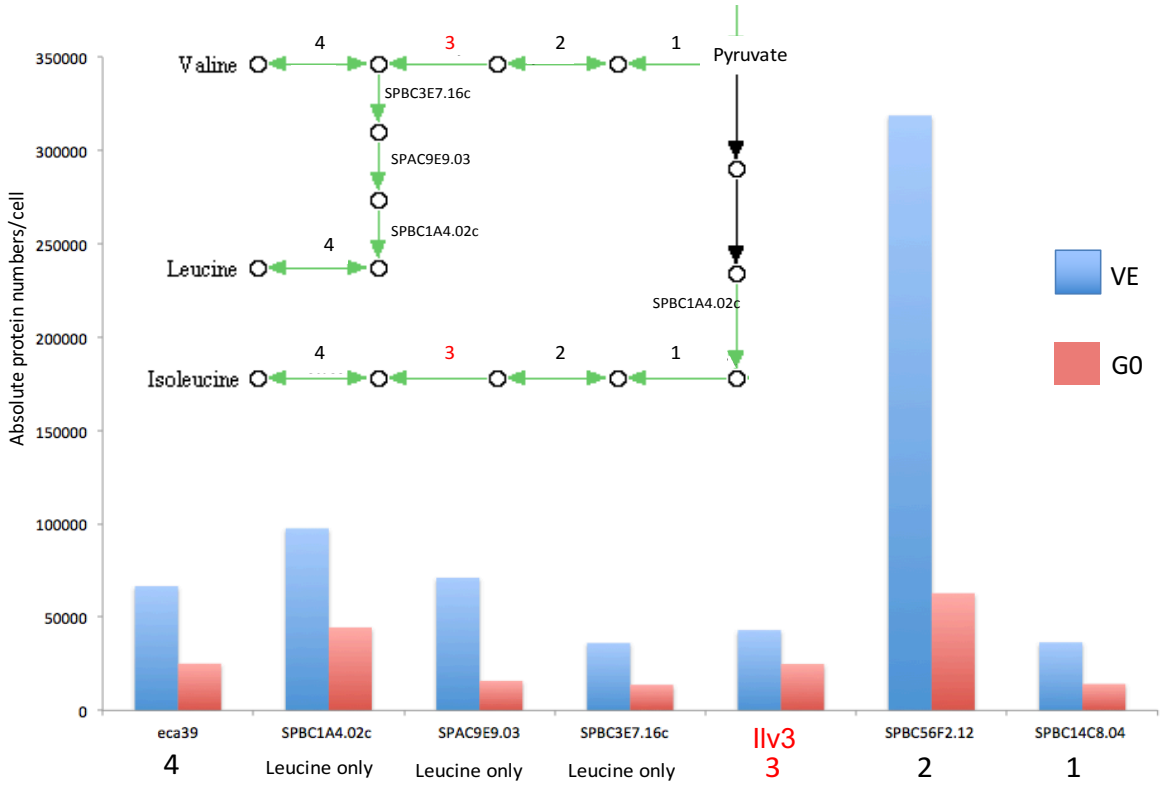

Figure 3.10. Branched-chain amino biosynthetic pathway. Overview in protein abundance of branched-chain amino acid biosynthetic proteins. The pathway is adapted from KEGG database (Kanehisa & Goto, 2000). Protein abundance per cell is inferred from Marguerat *et al*. 2012, which can be accessed via pombase.org database (Wood *et a*l., 2012). Dihydroxy-acid dehydratase is SPAC17G8.06c/Ilv3 marked in red font.

Homodimer formation is important for its catalytic activity (Flint et al., 1993). Amino acid alignments showed high conservation with *E. coli* DHAD (37 % ID) and *B. subtilis* DHAD (43% ID) (**Figure 3.11.**). However, besides two [4Fe-4S] binding sites, other functional sites have not been identified yet (**Figure 3.12.**). It seems that DHAD is a highly conserved protein. There are several overlapping amino acid residues which are still not characterized.

Phylogeny tree of Ilv3 homologs shows clear divergence from a common ancestor (**Figure 3.13**.) which support claim of Ilv3 homology to bacteria.

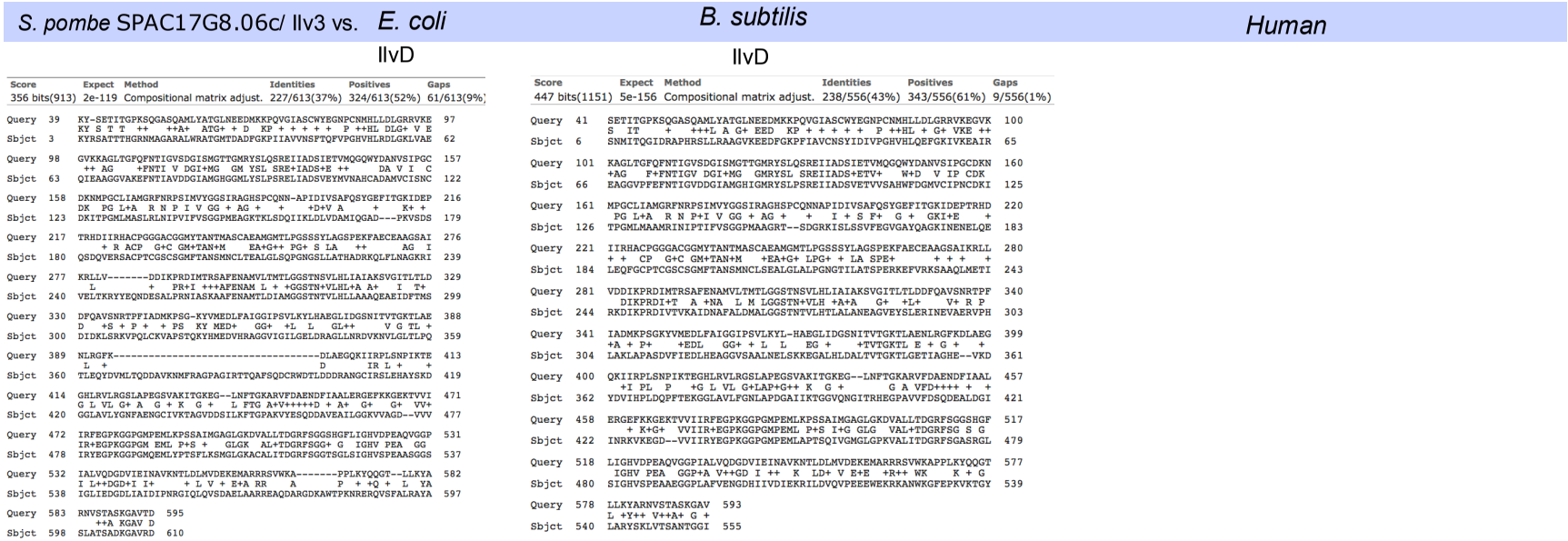

Figure 3.11. BLAST pairwise alignments against SPAC17G8.06c/ Ilv3. *S. pombe* sequences were separately run against *E. coli* and *B. subtilis*. No ortholog in human exists.

S. pombe	*E. coli*	E value	Identity (%)	Coverage (%)	Human	E value	Identity (%)	Coverage (%)	*B. subtilis*	E value	Identity (%)	Coverage (%)
IlvD	2.00E-119	37	93	NA	NA	NA	NA	NA	IlvD	5.00E-156	43	92

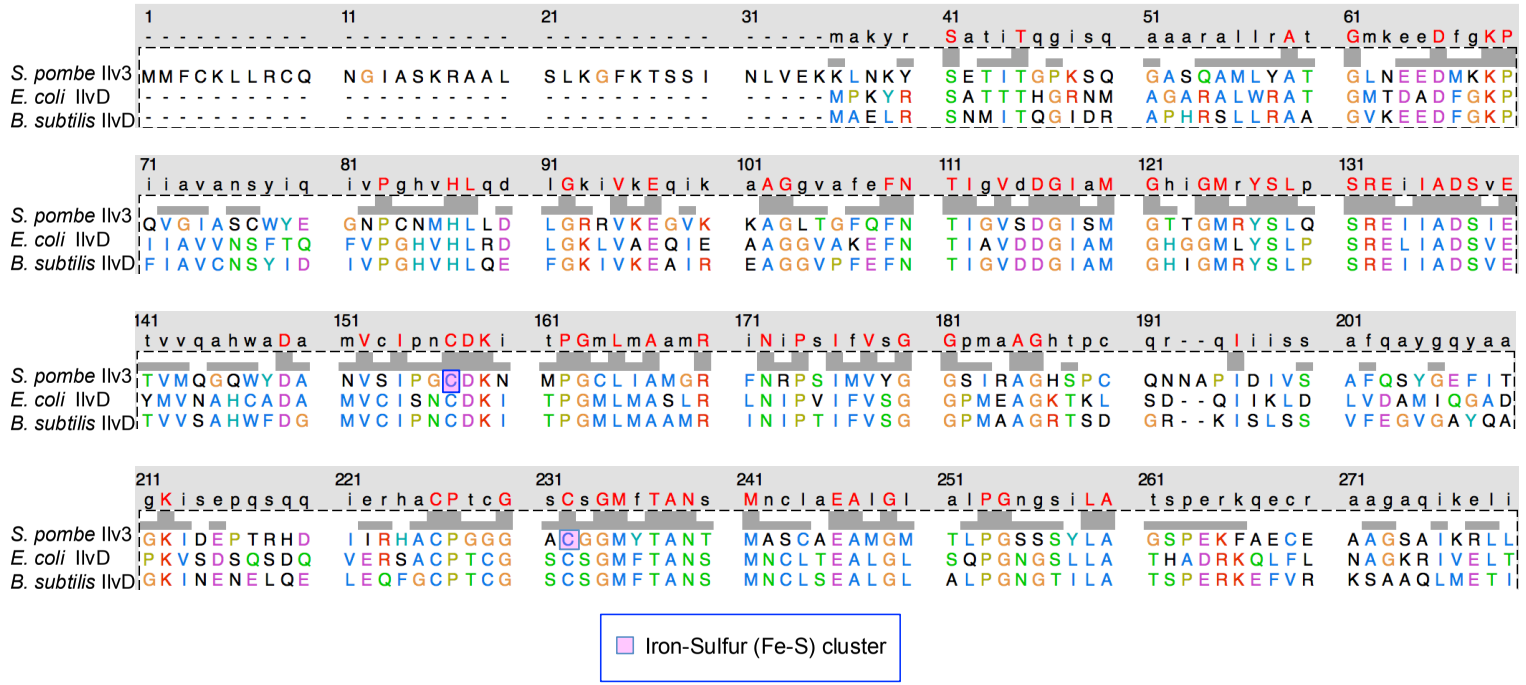

Figure 3.12. Alignment of *S. pombe* SPAC17G8.06c/ Ilv3 with its bacterial homologs. The two binding sites for construction of the 4Fe-4S clusters are overlapping. No crystal structures were resolved in any homolog. See next page for continuation of this alignment. especially in residues required for [4Fe-4S] cluster active sites (C157, C232; pink box) in which cysteine forms sulfide bridges

Figure 3.12. Alignment of *S. pombe* dihydroxy-acid dehydratase SPAC17G8.06c/ Ilv3 , *E. coli* and *B. subtilis* homologs (continued).Color scheme is based on ClustalX default setting which differentiates between residue type and frequency of occurence in the same column (consensus residue).

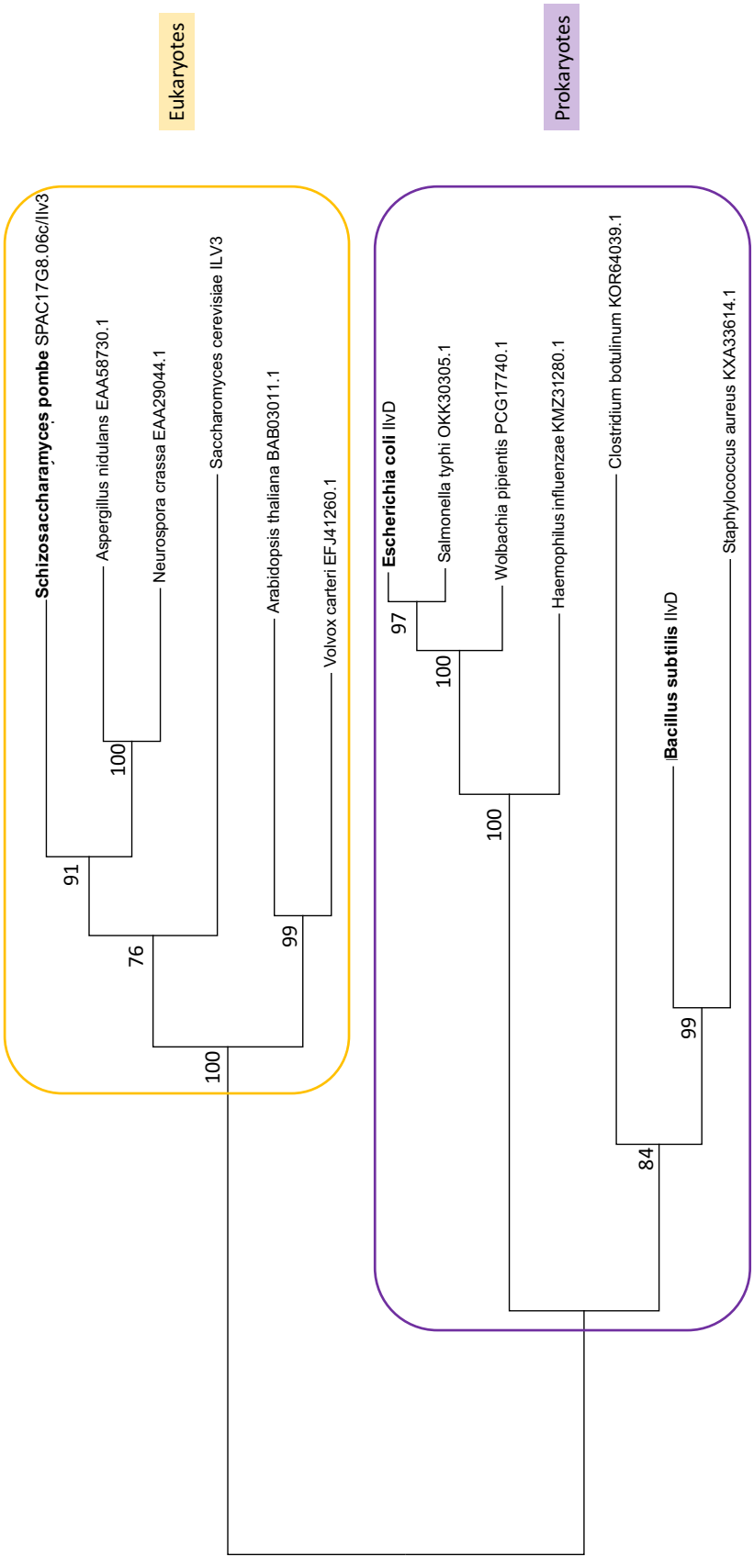

Figure 3.13. DHADH phylogeny reconstruction. Maximum likelihood phylogeny tree was computed with MEGA6. Node reliability is expressed with confidence percentage from 1,000 bootstrap repetitions. Based on node distribution eukaryotic (yellow) and prokaryotic (purple) dihydroxy-acid dehydratases can be differentiated. Node reliability is considered significant when confidence intervals are higher than 50%.

3.4.2. Carbon-nitrogen metabolism associated GZE enzymes- Gdh1 and Maa1

Besides the two above-mentioned enzymes Lys12 and Ilv3, situated in multi-step pathways, glutamate dehydrogenase Gdh1 and aspartate aminotransferase Maa1, generate amino acids in single reactions. Their products serve as precursors for other important nitrogen containing compounds. Gdh1 and Maa1 are associated with substrates from TCA cycle (**Figure 3.14.)**. While glycolytic enzyme levels are uniformly decreased upon G0, TCA cycle enzyme levels seem stable at G0 phase (Marguerat et al., 2012). Nevertheless, some fluctuation in relative changes can be seen among the TCA enzymes. It seems that levels of certain enzymes within the TCA cycle are increased, whereas others decrease upon G0 phase. This regulation of TCA cycle enzyme levels may modulate the flux through the cycle making the cycle responsive to conditions such as N starvation. For example, isocitrate dehydrogenase Idp1 levels seems to be decreased, but the isocitrate dehydrogenases Idh1 and Idh2 increase under G0 state. Although they catalyze similar reactions and produce 2-oxoglutarate (2-OG) both enzymatic reactions seem to be differentially regulated upon N starvation. The major difference is that Idp1 binds NADP+ (EC:1.1.1.42), whereas Idh1/2 bind NAD+ (EC:1.1.1.41). Depending on the protein abundance either NADP+ or NAD+ cofactor is used which alters the ratio in response to conditions. Gdh1 and Maa1 (blue arrow) are located at the periphery of the TCA cycle and use TCA cycle compounds as substrates. It is therefore likely that substrate availability through TCA cycle reactions, may modulate Gdh1 and Maa1 activity. But how do these two amino acid biosynthetic enzymes contribute to N starvation survival? A closer look on their degree of conservation may provide some hint for their contribution to an ancient N starvation mechanism.

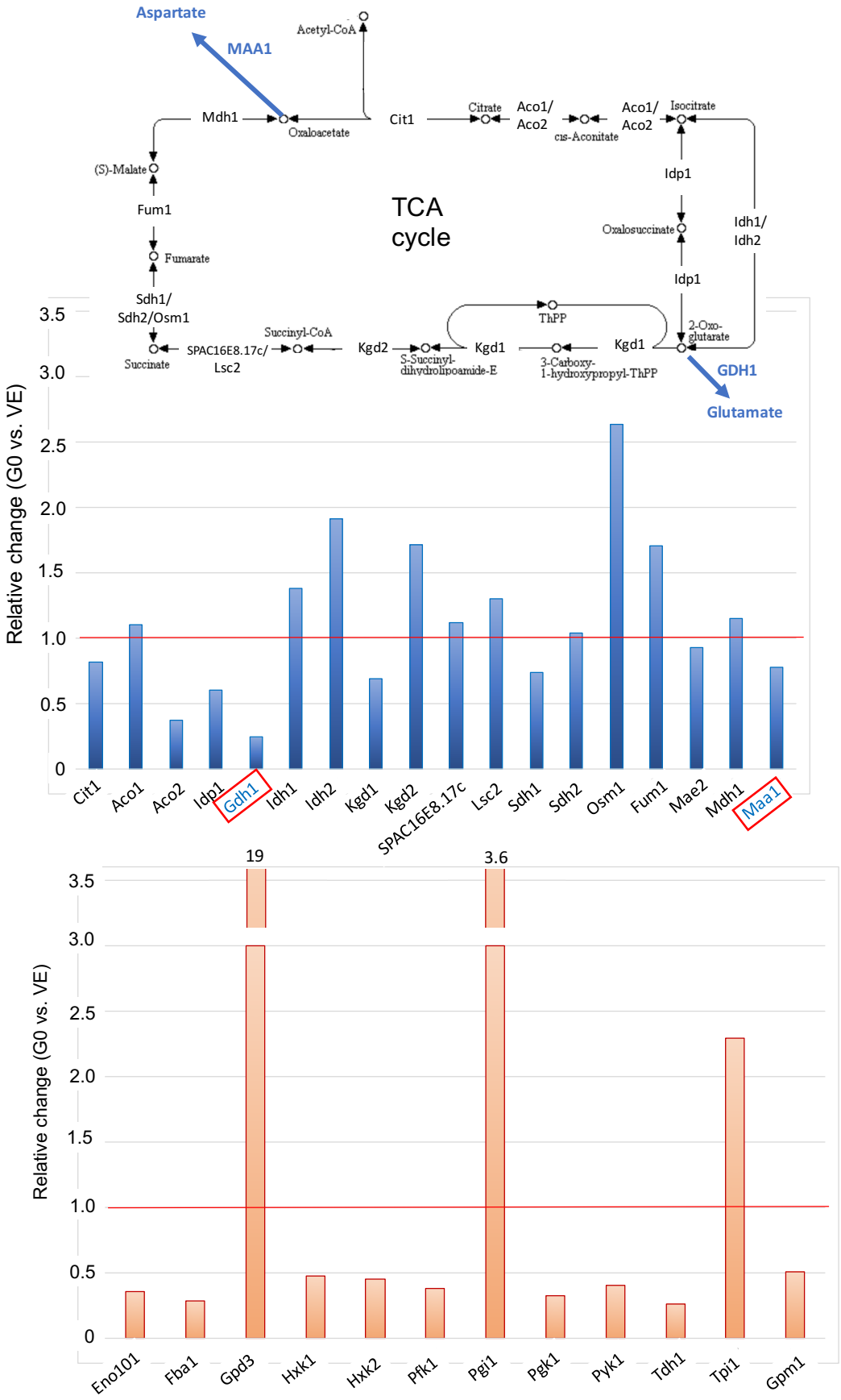

Figure 3.14. Relative protein level change of TCA cycle proteins. The overview of TCA cycle enzymes was adapted from KEGG database (Kanehisa & Goto, 2000). GZE

proteins glutamate dehydrogenase GDH1 and aspartate aminotransferase MAA1 are depicted in the figure (blue font). Protein abundance data for TCA cycle and glycolytic enzymes were inferred from Marguerat *et al*., 2012 accessed via pombase.org (Wood *et al*., 2012). Relative change of glycolytic enzymes serves as reference for sudden decrease upon G0 entry. Red line indicates relative change of 1 which signifies same protein levels in both G0 and VE states.

Gdh1 (~49 kDa) is predicted by homology to encode the mitochondrial $NADP^+$-dependent glutamate dehydrogenase (Gdh1) in *S. pombe* (DeLuna et al., 2001). Generally, NADP-GDH enzyme promotes the reversible reductive amination of 2-oxoglutarate (2-OG) and ammonia to glutamate (NADP-GDH, EC: 1.4.1.4). GDH is an essential enzyme contributing to the TCA cycle, ammonia assimilation/detoxification and energy metabolism (Lee et al., 2012). Gdh1 is localized to the cytoplasm, nucleus, as well as mitochondria (Hayashi et al., 2009) but it is still unclear at what conditions Gdh1 translocates within the cell compartments. Besides Gdh1, another GDH isoform SPCC132.04c, was reported to exist. In fact, *S. pombe* SPCC132.04c is a cytoplasmic NAD+ binding enzyme involved in the reverse reaction converting glutamate to 2-OG and ammonia (EC: 1.4.1.2) (Miller and Magasanik (1991). Therefore, it is of interest that only Gdh1 was observed to be essential for G0 survival. The bacterial homology candidates to Gdh1 are $NADP^+$-dependent glutamate dehydrogenase GdhA (50% ID) in *E. coli* and catabolic NAD-specific glutamate dehydrogenase RocG (33% ID) in *B. subtilis* (**Figure 3.15.)**. Conserved sites derived from 3SBO crystal structure (Totir et al., 2012) and additional information is used from (Sharkey et al., 2013) (**Figure 3.16.)**.

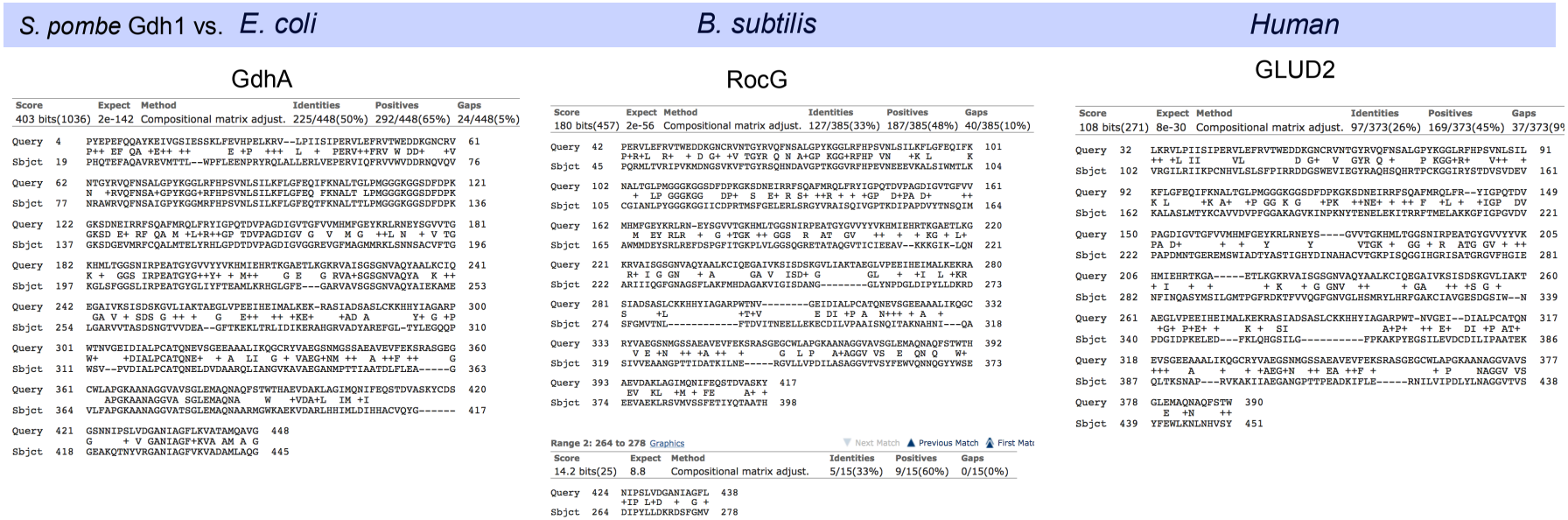

Figure 3.15. Pairwise alignments against Gdh1. *S. pombe*sequences were separately run against *E. coli*, *B. subtilis* and human databases.

S. pombe	*E. coli*	E value	Identity (%)	Coverage (%)	Human	E value	Identity (%)	Coverage (%)	*B. subtilis*	E value	Identity (%)	Coverage (%)
Gdh1	GdhA	2.00E-142	50	98	GLUD2	8.00E-30	25	79	RocG	1.00E-56	33	86

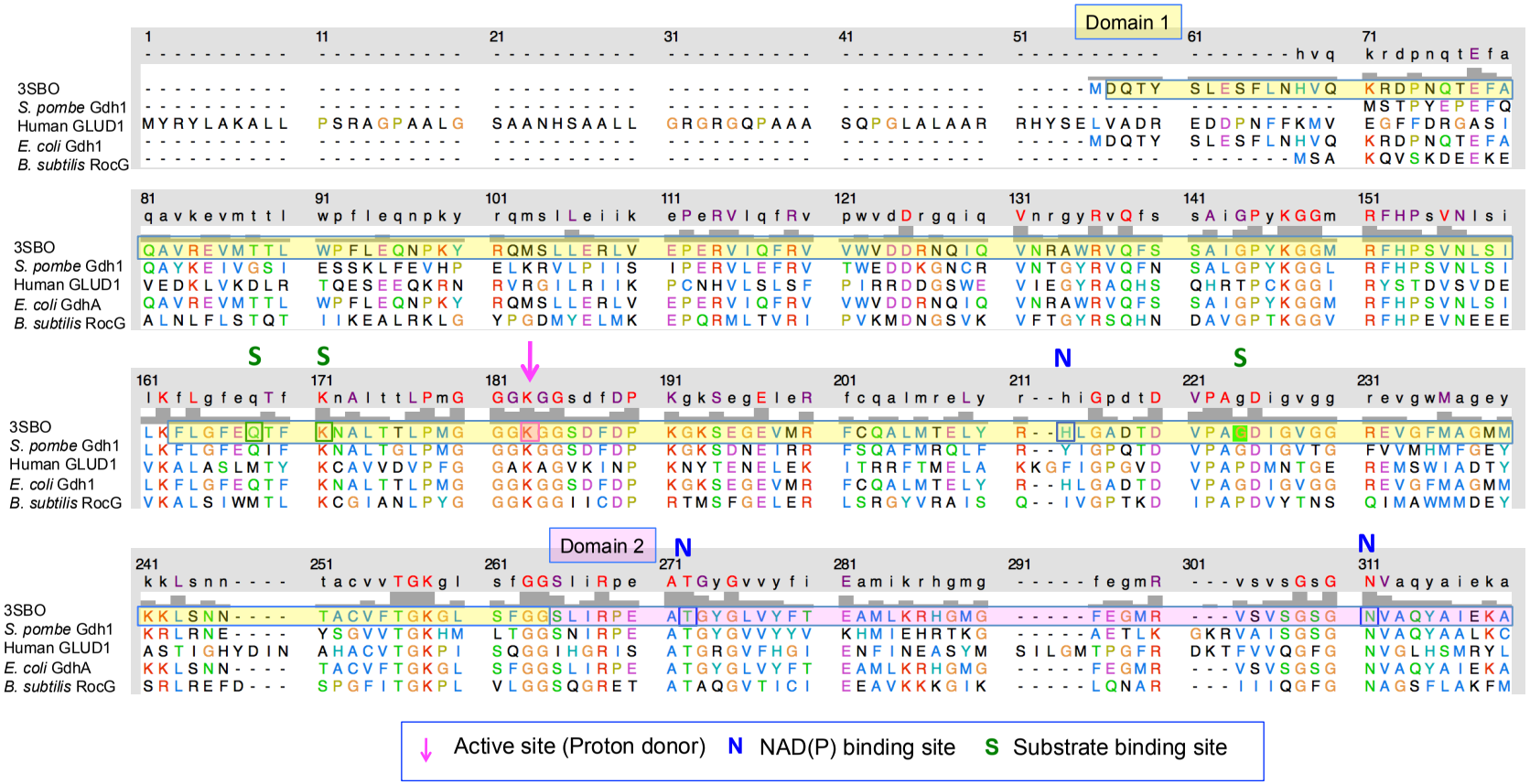

Figure 3.16. Alignment of *S. pombe* Gdh1 with its bacterial homologs. *E. coli* GdhA crystal structure 3SBO (Totir et al., 2012) is used as a reference. Domain info information is inferred from Sharkey *et al*. It is striking that many functional sites, including one proton donor (K183; red arrow), two substrate binding sites (K168, K171, G224; green S) and two NAD(P) binding sites (H214, T272, N311; blue N) are identical in all three organisms (Sharkey et al., 2013). See the next page for continuation of the alignment.

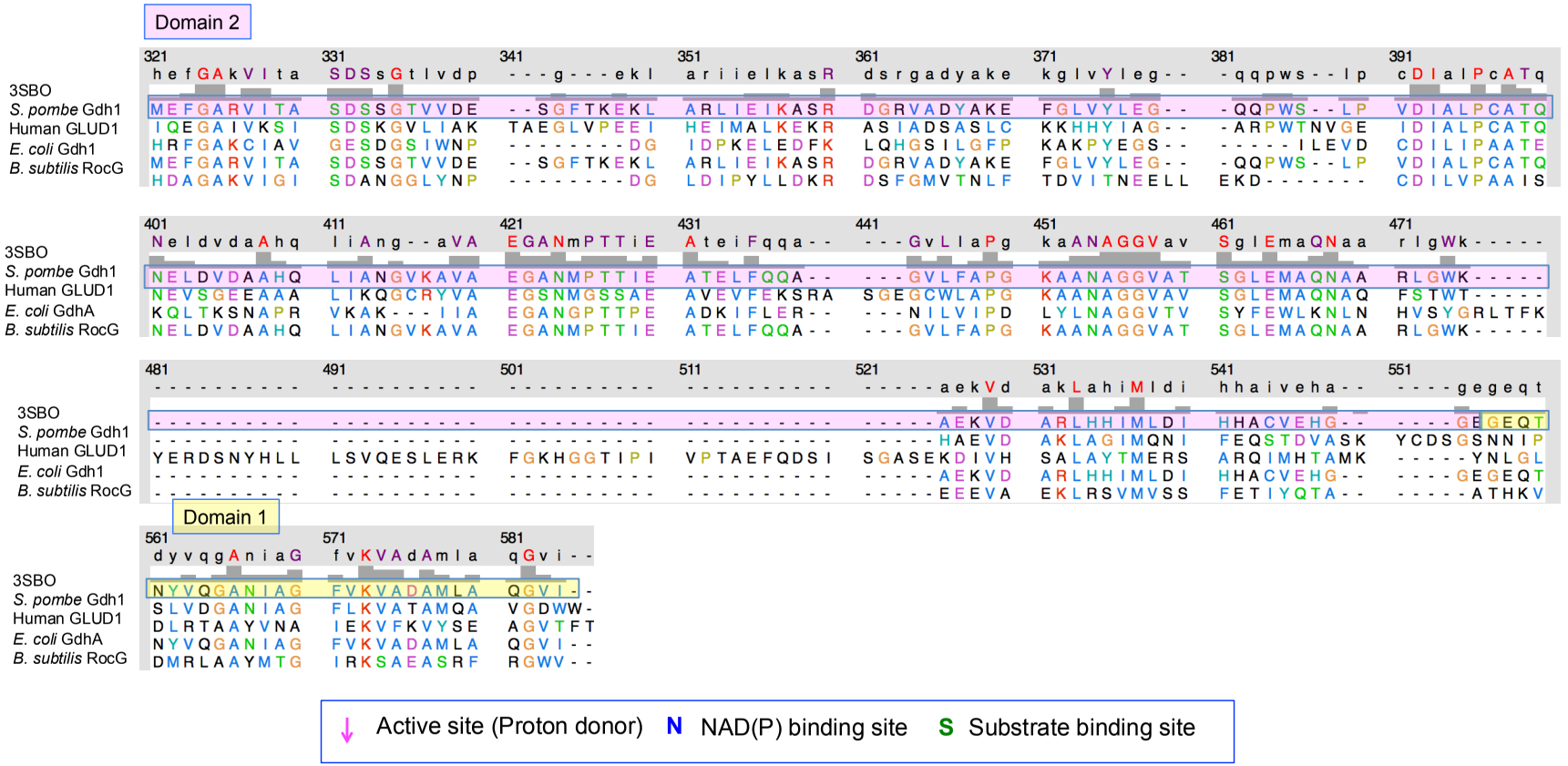

Figure 3.16. Alignment of *S. pombe* glutamate dehydrogenase Gdh1 (continued). *E. coli* GdhA crystal structure 3SBO (Totir et al., 2012).Color scheme is based on ClustalX default setting which differentiates between residue type and frequency of occurence in the same column (consensus residue).

In general aspartate aminotransferase uses oxoglutarate and glutamate as substrates for aspartate synthesis. Therefore, Gdh1 and Maa1 are linked to each other by the compounds oxoglutarate and glutamate.

The *S. pombe* aspartate amino transferase **Maa1** (~43 kDa) which transfers amine groups from L-aspartate to 2-oxoglutarate (AAT, EC 2.6.1.1). According to BLAST sequence comparison results, *E. coli* aspartate aminotransferase AspC (42% ID) displays higher homology to *S. pombe* Maa1 than *B. subtilis* YhdR (25% ID) (**Figure 3.17**.). In addition, high conservation at functional sites between *E. coli* and *S. pombe* AATs can be seen in **Figure 3.18** derived from crystal structure from 5EAA from (Jeffery et al., 2000). Also information from (Leistler et al., 1992) is used.

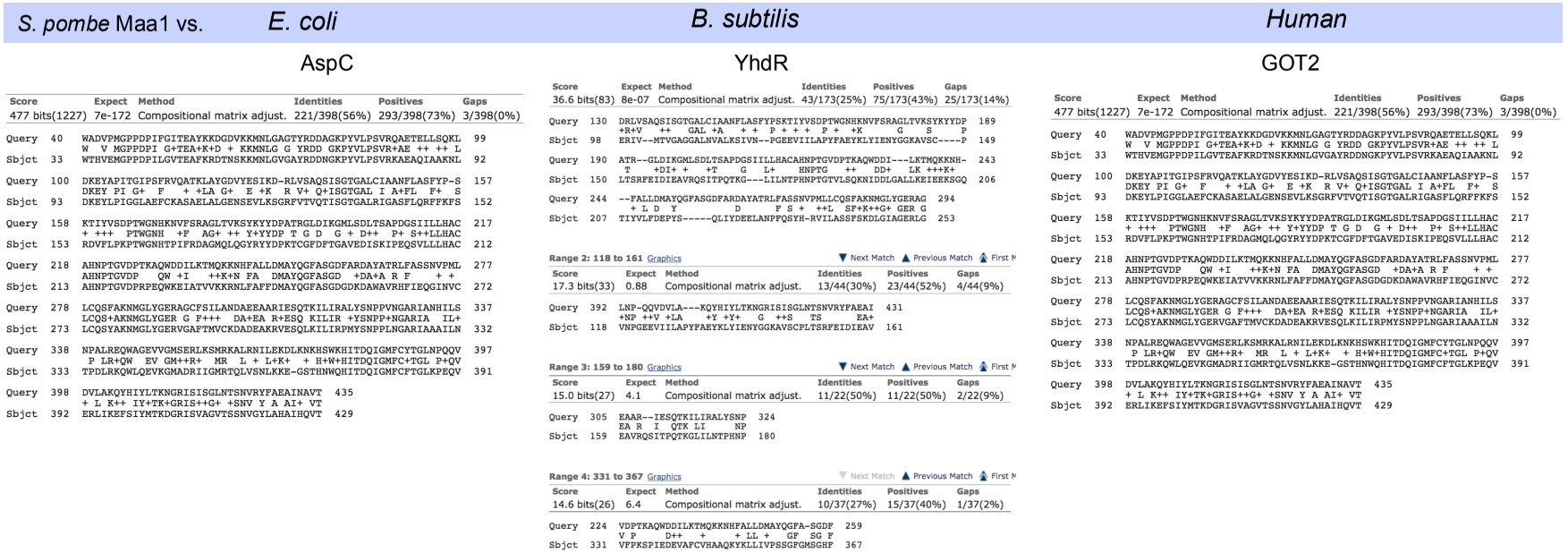

Figure 3.17. BLAST pairwise alignments against Maa1. *S. pombe* sequences were separately run against *E. coli*, *B. subtilis* and human databases.

S. pombe	*E. coli*	E value	Identity (%)	Coverage (%)	Human	E value	Identity (%)	Coverage (%)	*B. subtilis*	E value	Identity (%)	Coverage (%)
Maa1	AspC	7.00E-109	42	90	GOT2	7.00E-172	56	90	YhdR	8.00E-07	25	51

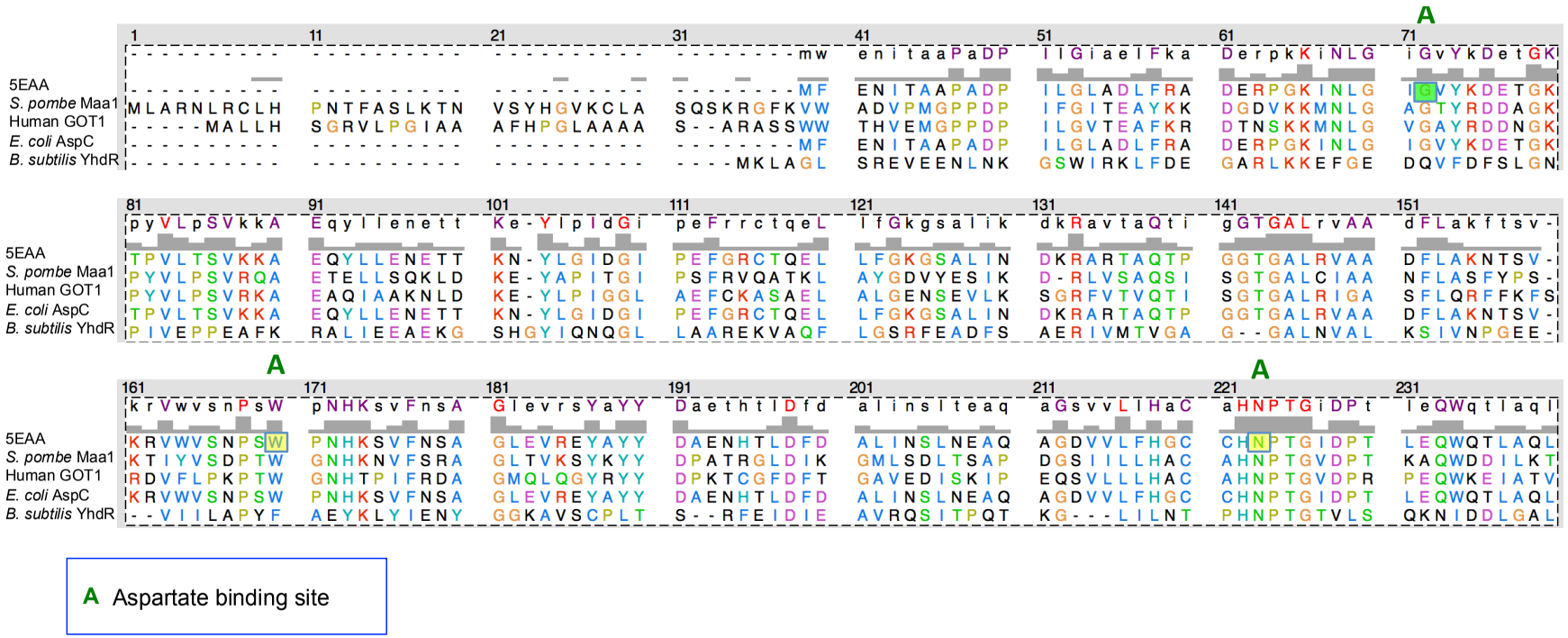

Figure 3.18. Alignment of Maa1 with its homologs. Functional information obtained from *E. coli AspC* crystal structure 5EAA (Jeffery et al., 1998). See the next page for continuation of alignment. In fact, aspartate-binding sites (G72, W167, N220) are conserved (red box, green arrow). High number of active sites (Y103, D248, Y251, K284, R318, Y407) (yellow arrow) from *E. coli* AspC is conserved in *S. pombe*. The catalytic site, being essential for covalent binding to the coenzyme PLP (Leistler et al., 1992).

Figure 3.18. Alignment of Maa1 with its bacterial homologs (continued).Color scheme is based on ClustalX default setting which differentiates between residue type and frequency of occurence in the same column (consensus residue).

3.4.2.1. Investigating sequence ID variation in selected GZE homologs

As previously mentioned, *B. subtilis* RocG shows less identity to *S. pombe* Gdh1, than compared with the alignment *S. pombe* Gdh1- *E. coli* GdhA. Due to the big difference in sequence identities, sequence alignments will be separately looked at. In fact, functionally *B. subtilis* RocG differs greatly from *E. coli* and *S. pombe* homology candidates. RocG is regulated by arginine and catalyzes glutamate degradation only. *S. pombe* Gdh1and *E. coli* GdhA, on the other hand, are regulated by 2-OG levels and catalyze glutamate biosynthesis (Chubukov and Sauer, 2014).

Despite all eight GZE proteins are conserved, sequence identity was highly variable among *E. coli*, *S. pombe* towards *B. subtilis*. In fact, around 17 per cent points difference was seen in BLASTp alignments of *S. pombe* glutamate dehydrogenase Gdh1 versus *E. coli* GdhA (50% ID) and versus *B. subtilis* RocG (33% ID). The same goes for aspartate aminotransferase Maa1 versus *E. coli* AspC (42 % ID) compared to Maa1 versus *B. subtilis* YhdR (25% ID) (**Table 3.3.**). Moreover, difference of 12 per cent points were seen in alignments between ubiquinone methyltransferase Coq5 versus *E. coli* Coq5 (45% ID) and Coq5 versus *B. subtilis* MenG (33% ID) which will be investigated further in section 3.4.2.1. on page 65. In fact, alignments to SodA from *B. subtilis* yield a slightly higher sequence identity value than observed in the alignment to *E. coli* SodA. However, in this case both bacterial Sod2 homologs align to *S. pombe* with a sequence ID of more than 35% which is still considered reasonably high. Therefore, the question is why does such a high variability among homologs exist in these three GZE proteins? Also, do the sequence changes correspond to different function of the bacterial protein? As previously mentioned gram-positive *E. coli* and gram-negative *B. subtilis* can be distinguished

based on call wall morphology. Based on presence of an outer membrane, masking the peptidoglycan layer, or a thicker peptidoglycan layer without any outer membrane Therefore, their cell wall morphologies can be visualized and distinguished with the gram stain which cannot pass through the outer membrane in *E. coli* to stain the peptidoglycan layer. On the other hand, *B. subtilis* lacks an outer membrane causing the gram agent to stick to the peptidoglycan layer. Apart from the differences in cell wall morphologies, *E. coli* and *B. subtilis* employ different starvation response modes being either a quiescent state or forming endospores (Tocheva et al., 2016). In fact, *E. coli* transits into a resting phase upon starvation just like *S. pombe*, whereas *B. subtilis* differentiates into dormant spores with low metabolic activity (Chubukov and Sauer, 2014).

The question therefore is whether the sequence changes in the aspartate aminotransferase homologs from *E. coli* and *S. pombe* arose due to adaptations to quiescence survival, whereas the homolog found in *B. subtilis* is functional for endospore formation? To make a better judgment about this possibility more sequences need to be compared from a more diverse range of organisms which will be discussed in the next section.

Is degree of conservation in GZE proteins linked to prokaryotic starvation mode?

It would be reasonable to assume that these features may be behind the sequence variability observed in both bacterial species. However, in order to rule out any other factor behind the differences, proteins sequences of a defined set of selected eukaryotic homologs were used. Bacterial species which can or cannot form spores were selected.

Bacterial species preferentially from diverse clades were selected. It seems that endospore forming bacteria are predominantly gram-positive but there are also exospore forming species such as *Streptomyces coelicolor.* Exospores are formed outside the bacterial cell in contrast to endospores (Chandra and Chater, 2014). Nevertheless, just a few gram-negative bacteria are able to form endospores. *Myxococcus xanthus* was selected as an example for gram-negative endospore forming example. The other gram-negative bacterium is the cyanobacterial species *Anabaena cylindrica*, which was reported to differentiate spore-like cells called akinetes. These four were taken as examples because sufficient data exists about their cellular states in responses to starvation (Claessen et al., 2014). Bacterial endospores should not be compared with fungal spores. In fact, fungal spore formation is considered as a different process since it is part of the vegetative life cycle rather than a survival response as seen in bacteria. In contrast, bacterial spore formation does not require mating since it is asexual (Black, 2011). Considering *S. pombe,* it is able to form spores when both mating types are present. However, in absence of mating, *S. pombe* transfers into quiescence state. Consequently, this study focused on condition in *S. pombe* which lead to quiescence induced upon N starvation(Yanagida, 2009).

For this approach phylogeny trees generated by MEGA6 proved great help in categorizing the respective protein sequences. It is essential to stress that phylogeny, or evolutionary distance, is not investigated, rather the degree of sequence identity variation among the selected organisms. For the investigation 26 organisms are used (**Table 3.4.**) and information about their energy metabolism, cell wall physiology (gram stain), and habitat is used as reference to interpret a potential functional reason for sequence variance among the phylogenic groupings.

Table 3.4. Variable degree of conservation among GZE proteins. A higher portion of *S. pombe* alignments to *E. coli* have a higher sequence identity than alignments to *B. subtilis* proteins. Especially, alignments to mitochondria-located GZ2E proteins (green font) allocate on top. As a matter of fact, Maa1, Gdh1 and Coq5 show variable degrees of conservation to the two bacterial species. In fact, alignments to *E. coli* rank high (sequence ID value >40%) and low (sequence ID <35%) when aligned to *B. subtilis*. Homologs to Mhf1 are not displayed since *E. coli* and *B. subtilis* homology candidates seem to be involved in different.

E. coli	*B. subtilis*
High>40%	
Glutamate dehydrogenase Gdh1	Superoxide dismutase Sod2
C-methyltransferase Coq5	Dihydroxy-acid dehydratase Ilv3
Superoxide dismutase Sod2	
Aspartate aminotransferase Maa1	
Medium35-40%	
Dihydroxy-acid dehydratase Ilv3	
Homoisocitrate dehydrogenase Lys12	
Low<35%	
DNA helicase Fft3	Homoisocitrate dehydrogenase Lys12
Protein chaperone Ssz1	Glutamate dehydrogenase Gdh1
Abc1-like kinase SPBC21C3.03	C-methyltransferase Coq5
NADH dehydrogenase Nde1	DNA helicase Fft3
Methyl-THF-reductase Mtd1	NADH dehydrogenase Nde1
Ornithine decarboxylase Spe1	Protein chaperone Ssz1
Vitamin H transporter Vht1	Methyl-THF-reductase Mtd1
60S ribosomal protein L10	Aspartate aminotransferase Maa1
	Ornithine decarboxylase Spe1
	Abc1-like kinase SPBC21C3.03
	Vitamin H transporter Vht1
	60S ribosomal protein L10

Table 3.5. Overview of the organisms used for phylogeny study. Twenty-six species are listed together with information about their cell wall physiology, categorized by the gram stain results being either positive (red) or negative (blue), energy metabolism, habitat and starvation response. *Fungi produce spores after sexual mating which is different from bacterial spores.

Organism	Phylogeny	Energy metabolism	Habitat	Starvation mode	References
Streptococcus pneumoniae	Bacteria	Facultative anaerobic	Human	Non-spore	Patterson, 1996
Corynebacterium glutamicum	Bacteria	Facultative anearobic	Soil	Non-spore	Matsushita, 2013
Staphylococcus aureus	Bacteria	Facultative anearobic	Human	Non-spore	Foster, 1996
Mycobacterium tuberculosis	Bacteria	Obligate aerobic	Human	Spore-like	McMurray, 1996
Streptomyces coelicolor	Bacteria	Obligate aerobic	Soil, aqueous environment	Spore	Chater, 1992
Clostridium botulinum	Bacteria	Obligate anaerobic	Soil, aquaoues environments	Spore	Wells & Willkins, 1996
Bacillus subtilis	Bacteria	Facultative anaerobic	Soil, environment	Spore	Turnbull, 1996
Myxococcus xanthus	Bacteria	Obligate aerobic	Soil	Spore	McCleary *et al.*, 1991
Shewanella putrefaciens	Bacteria	Facultative anaerobic	Fish, marine environemnts	Non-spore	Masataka, 2014
Pseudomonas aeruginosa	Bacteria	Facultative anaerobic	Soil, water, vegetation, animals	Non-spore	Iglewski, 1996
Salmonella typhi	Bacteria	Facultative anaerobic	Human	Non-spore	Giannella, 1996
Haemophilus influenzae	Bacteria	Facultative anaerobic	Human	Non-spore	Musher, 1996
Providencia stuartii	Bacteria	Facultative anaerobic	Soil, water sewage	Non-spore	Manos & Belas, 2006
Thermus thermophilus	Bacteria	Obligate aerobic	Thermal springs	Non-spore	Ohtani *et al*., 2010
Rickettsia prowazekii	Bacteria	Obligate aerobic	Obligate intracellular	Non-spore	Walker, 1996
Escherichia coli	Bacteria	Facultative anaerobic	Human (commensal)	Non-spore	Guentzel, 1996
Synechocystis sp.	Cyanobacterium	Photosynthetic	Fresh water	Non-spore	Kaneko *et al*., 1996
Anabaena cylindrica	Cyanobacterium	Photosynthetic	Fresh water	Spore	Simon, 1977
Haloferax mediterranei	Archaea	Facultative anaerobic	Hypersaline, aquaeous environm	Non-spore	Oren, 2002
Chlorella variabillis	Eukarya	Photosynthetic	Marine environment	Non-spore	Blanc *et al*., 2010
Arabidopsis thaliana	Eukarya	Photosynthetic	Land	Non-spore	Hamburger & Kramhoft, 1982
Human	Eukarya	Obligate aerobic	Land	Non-spore	Olszewski & Llinas, 2011
Plasmodium falciparum	Eukarya	Facultative anaerobic	Obligate intracellular	Non-spore	Garder *et al*.,2002
Neurospora crassa	Eukarya	Obligate aerobic	Land	Spore*	Nargang & Rapaport, 2007; Schmit & Brody, 1976
Aspergillus nidulans	Eukarya	Obligate aerobic	Land	Spore*	Willger *et al*.,2009
Schizosaccharomyces pombe	Eukarya	Facultative aerobic	Land	Quiescent/spore*	Hamburger & Kramhoft, 1982

*Spores are formed after sexual mating, part of fungal life cycle

Glutamate dehydrogenase isoforms linked to cofactor specificity

A phylogenic tree for glutamate dehydrogenases from 26 different species was computed using the MEGA6 tool (Tamura et al., 2013). Branch topology rather than evolutionary distance will provide some hint to the above-mentioned questions of factors influencing the variance in the respective enzymes. The original phylogeny results with information on branch lengths are available in **Figure S1.** According to the condensed (bootstrap confidence 50% or more) phylogenic tree for glutamate dehydrogenases (GDH) in Figure **3.19.,** bacterial GDHs allocate into two main nodes A and B. Node A consists of large bacterial GDH isoforms which bind NAD+. One of these, *Rickettsia prowazekii*, is considered an intracellular obligate which means that it cannot survive without a host animal. It is likely that *R. prowazekii* GDH is essential for catabolizing glutamate which originates from the host (Walker, 1996). GDHs in node B diverge into subnodes which may be based on the cofactor specifcity. This finding is in accordance to previous reports about different types of GDH proteins based on the preference to bind either NAD+, NADP+ and both (Sharkey and Engel, 2008). Cofactor specificity influences the direction of glutamate metabolism being either catabolic (NAD+) or synthetic (NADP+). Node B3 consists of NADP+-binding GDH isoforms which are prokaryotic and eukaryotic. NADP+ binding enzymes, like *S. pombe* Gdh1 and *E. coli* GdhA promote glutamate synthesis from ammonium and are therefore part of the ammonium assimilation pathway (Kumar and Shimizu, 2010). Node B2 contains bacterial GDH isoforms which mostly bind NAD+ and catabolize glutamate. Node B2 also contains eukaryotic GDH isoforms, which are able to bind both NADP+ and NAD+, and therefore have dual specificity (Minambres, 2000). Node B3 consists of fungal NAD+ binding GDH isoforms which are involved in glutamate c

catabolism because exclusively NAD+-binding GDH enzymes catalyze glutamate catabolic reactions (Halsey et al., 2017).

In summary, variances in sequence identity values among the GDH isoforms can be explained by a different cofactor binding preference. The identity variance between the *E. coli* and *B. subtilis* alignments is likely based on NADP+ binding GdhA in *E. coli* and NAD+ binding RocG in *B. subtilis* which have different effect on glutamate metabolism. NAD+ binding GDHs are known to catalyze the glutamate catabolic reaction, whereas NADP+ specific GDHs synthesize glutamate (Miller and Magasanik (1991).

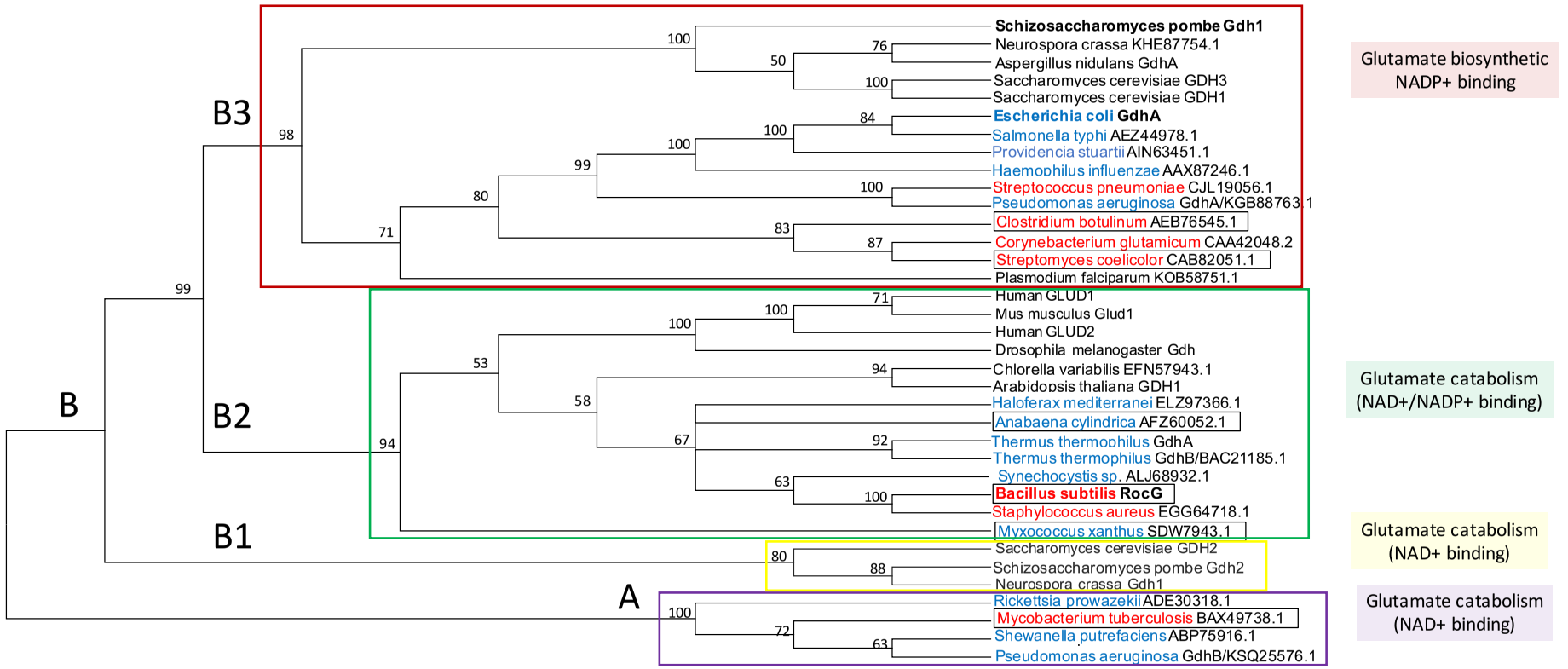

Figure 3.19. Branch topology of Gdh1 and homologs. Maximum likelihood with 1000 bootstrap repetions was computed using MEGA6 tool. Confidence intervals above 50% are shown. Four nodules are seen. Gdh1 homologs seem to localize into nodules based on their functions being either glutamate catabolic (red box) or synthetic (orange and green boxes). Gram-negative bacteria are colored in blue font, whereas gram-positive are in red font. The official protein names are used if available, otherwise GenBank® namings are used (sequences accessible at https://www.ncbi.nlm.nih.gov/genbank). Proteins from spore-forming bacteria are put into black brackets. Information on cofactor specificity is inferred from GeneBank database.

High variability of identity among aspartate aminotransferases

A phylogenic tree for aspartate aminotransferases from 26 different species was generated with Maximum likelihood, with 1,000 bootstrap repetitions, was computed using MEGA6 tool (Tamura et al., 2013). Since branch topology rather than evolutionary distance will give a clear answer to the above-mentioned questions of factors influencing the variance in the respective enzymes, a condensed tree is generated by setting the confidence interval to 50% and more. Consequently, non-significant nodes are not included and evolutionary distance cannot be inferred. The original phylogeny results with information on branch lengths are available in **Figure S2**.

Some organisms, predominantly gram-positive bacteria such as *B. subtilis* (Turnbull, 1996) and *C. botulinum* (Wells & Willkins, 1996*)*, contain more than one aspartate aminotransferase (AAT) proteins. Nevertheless, for are whole picture of AAT characteristics these AAT sequences are included. Considering the eukaryotic organisms, which contain multiple AAT isoforms in different cellular compartments, only the mitochondrial aspartate aminotransferase orthologs were included in the alignment. In the phylogeny tree, AAT proteins diverge into two branched (**Figure 3.20.**). One of which consists of gram-negative, non-sporulation bacteria which are considered as human pathogens such as *Salmonella typhirium* (Giannella, 1996), *Haemophilus influenzae* (Musher, 1996) and other bacterial species which were found in animals *Pseudomonas aeruginosa* (Iglewski, 1996) and *Shewanella putrifaciens* (Masataka, 2014). Allocation of AAT from the gram-positive *S. pneumoniae* (Patterson, 1996) into branch A is an exception since most of the gram-positive bacteria from this study appear in the more distant branch (B). Also, eukaryotic AATs from

human, *Plasmodium falciparum* (Gardner et al., 2002, Olszewski and Llinas, 2011), *Arabidopsis thaliana* (Hamburger, 1982) and the fungal species *Neurospora crassa* (Nargang and Rapaport, 2007), *Aspergillus nidulans* (Willger et al., 2009). Branch B seems to be more diverse comprising AATs from cyanobacteria, archaea and both sporulating and non-sporulating bacterial species. It is however striking that all AATs from the sporulating bacteria *B. subtilis*, *Streptomyces coelicolor* (Chater, 1992) and *Clostridium botulinum* (Wells, 1996), including gram-negative species *Anabaena cylindrica* (Simon, 1977) and *Myxococcus xanthus* (McCleary et al., 1991), are found in branch B. It was reported that *M. xanthus* has an unusual peptidoglycan layer (Bui et al., 2009). The finding of two structural groups is in accordance to previous phylogeny study which claimed that two AAT categories exist: Ia group and Ib group (Wu et al., 2011). However, the idea to compare individual bacteria species properties to judge functional difference between these two AAT groups is a new approach presented in this study.

All in all, it appears that AATs generally differ among bacteria with different cell wall physiology (gram-positive or negative). Although the ability of spore formation is predominantly seen in gram-positive bacteria, sporulating gram-negative bacteria exist. In fact, *M. xanthus* and *A. cylindrica* AAT homologs allocate with the gram-positive bacteria in phylogenic branch B. In addition, gram-negative bacteria which are considered environmental organisms such as *Synechocystis sp*. (Kaneko et al., 1996) and even extremophiles like *Thermus thermophilus* (Ohtani et al., 2010) and *Haloferax mediterranei* (Oren, 2002) also allocate to branch B. Despite being gram-negative *T. thermophilus* cell wall physiology shows similarities to gram-positive species (Quintela et al., 1995), whereas archaeal cell wall in *H. mediterranei* shows

fundamental differences to bacteria (Albers & Meyer, 2011). Therefore, branch B not only comprises a wider range of variable AAT isoforms, than branch A, but it also comprises AATs from bacteria with diverse cell wall physiology, which appears rather uniform and specialized in bacteria found in branch A.

Since it is assumed that gram-negative bacteria evolved from spores of ancient gram-positive species, it is likely that environmental gram-negative bacteria retained the ancient version of the AATs (Errington, 2013). A probable functional setting of the ancient AAT may be the peptidoglycan layer synthesis for the cell wall. In fact, peptidoglycan is synthesized via lysine which originates from aspartate (Hudson, 2017). In fact, the two AAT isoforms in *B. subtilis*, AspB and YhdR, share high similarities to DAP aminotransferase (99% CR, 42% ID, 5.00E-95 and 88% CR, 4.00E-42, 28%) which is involved in peptidoglycan synthesis. On the other hand, *E. coli* AspC, which localizes to phylogenic branch A, displays high similarity to the aromatic acid amino transferase TyrB (100% CR, 2.00E-118, 43% ID). In fact, studies show that TyrB and AspC are able to compensate each other's functions (Lal et al., 2014).

An ancient AAT function may be involved in contributing to the cell wall peptidoglycan which is an essential component of the spore wall. Peptidoglycan is synthesized from aspartate which suggest that aspartate aminotransferases in gram-positive bacteria are essential for generating precursors for cell wall components. Gram-negative bacteria and gram-positive species, that colonize animals, may not suffer under harsh environmental conditions compared to soil bacteria. Therefore, a thick peptidoglycan layer is not required in the latter. It is therefore likely that AAT function changed throughout evolution into contributing to the synthesis of other N

compounds which are required for quiescence survival rather than cell wall thickening during sporulation. These findings may explain the distinct difference in sequence identities found in the BLASTp homology search for Maa1.

Maa1 alignments against *B. subtilis* aspartate amino transferase YhdR yield a lesser identity, than observed in alignments against *E. coli* AspC. This is very likely due to different roles of the AATs in both organisms. The AspC functional role is more similar in *S. pombe* since it is likely involved in amino acid pool generation, rather than supplying compounds for cell wall as seen in gram-positive and/or spore-forming bacteria.

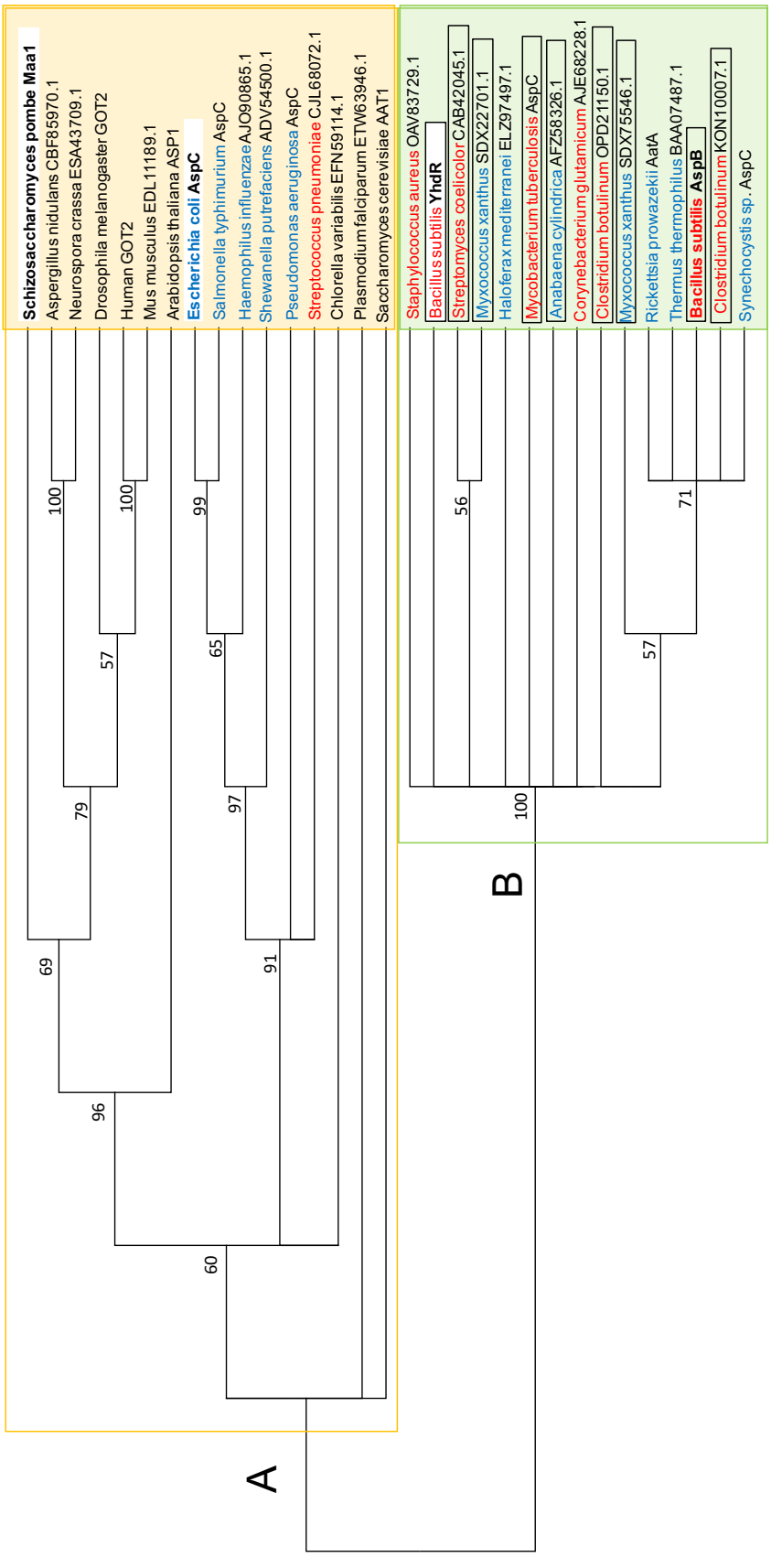

Figure 3.20. Branch topology of Maa1 and homologs. The various Maa1 homologs diverge into two nodes. *S. pombe* Maa1 localizes together with eukaryotic homologs (black font) and *E. coli* AspC into one node (orange box). The remaining bacterial species which include gram-positive (red font), spore-forming (black box and environmental gram-negative bacteria is the other noder (green box). Condensed phylogenic tree was generated by computing Maximum likelihood with 1,000 bootstrap repetitions using the MEGA6 tool. Bootstrap confidence intervals are depicted above 50%. Proteins from spore-forming bacteria are put into black brackets. Official protein names are used if available, otherwise GenBank® namings are used (sequences accessible at https://www.ncbi.nlm.nih.gov/genbank). .

3.5. The electron transfer associated Nde1 and Coq5

The two genes which encode enzymes NADH dehydrogenase Nde1 and ubiquinone methyltransferase Coq5. Nde1 is considered as the entry point into the electron transfer chain (ETC), whereas Coq5 is indirectly involved by contributing to ubiquinone synthetic pathway. Ubiquinone accepts electrons from NADH dehydrogenase and is part of the ETC.

The alternative NADH dehydrogenase Nde1

Nde1/SPBC947.15c **(**~61 kDa) is predicted to encode NADH dehydrogenase inferred from homology (NADH-DH, EC: 1.6.5.9) (Luttik et al., 1998, Overkamp et al., 2000). In *S. pombe* there are two NADH dehydrogenase proteins: Nde1 and Nde2. But only deletion of *nde1* caused viability loss during N starvation conditions.

When considering respiratory chain protein abundance data (Marguerat et al., 2012), Nde1 appears slightly increased (1.5-fold) upon G0 phase entry, in contrast to the other non-GZE NADH dehydrogenase Nde2 which is unchanged (**Figure 3.21**.). Also, relative change of protein abundance of other respiratory chain enzymes seems to remain stable even under G0 phase. Especially, when comparing with glycolytic enzymes, which mostly decrease upon G0, respiratory protein levels do not radically change in abundance. Based on these data Nde1 seem to be required upon G0 phase.

Figure 3.21. Relative changes in respiratory chain protein levels. Relative changes in glycolytic protein abundance is displayed in separate graph. It serves as a reference, showing the uniform decrease of glycolytic protein abundance upon G0 phase. In contrast, respiratory protein levels remain relatively constant even upon G0 conditions. This suggests that levels of respiratory enzymes are maintained at G0.

Protein abundance data are based on Marguerat et al., 2012 accessed via pombase.org (Wood et al., 2012).

Sequence comparison identified Nde1 homologs in *E. coli* (25% ID) and *B. subtilis* (28% ID) (**Figure 3.22.)**. Aligning and comparing the corresponding protein sequence with *S. pombe* and bacterial homolog candidates led to the observation there are a few identical residues from 4G74 (Feng et al., 2012) (**Figure 3.23**.).

The NADH dehydrogenase phylogeny reconstruction results (**Figure 3.24**.) support this study's BLAST homology claim.

However, it is unclear why Δ*nde1*, and not Δ*nde2*, showed sensitivity to four-week-long N starvation conditions. According to the phylogeny reconstruction Nde1 and Nde2 are relatively closely related. It is likely that other factors play a role in Nde1 importance for G0 survival.

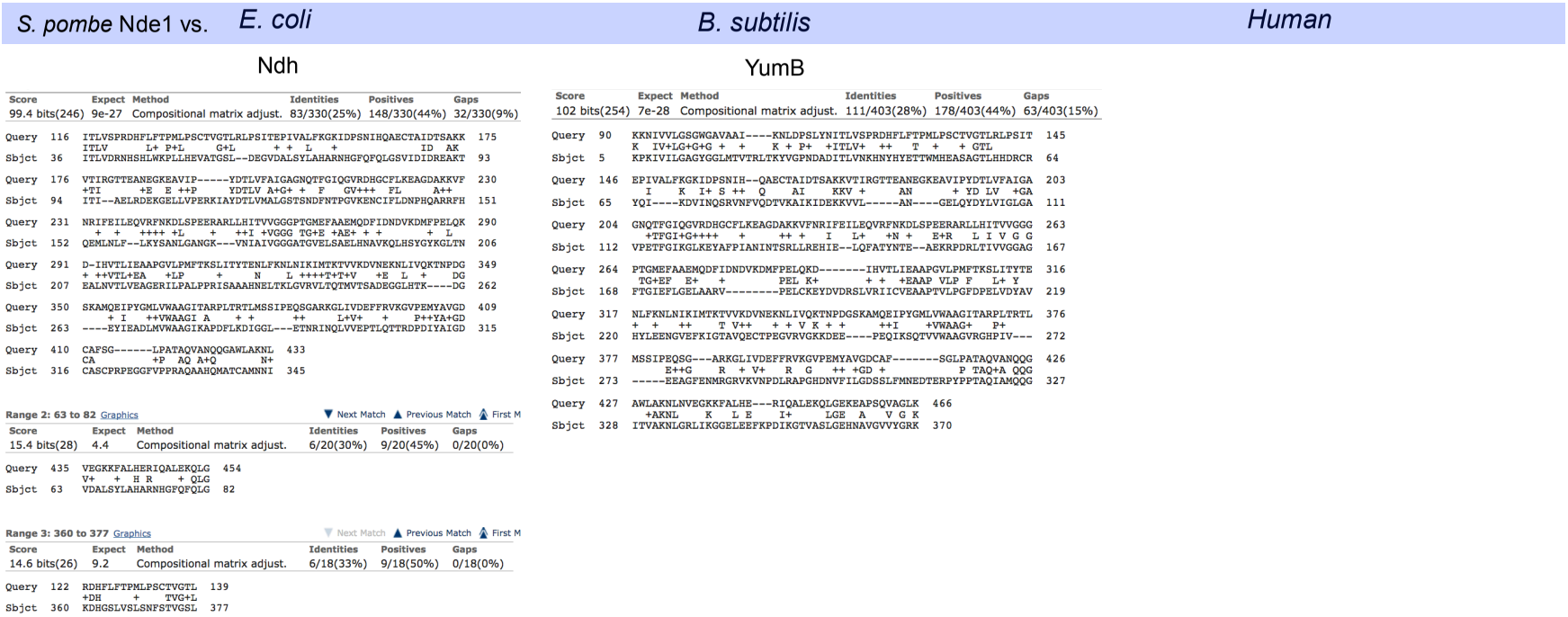

Figure 3.22. BLAST pairwise alignments against Nde1. *S. pombe* sequences were separately run against *E. coli* and *B. subtilis*. No ortholog were found in human.

S. pombe	*E. coli*	E value	Identity (%)	Coverage (%)	Human	E value	Identity (%)	Coverage (%)	*B. subtilis*	E value	Identity (%)	Coverage (%)
Ndh	9.00E-27	25	61	NA	NA	NA	NA	NA	YumB	7.00E-28	28	68

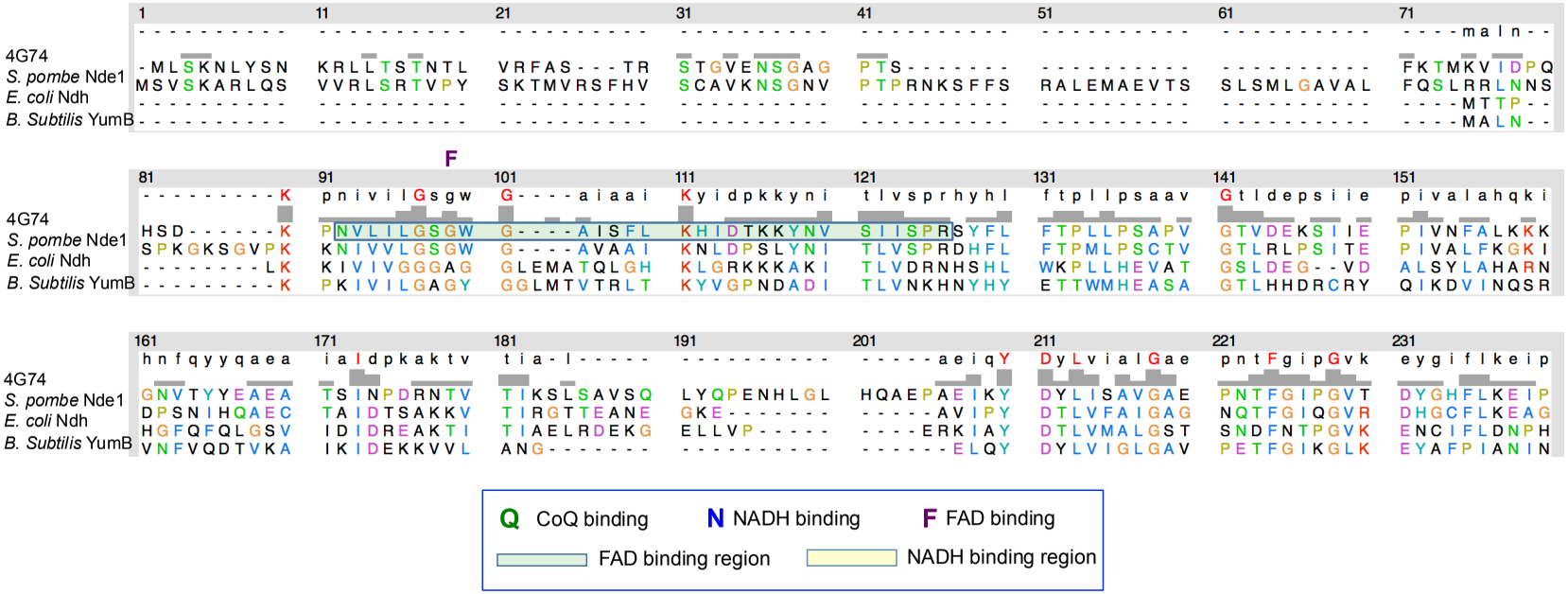

Figure 3.23. Protein alignment of Nde1 against bacterial homologs. The functional sites were derived from Feng *et al.* 2012 crystal structure 4G74. NADH binding sites appear well conserved in contrast to FAD and ubiquinone (CoQ) residues. See next page for continuation of this alignment.Chimeria software was used to generate alignment.

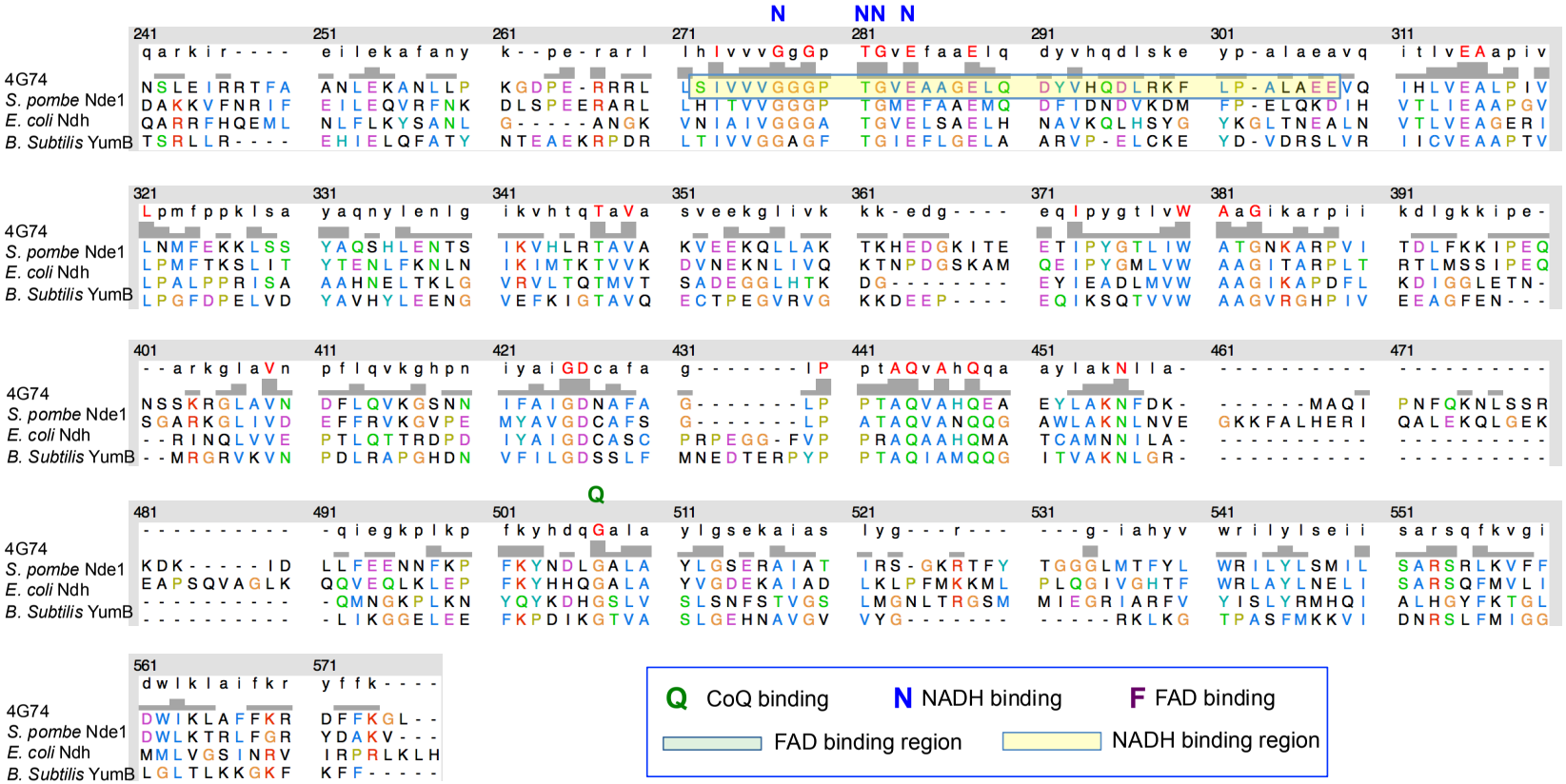

Figure 3.23. Protein alignment of Nde1 against bacterial homologs. (continued) The functional sites were derived from Feng *et al.* 2012 crystal structure 4G74. Color scheme is based on ClustalX default setting which differentiates between residue type and frequency of occurence in the same column (consensus residue).

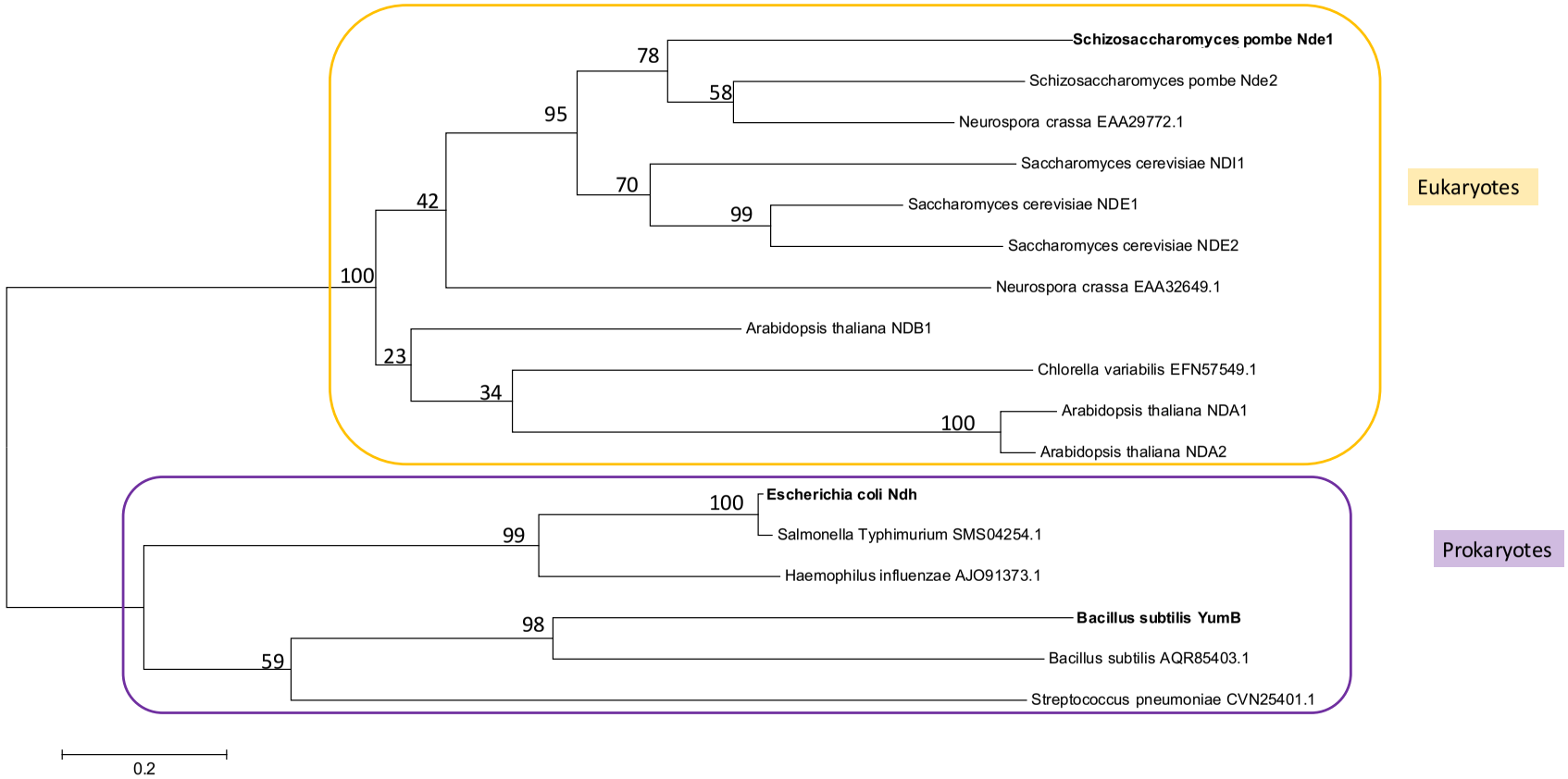

Figure 3.24. Alternative NADH dehdyrogenase phyloheny reconstruction. Maximum likelihood phylogeny tree was computed for functional homologs using MEGA6. Node reliability is expressed with confidence percentage from 1,000 bootstrap repetions. Based on the node distribution eukaryotic (yellow) and prokaryotic (purple) alternative NADH dehydrogenases can be differentiated. Node reliability is considered high when confidence intervals are higher than 50%.

Coq5 - Generator of CoQ precursor pool

Nde1 electron transfer activity depends on presence of ubiquinone CoQ. It is therefore no surprise that Coq5, a ubiquinone biosynthetic protein, is among the GZE proteins. Notably, out of the many ubiquinone biosynthetic enzymes, only Coq5 was found to be essential for N starvation survival. **Coq5 (**34 kDa) is an S- adenosyl-L-methionine (SAM)-dependent methyltransferase (COQ5, EC: 2.1.1.201) based on homology (Uchida et al., 2000). It catalyzes the C-methylation step from 2-methoxy-6-polyprenyl-1,4-benzoquinone to 2-methoxy-5-methyl-6-polyprenyl-1,4-benzoquinone (demethoxy quinone, DMQ) (Barkovich et al., 1997). The end-product DMQ is the substrate for Coq7 the final step in ubiquinone (Coenzyme Q; CoQ) synthetic reaction (Gonzalez-Mariscal et al., 2014).

Similar to lysine and branched-chain amino acids, CoQ is produced via several steps. Coq5 is the sole GZE protein which is part of the ubiquinone biosynthetic pathway (**Figure 3.25**.). Most of the enzymes from the ubiquinone pathway are conserved, nevertheless, only Coq5 is essential for the regeneration from our-week-long N starvation. To understand why Coq5 differs from the other CoQ biosynthetic enzymes, protein abundances from all ubiquinone enzymes were obtained as described previously for Lys12 and Ilv3. In fact, Coq5 protein abundance during vegetative (VE) state is the highest among the enzymes from the CoQ biosynthetic pathway(Marguerat et al., 2012). Nevertheless, upon G0 entry Coq5 protein levels decrease. Still, they appear higher compared to other CoQ biosynthetic enzymes. It is likely that Coq5 function is essential during VE phase to promote ubiquinone precursor compound. Sudden decrease in Coq5 levels may affect the flux through ubiquinone biosynthesis upon G0. The differences in protein abundance may be due to enzyme-specific

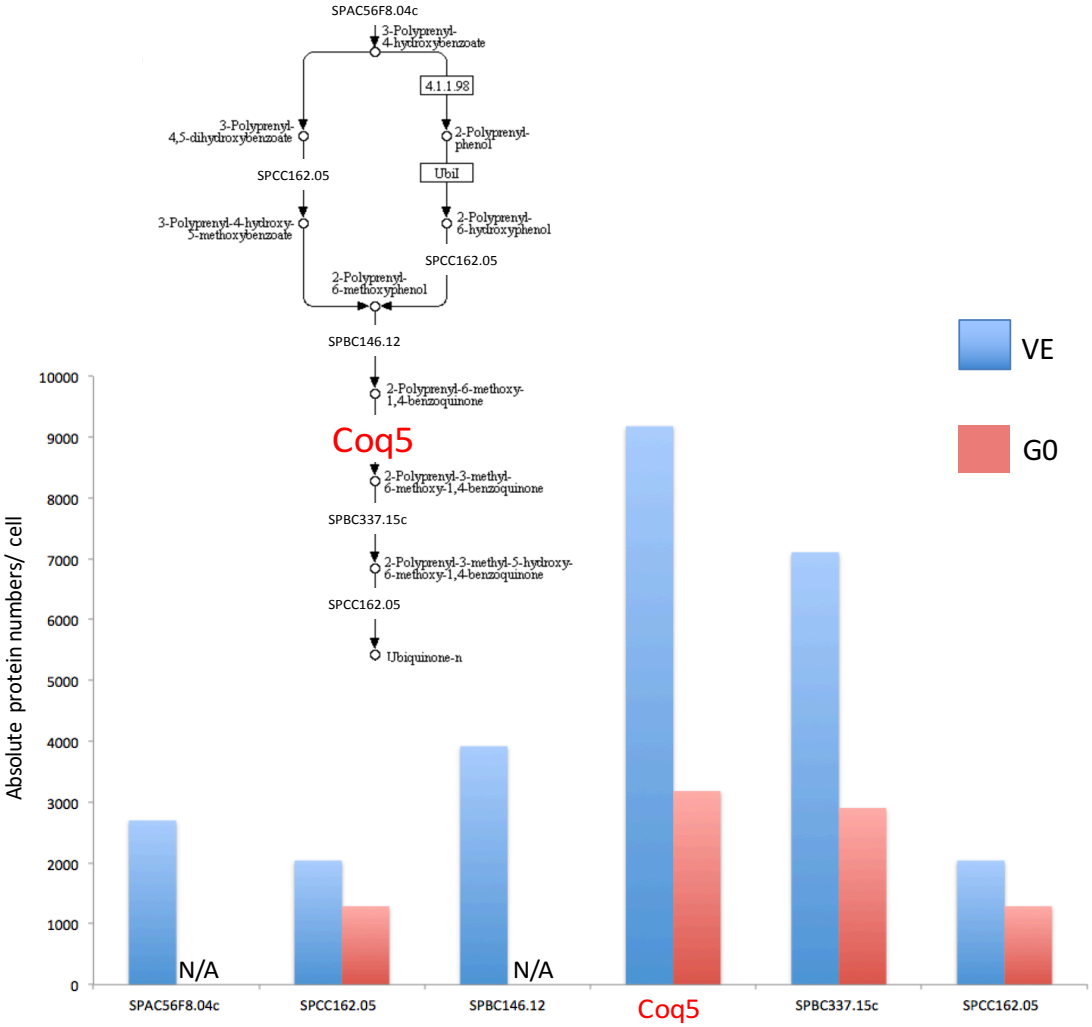

Figure 3.25. CoQ biosynthetic pathway. Fluctuation in protein abundance of ubiquinone biosynthetic proteins during vegetative (blue) and G0 (red) states. The CoQ biosynthetic pathway is adapted from KEGG database (Kanehisa & Goto, 2000). Protein abundance per cell was inferred from Marguerat *et al*. 2012, accessed via pombase.org database (Wood *et al*., 2012). GZE ubiquinone methyltransferase Coq5 is marked in red font. Data which were not available in G0 state are marked with N/A.

regulation. There are still unknown factors which lead to G0 essentiality of Coq5.

The CoQ biosynthetic pathway is a relatively well conserved mechanism. Only Coq5 was shown to be a conserved GZE protein. It contains a SAM-dependent

methyltransferase domain forming a dimer topology (Dai et al., 2014). *E. coli* UbiE (44% ID) is the potential homolog to *S. pombe* Coq5 which is a bifunctional enzyme involved in the synthesis of CoQ and menaquinone (MQ) (Lee et al., 1997). On the other hand, *B. subtilis* MenG (32% ID), is essential for conversion of demethylmenaquinone (DMMQ) to MQ (**Figure 3.26.**). and shares some similarities with COQ5. Common SAM binding involved sites (orange, blue and yellow triangle) are found in *E. coli*, *B*. *subtilis* and *S. pombe* (**Figure 3.27.**). Crystal structure 4OBW (Dai et al., 2014) is loaded in Chimera program to identify conserved sites.

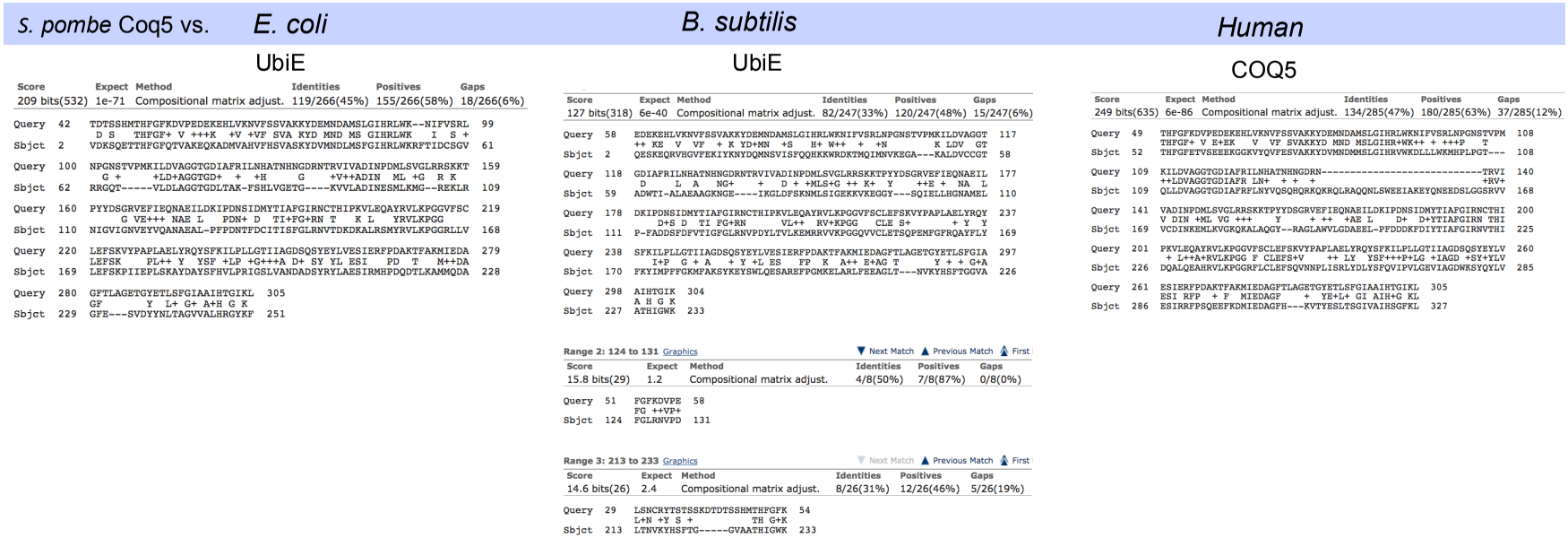

Figure 3.26. BLAST pairwise alignments against Coq5. *S. pombe* sequences were separately run against *E. coli*, *B. subtilis* and human databases.

S. pombe	*E. coli*	E value	Identity (%)	Coverage (%)	Human	E value	Identity (%)	Coverage (%)	*B. subtilis*	E value	Identity (%)	Coverage (%)
Coq5	UbiE	1.00E-71	45	86	COQ5	6.00E-86	47	84	MenG/UbiE	6.00E-40	33	90

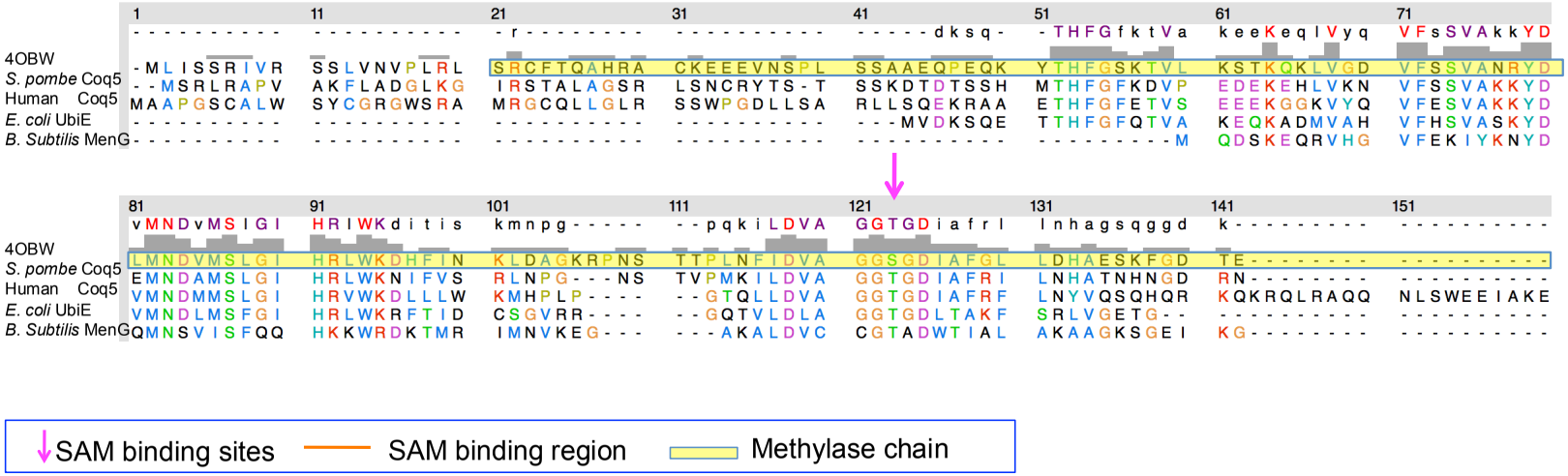

Figure 3.27. Alignment against Coq5 and its homologs. Functional sites are inferred from *S. cerevisiae* Coq5 crystal structure 4OBW (Dai *et al*., 2014).

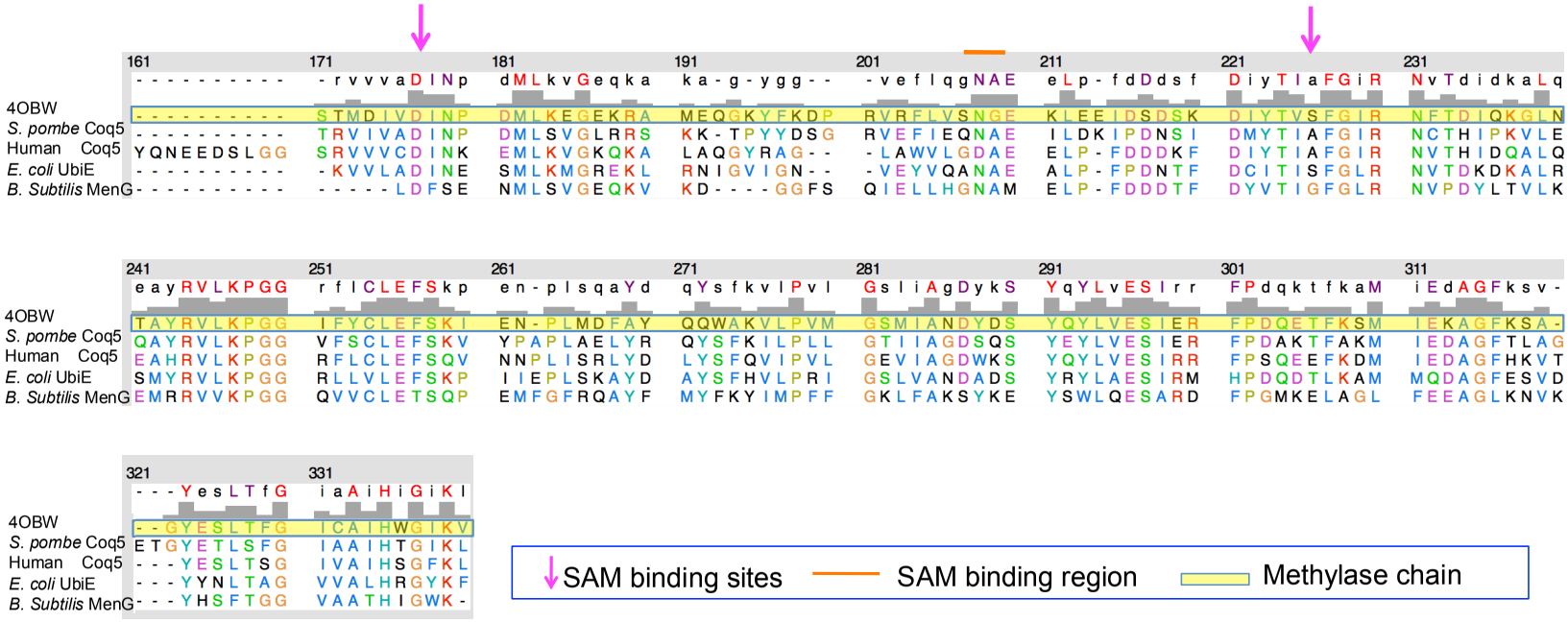

Figure 3.27. Alignment against Coq5 and its homologs. Functional sites inferred from *S. cerevisiae* Coq5 crystal structure 4OBW (Dai *et al.*, 2014). Color scheme is based on ClustalX default setting which differentiates between residue type and frequency of occurence in the same column (consensus residue).

3.5.1. Investigating sequence ID variation among Coq5 homologs

Similar to the previously mentioned Maa1 and Gdh1, in order to investigate sequential variance which may be an effect of changes in physiology and metabolism of the bacterial species during evolution, a condensed phylogenic tree for Coq5 was generated **(Figure 3.28**.) The original tree can be found in Figure **S3**. The phylogenic tree for Coq5 differs from the two previous phylogenic trees, since no clear branching takes place. On the contrary, it appears that Coq5 homologs form speciation nodes branch based on the isoprenoid they are synthesizing. In fact, there are two main types of electron accepting isoprenoid compounds prenylquinones, including plastoquinone and ubiquinone (Liu and Lu, 2016), and naphthoquinones including menaquinone and demethylmenaquinone (Soballe and Poole, 1999). They are involved in energy generation under different oxygen conditions (Meganathan, 2001). Therefore, they differ in redox potential with ubiquinone having the highest, and menaquinone the lowest value (Hollander, 1976). (Demethyl-) menaquinone synthesizing Coq5 homologs are predominantly seen in gram-positive bacteria, whereas gram-negative facultative anaerobes like *E. coli* synthesize both ubiquinone and menaquinone dependent on environmental oxygen conditions.

The Coq5 homolog in *B. subtilis* produces menaquinone (Lee et al., 1997). In fact, menaquinone was reported to be involved in regulating sporulation (Escamilla et al., 1988). It is unclear whether ubiquinone has the same effect on quiescent cells.

Based on the phylogeny the difference in identities between Coq5 alignments to *E. coli* and *B. subtilis* may be explained by different types of lipoquinones used in the organism for electron transfer reactions. Throughout the evolutionary progress occurrence and preference for a certain type of lipoquinone has changed.

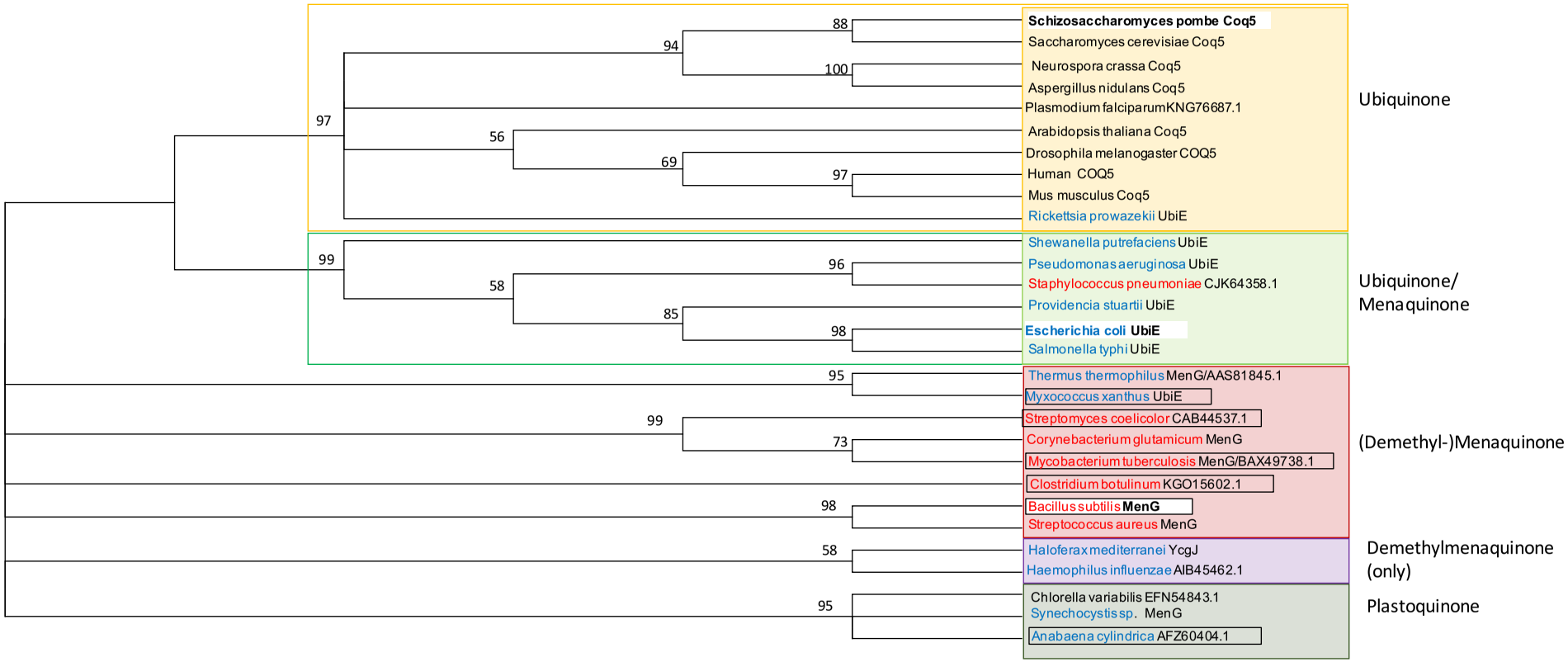

Figure 3.28. Branch topology of Coq5 and homologs. Condensed phylogenic tree was generated by computing Maximum likelihood with 1,000 bootstrap repetitions using the MEGA tool. Bootstrap confidence intervals are depicted above 50%. Gram-negative bacteria are colored in blue font, whereas gram-positive are red. Official protein names are used if available, otherwise GeneBank® namings are used. Proteins from spore-forming bacteria are put into black brackets. Information on the enzymatic product, being either ubiquinone or menaquinone, is inferred from the entry in GeneBank and uniprot.

3.6. Protein of uncharacterized function

Similar to Nde1 and Coq5, the uncharacterized **SPBC21C3.03** suffers from mild viability impairment during -N incubation. Not much is known about SPBC21C3.03 despite its designation to the **a**ctivity of **b**c1 **c**omplex-**l**ike **k**inase 1 (ABC-like kinase 1) protein family which is represented in all domains of life. Since a possible role in cytochrome bc1 complex (respiratory complex III) activity was rejected (Hsieh et al., 2004), call for re-naming the family into UbiB family was made based on recent insights (Stefely et al., 2015). Therefore, this manuscript adopted the latest nomenclature for this conserved protein family.

SPBC21C3.03 is localized only to the mitochondria which is inferred from information from its homolog (Matsuyama et al., 2006). In *S. pombe* three other mitochondria-located UbiB family members were reported: SPAC10F6, SPBC15C4.02 and Coq8.

The *ubiB* gene in *E. coli* and other gram-negative bacteria forms an operon together with *ubiE* which is the ortholog to *S. pombe* Coq5 (Poon et al., 2000). Therefore, bacterial ubiquinone biosynthetic methyltransferase *ubiE* and the uncharacterized *ubiB* share one operon which may be a hint for their roles in ubiquinone synthesis. Furthermore, bacterial UbiB was suggested to be a regulator of the newly identified protein UbiI, an FAD/NAD(P)-binding hydroxylase, involved in aerobic CoQ synthesis (Hajj Chehade et al., 2013). BLAST search found that UbiI shares high sequence similarity to *S. pombe* monooxygenase Coq6 (E-value 4E-29, identity 25% coverage 97%; and E-value 4E-46, identity 30%, coverage 93%)**.** *E. coli* UbiB and *B. subtilis* UbiB show similarity to *S. pombe* SPBC21C3.03 (**Figure 3.29.**). Functional sites remain uncharacterized.

However, bacterial UbiB shows considerate similarity to the other three *S. pombe* family members as well (**Figure S4**).

Nevertheless, *S. pombe* protein shares functional residues with *E. coli* and *B. subtilis* UbiB active sites (D456; violet box) and ATP binding sites (K323; blue box).

Functional sites in eukaryotic Coq8/ADCK3 were characterized recently but not in other UbiB protein isoforms (Stefely et al., 2015). The information was used when aligning the four *S. pombe* UbiB members to the bacterial UbiB protein. Difference between Coq8 and the other three can be seen when dividing the sequences into regions N lobe, A-rich motif, catalytic loop (**Figure 3.30.**) which were defined by previous crystal structure study results from (Stefely et al., 2015). This study shows that Coq8 catalytic loop differs from the bacterial and from the catalytic loops found in three *S. pombe* isoforms. However, its A-rich motif is fairly similar to bacterial UbiB, whereas varies in the three isoforms. It is likely that the four *S. pombe* UbiB isoforms arose from an ‘ancient’ UbiB protein.

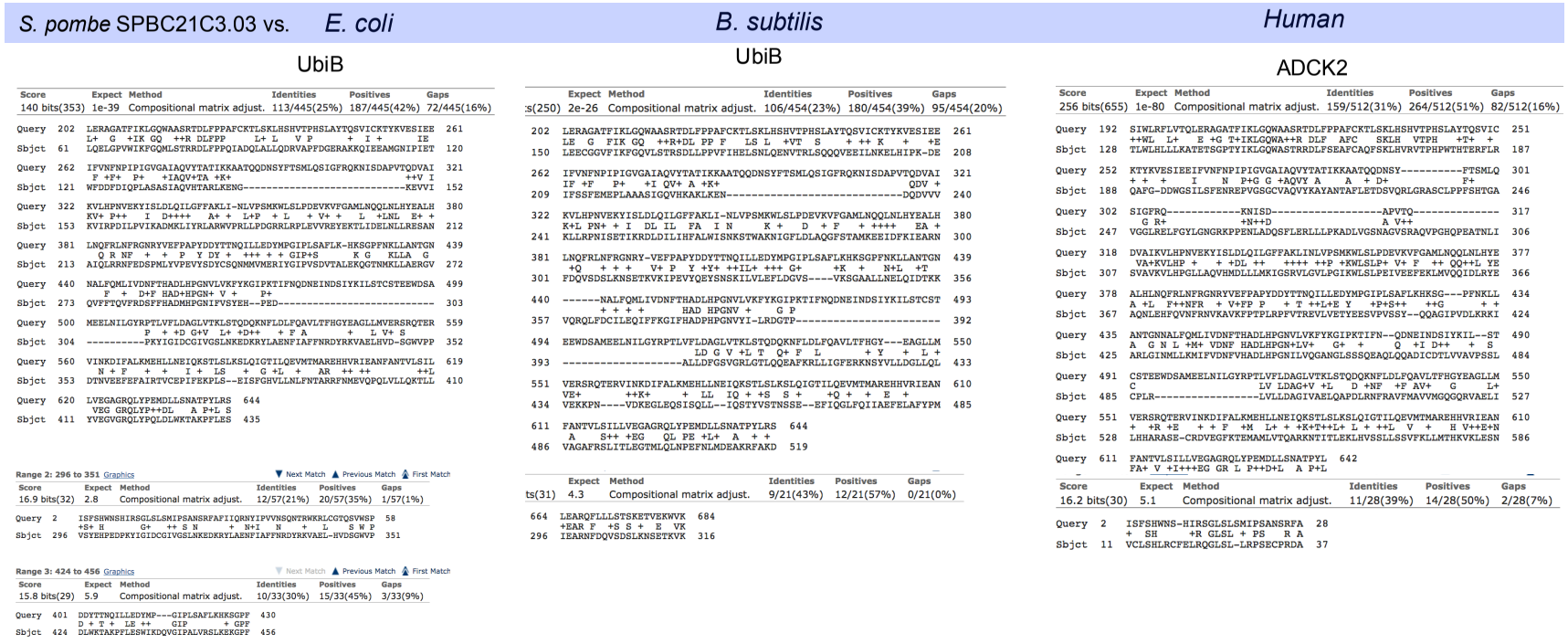

Figure 3.29. BLAST pairwise alignments against SPBC21C3.03. *S. pombe* sequences were separately run against *E. coli*, *B. subtilis* and human databases.

S. pombe	***E. coli***	E value	Identity (%)	Coverage (%)	Human	E value	Identity (%)	Coverage (%)	***B. subtilis***	E value	Identity (%)	Coverage (%)
SPBC21C3.03	UbiB	1.00E-39	25	72	ADCK2	1.00E-80	31	69	UbiB	2.00E-26	23	67

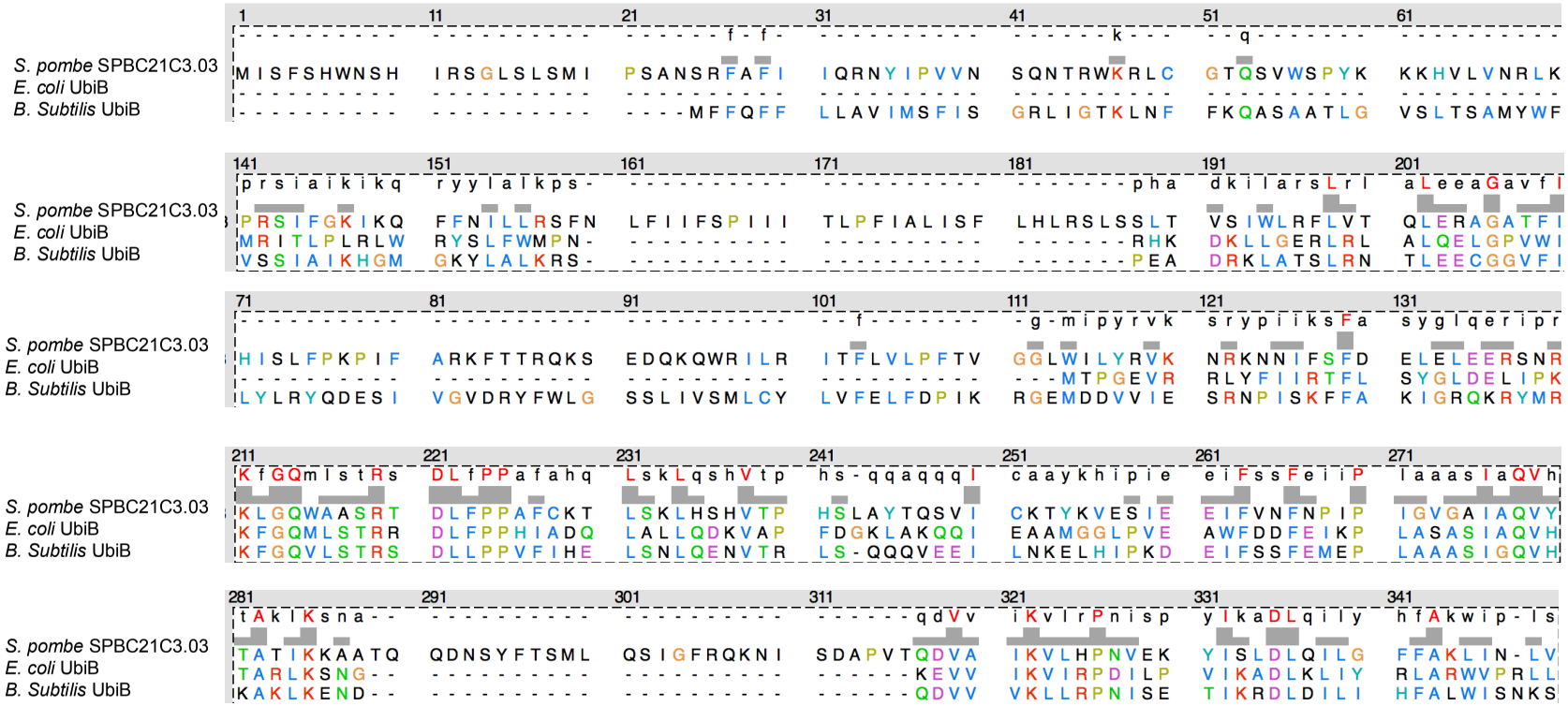

Figure 3.30. Alignment against SPBC21C3.03 and its homologs. No crystal structures exist for UbiB family proteins. See next page for continuation.

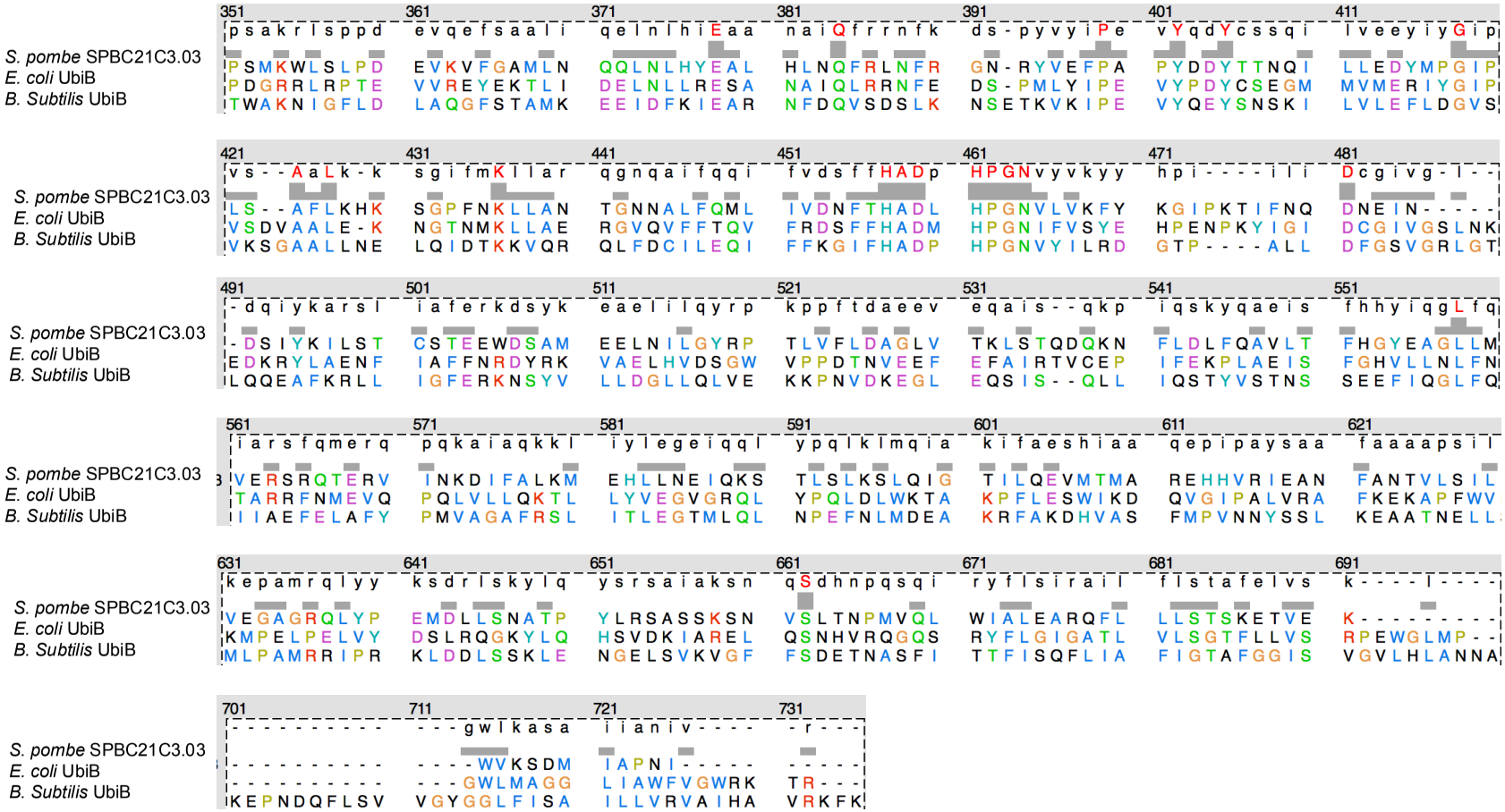

Figure 3.30. Alignment against SPBC21C3.03 and its homologs. (continued). According to Stefely *et al*., the region starting from H457 to N464 is the kinase-like region.Color scheme is based on ClustalX default setting which differentiates between residue type and frequency of occurence in the same column (consensus residue).

To visualize what family member is closest to bacterial ancestor, a phylogenic tree for the UbiB family is displayed in **Fig 3.31.** In addition to *E. coli*, *B. subtilis* and human homologs, UbiB family members found in mouse, *S. cerevisiae*, *N. crassa*, *S. typhi* and *C. botulinum* were selected. In eukaryotes, more than one UbiB family protein exists, therefore, all of them were included. Based on the phylogeny reconstruction Coq8 homologs (purple box) are more distant from the others. Human ADCK1 and ADCK5 form one node with *S. pombe* SPAC10F6, SPBC15C4.02 and their fungal homologs (blue box). In the end, SPBC21C3.03 and its homologs form a separate node which incudes ancient type of UbiB protein. SPBC21C3.03 seems to be closest to the bacterial ancestor UbiB.

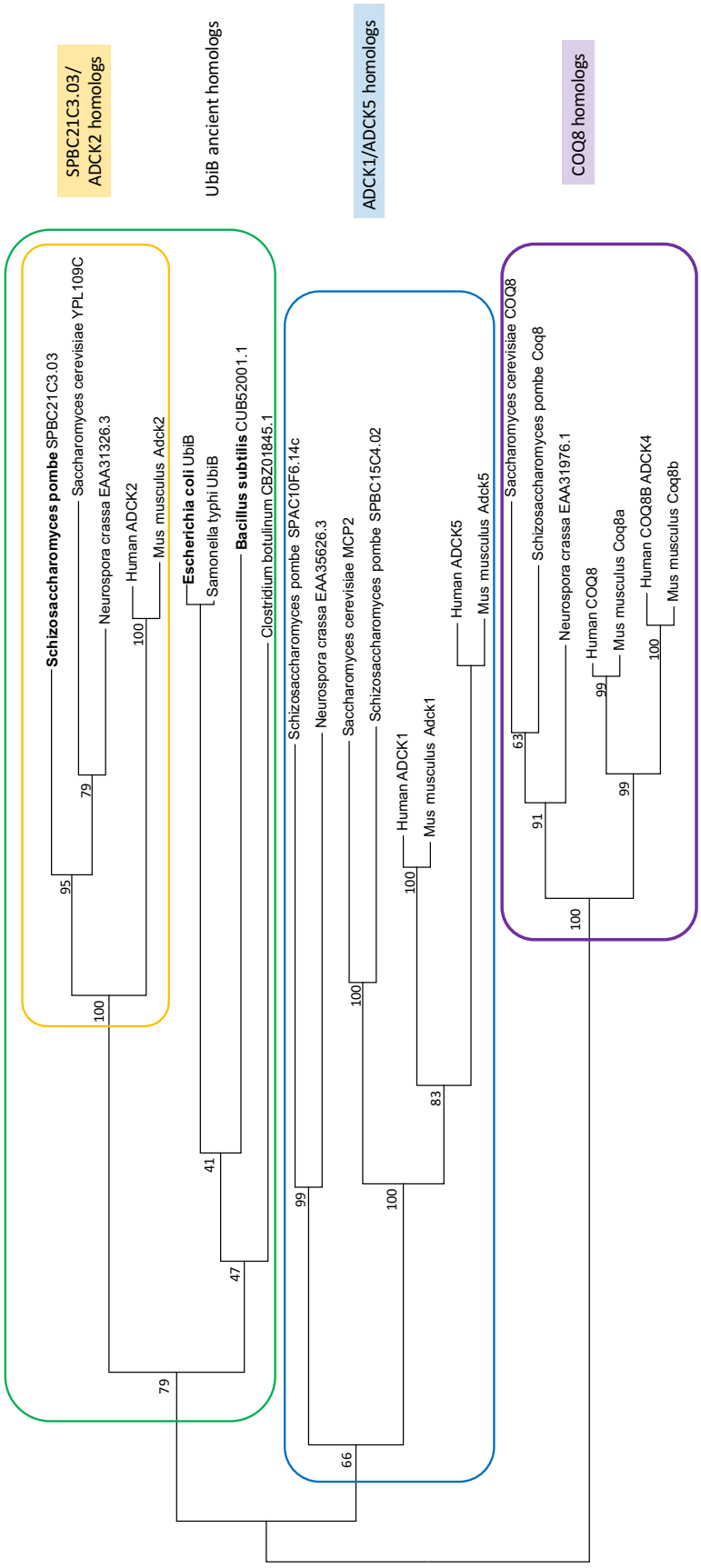

Figure 3.31. UbiB family phylogeny reconstruction. Maximum likelihood phylogeny tree was computed for the conserved Abc1-like kinase/UbiB familiy members using MEGA6. Node reliability is expressed with confidence percentage from 1,000 bootstrap repetions.Node reliability is considered high when confidence intervals are higher than 50%.

3.6.1. Protein function of SPBC21C3.03, a UbiB family member, remains unclear

Three experimental approaches were performed with the aim to characterize Δ*SPBC21C3.03* deletion mutant phenotype in comparison to WT. Initially, morphological features during vegetative and G0 phases were investigated under the microscope which did not show any clear differences among the wild type and deletion mutants of the four *S. pombe* UbiB family members Δ*SPBC21C3.03,* Δ*SPAC10F6.14c*, Δ*SPBC15C4.02* and Δ*coq8* (**Figure S5 and S6**). The pictures were taken with the help of Ms. Yuria Tahara, a technician in the lab.

As a next step, physiological differences are investigated among the UbiB family members. Growth sensitivity assessment in response to drugs can be used to characterize mutant features distinct from WT. Inability to form colonies in media treated with certain chemical agents might indicate requirement for the gene to overcome the external conditions, a link between the gene and the inhibited pathway can be speculated. The individual results of the spot tests for growth sensitivity are shown in **Figures S6 to S21**. In summary, Δ*SPBC21C3.03* showed sensitivity to hydrogen peroxide treatment which is in accordance to the findings that SPBC21C3.03 expression increases upon H_2O_2 treatment (Chen et al., 2003). An overall summary of the drug screening effects on all the four UbiB family mutants is displayed in **Figure S22**.

A last experimental set-up aimed to identify whether mutant phenotypes of Δ*SPBC21C3.03* appear during N starvation. However, upon treatment with H_2O_2 N-starved Δ*SPBC21C3.03* did not show any differences from WT control strain (**Figures S23 and S24**). It is likely that other factors may have influenced the outcomes of the experiments. In fact, a major part of *SPBC21C3.03* coding region was found to overlap

with the 3' UTR (untranslated region) of the mitochondrial ribosomal protein L34 encoding gene *SPBC21C3.04c*. There is some evidence for *SPBC21C3.04c* mRNA stabilizing polyadenylation sites located on the sequence overlapping *SPBC21C3.03* coding region (Schlackow et al., 2013). An overview of the differential polyadenylation sites for *SPBC21C3.03* found by Schlackow et al., 2013 was generated (**Figure S25**). Unlike *SPBC21C3.03*, the other four *S. pombe* UbiB family members did not show any polyadenylation sites at quiescence (not shown). It is likely that upon deletion of *SPBC21C3.03* polyadenylation sites are removed and thus, alter mRNA stability of *SPBC21C3.04c*. Also, *SPBC21C3.03* deletion shows genetic interactions with many nuclear genes, involved in splicing and silencing (Ryan et al., 2012)

Therefore, more work needs to be done in order elucidate the importance of SPBC21C3.03 during quiescence survival. This study, however, focuses on the search for a conserved quiescence mechanism and shall not divert into a single gene study.

3.7. Summary of the phylogeny study and literature review

Based on the homology study the seven conserved mitochondria-localized GZE proteins can be grouped into three categories based on their functions: Superoxide scavenging, amino acid biosynthetic and NADH cofactor regenerating electron transfer component (**Figure 3.32.**). Initially, SPBC21C3.03 was found to be a conserved GZE protein. However, due to some subsequent findings it needs further confirmation whether SPBC21C3.03 deletion is causing any secondary effects on mRNA stability in its adjacent gene. Interestingly, the time points of long-term G0 survival ability decrease, as mentioned above, follows a pattern which corresponds to their functional grouping. Since superoxide dismutase Sod2 depletion has significant implications on viability upon G0 state, oxygen-related reactions within the mitochondria may be involved. It appears therefore as reasonable to check for any abnormalities concerning respiration in the mutants under N starvation induced quiescence. The next step will deal with the investigation of oxygen consumption in the seven mutants.

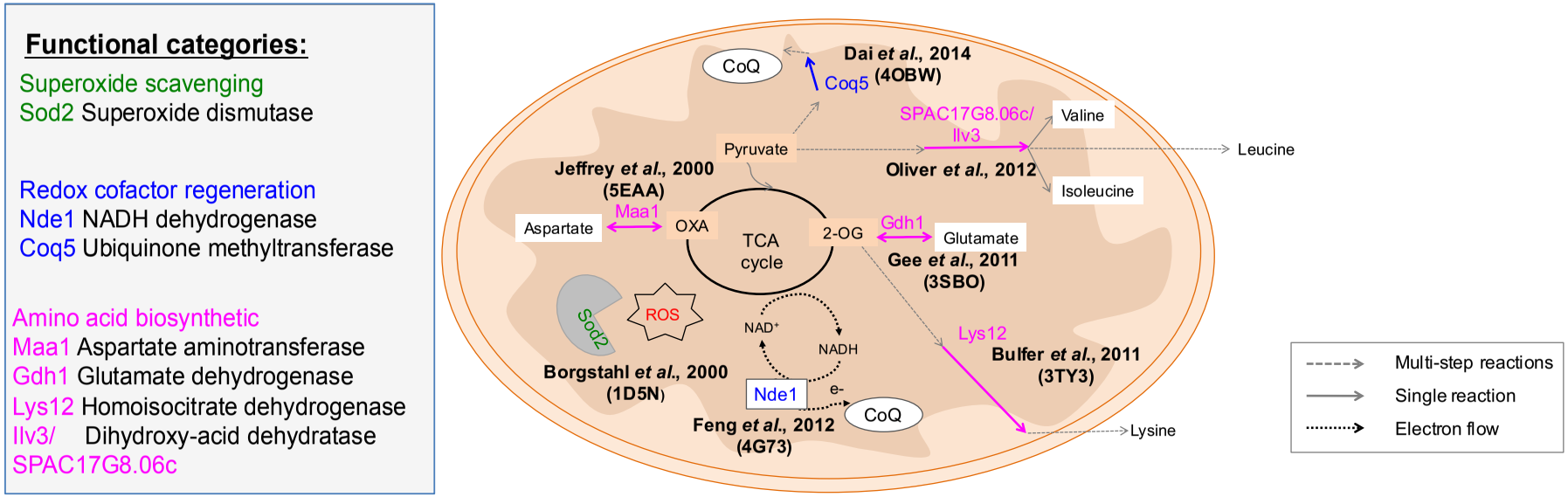

Figure 3.32. Functional setting of conserved GZE proteins within mitochondria. Seven gene products localized to the mitochondria were reported to be essential for G0 phase survival under N starvation in *S. pombe*. GZE mechanisms within the mitochondria comprise superoxide scavenging, the redox cofactor regenerating and amino acid biosynthetic reactions. One gene could not be allocated: SPBC21C3.03 whose function is unknown. Therefore, it must be regarded separately from the other gene products.

3.8. Oxygen consumption measurements

Literature review of the functional importance of the three GZE gene products superoxide dismutase Sod2, NADH dehydrogenase Nde1 and methyltransferase Coq5 implies a role for the respiratory electron transfer chain. Hence, to check whether depletion of these selected GZE genes does indeed influence respiratory outcome, oxygen consumption rates (OCR) were investigated in this part. Respiratory activity in *S. pombe* can be deduced from the oxygen consumption rate using the flux analyzer Seahorse XF-96 from Bioscience. It is known that, *S. pombe* displays some basal respiratory activity when grown in the synthetic minimal medium EMM2+N, in addition to generating energy via the fermentative pathway. Also, the rate of oxygen consumption was shown to be dependent upon glucose levels in the EMM2 media (Takeda et al., 2015).

Initial OCR measurements were performed with wild type 972h- under vegetative conditions and under G state, respectively. The experiments were performed by Ms. Ayaka Mori a technical staff in the G0 cell unit. Since OCR measurement *in S. pombe* with Seahorse XF-96 is a widely unreported approach, the ideal cell concentration for measurements had to be determined. The experiments were performed using four different concentration of wild type strain: $1x10^6$, $2.5x10^6$, $5x10^6$ and $7.5x10^6$ cells/mL. During the measurements, it was noted that a cell concentration at 5 $x10^6$ cells/mL and more caused the maximum measurement capacity of the machine to be reached during vegetative state (**Figure 3.33.)**. In order to prevent inaccurate readings cell concentration higher than $2.5x10^6$ cells/mL were omitted. OCR in G0 cells seems to be lower than in vegetative state. This may be due to lower cell volume in quiescent cells. In fact, cell volume ratio of proliferating to quiescent

cells are approximately 3:1 (Shimanuki et al., 2007), cell concentration in the samples was adjusted to make up for the smaller cell size. In other words, measurements of vegetative state samples were performed at cell concentration $1x10^6$ cells/mL, whereas samples with G0 cells were measured at a concentration of $2.5x10^6$ cells/mL.

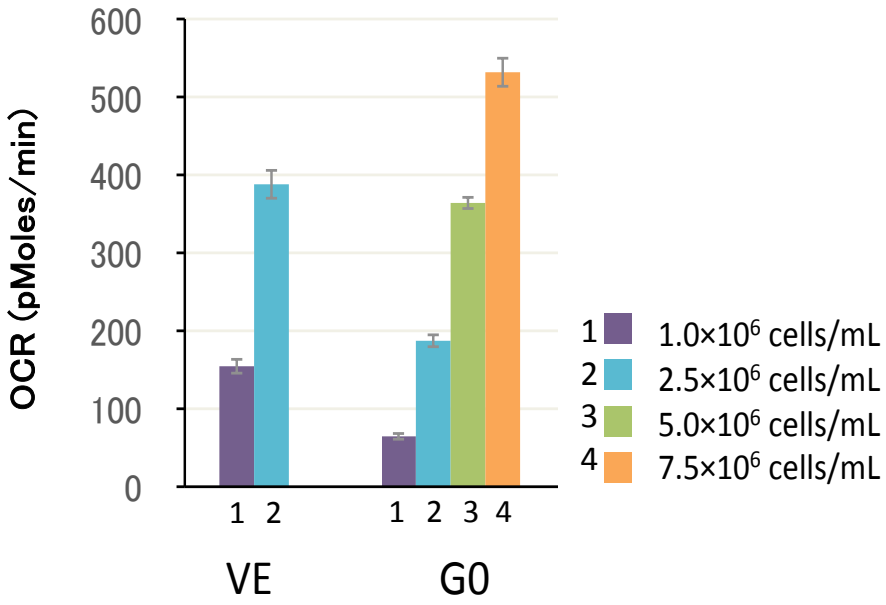

Figure 3.33. Oxygen consumption rates in WT during VE and G0. Wild type (WT) OCR measurements were performed using different cell number concentrations. Data obtained from Ms. Ayaka Mori.

Based on the initial wild type OCR measurements, a 2.5x greater cell concentration is ideal for comparing oxygen consumption rates between vegetative and quiescent cells. The OCR measurements showed that basal respiratory activity is detectable under vegetative state and seems unchanged during quiescence. The OCR among the mutants seems to vary greatly in VE (**Figure 3.34**) and G0 (**Figure 3.35**).

Especially, among amino acid biosynthetic deletion mutants, OCR outcomes vary greatly. Especially under VE state the OCR levels among the seven deletion mutants are variable.

These OCR results argue against the functional categorization, mentioned in **Figure 3.32** which seems unreasonable. In order to investigate a secondary factor behind the OCR variations, cell morphologies were observed under the microscope. The cell imaging, at both VE and G0, showed that cell shape and size are indeed aberrant among the mutants when compared to WT. This may explain the seemingly diverse OCR behavior among the mutants. In fact, a bigger cell size is linked to an increased OCR which was observed in Δ*coq5* and Δ*ilv3* at VE and G0 states. On the other hand, a smaller cell size causes a decrease in OCR which was observed in Δ*gdh1* and Δ*maa1* under VE conditions.

In contrast to the majority of deletion mutants, which are variable in sizes, Δ*sod2* cell morphology does not differ from WT. Nevertheless, Δ*sod2* OCR is the lowest among the deletion mutant. Since its size is comparable to WT, the low OCR readings can be considered as a true Δ*sod2* mutant phenotype. It seems that Δ*sod2* has an effect on oxygen consumption. During vegetative state viability of Δ*sod2* is not affected, but only during N starvation the abolished Δ*sod2* suffers from a radical viability loss. The abolished OCR may be a hint for the functional importance of Sod2 during N starvation.

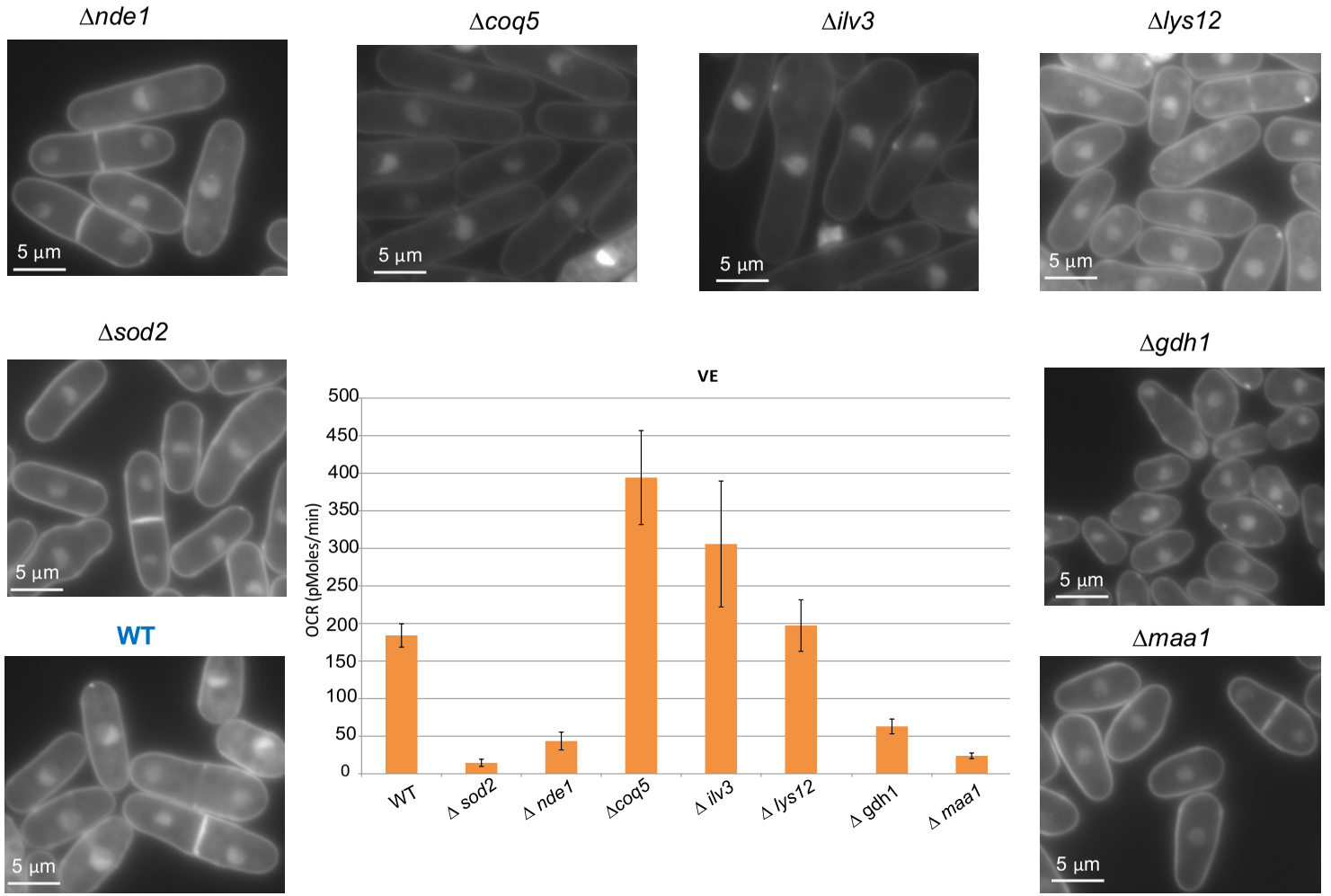

Figure 3.34. Oxygen consumption rates of deletion strains in vegetative state. Oxygen consumption was measured at a cell concentration of 1x10^6 cells/mL. The means of oxygen consumption rates (OCR) are indicated in pMoles/min with standard deviations are indicated. The number of measurements for VE strains are as follows ten for WT and four for Δ*sod2. OCR m*easurements were performed by Ms. Ayaka Mori. Images of mutants and WT were obtained with assisstence from Ms. Yuria Tahara. DAPI nuclear stain was applied.

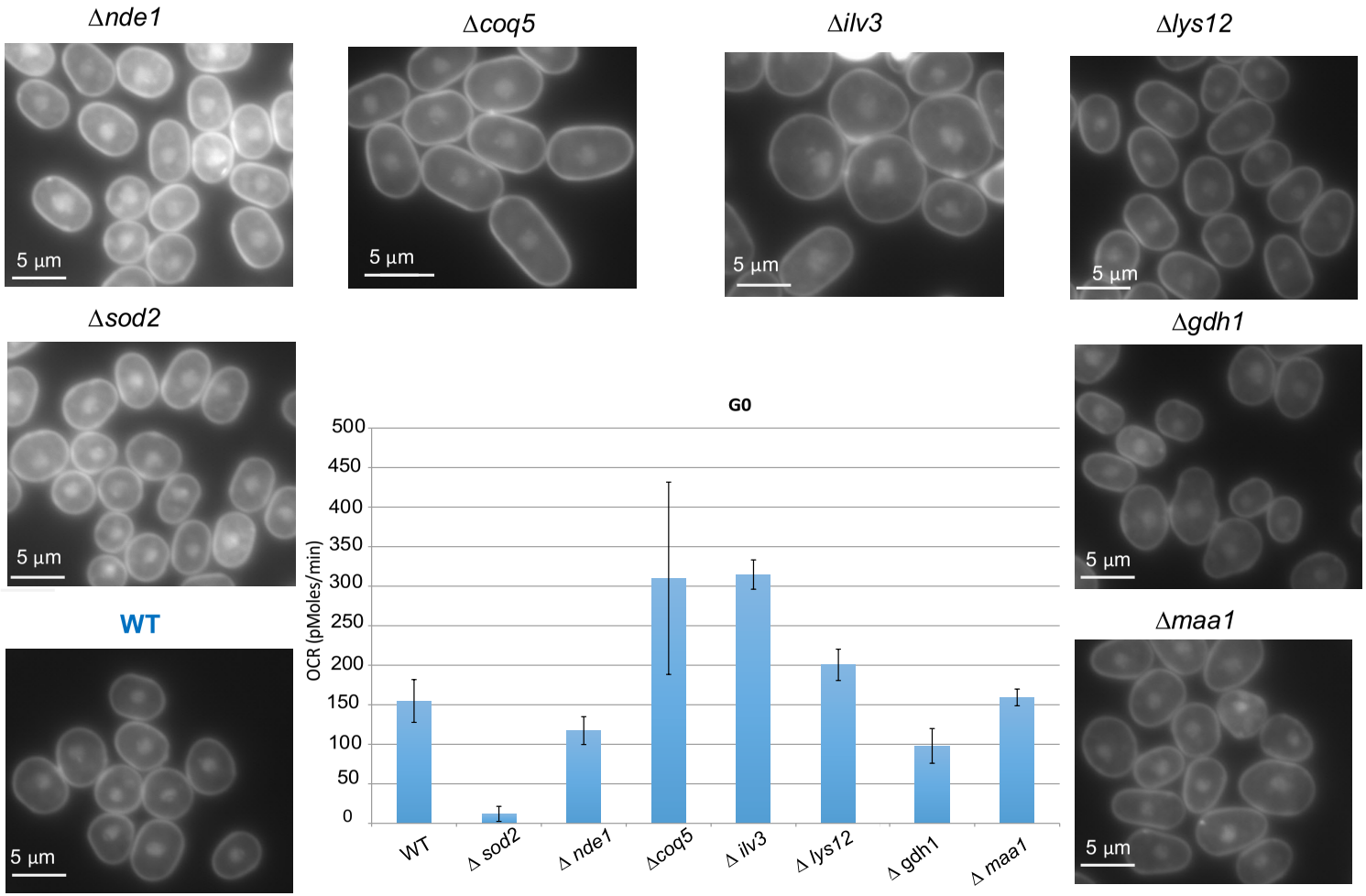

Figure 3.35. Oxygen consumption rates of deletion strains in G0. Oxygen measurement was performed at a cell concentration of 2.5x10^6 cells/mL. The means of oxygen consumption rates (OCR) are indicated in pMoles/min with standard deviations are indicated. The numbers of measurements for G0 phase cell strains are as follows: Nine measurement round for WT, two for Δ*coq5*, three for Δ*sod2*, Δ*nde1*, Δ*maa1*, four for Δ*lys12*, Δ*gdh1* were performed. *OCR m*easurements were performed by Ms. Ayaka Mori. Images of mutants and WT were obtained with assisstence from Ms. Yuria Tahara. DAPI nuclear stain was applied.

Summary of OCR measurements

Cell imaging showed that cell size differs among the mutants when compared to wild type strain. The differences in cell size may explain varying OCR levels in mutants. Smaller cells (Δ*maa1* and Δ*gdh1*) have lower OCR, whereas bigger cells (Δ*coq5* and Δ*ilv3*) showed increased OCR. On the other hand, Δ*sod2*, which does not differ greatly from WT cell size, shows the most radical OCR decline among the seven mutants. The OCR measurement supports the vital role of Sod2 in N starvation survival. Of course, more future experimental measures are necessary to get a correct picture. In order to get more accurate readings, OCR results need to be normalized to the cell size, i.e. volume. Another approach may be to normalize the readings to the protein content which makes the OCR values easier to compare and thus, interpret.

4. Discussion

4.1. Mitochondria – The central hub for conserved N starvation survival

Based on this study's homology criteria 14 from 89 G0 essential (GZE) proteins qualify as highly conserved. A high portion of these highly conserved GZE 50% (7/14) are mitochondria-localized, whereas 42% (6/14) locate in the cytoplasm and only one conserved GZE protein is is situated in the nucleus. Above all, most of these conserved mitochondrial GZE proteins rank at the top among the homology candidates. Since the seven GZE proteins localize to the mitochondria, this study focused on the mitochondrial contribution in the regeneration from N starvation induced G0 phase. Phylogenetic profiles of the highly conserved mitochondria-localized GZE proteins are generated. Phylogenetic profiling has been claimed to be an efficient method for predicting protein function and potential functional relationships based on protein conservation (Pellegrini, 2012).Previous studies using BLAST approaches successfully described highly conserved pathways, such as glycolysis (Canback et al., 2002) and the TCA cycle (Cavalcanti et al., 2014). Phylogenetic profiling is based on the assumption that commonly shared mechanisms involve a set of conserved enzymes (Peregrin-Alvarez et al., 2009). Therefore, this study analyze the ancient relationship between the seven GZE conserved enzymes which are essential for the regenerative capability from quiescence. Since they share a common localiztion within the cell, which is the mitochondria, a mitochondrial role in N starvation survival is proposed.

Since mitochondrial origin was proposed to be prokaryotic (Yang et al., 1985) it seems reasonable that mitochondrial proteins are conserved in bacteria. However, this assumption may appear slightly simplistic. While it is true that a portion

of prokaryotic proteins was contained in the proto-mitochondrial structure, evolutionary time led to modifications within the mitochondria and host cells. In fact, several protein transfers between different cellular compartments and the mitochondrion is presumed to have taken place (Kurland and Andersson, 2000).

According to the latest pombase.org listing, less than half of the mitochondrial proteome is bacterially conserved. The remaining proteins are either *S. pombe* specific or conserved between eukaryotes only. Overall, there are 980 *S. pombe* proteins, which are conserved in bacteria, and only 301 of these localize to the mitochondria (**Figure 4.1.**) which rejects the assumption that bacterially conserved proteins are predominantly found in the mitochondria. When compared to the whole *S. pombe* conserved proteome, the GZE protein proportion is around 1.5% which is nearly similar to the cytoplasmic/nuclear GZE proportion (1.2%). In mitochondria, on the other hand, the proportion of conserved GZE is 2.3%, nearly double of that found outside the mitochondrion.

The percentage among GZE proteins with high conservation to prokaryotes is relatively low (16%). This is in contrast to the nearly 60% of GZE protein alignments against human sequences which fulfill this study's homology criteria. In fact, G0 survival seems to be an evolutionary 'modern' process. Nevertheless, the few bacterially conserved GZE may promote ancient reactions which were shown to be essential for G0 survival (Sajiki et al., publication in progress). Nevertheless, ancient reactions may be still active contributing to N starvation regeneration. The predominantly localize to the mitochondria.

These mitochondrial reactions, which are assumed to contribute to the ancient N starvation survival mechanism, can be categorized into three groups based on their function:

Superoxide scavenging, electron transfer-associated and amino acid biosynthetic enzymes. An overview of the functional involvement is presented in **Figure 4.2**.

Four out of the mitochondria-localized GZE are amino acid biosynthetic. According to pombase.org (Wood et al., 2012) around 82% (14/17) of the conserved amino acid biosynthetic enzymes in the mitochondria are involved in biosynthetic steps contributing to either branched-chain amino acids (BCAAs), lysine, aspartate or glutamate. there are 17 bacterially conserved amino acid biosynthetic enzymes which include both GZE and non-GZE proteins. It is of interest that each of the four amino acid biosynthetic GZE enzymes contributes to one of these four amino

acid groups. This finding stresses the mitochondrion as an ancient hub for amino acid biosynthetic pathways. Also, it supports the importance of the seven GZE enzymes which are likely involved in the regulation of these ancient processes. Therefore, the accumulation of highly conserved GZE proteins in mitochondria may not be merely due to the prokaryotic origin of the mitochondria. It may be based on functional context.

The pattern of viability decrease upon four-week-long N starvation differs among the functional categories which may be a hint that these three groups may be involved in three independent processes. In fact, it was suggested that proteins with same phylogenetic profiles may show the same phenotypic effect since their function depends on each other (Pellegrini, 2012). In fact, wild type *S. pombe* is able to survive N starved conditions for more than three months, i.e. 12 weeks.

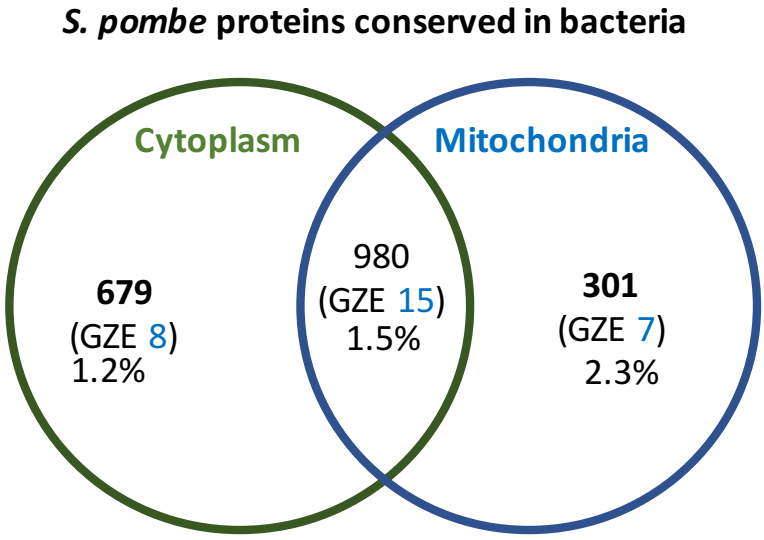

Figure 4.1. Cellular localization of *S. pombe* proteins conserved in bacteria. Based on information obtained from pombase.org (Wood *et al.,* 2012), around 980 *S. pombe* proteins are conserved in bacteria. Around a third of these localize to the mitochondria, the rest is distributed throughout the cell in different compartments. Information retrieved 10th October 2017 from pombase.org (Wood *et al*., 2012). This study identified 15 conserved GZE proteins. Nevertheless, 14 fitted into the criteria of highly conserved GZE proteins.

N starvation survival makes the cell more resistant to stresses (Su et al., 1996). It usually takes more than a single deletion mutation to disturb the G0 survival process (Sajiki *et al*., publication in progress). This may be due to compensatory mechanisms. Therefore, the viability decrease following the four weeks of N starvation, as seen in the seven deletion mutants is considered of significance. The most rapid viability loss was observed in Δ*sod2* strain, whereas in the remaining six, viability decreased considerably slower in the course of the four-week long N incubation. In contrast, amino acid biosynthetic enzymes suffer from diminished viability around the mid-point of N starvation.

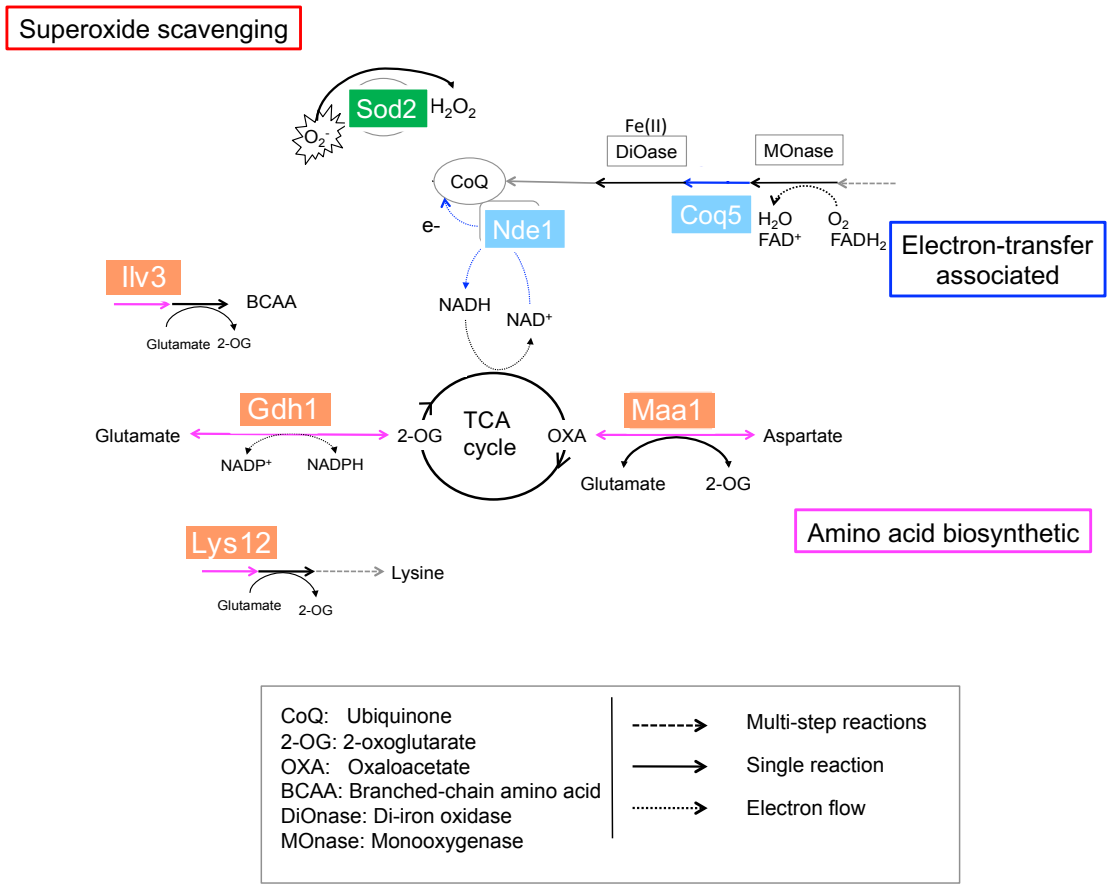

Figure 4.2. Overview of ancient N starvation reactions. Sod2 is an essential protein whose primary role is scavenging of superoxide. NADH dehydrogenase Nde1 is assumed to be involved in replenishing redox cofactor NAD+ to drive TCA cycle functions. Coq5 activity may be responsive to changes in oxygen levels. In fact, the upstream protein Coq6, a monooxygenase, produces Coq5 substrate by using oxygen, it catalyzes an oxygen-limited reaction. Ilv3 contains a highly oxygen-sensitive redox center (4Fe-4S). Its activity may be switched-off by an increase in oxygen level. Its inactivation may re-model branched-chain amino acid (BCAA) biosynthetic flux. Maa1 and Gdh1 are TCA cycle associated enzymes which directly supply compounds into the cycle.

Importance of amino acid pool synthesis and maintenance

It is likely that these four amino acid biosynthetic enzymes are essential for generating sufficient level of amino acids. Therefore, the level of amino acids generated during vegetative state contributes to the starvation survival by promoting N compound recycling pathways (Takeda et al., 2010). In this way the scarce intracellular N pool is re-distributed during quiescence (Sajiki et al., 2013). The phenomenon of N-sparing was observed in the microalgae *Chlamydomonas reinhardtii* under N starvation (Schmollinger et al., 2014). In this process heavily N-loaded amino acids, such as arginine, histidine and proline etc., into more favorable, 'N-lighter' ones. Extensive metabolome studies exist in the microalgae such as *C. reinhardtii* (Valledor et al., 2014) or diatom species (Hockin et al., 2012, Levitan et al., 2015) which support the importance of TCA cycle during N starvation. Gdh1 and Maa1 catalyze reactions by using the TCA cycle compounds 2-oxoglutarate and oxaloacetate, respectively. In fact, it was reported that TCA cycle and glutamate dehydrogenase activities were increased within 6-24h of N starvation (Park et al., 2015). Aspartate aminotransferase function, on the other hand, was increased in the initial time of N starvation (0-4h) but had decreased in the course of incubation in -N which suggests different time points of action. Also, levels of certain TCA cycle enzymes, such as isocitrate dehydrogenase isoforms Idp1and Idh1/2, fluctuate depending on the growth conditions (Marguerat et al., 2012).. Protein abundance data suggest that part of TCA cycle reactions is active under specific conditions such as N starvation.

However, if the cell fails to maintain an appropriate level of amino acids during vegetative growth, the recycling output during times of scarcity is assumed to

fail in reaching full capacity to promote viability. One example may be lysine which is an essential constituent of ribosomes. In *E. coli* lysine, arginine and glutamate, the latter two are highly N rich, are predominantly incorporated into ribosomes (Spahr, 1962). During amino acid scarcity ribosomes are selectively degraded in order to replenish the low amino acid pools. This a process of ribosomal degradation upon starvation was widely reported (Kraft et al., 2008, Durfee et al., 2008). Unlike in *S. pombe*, *E. coli* does not have a protein degradation machinery but relies on proteases which degrade ribosomes during nitrogen starvation (Kuroda et al., 2001). Besides lysine, levels of branched-chain amino acids were reported to be critical for starvation response activation in prokaryotes (Shivers and Sonenshein, 2004, Tojo et al., 2008). Since Ilv3 is a redox protein, due to its iron-sulfur clusters [4Fe-4S], it is likely to be affected by oxygen by-products. Therefore, it was suggested to serve as a

potential oxidative switch (Flint et al., 1993, Henard et al., 2010). In fact, this study reports that OCR appears unchanged upon G0 phase in wild type. This finding suggests that oxygen-consuming reactions are still active upon G0 conditions. It seems that failure to promote these oxygen-consuming processes have grave impact on regenerative ability following N starvation. The effect was observed in Δ*sod2* which had abolished OCR and also the most radical viability loss upon G0 phase. What is important to stress is that respiration in *S. pombe* was not observed in rich media but in minimal medium EMM2+N. So what is the role of respiratory reactions for N starvation survival?

Role of respiration under EMM2+N – Potential link to amino acid biosynthesis?

One essential hint, which may explain the difference in respiratory behavior under rich and minimal media, is that EMM2+N media are not supplemented with amino acids which need to be actively synthesized. *S. pombe* tends to generate energy by fermentation at vegetative state in EMM2+N. Why the need for respiration then? Respiration in EMM2+N with plenty of glucose was shown to be dispensible (Takeda et al., 2015) due to preference for fermentation. Nevertheless, it was reported that respiratory chain enzymes are essential for growth in EMM2+N (Malecki et al., 2016). In fact, treatment with respiratory chain inhibitory drug antimycin A led to slower growth in EMM2+N conditions, but was irrelevant in growth on rich media. Depletion of aspartate aminotransferase was reported to lead to a slower cell growth in bacteria (Liu et al., 2014). In fact, aspartate was shown be involved in regulating cell cycle which stresses the importance of an appropriate amino acid pool for growth and survival. Since EMM2+N lacks amino acids, a possible explanation for respiratory need may be the requirement of *S. pombe* to synthesize amino acids from ammonium chloride (**Figure 4.3).** This argues for a new function of respiratory reactions as the driving force of amino acid biosynthetic processes.

Among the seven, the two GZE enzymes Coq5 and Nde1 are associated with redox reactions supporting the respiratory chain. It was reported that alternative NADH dehydrogenases, found in fungi and plants but not in humans, are involved in oxidative stress management rather than ATP production (Voulgaris et al., 2012). In *S. cerevisiae*, the distant cousin of *S. pombe,* alternative NADH dehydrogenases homologous to *S. pombe* Nde1, are thought to be linked to maintaining the ratio of the redox couple $NADH/NAD^+$ (Vemuri et al., 2007). Based on these findings we suggest the role of

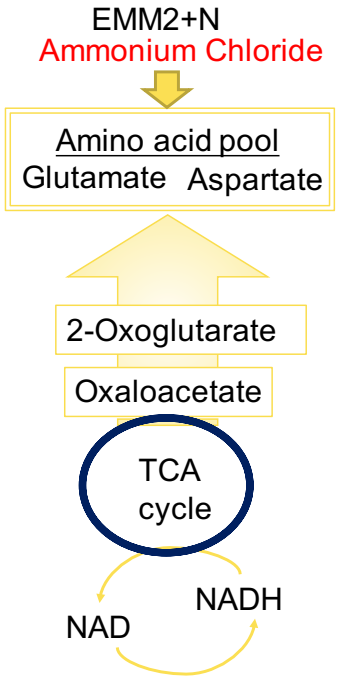

Figure 4.3 Amino acid pool generating mechanism. Possible mechanism driving amino acid biosynthesis during incubation in minimal medium EMM2 which contains only ammonium chloride as sole N source. Since no amino acids are included in EMM2+N medium, the cell needs to generate amino acids *de novo* from assimilated ammonium chloride. The TCA cycle compound 2-oxoglutarate is necessary to generate glutamate which is needed for reactions contributing to other amino acids. Also, TCA compound oxaloacetate is necessary to generate aspartate which contributes to various N compounds such as urea and nucleotides.

Nde1 is important for recycling the cofactor NADH into the oxidized form NAD+ to drive processes such as the TCA cycle. It is likely that the ratio of redox factors modulates metabolic flux. For example, it is known that NADH acts as an allosteric effector affecting activity of pyruvate dehydrogenase and other TCA cycle enzymes (Berg, 2002).

Coq5, on the other hand, is indirectly linked to respiratory chain since it is involved in the pathway which generates the electron acceptor ubiquinone. In the

biosynthetic chain, Coq5 is preceded by a yet unknown monooxygenase which consumes oxygen to generate the Coq5 substrate (Ozeir et al., 2011). Also, a di-iron oxygenase uses the Coq5 generated compound in the last step of ubiquinone synthesis (Stenmark et al., 2001). Coq5 is therefore surrounded by redox active enzymes which may affect Coq5 activity upon changes in oxygen levels.

4.1. Conclusion

This study generated phylogenetic profiles of seven conserved mitochondria-localized proteins which were shown to be required for efficient N starvation regeneration in *S. pombe*. According to the literature results these seven G0 essential (GZE) proteins can be divided into three functional groups which is also experimentally supported by time point of viability decrease. This study mentions evidence that GZE may be involved in promoting and maintaining a sufficient pool of lysine, BCAAs, glutamate and aspartate. Consequently, due to their common localization, the main biosynthetic hub for the amino acid pool appears to be situated in the mitochondria. Also, redox-driven and oxygen-consuming reactions need to be active to survive quiescence. Among the seven GZE, only mitochondrial superoxide dismutase Sod2 depletion radically affected oxygen consumption rates in the mutant strain which may be a cause for the rapid viability loss upon N starvation. However, more experimental evidence is needed to support this study's findings. Mass-spectroscopic approach, for instance, may serve to clarify whether amino acid levels are changed or whether levels of compounds, such as oxoglutarate or oxaloacetate, which are used as substrates in biosynthetic pathways, are affected in the specified GZE mutants. Most importantly, understanding Sod2's role in oxygen consumption may be the next approach.

5. References

AGRAWAL, A., BRENDEL, V. P. & HUANG, X. 2008. Pairwise statistical significance and empirical determination of effective gap opening penalties for protein local sequence alignment. *Int J Comput Biol Drug Des,* 1**,** 347-67.

ARAVIND, L., WATANABE, H., LIPMAN, D. J. & KOONIN, E. V. 2000. Lineage-specific loss and divergence of functionally linked genes in eukaryotes. *Proc Natl Acad Sci U S A,* 97**,** 11319-24.

AUGENLICHT, L. H. & BASERGA, R. 1974. Changes in the G0 state of WI-38 fibroblasts at different times after confluence. *Exp Cell Res,* 89**,** 255-62.

BAHLER, J., WU, J. Q., LONGTINE, M. S., SHAH, N. G., MCKENZIE, A., 3RD, STEEVER, A. B., WACH, A., PHILIPPSEN, P. & PRINGLE, J. R. 1998. Heterologous modules for efficient and versatile PCR-based gene targeting in Schizosaccharomyces pombe. *Yeast,* 14**,** 943-51.

BARKOVICH, R. J., SHTANKO, A., SHEPHERD, J. A., LEE, P. T., MYLES, D. C., TZAGOLOFF, A. & CLARKE, C. F. 1997. Characterization of the COQ5 gene from Saccharomyces cerevisiae. Evidence for a C-methyltransferase in ubiquinone biosynthesis. *J Biol Chem,* 272**,** 9182-8.

BENSON, D. A., KARSCH-MIZRACHI, I., LIPMAN, D. J., OSTELL, J. & WHEELER, D. L. 2004. GenBank: update. *Nucleic Acids Res,* 32**,** D23-6.

BENSON, D. A., KARSCH-MIZRACHI, I., LIPMAN, D. J., OSTELL, J. & WHEELER, D. L. 2005. GenBank. *Nucleic Acids Res,* 33**,** D34-8.

BERG, J. M. T., J.L.; STYRER L. 2002. Entry to the Citric Acid Cycle and Metabolism Through It Are Controlled. *Biochemistry.* 5th ed. New York: WH Freeman & Co.

BERMAN, H. M., WESTBROOK, J., FENG, Z., GILLILAND, G., BHAT, T. N., WEISSIG, H., SHINDYALOV, I. N. & BOURNE, P. E. 2000. The Protein Data Bank. *Nucleic Acids Res,* 28**,** 235-42.

BLACK, J. G. 2011. Characteristics of Prokaryotic and Eukaryotic Cells. *Microbiology: Principles and Explorations.* New York: John Willey & Sons.

BLATTNER, F. R., PLUNKETT, G., 3RD, BLOCH, C. A., PERNA, N. T., BURLAND, V., RILEY, M., COLLADO-VIDES, J., GLASNER, J. D., RODE, C. K., MAYHEW, G. F., GREGOR, J., DAVIS, N. W., KIRKPATRICK, H. A., GOEDEN, M. A., ROSE, D. J., MAU, B. & SHAO, Y. 1997. The complete genome sequence of Escherichia coli K-12. *Science,* 277**,** 1453-62.

BORGSTAHL, G. E., PARGE, H. E., HICKEY, M. J., BEYER, W. F., JR., HALLEWELL, R. A. & TAINER, J. A. 1992. The structure of human mitochondrial manganese superoxide dismutase reveals a novel tetrameric interface of two 4-helix bundles. *Cell,* 71**,** 107-18.

BORGSTAHL, G. E., POKROSS, M., CHEHAB, R., SEKHER, A. & SNELL, E. H. 2000. Cryo-trapping the six-coordinate, distorted-octahedral active site of manganese superoxide dismutase. *J Mol Biol,* 296**,** 951-9.

BREN, A., PARK, J. O., TOWBIN, B. D., DEKEL, E., RABINOWITZ, J. D. & ALON, U. 2016. Glucose becomes one of the worst carbon sources for E.coli on poor nitrogen sources due to suboptimal levels of cAMP. *Sci Rep,* 6**,** 24834.

BUI, N. K., GRAY, J., SCHWARZ, H., SCHUMANN, P., BLANOT, D. & VOLLMER, W. 2009. The peptidoglycan sacculus of Myxococcus xanthus has unusual

structural features and is degraded during glycerol-induced myxospore development. *J Bacteriol,* 191**,** 494-505.

BULFER, S. L., HENDERSHOT, J. M. & TRIEVEL, R. C. 2012. Crystal structure of homoisocitrate dehydrogenase from Schizosaccharomyces pombe. *Proteins,* 80**,** 661-6.

CANBACK, B., ANDERSSON, S. G. & KURLAND, C. G. 2002. The global phylogeny of glycolytic enzymes. *Proc Natl Acad Sci U S A,* 99**,** 6097-102.

CAVALCANTI, J. H., ESTEVES-FERREIRA, A. A., QUINHONES, C. G., PEREIRA-LIMA, I. A., NUNES-NESI, A., FERNIE, A. R. & ARAUJO, W. L. 2014. Evolution and functional implications of the tricarboxylic acid cycle as revealed by phylogenetic analysis. *Genome Biol Evol,* 6**,** 2830-48.

CHANDRA, G. & CHATER, K. F. 2014. Developmental biology of Streptomyces from the perspective of 100 actinobacterial genome sequences. *FEMS Microbiol Rev,* 38**,** 345-79.

CHATER, K. F. 1992. Streptomyces coelicolor: a Mycelial, Spore-Bearing Prokaryote. *Development: The molecular genetic Approach.* Berlin Heidelberg: Springer-Verlag Berlin Heidelberg.

CHEN, D., TOONE, W. M., MATA, J., LYNE, R., BURNS, G., KIVINEN, K., BRAZMA, A., JONES, N. & BAHLER, J. 2003. Global transcriptional responses of fission yeast to environmental stress. *Mol Biol Cell,* 14**,** 214-29.

CHUBUKOV, V. & SAUER, U. 2014. Environmental dependence of stationary-phase metabolism in Bacillus subtilis and Escherichia coli. *Appl Environ Microbiol,* 80**,** 2901-9.

CLAESSEN, D., ROZEN, D. E., KUIPERS, O. P., SOGAARD-ANDERSEN, L. & VAN WEZEL, G. P. 2014. Bacterial solutions to multicellularity: a tale of biofilms, filaments and fruiting bodies. *Nat Rev Microbiol,* 12**,** 115-24.

COSTELLO, G. R., L.; BEACH, D. 1986. Fission yeast enters the stationary phase G0 state from either mitotic G1 or G2. *Current Genetics,* 11**,** 119.

DAI, Y. N., ZHOU, K., CAO, D. D., JIANG, Y. L., MENG, F., CHI, C. B., REN, Y. M., CHEN, Y. & ZHOU, C. Z. 2014. Crystal structures and catalytic mechanism of the C-methyltransferase Coq5 provide insights into a key step of the yeast coenzyme Q synthesis pathway. *Acta Crystallogr D Biol Crystallogr,* 70**,** 2085-92.

DECOTTIGNIES, A., SANCHEZ-PEREZ, I. & NURSE, P. 2003. Schizosaccharomyces pombe essential genes: a pilot study. *Genome Res,* 13**,** 399-406.

DELUNA, A., AVENDANO, A., RIEGO, L. & GONZALEZ, A. 2001. NADP-glutamate dehydrogenase isoenzymes of Saccharomyces cerevisiae. Purification, kinetic properties, and physiological roles. *J Biol Chem,* 276**,** 43775-83.

DURFEE, T., HANSEN, A. M., ZHI, H., BLATTNER, F. R. & JIN, D. J. 2008. Transcription profiling of the stringent response in Escherichia coli. *J Bacteriol,* 190**,** 1084-96.

EISENER-DORMAN, A. F., LAWRENCE, D. A. & BOLIVAR, V. J. 2009. Cautionary insights on knockout mouse studies: the gene or not the gene? *Brain Behav Immun,* 23**,** 318-24.

ERRINGTON, J. 2013. L-form bacteria, cell walls and the origins of life. *Open Biol,* 3**,** 120143.

ESCAMILLA, J. E., BARQUERA, B., RAMIREZ, R., GARCIA-HORSMAN, A. & DEL ARENAL, P. 1988. Role of menaquinone in inactivation and activation of the Bacillus cereus forespore respiratory system. *J Bacteriol,* 170**,** 5908-12.

EVANS, T., ROSENTHAL, E. T., YOUNGBLOM, J., DISTEL, D. & HUNT, T. 1983. Cyclin: a protein specified by maternal mRNA in sea urchin eggs that is destroyed at each cleavage division. *Cell,* 33**,** 389-96.

FANTES, P. & NURSE, P. 1977. Control of cell size at division in fission yeast by a growth-modulated size control over nuclear division. *Exp Cell Res,* 107**,** 377-86.

FANTES, P. A. & NURSE, P. 1978. Control of the timing of cell division in fission yeast. Cell size mutants reveal a second control pathway. *Exp Cell Res,* 115**,** 317-29.

FENG, Y., LI, W., LI, J., WANG, J., GE, J., XU, D., LIU, Y., WU, K., ZENG, Q., WU, J. W., TIAN, C., ZHOU, B. & YANG, M. 2012. Structural insight into the type-II mitochondrial NADH dehydrogenases. *Nature,* 491**,** 478-82.

FLINT, D. H., EMPTAGE, M. H., FINNEGAN, M. G., FU, W. & JOHNSON, M. K. 1993a. The role and properties of the iron-sulfur cluster in Escherichia coli dihydroxy-acid dehydratase. *J Biol Chem,* 268**,** 14732-42.

FLINT, D. H., TUMINELLO, J. F. & EMPTAGE, M. H. 1993b. The inactivation of Fe-S cluster containing hydro-lyases by superoxide. *J Biol Chem,* 268**,** 22369-76.

FONDI, M., BRILLI, M., EMILIANI, G., PAFFETTI, D. & FANI, R. 2007. The primordial metabolism: an ancestral interconnection between leucine, arginine, and lysine biosynthesis. *BMC Evol Biol,* 7 Suppl 2**,** S3.

GARDNER, M. J., HALL, N., FUNG, E., WHITE, O., BERRIMAN, M., HYMAN, R. W., CARLTON, J. M., PAIN, A., NELSON, K. E., BOWMAN, S., PAULSEN, I. T., JAMES, K., EISEN, J. A., RUTHERFORD, K., SALZBERG, S. L., CRAIG, A., KYES, S., CHAN, M. S., NENE, V., SHALLOM, S. J., SUH, B., PETERSON, J., ANGIUOLI, S., PERTEA, M., ALLEN, J., SELENGUT, J., HAFT, D., MATHER, M. W., VAIDYA, A. B., MARTIN, D. M., FAIRLAMB, A. H., FRAUNHOLZ, M. J., ROOS, D. S., RALPH, S. A., MCFADDEN, G. I., CUMMINGS, L. M., SUBRAMANIAN, G. M., MUNGALL, C., VENTER, J. C., CARUCCI, D. J., HOFFMAN, S. L., NEWBOLD, C., DAVIS, R. W., FRASER, C. M. & BARRELL, B. 2002. Genome sequence of the human malaria parasite Plasmodium falciparum. *Nature,* 419**,** 498-511.

GIANNELLA, R. A. 1996. Salmonella. *In:* BARON, S. (ed.) *Medical Microbiology.* 4th ed. Galveston (TX): University of Texas Medical Branch at Galveston.

GONZALEZ-MARISCAL, I., GARCIA-TESTON, E., PADILLA, S., MARTIN-MONTALVO, A., POMARES VICIANA, T., VAZQUEZ-FONSECA, L., GANDOLFO DOMINGUEZ, P. & SANTOS-OCANA, C. 2014. The regulation of coenzyme q biosynthesis in eukaryotic cells: all that yeast can tell us. *Mol Syndromol,* 5**,** 107-18.

HAGAN, I. M., GRALLERT, A. & SIMANIS, V. 2016. Analysis of the Schizosaccharomyces pombe Cell Cycle. *Cold Spring Harb Protoc,* 2016**,** pdb top082800.

HAJJ CHEHADE, M., LOISEAU, L., LOMBARD, M., PECQUEUR, L., ISMAIL, A., SMADJA, M., GOLINELLI-PIMPANEAU, B., MELLOT-DRAZNIEKS, C., HAMELIN, O., AUSSEL, L., KIEFFER-JAQUINOD, S., LABESSAN, N., BARRAS, F., FONTECAVE, M. & PIERREL, F. 2013. ubiI, a new gene in Escherichia coli coenzyme Q biosynthesis, is involved in aerobic C5-hydroxylation. *J Biol Chem,* 288**,** 20085-92.

HALSEY, C. R., LEI, S., WAX, J. K., LEHMAN, M. K., NUXOLL, A. S., STEINKE, L., SADYKOV, M., POWERS, R. & FEY, P. D. 2017. Amino Acid Catabolism in

Staphylococcus aureus and the Function of Carbon Catabolite Repression. *MBio,* 8.

HAMBURGER, K., ; KRAMHOFT, B. 1982. Respiration and fermentation during growth and starvation in the fission yeast, Schizosaccharomyces pombe. *Carlsberg Research Communications,* 47.

HARTWELL, L. H. & WEINERT, T. A. 1989. Checkpoints: controls that ensure the order of cell cycle events. *Science,* 246**,** 629-34.

HAURYLIUK, V., ATKINSON, G. C., MURAKAMI, K. S., TENSON, T. & GERDES, K. 2015. Recent functional insights into the role of (p)ppGpp in bacterial physiology. *Nat Rev Microbiol,* 13**,** 298-309.

HAYASHI, A., DING, D. Q., TSUTSUMI, C., CHIKASHIGE, Y., MASUDA, H., HARAGUCHI, T. & HIRAOKA, Y. 2009. Localization of gene products using a chromosomally tagged GFP-fusion library in the fission yeast Schizosaccharomyces pombe. *Genes Cells,* 14**,** 217-25.

HAYASHI, T., FUJITA, Y., IWASAKI, O., ADACHI, Y., TAKAHASHI, K. & YANAGIDA, M. 2004. Mis16 and Mis18 are required for CENP-A loading and histone deacetylation at centromeres. *Cell,* 118**,** 715-29.

HAYASHI, T., HATANAKA, M., NAGAO, K., NAKASEKO, Y., KANOH, J., KOKUBU, A., EBE, M. & YANAGIDA, M. 2007. Rapamycin sensitivity of the Schizosaccharomyces pombe tor2 mutant and organization of two highly phosphorylated TOR complexes by specific and common subunits. *Genes Cells,* 12**,** 1357-70.

HENARD, C. A., BOURRET, T. J., SONG, M. & VAZQUEZ-TORRES, A. 2010. Control of redox balance by the stringent response regulatory protein promotes antioxidant defenses of Salmonella. *J Biol Chem,* 285**,** 36785-93.

HOCKIN, N. L., MOCK, T., MULHOLLAND, F., KOPRIVA, S. & MALIN, G. 2012. The response of diatom central carbon metabolism to nitrogen starvation is different from that of green algae and higher plants. *Plant Physiol,* 158**,** 299-312.

HOFFMAN, C. S., WOOD, V. & FANTES, P. A. 2016. Corrigendum. An Ancient Yeast for Young Geneticists: A Primer on the Schizosaccharomyces pombe Model System. *Genetics,* 202**,** 1241.

HSIEH, E. J., DINOSO, J. B. & CLARKE, C. F. 2004. A tRNA(TRP) gene mediates the suppression of cbs2-223 previously attributed to ABC1/COQ8. *Biochem Biophys Res Commun,* 317**,** 648-53.

HUDSON, A. O. S., M.A.; PEARCE, F.G.; DOBSON, R.C.J 2017. Lysine biosynthesis in microorganisms. *In:* D'MELLO, J. P. F. D. (ed.) *The Handbook of Microbial Metabolism of Amino acids.* UK, USA: CABI international.

IGLEWSKI, B. H. 1996. Pseudomonas. *In:* BARON, S. (ed.) *Medical Microbiology.* 4th ed. Galveston (TX): University of Texas Medical Branch at Galveston.

IIDA, H. & YAHARA, I. 1984. Specific early-G1 blocks accompanied with stringent response in Saccharomyces cerevisiae lead to growth arrest in resting state similar to the G0 of higher eucaryotes. *J Cell Biol,* 98**,** 1185-93.

JEFFERY, C. J., GLOSS, L. M., PETSKO, G. A. & RINGE, D. 2000. The role of residues outside the active site: structural basis for function of C191 mutants of Escherichia coli aspartate aminotransferase. *Protein Eng,* 13**,** 105-12.

JEONG, J. H., KWON, E. S. & ROE, J. H. 2001. Characterization of the manganese-containing superoxide dismutase and its gene regulation in stress response

of Schizosaccharomyces pombe. *Biochem Biophys Res Commun,* 283**,** 908-14.

JIA, Y., TOMITA, T., YAMAUCHI, K., NISHIYAMA, M. & PALMER, D. R. 2006. Kinetics and product analysis of the reaction catalysed by recombinant homoaconitase from Thermus thermophilus. *Biochem J,* 396**,** 479-85.

KANEHISA, M. & GOTO, S. 2000. KEGG: kyoto encyclopedia of genes and genomes. *Nucleic Acids Res,* 28**,** 27-30.

KANEKO, T., SATO, S., KOTANI, H., TANAKA, A., ASAMIZU, E., NAKAMURA, Y., MIYAJIMA, N., HIROSAWA, M., SUGIURA, M., SASAMOTO, S., KIMURA, T., HOSOUCHI, T., MATSUNO, A., MURAKI, A., NAKAZAKI, N., NARUO, K., OKUMURA, S., SHIMPO, S., TAKEUCHI, C., WADA, T., WATANABE, A., YAMADA, M., YASUDA, M. & TABATA, S. 1996. Sequence analysis of the genome of the unicellular cyanobacterium Synechocystis sp. strain PCC6803. II. Sequence determination of the entire genome and assignment of potential protein-coding regions (supplement). *DNA Res,* 3**,** 185-209.

KENSCHE, P. R., VAN NOORT, V., DUTILH, B. E. & HUYNEN, M. A. 2008. Practical and theoretical advances in predicting the function of a protein by its phylogenetic distribution. *J R Soc Interface,* 5**,** 151-70.

KIM, S. & LEE, S. B. 2006. Catalytic promiscuity in dihydroxy-acid dehydratase from the thermoacidophilic archaeon Sulfolobus solfataricus. *J Biochem,* 139**,** 591-6.

KOHDA, T. A., TANAKA, K., KONOMI, M., SATO, M., OSUMI, M. & YAMAMOTO, M. 2007. Fission yeast autophagy induced by nitrogen starvation generates a nitrogen source that drives adaptation processes. *Genes Cells,* 12**,** 155-70.

KOTARU, A., R.; JOSHI, R.C. 2009. Classification of phylogenetic profiles for protein function prediction: An SVM approach. *In:* RANKA, S. (ed.) *Contemporary Computing.* Berlin, Heidelberg: Springer.

KRAFT, C., DEPLAZES, A., SOHRMANN, M. & PETER, M. 2008. Mature ribosomes are selectively degraded upon starvation by an autophagy pathway requiring the Ubp3p/Bre5p ubiquitin protease. *Nat Cell Biol,* 10**,** 602-10.

KRISTELL, C., ORZECHOWSKI WESTHOLM, J., OLSSON, I., RONNE, H., KOMOROWSKI, J. & BJERLING, P. 2010. Nitrogen depletion in the fission yeast Schizosaccharomyces pombe causes nucleosome loss in both promoters and coding regions of activated genes. *Genome Res,* 20**,** 361-71.

KUMAR, R. & SHIMIZU, K. 2010. Metabolic regulation of Escherichia coli and its gdhA, glnL, gltB, D mutants under different carbon and nitrogen limitations in the continuous culture. *Microb Cell Fact,* 9**,** 8.

KUNST, F., OGASAWARA, N., MOSZER, I., ALBERTINI, A. M., ALLONI, G., AZEVEDO, V., BERTERO, M. G., BESSIERES, P., BOLOTIN, A., BORCHERT, S., BORRISS, R., BOURSIER, L., BRANS, A., BRAUN, M., BRIGNELL, S. C., BRON, S., BROUILLET, S., BRUSCHI, C. V., CALDWELL, B., CAPUANO, V., CARTER, N. M., CHOI, S. K., CORDANI, J. J., CONNERTON, I. F., CUMMINGS, N. J., DANIEL, R. A., DENZIOT, F., DEVINE, K. M., DUSTERHOFT, A., EHRLICH, S. D., EMMERSON, P. T., ENTIAN, K. D., ERRINGTON, J., FABRET, C., FERRARI, E., FOULGER, D., FRITZ, C., FUJITA, M., FUJITA, Y., FUMA, S., GALIZZI, A., GALLERON, N., GHIM, S. Y., GLASER, P., GOFFEAU, A., GOLIGHTLY, E. J., GRANDI, G., GUISEPPI, G., GUY, B. J., HAGA, K., HAIECH, J., HARWOOD, C. R., HENAUT, A., HILBERT, H., HOLSAPPEL, S., HOSONO, S., HULLO, M. F., ITAYA, M., JONES, L., JORIS, B., KARAMATA, D., KASAHARA, Y., KLAERR-

BLANCHARD, M., KLEIN, C., KOBAYASHI, Y., KOETTER, P., KONINGSTEIN, G., KROGH, S., KUMANO, M., KURITA, K., LAPIDUS, A., LARDINOIS, S., LAUBER, J., LAZAREVIC, V., LEE, S. M., LEVINE, A., LIU, H., MASUDA, S., MAUEL, C., MEDIGUE, C., MEDINA, N., MELLADO, R. P., MIZUNO, M., MOESTL, D., NAKAI, S., NOBACK, M., NOONE, D., O'REILLY, M., OGAWA, K., OGIWARA, A., OUDEGA, B., PARK, S. H., PARRO, V., POHL, T. M., PORTELLE, D., PORWOLLIK, S., PRESCOTT, A. M., PRESECAN, E., PUJIC, P., PURNELLE, B., et al. 1997. The complete genome sequence of the gram-positive bacterium Bacillus subtilis. *Nature,* 390**,** 249-56.

KURLAND, C. G. & ANDERSSON, S. G. 2000. Origin and evolution of the mitochondrial proteome. *Microbiol Mol Biol Rev,* 64**,** 786-820.

KURODA, A., NOMURA, K., OHTOMO, R., KATO, J., IKEDA, T., TAKIGUCHI, N., OHTAKE, H. & KORNBERG, A. 2001. Role of inorganic polyphosphate in promoting ribosomal protein degradation by the Lon protease in E. coli. *Science,* 293**,** 705-8.

LAL, P. B., SCHNEIDER, B. L., VU, K. & REITZER, L. 2014. The redundant aminotransferases in lysine and arginine synthesis and the extent of aminotransferase redundancy in Escherichia coli. *Mol Microbiol,* 94**,** 843-56.

LANCIEN, M., GADAL, P. & HODGES, M. 2000. Enzyme redundancy and the importance of 2-oxoglutarate in higher plant ammonium assimilation. *Plant Physiol,* 123**,** 817-24.

LARKIN, M. A., BLACKSHIELDS, G., BROWN, N. P., CHENNA, R., MCGETTIGAN, P. A., MCWILLIAM, H., VALENTIN, F., WALLACE, I. M., WILM, A., LOPEZ, R., THOMPSON, J. D., GIBSON, T. J. & HIGGINS, D. G. 2007. Clustal W and Clustal X version 2.0. *Bioinformatics,* 23**,** 2947-8.

LEE, P. T., HSU, A. Y., HA, H. T. & CLARKE, C. F. 1997. A C-methyltransferase involved in both ubiquinone and menaquinone biosynthesis: isolation and identification of the Escherichia coli ubiE gene. *J Bacteriol,* 179**,** 1748-54.

LEE, Y. J., KIM, K. J., KANG, H. Y., KIM, H. R. & MAENG, P. J. 2012. Involvement of GDH3-encoded NADP+-dependent glutamate dehydrogenase in yeast cell resistance to stress-induced apoptosis in stationary phase cells. *J Biol Chem,* 287**,** 44221-33.

LEISTLER, B., HEROLD, M. & KIRSCHNER, K. 1992. Collapsed intermediates in the reconstitution of dimeric aspartate aminotransferase from Escherichia coli. *Eur J Biochem,* 205**,** 603-11.

LEVITAN, O., DINAMARCA, J., ZELZION, E., LUN, D. S., GUERRA, L. T., KIM, M. K., KIM, J., VAN MOOY, B. A., BHATTACHARYA, D. & FALKOWSKI, P. G. 2015. Remodeling of intermediate metabolism in the diatom Phaeodactylum tricornutum under nitrogen stress. *Proc Natl Acad Sci U S A,* 112**,** 412-7.

LIU, F., QIMUGE, HAO, J., YAN, H., BACH, T., FAN, L. & MORIGEN 2014. AspC-mediated aspartate metabolism coordinates the Escherichia coli cell cycle. *PLoS One,* 9**,** e92229.

LIU, M. & LU, S. 2016. Plastoquinone and Ubiquinone in Plants: Biosynthesis, Physiological Function and Metabolic Engineering. *Front Plant Sci,* 7**,** 1898.

LUKAS, H., REIMANN, J., KIM, O. B., GRIMPO, J. & UNDEN, G. 2010. Regulation of aerobic and anaerobic D-malate metabolism of Escherichia coli by the LysR-type regulator DmlR (YeaT). *J Bacteriol,* 192**,** 2503-11.

LUTTIK, M. A., OVERKAMP, K. M., KOTTER, P., DE VRIES, S., VAN DIJKEN, J. P. & PRONK, J. T. 1998. The Saccharomyces cerevisiae NDE1 and NDE2 genes encode separate mitochondrial NADH dehydrogenases catalyzing the oxidation of cytosolic NADH. *J Biol Chem,* 273**,** 24529-34.

MALECKI, M., BITTON, D. A., RODRIGUEZ-LOPEZ, M., RALLIS, C., CALAVIA, N. G., SMITH, G. C. & BAHLER, J. 2016. Functional and regulatory profiling of energy metabolism in fission yeast. *Genome Biol,* 17**,** 240.

MALIK, R. & VIOLA, R. E. 2010. Structural characterization of tartrate dehydrogenase: a versatile enzyme catalyzing multiple reactions. *Acta Crystallogr D Biol Crystallogr,* 66**,** 673-84.

MARGUERAT, S., SCHMIDT, A., CODLIN, S., CHEN, W., AEBERSOLD, R. & BAHLER, J. 2012. Quantitative analysis of fission yeast transcriptomes and proteomes in proliferating and quiescent cells. *Cell,* 151**,** 671-83.

MASATAKA, S. 2014. The Family Shewanellaceae. *In:* ROSENBERG, E. D., E.F.,; LORY, S.; STACKEBRANDT, E.; THOMPSON, F. (ed.) *The Prokaryotes: Gammaproteobacteria.* Berlin Heidelberg: Springer Verlag.

MASUDA, F., ISHII, M., MORI, A., UEHARA, L., YANAGIDA, M., TAKEDA, K. & SAITOH, S. 2016. Glucose restriction induces transient G2 cell cycle arrest extending cellular chronological lifespan. *Sci Rep,* 6**,** 19629.

MATSUYAMA, A., ARAI, R., YASHIRODA, Y., SHIRAI, A., KAMATA, A., SEKIDO, S., KOBAYASHI, Y., HASHIMOTO, A., HAMAMOTO, M., HIRAOKA, Y., HORINOUCHI, S. & YOSHIDA, M. 2006. ORFeome cloning and global analysis of protein localization in the fission yeast Schizosaccharomyces pombe. *Nat Biotechnol,* 24**,** 841-7.

MCCLEARY, W. R., ESMON, B. & ZUSMAN, D. R. 1991. Myxococcus xanthus protein C is a major spore surface protein. *J Bacteriol,* 173**,** 2141-5.

MILLER, S. M. & MAGASANIK, B. 1991. Role of the complex upstream region of the GDH2 gene in nitrogen regulation of the NAD-linked glutamate dehydrogenase in Saccharomyces cerevisiae. *Mol Cell Biol,* 11**,** 6229-47.

MINAMBRES, B. O., E. R.; JENSEN, R. A, LUENGO, J. M. 2000. A new class of glutamate dehydrogenases (GDH). *J. of Bio. Chem.,* 275**,** 39529- 39542.

MIYAZAKI, J., ASADA, K., FUSHINOBU, S., KUZUYAMA, T. & NISHIYAMA, M. 2005. Crystal structure of tetrameric homoisocitrate dehydrogenase from an extreme thermophile, Thermus thermophilus: involvement of hydrophobic dimer-dimer interaction in extremely high thermotolerance. *J Bacteriol,* 187**,** 6779-88.

MIYAZAKI, K. 2005. Bifunctional isocitrate-homoisocitrate dehydrogenase: a missing link in the evolution of beta-decarboxylating dehydrogenase. *Biochem Biophys Res Commun,* 331**,** 341-6.

MOCHIDA, S. & YANAGIDA, M. 2006. Distinct modes of DNA damage response in S. pombe G0 and vegetative cells. *Genes Cells,* 11**,** 13-27.

MORENO-HAGELSIEB, G. & LATIMER, K. 2008. Choosing BLAST options for better detection of orthologs as reciprocal best hits. *Bioinformatics,* 24**,** 319-24.

MURRAY, A. W., SOLOMON, M. J. & KIRSCHNER, M. W. 1989. The role of cyclin synthesis and degradation in the control of maturation promoting factor activity. *Nature,* 339**,** 280-6.

MUSHER, D. M. 1996. Haemophilus Species. *In:* BARON, S. (ed.) *Medical Microbiology.* 4th ed. Galveston (TX): University of Texas Medical Branch at Galveston.

NAKASHIMA, A., HASEGAWA, T., MORI, S., UENO, M., TANAKA, S., USHIMARU, T., SATO, S. & URITANI, M. 2006. A starvation-specific serine protease gene, isp6+, is involved in both autophagy and sexual development in Schizosaccharomyces pombe. *Curr Genet,* 49**,** 403-13.

NARGANG, F. E. & RAPAPORT, D. 2007. Neurospora crassa as a model organism for mitochondrial biogenesis. *Methods Mol Biol,* 372**,** 107-23.

NISHIDA, H., NISHIYAMA, M., KOBASHI, N., KOSUGE, T., HOSHINO, T. & YAMANE, H. 1999. A prokaryotic gene cluster involved in synthesis of lysine through the amino adipate pathway: a key to the evolution of amino acid biosynthesis. *Genome Res,* 9**,** 1175-83.

NORBURY, C. J. & NURSE, P. 1989. Control of the higher eukaryote cell cycle by p34cdc2 homologues. *Biochim Biophys Acta,* 989**,** 85-95.

NURSE, P., THURIAUX, P. & NASMYTH, K. 1976. Genetic control of the cell division cycle in the fission yeast Schizosaccharomyces pombe. *Mol Gen Genet,* 146**,** 167-78.

OHTANI, N., TOMITA, M. & ITAYA, M. 2010. An extreme thermophile, Thermus thermophilus, is a polyploid bacterium. *J Bacteriol,* 192**,** 5499-505.

OLSZEWSKI, K. L. & LLINAS, M. 2011. Central carbon metabolism of Plasmodium parasites. *Mol Biochem Parasitol,* 175**,** 95-103.

OREN, A. 2002. Molecular ecology of extremely halophilic Archaea and Bacteria. *FEMS Microbiol Ecol,* 39**,** 1-7.

OVERKAMP, K. M., BAKKER, B. M., KOTTER, P., VAN TUIJL, A., DE VRIES, S., VAN DIJKEN, J. P. & PRONK, J. T. 2000. In vivo analysis of the mechanisms for oxidation of cytosolic NADH by Saccharomyces cerevisiae mitochondria. *J Bacteriol,* 182**,** 2823-30.

OZEIR, M., MUHLENHOFF, U., WEBERT, H., LILL, R., FONTECAVE, M. & PIERREL, F. 2011. Coenzyme Q biosynthesis: Coq6 is required for the C5-hydroxylation reaction and substrate analogs rescue Coq6 deficiency. *Chem Biol,* 18**,** 1134-42.

PARDEE, A. B. 1974. A restriction point for control of normal animal cell proliferation. *Proc Natl Acad Sci U S A,* 71**,** 1286-90.

PARK, J. J., WANG, H., GARGOURI, M., DESHPANDE, R. R., SKEPPER, J. N., HOLGUIN, F. O., JUERGENS, M. T., SHACHAR-HILL, Y., HICKS, L. M. & GANG, D. R. 2015. The response of Chlamydomonas reinhardtii to nitrogen deprivation: a systems biology analysis. *Plant J,* 81**,** 611-24.

PATTERSON, M. J. 1996. Streptococcus. *In:* BARON, S. (ed.) *Medical Microbiolohy.* 4th ed. Glveston (TX): University of Texas Medical Branch at Galveston.

PAVLOPOULOS, G. A., SOLDATOS, T. G., BARBOSA-SILVA, A. & SCHNEIDER, R. 2010. A reference guide for tree analysis and visualization. *BioData Min,* 3**,** 1.

PEARSON, W. R. 2013. An introduction to sequence similarity ("homology") searching. *Curr Protoc Bioinformatics,* Chapter 3**,** Unit3 1.

PELLEGRINI, M. 2012. Using phylogenetic profiles to predict functional relationships. *Methods Mol Biol,* 804**,** 167-77.

PEREGRIN-ALVAREZ, J. M., SANFORD, C. & PARKINSON, J. 2009. The conservation and evolutionary modularity of metabolism. *Genome Biol,* 10**,** R63.

PETTERSEN, E. F., GODDARD, T. D., HUANG, C. C., COUCH, G. S., GREENBLATT, D. M., MENG, E. C. & FERRIN, T. E. 2004. UCSF Chimera--a visualization system for exploratory research and analysis. *J Comput Chem,* 25**,** 1605-12.

PEVSNER, J. 2003. Pairwise sequence alignment. *Bioinformatics and Functional Genomics.* Hoboken, New Jerey: John Wiley & Sons.

POON, W. W., DAVIS, D. E., HA, H. T., JONASSEN, T., RATHER, P. N. & CLARKE, C. F. 2000. Identification of Escherichia coli ubiB, a gene required for the first monooxygenase step in ubiquinone biosynthesis. *J Bacteriol,* 182**,** 5139-46.

PORTA, J., VAHEDI-FARIDI, A. & BORGSTAHL, G. E. 2010. Structural analysis of peroxide-soaked MnSOD crystals reveals side-on binding of peroxide to active-site manganese. *J Mol Biol,* 399**,** 377-84.

RENVOISE, M., BONHOMME, L., DAVANTURE, M., VALOT, B., ZIVY, M. & LEMAIRE, C. 2014. Quantitative variations of the mitochondrial proteome and phosphoproteome during fermentative and respiratory growth in Saccharomyces cerevisiae. *J Proteomics,* 106**,** 140-50.

RITTERSHAUS, E. S., BAEK, S. H. & SASSETTI, C. M. 2013. The normalcy of dormancy: common themes in microbial quiescence. *Cell Host Microbe,* 13**,** 643-51.

ROST, B. 1999. Twilight zone of protein sequence alignments. *Protein Eng,* 12**,** 85-94.

ROSZAK, D. B. & COLWELL, R. R. 1987. Survival strategies of bacteria in the natural environment. *Microbiol Rev,* 51**,** 365-79.

ROUX, A. E., QUISSAC, A., CHARTRAND, P., FERBEYRE, G. & ROKEACH, L. A. 2006. Regulation of chronological aging in Schizosaccharomyces pombe by the protein kinases Pka1 and Sck2. *Aging Cell,* 5**,** 345-57.

RUSSELL, P. & NURSE, P. 1987. Negative regulation of mitosis by wee1+, a gene encoding a protein kinase homolog. *Cell,* 49**,** 559-67.

RYAN, C. J., ROGUEV, A., PATRICK, K., XU, J., JAHARI, H., TONG, Z., BELTRAO, P., SHALES, M., QU, H., COLLINS, S. R., KLIEGMAN, J. I., JIANG, L., KUO, D., TOSTI, E., KIM, H. S., EDELMANN, W., KEOGH, M. C., GREENE, D., TANG, C., CUNNINGHAM, P., SHOKAT, K. M., CAGNEY, G., SVENSSON, J. P., GUTHRIE, C., ESPENSHADE, P. J., IDEKER, T. & KROGAN, N. J. 2012. Hierarchical modularity and the evolution of genetic interactomes across species. *Mol Cell,* 46**,** 691-704.

SAITOH, S. & YANAGIDA, M. 2014. Does a shift to limited glucose activate checkpoint control in fission yeast? *FEBS Lett,* 588**,** 2373-8.

SAJIKI, K., HATANAKA, M., NAKAMURA, T., TAKEDA, K., SHIMANUKI, M., YOSHIDA, T., HANYU, Y., HAYASHI, T., NAKASEKO, Y. & YANAGIDA, M. 2009. Genetic control of cellular quiescence in S. pombe. *J Cell Sci,* 122**,** 1418-29.

SAJIKI, K., PLUSKAL, T., SHIMANUKI, M. & YANAGIDA, M. 2013. Metabolomic analysis of fission yeast at the onset of nitrogen starvation. *Metabolites,* 3**,** 1118-29.

SAKA, Y., FANTES, P., SUTANI, T., MCINERNY, C., CREANOR, J. & YANAGIDA, M. 1994. Fission yeast cut5 links nuclear chromatin and M phase regulator in the replication checkpoint control. *EMBO J,* 13**,** 5319-29.

SALDIVIA, M., CEBALLOS-PEREZ, G., BART, J. M. & NAVARRO, M. 2016. The AMPKalpha1 Pathway Positively Regulates the Developmental Transition from Proliferation to Quiescence in Trypanosoma brucei. *Cell Rep,* 17**,** 660-670.

SCHLACKOW, M., MARGUERAT, S., PROUDFOOT, N. J., BAHLER, J., ERBAN, R. & GULLEROVA, M. 2013. Genome-wide analysis of poly(A) site selection in Schizosaccharomyces pombe. *RNA,* 19**,** 1617-31.

SCHMOLLINGER, S., MUHLHAUS, T., BOYLE, N. R., BLABY, I. K., CASERO, D., METTLER, T., MOSELEY, J. L., KROPAT, J., SOMMER, F., STRENKERT, D., HEMME, D., PELLEGRINI, M., GROSSMAN, A. R., STITT, M., SCHRODA, M. & MERCHANT, S. S. 2014. Nitrogen-Sparing Mechanisms in Chlamydomonas Affect the Transcriptome, the Proteome, and Photosynthetic Metabolism. *Plant Cell,* 26**,** 1410-1435.

SHARKEY, M. A. & ENGEL, P. C. 2008. Apparent negative co-operativity and substrate inhibition in overexpressed glutamate dehydrogenase from Escherichia coli. *FEMS Microbiol Lett,* 281**,** 132-9.

SHARKEY, M. A., OLIVEIRA, T. F., ENGEL, P. C. & KHAN, A. R. 2013. Structure of NADP(+)-dependent glutamate dehydrogenase from Escherichia coli--reflections on the basis of coenzyme specificity in the family of glutamate dehydrogenases. *FEBS J,* 280**,** 4681-92.

SHERR, C. J. 1996. Cancer cell cycles. *Science,* 274**,** 1672-7.

SHIMANUKI, M., CHUNG, S. Y., CHIKASHIGE, Y., KAWASAKI, Y., UEHARA, L., TSUTSUMI, C., HATANAKA, M., HIRAOKA, Y., NAGAO, K. & YANAGIDA, M. 2007. Two-step, extensive alterations in the transcriptome from G0 arrest to cell division in Schizosaccharomyces pombe. *Genes Cells,* 12**,** 677-92.

SHIMIZU, K. 2013. Regulation Systems of Bacteria such as Escherichia coli in Response to Nutrient Limitation and Environmental Stresses. *Metabolites,* 4**,** 1-35.

SHIVERS, R. P. & SONENSHEIN, A. L. 2004. Activation of the Bacillus subtilis global regulator CodY by direct interaction with branched-chain amino acids. *Mol Microbiol,* 53**,** 599-611.

SIMON, R. D. 1977. Sporulation in the filamentous cyanobacterium Anabaena cylindrica. The course of spore formation. *Arch Microbiol,* 111**,** 283-8.

SOBALLE, B. & POOLE, R. K. 1999. Microbial ubiquinones: multiple roles in respiration, gene regulation and oxidative stress management. *Microbiology,* 145 (Pt 8)**,** 1817-30.

SPAHR, P. F. 1962. Amino acid composition of ribosomes from Escherichia coli. *J Mol Biol,* 4**,** 395-406.

SPERKA, T., WANG, J. & RUDOLPH, K. L. 2012. DNA damage checkpoints in stem cells, ageing and cancer. *Nat Rev Mol Cell Biol,* 13**,** 579-90.

STEFELY, J. A., REIDENBACH, A. G., ULBRICH, A., ORUGANTY, K., FLOYD, B. J., JOCHEM, A., SAUNDERS, J. M., JOHNSON, I. E., MINOGUE, C. E., WROBEL, R. L., BARBER, G. E., LEE, D., LI, S., KANNAN, N., COON, J. J., BINGMAN, C. A. & PAGLIARINI, D. J. 2015. Mitochondrial ADCK3 employs an atypical protein kinase-like fold to enable coenzyme Q biosynthesis. *Mol Cell,* 57**,** 83-94.

STENMARK, P., GRUNLER, J., MATTSSON, J., SINDELAR, P. J., NORDLUND, P. & BERTHOLD, D. A. 2001. A new member of the family of di-iron carboxylate proteins. Coq7 (clk-1), a membrane-bound hydroxylase involved in ubiquinone biosynthesis. *J Biol Chem,* 276**,** 33297-300.

SU, S. S., TANAKA, Y., SAMEJIMA, I., TANAKA, K. & YANAGIDA, M. 1996. A nitrogen starvation-induced dormant G0 state in fission yeast: the establishment from uncommitted G1 state and its delay for return to proliferation. *J Cell Sci,* 109 (Pt 6)**,** 1347-57.

SUN, J., XU, J., LIU, Z., LIU, Q., ZHAO, A., SHI, T. & LI, Y. 2005. Refined phylogenetic profiles method for predicting protein-protein interactions. *Bioinformatics,* 21**,** 3409-15.

TAKAHASHI, H., SUZUKI, T., SHIRAI, A., MATSUYAMA, A., DOHMAE, N. & YOSHIDA, M. 2011. Mitochondrial localization of fission yeast manganese superoxide dismutase is required for its lysine acetylation and for cellular stress resistance and respiratory growth. *Biochem Biophys Res Commun,* 406**,** 42-6.

TAKEDA, K., STARZYNSKI, C., MORI, A. & YANAGIDA, M. 2015. The critical glucose concentration for respiration-independent proliferation of fission yeast, Schizosaccharomyces pombe. *Mitochondrion,* 22**,** 91-5.

TAKEDA, K. & YANAGIDA, M. 2010. In quiescence of fission yeast, autophagy and the proteasome collaborate for mitochondrial maintenance and longevity. *Autophagy,* 6**,** 564-5.

TAKEDA, K., YOSHIDA, T., KIKUCHI, S., NAGAO, K., KOKUBU, A., PLUSKAL, T., VILLAR-BRIONES, A., NAKAMURA, T. & YANAGIDA, M. 2010. Synergistic roles of the proteasome and autophagy for mitochondrial maintenance and chronological lifespan in fission yeast. *Proc Natl Acad Sci U S A,* 107**,** 3540-5.

TAMURA, K., STECHER, G., PETERSON, D., FILIPSKI, A. & KUMAR, S. 2013. MEGA6: Molecular Evolutionary Genetics Analysis version 6.0. *Mol Biol Evol,* 30**,** 2725-9.

TEMIN, H. M. 1971. Stimulation by serum of multiplication of stationary chicken cells. *J Cell Physiol,* 78**,** 161-70.

THE UNIPROT, C. 2017. UniProt: the universal protein knowledgebase. *Nucleic Acids Res,* 45**,** D158-D169.

TOCHEVA, E. I., ORTEGA, D. R. & JENSEN, G. J. 2016. Sporulation, bacterial cell envelopes and the origin of life. *Nat Rev Microbiol,* 14**,** 535-542.

TOJO, S., SATOMURA, T., KUMAMOTO, K., HIROOKA, K. & FUJITA, Y. 2008. Molecular mechanisms underlying the positive stringent response of the Bacillus subtilis ilv-leu operon, involved in the biosynthesis of branched-chain amino acids. *J Bacteriol,* 190**,** 6134-47.

TOTIR, M., ECHOLS, N., NANAO, M., GEE, C. L., MOSKALEVA, A., GRADIA, S., IAVARONE, A. T., BERGER, J. M., MAY, A. P., ZUBIETA, C. & ALBER, T. 2012. Macro-to-micro structural proteomics: native source proteins for high-throughput crystallization. *PLoS One,* 7**,** e32498.

UCHIDA, N., SUZUKI, K., SAIKI, R., KAINOU, T., TANAKA, K., MATSUDA, H. & KAWAMUKAI, M. 2000. Phenotypes of fission yeast defective in ubiquinone production due to disruption of the gene for p-hydroxybenzoate polyprenyl diphosphate transferase. *J Bacteriol,* 182**,** 6933-9.

VALLEDOR, L., FURUHASHI, T., RECUENCO-MUNOZ, L., WIENKOOP, S. & WECKWERTH, W. 2014. System-level network analysis of nitrogen starvation and recovery in Chlamydomonas reinhardtii reveals potential new targets for increased lipid accumulation. *Biotechnol Biofuels,* 7**,** 171.

VELASCO, J. A., CANSADO, J., PENA, M. C., KAWAKAMI, T., LABORDA, J. & NOTARIO, V. 1993. Cloning of the dihydroxyacid dehydratase-encoding gene (ILV3) from Saccharomyces cerevisiae. *Gene,* 137**,** 179-85.

VEMURI, G. N., EITEMAN, M. A., MCEWEN, J. E., OLSSON, L. & NIELSEN, J. 2007. Increasing NADH oxidation reduces overflow metabolism in Saccharomyces cerevisiae. *Proc Natl Acad Sci U S A,* 104**,** 2402-7.

VO, T. V., DAS, J., MEYER, M. J., CORDERO, N. A., AKTURK, N., WEI, X., FAIR, B. J., DEGATANO, A. G., FRAGOZA, R., LIU, L. G., MATSUYAMA, A., TRICKEY, M.,

HORIBATA, S., GRIMSON, A., YAMANO, H., YOSHIDA, M., ROTH, F. P., PLEISS, J. A., XIA, Y. & YU, H. 2016. A Proteome-wide Fission Yeast Interactome Reveals Network Evolution Principles from Yeasts to Human. *Cell,* 164**,** 310-23.

VOROBIEVA, A. A., KHAN, M. S. & SOUMILLION, P. 2014. Escherichia coli D-malate dehydrogenase, a generalist enzyme active in the leucine biosynthesis pathway. *J Biol Chem,* 289**,** 29086-96.

VOULGARIS, I., O'DONNELL, A., HARVEY, L. M. & MCNEIL, B. 2012. Inactivating alternative NADH dehydrogenases: enhancing fungal bioprocesses by improving growth and biomass yield? *Sci Rep,* 2**,** 322.

WALKER, D. H. 1996. Rickettsiae. *In:* BARON, S. (ed.) *Medical Microbiology.* 4th ed. Galveston (TX): University of Texas at Galveston.

WELLS, C. L. W., T.D. 1996. Clostridia:Sporeforming anaerobic bacilli. *In:* BARON, S. (ed.) *Medical Microbiology.* 4th ed. Galveston (TX): University of Texas Medical Branch at Galveston.

WILHELM, B. T., MARGUERAT, S., WATT, S., SCHUBERT, F., WOOD, V., GOODHEAD, I., PENKETT, C. J., ROGERS, J. & BAHLER, J. 2008. Dynamic repertoire of a eukaryotic transcriptome surveyed at single-nucleotide resolution. *Nature,* 453**,** 1239-43.

WILLGER, S. D., GRAHL, N. & CRAMER, R. A., JR. 2009. Aspergillus fumigatus metabolism: clues to mechanisms of in vivo fungal growth and virulence. *Med Mycol,* 47 Suppl 1**,** S72-9.

WOOD, V., GWILLIAM, R., RAJANDREAM, M. A., LYNE, M., LYNE, R., STEWART, A., SGOUROS, J., PEAT, N., HAYLES, J., BAKER, S., BASHAM, D., BOWMAN, S., BROOKS, K., BROWN, D., BROWN, S., CHILLINGWORTH, T., CHURCHER, C., COLLINS, M., CONNOR, R., CRONIN, A., DAVIS, P., FELTWELL, T., FRASER, A., GENTLES, S., GOBLE, A., HAMLIN, N., HARRIS, D., HIDALGO, J., HODGSON, G., HOLROYD, S., HORNSBY, T., HOWARTH, S., HUCKLE, E. J., HUNT, S., JAGELS, K., JAMES, K., JONES, L., JONES, M., LEATHER, S., MCDONALD, S., MCLEAN, J., MOONEY, P., MOULE, S., MUNGALL, K., MURPHY, L., NIBLETT, D., ODELL, C., OLIVER, K., O'NEIL, S., PEARSON, D., QUAIL, M. A., RABBINOWITSCH, E., RUTHERFORD, K., RUTTER, S., SAUNDERS, D., SEEGER, K., SHARP, S., SKELTON, J., SIMMONDS, M., SQUARES, R., SQUARES, S., STEVENS, K., TAYLOR, K., TAYLOR, R. G., TIVEY, A., WALSH, S., WARREN, T., WHITEHEAD, S., WOODWARD, J., VOLCKAERT, G., AERT, R., ROBBEN, J., GRYMONPREZ, B., WELTJENS, I., VANSTREELS, E., RIEGER, M., SCHAFER, M., MULLER-AUER, S., GABEL, C., FUCHS, M., DUSTERHOFT, A., FRITZC, C., HOLZER, E., MOESTL, D., HILBERT, H., BORZYM, K., LANGER, I., BECK, A., LEHRACH, H., REINHARDT, R., POHL, T. M., EGER, P., ZIMMERMANN, W., WEDLER, H., WAMBUTT, R., PURNELLE, B., GOFFEAU, A., CADIEU, E., DREANO, S., GLOUX, S., et al. 2002. The genome sequence of Schizosaccharomyces pombe. *Nature,* 415**,** 871-80.

WOOD, V., HARRIS, M. A., MCDOWALL, M. D., RUTHERFORD, K., VAUGHAN, B. W., STAINES, D. M., ASLETT, M., LOCK, A., BAHLER, J., KERSEY, P. J. & OLIVER, S. G. 2012. PomBase: a comprehensive online resource for fission yeast. *Nucleic Acids Res,* 40**,** D695-9.

WU, H. J., YANG, Y., WANG, S., QIAO, J. Q., XIA, Y. F., WANG, Y., WANG, W. D., GAO, S. F., LIU, J., XUE, P. Q. & GAO, X. W. 2011. Cloning, expression and

characterization of a new aspartate aminotransferase from Bacillus subtilis B3. *FEBS J,* 278**,** 1345-57.

YANAGIDA, M. 2000. Cell cycle mechanisms of sister chromatid separation; roles of Cut1/separin and Cut2/securin. *Genes Cells,* 5**,** 1-8.

YANAGIDA, M. 2009. Cellular quiescence: are controlling genes conserved? *Trends Cell Biol,* 19**,** 705-15.

YANG, D., OYAIZU, Y., OYAIZU, H., OLSEN, G. J. & WOESE, C. R. 1985. Mitochondrial origins. *Proc Natl Acad Sci U S A,* 82**,** 4443-7.

YOUNG, P. G. & FANTES, P. A. 1987. Schizosaccharomyces pombe mutants affected in their division response to starvation. *J Cell Sci,* 88 (Pt 3)**,** 295-304.

ZETTERBERG, A. & LARSSON, O. 1985. Kinetic analysis of regulatory events in G1 leading to proliferation or quiescence of Swiss 3T3 cells. *Proc Natl Acad Sci U S A,* 82**,** 5365-9.

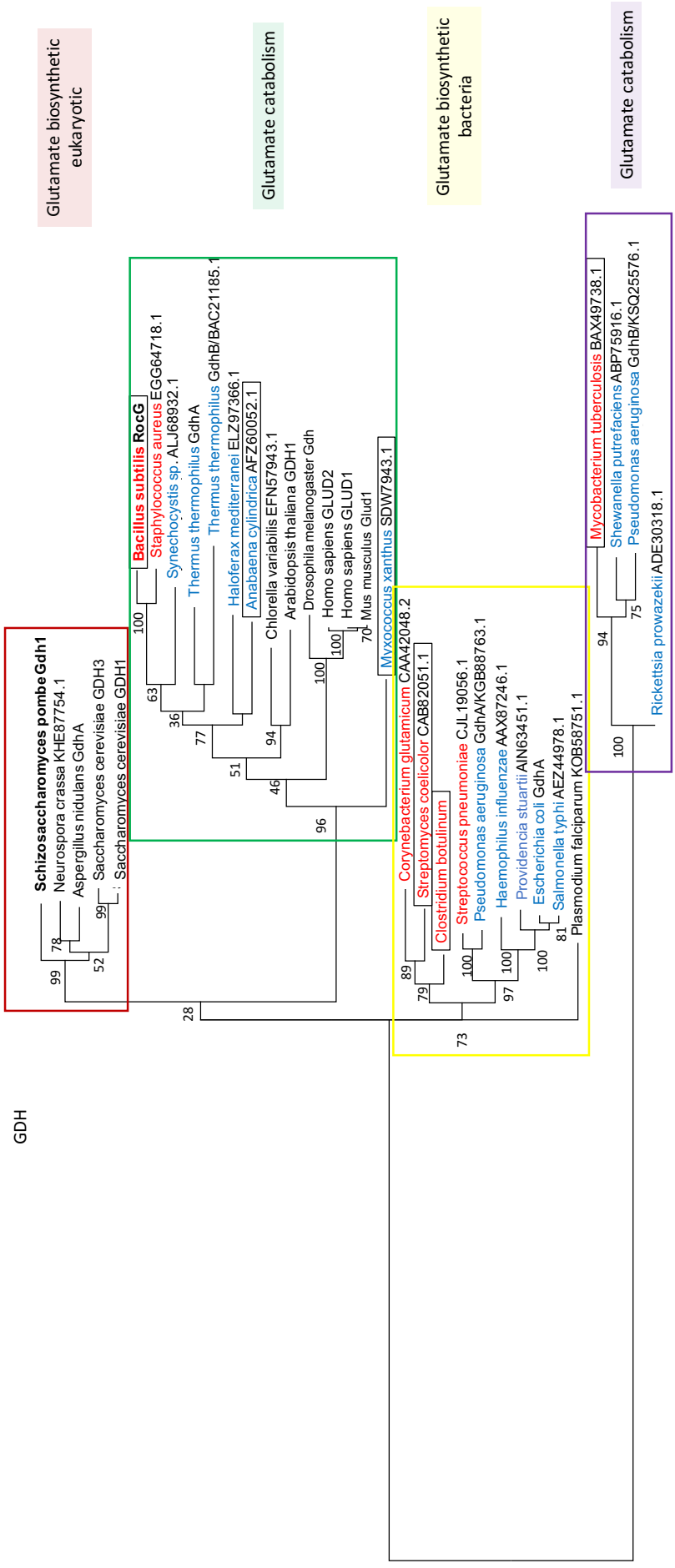

Figure S1 Phylogenic reconstruction of Gdh1 homologs. Maximum likelihood with 1000 bootstrap repeats was computed using MEGA tool. Bootstrap confidence is depicted. Bacterial species are differentiated between gram-positives (red font) and gram-negatives (blue font). In additions spore-forming bacteria are presented in black boxes.

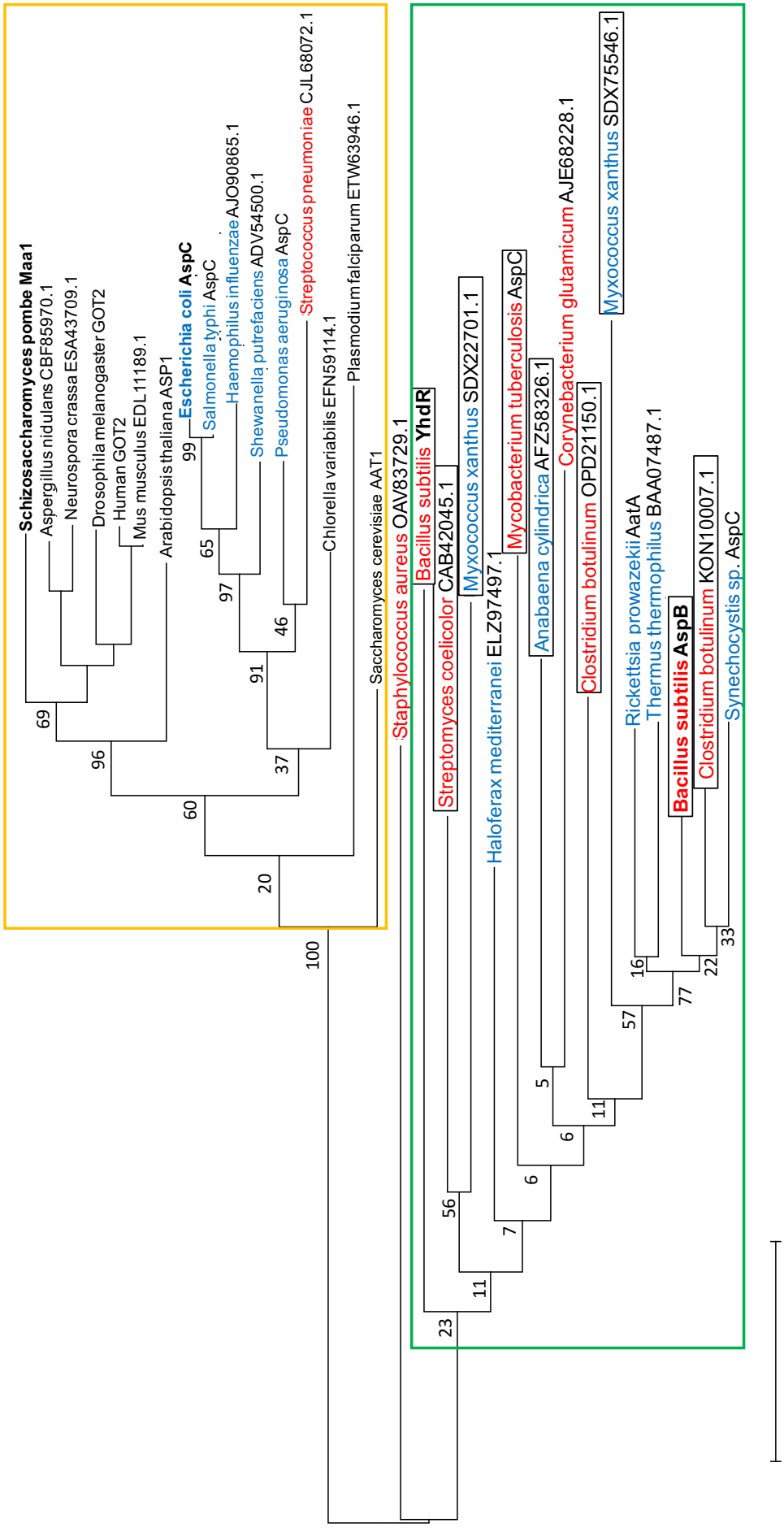

Figure S2 Phylogenic reconstruction of Maa1 homologs. Maximum likelihood with 1000 bootstrap repeats was computed using MEGA tool. Bootstrap confidence is depicted. Bacterial species are differentiated between gram-positives (red font) and gram-negatives (blue font). In additions spore-forming bacteria are presented in black boxes.

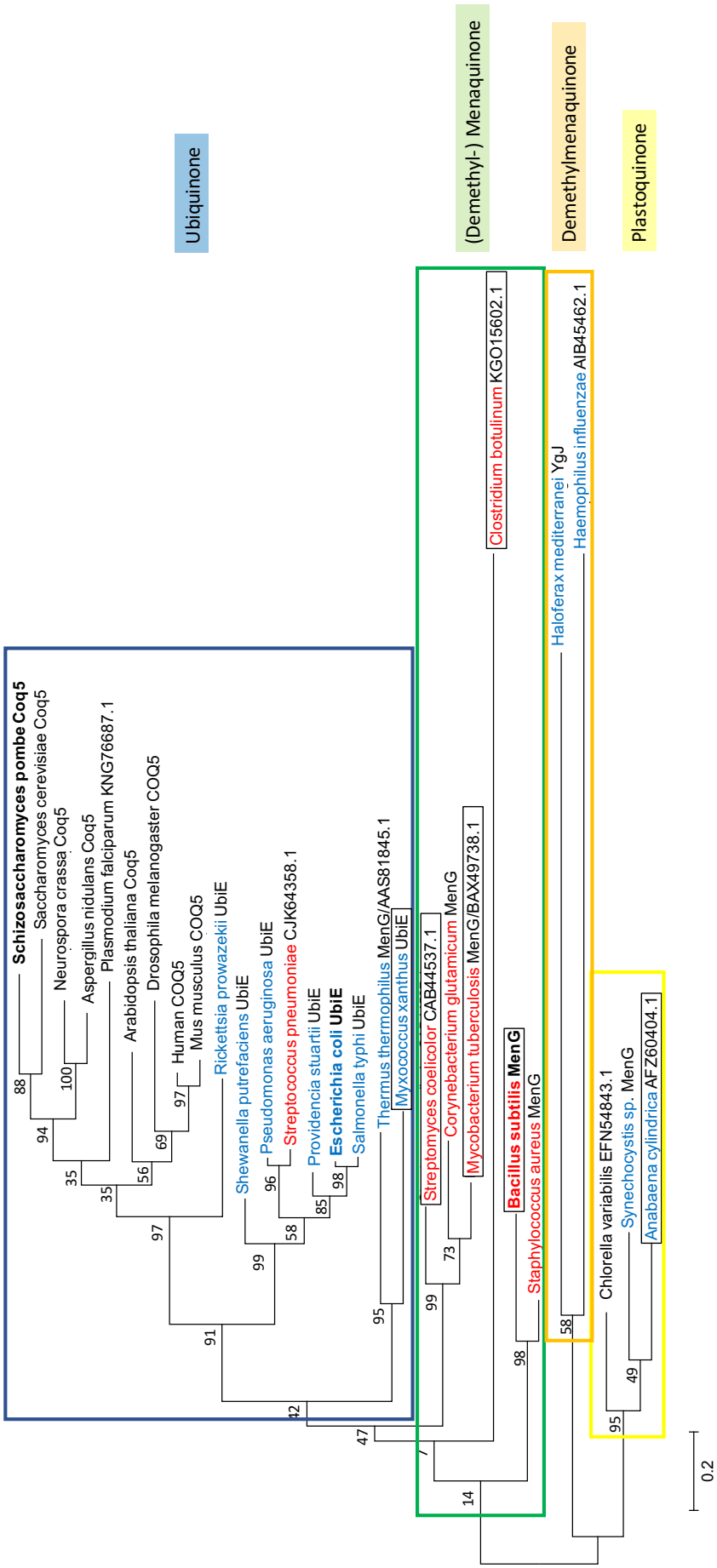

Figure S3 Phylogenic reconstruction of Coq5 homologs. Maximum likelihood with 1000 bootstrap repetitions was computed using MEGA tool. Bootstrap confidence is depicted. Bacterial species are differentiated between gram-positives (red font) and gram-negatives (blue font). In additions spore-forming bacteria are presented in black boxes.

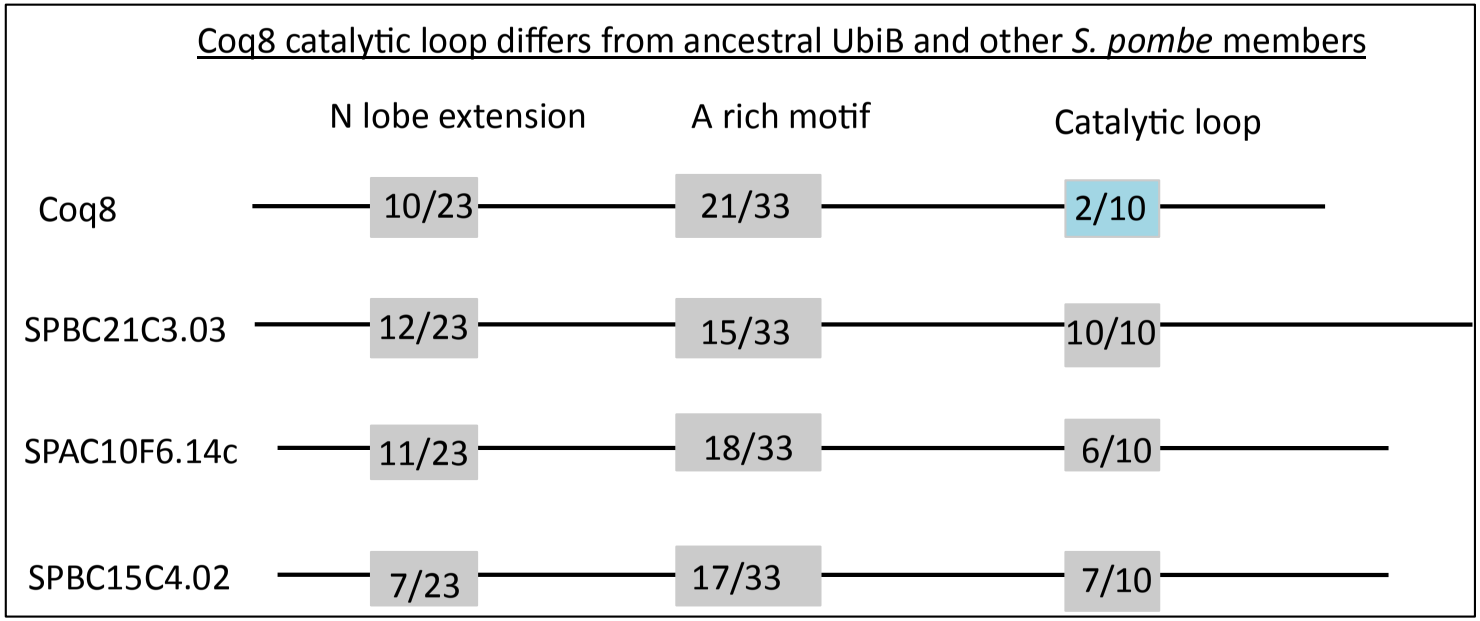

Figure S4 Sequence comparison between *S. pombe* UbiB family members and bacterial UbiB. Clustal W protein sequence alignments with SPBC21C3.03, SPAC10F6.14c, SPBC14C4.02*, Coq8 and E. oli* UbiB were made (not shown). Specific conserved sites were compared between individual S. pombe UbiB family members and bacterial UbiB. The number of identical residues against the number of residues in the selected cluster are indicated.

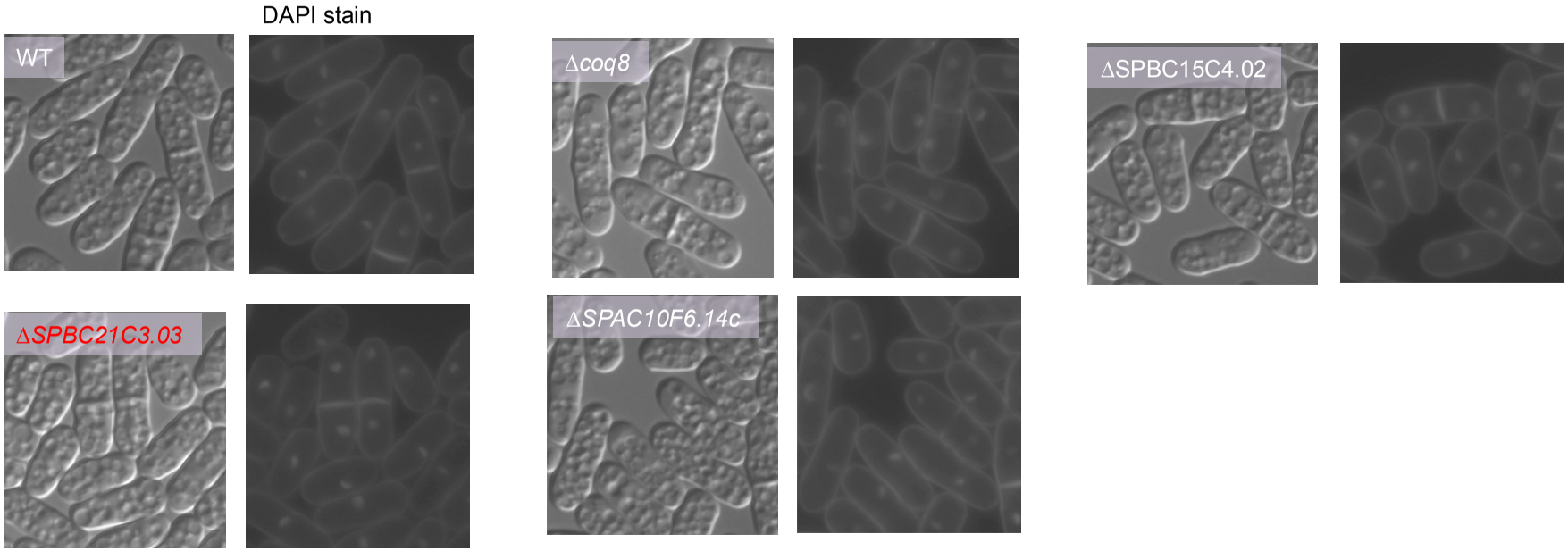

Figure S5 Cell morphology in vegetative state. No significant difference between wild type (WT) and mutants: GZE Δ*SPBC21C3.03* (red font), Δ*SPAC10F6.14c,* Δ*SPBC14C4.02.* Pictures were taken with the help of Ms. Yuria Tahara from the G0 cell unit.

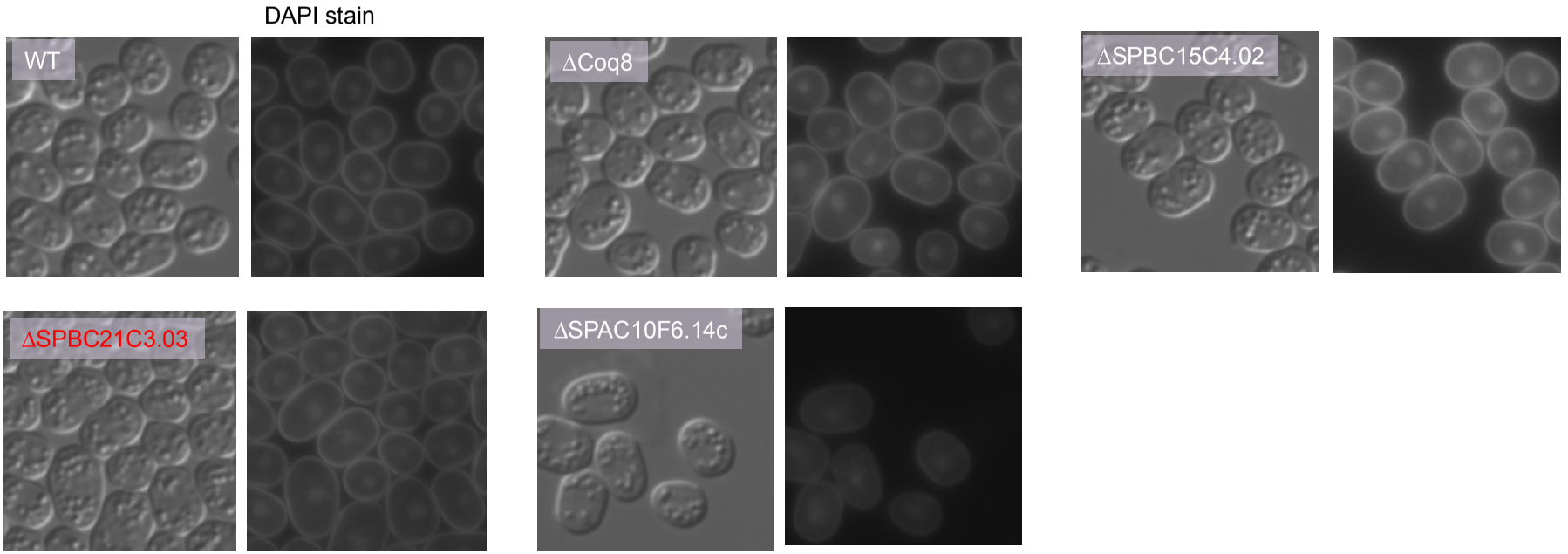

Figure S6 Cell morphology in G0 state. 24h after N starvation cells becomes round and enter G0 phase. No significant difference between wild type (WT) and mutants ΔSPBC21C3.03 (GZE, red), ΔSPAC10F6.14c , ΔSPBC14C4.02 were observed. Pictures were taken with the help of Ms. Yuria Tahara from the G0 cell unit.

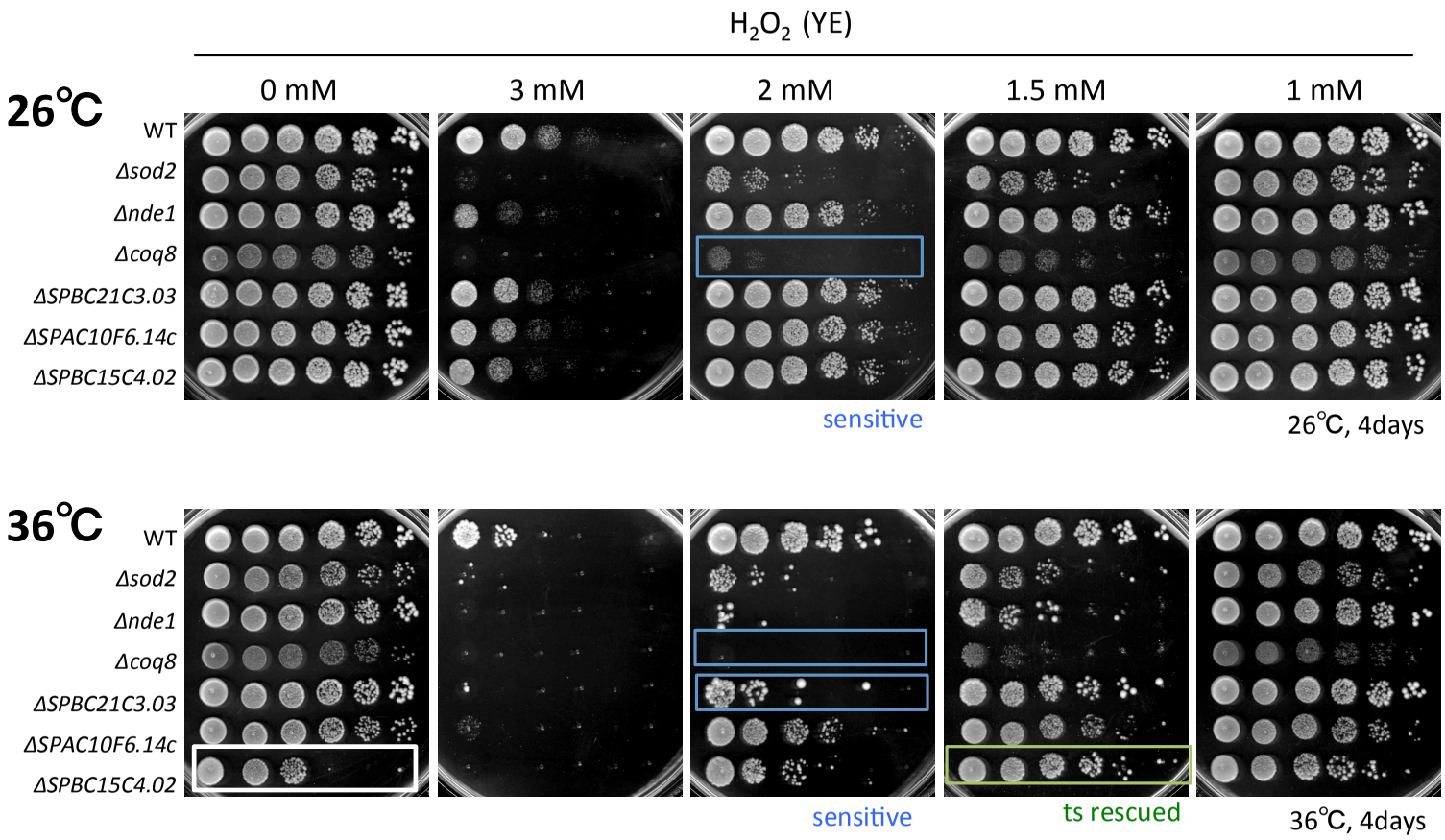

Figure S7 Oxidative stress inducing hydrogen peroxide (H_2O_2) screening. Mutant strains showing growth changes on drug-treated YE (2 % yeast extract) agar medium compared to wild type control (WT) with Δ*sod2* as oxidative stress sensitive positive control are shown: Temperature sensitive (ts) Δ*SPBC15C4.02* (white box), with ts rescued phenotype at 1.5mM H_2O_2 (green box), H_2O_2 sensitive Δ*coq8* and Δ*SPC21C3.03* (blue box)

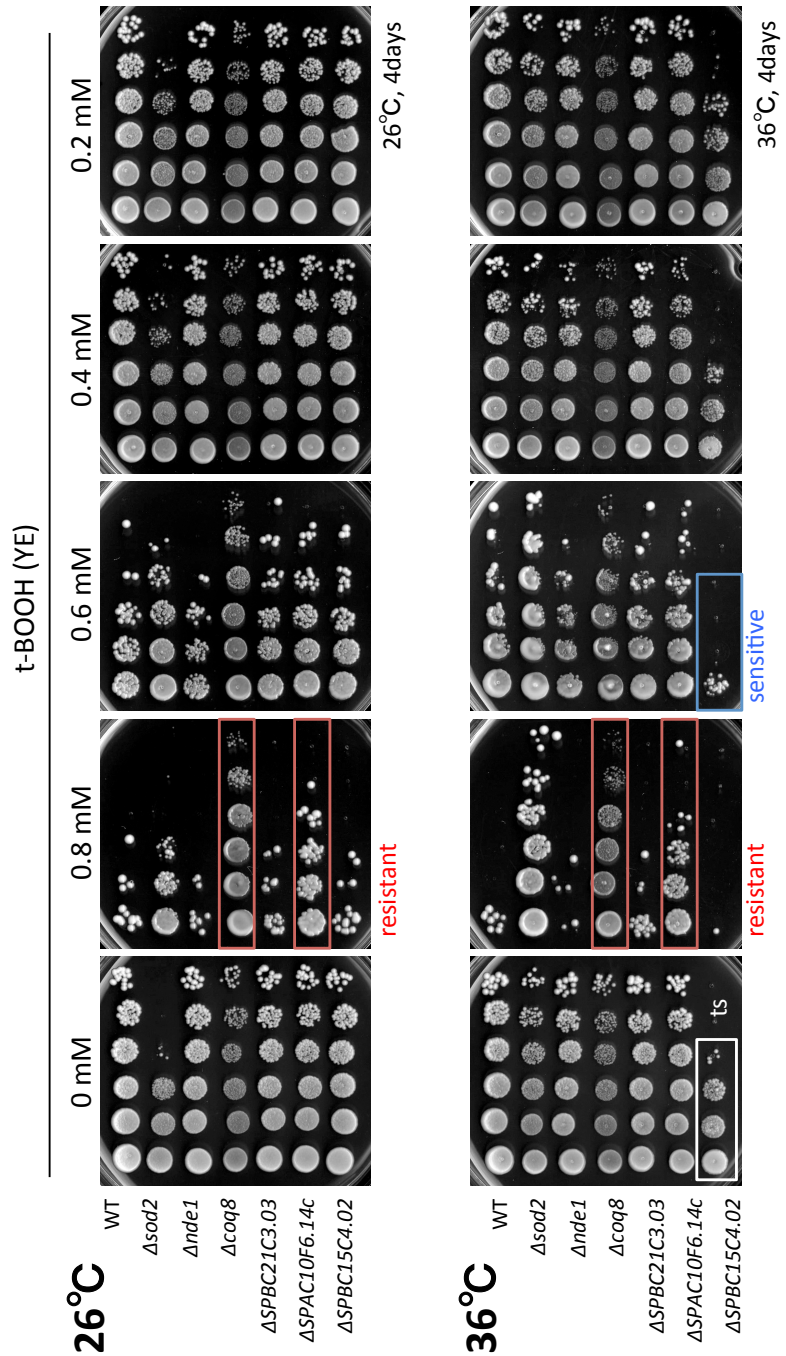

Figure S8 Oxidative stress inducing t-BOOh screening. Mutant strains showing growth changes on drug-treated YE (2 % yeast extract) agar medium compared to wild type control (WT) are shown: Temperature sensitive (ts) Δ*SPBC15C4.02* (white box), with t-BOOh sensitive phenotype at 0.6 mM t-BOOH (blue box), drug resistant Δ*coq8* and Δ*SPAC10F6.14c* (red box).

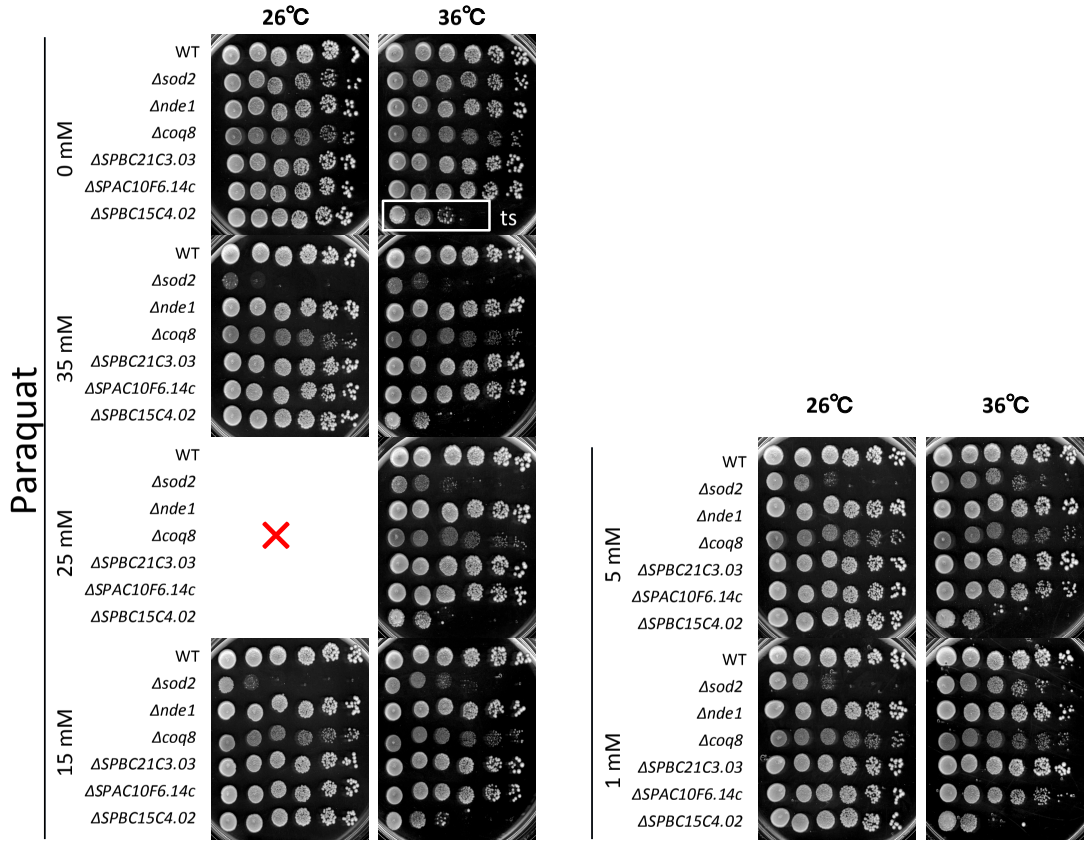

Figure S9 Oxidative stress inducing paraquat screening. Mutant strains showing growth changes on drug-treated YE (2 % yeast extract) agar medium compared to wild type control (WT) with Δ*sod2* as oxidative stress sensitive positive control are shown: Temperature sensitive (ts) Δ*SPBC15C4.02* (white box) in drug-untreated YE medium.

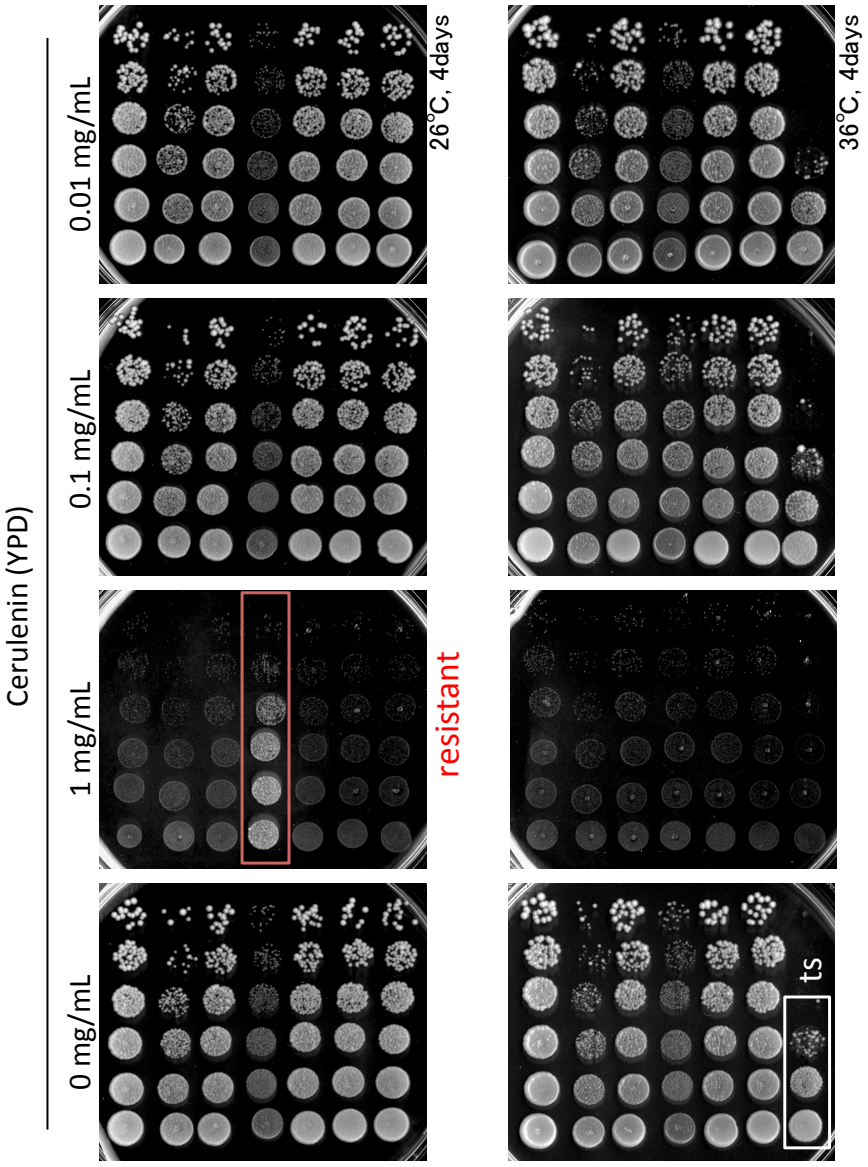

Figure S10 Fatty acid synthetase inhibiting cerulenin screening. Mutant strains showing growth changes on drug-treated YPD (2 % yeast extract + polypeptone, D-glucose) agar medium compared to wild type control (WT) are shown: Temperature sensitive (ts) Δ*SPBC15C4.02* (white box), drug resistant Δ*coq8* (red box).

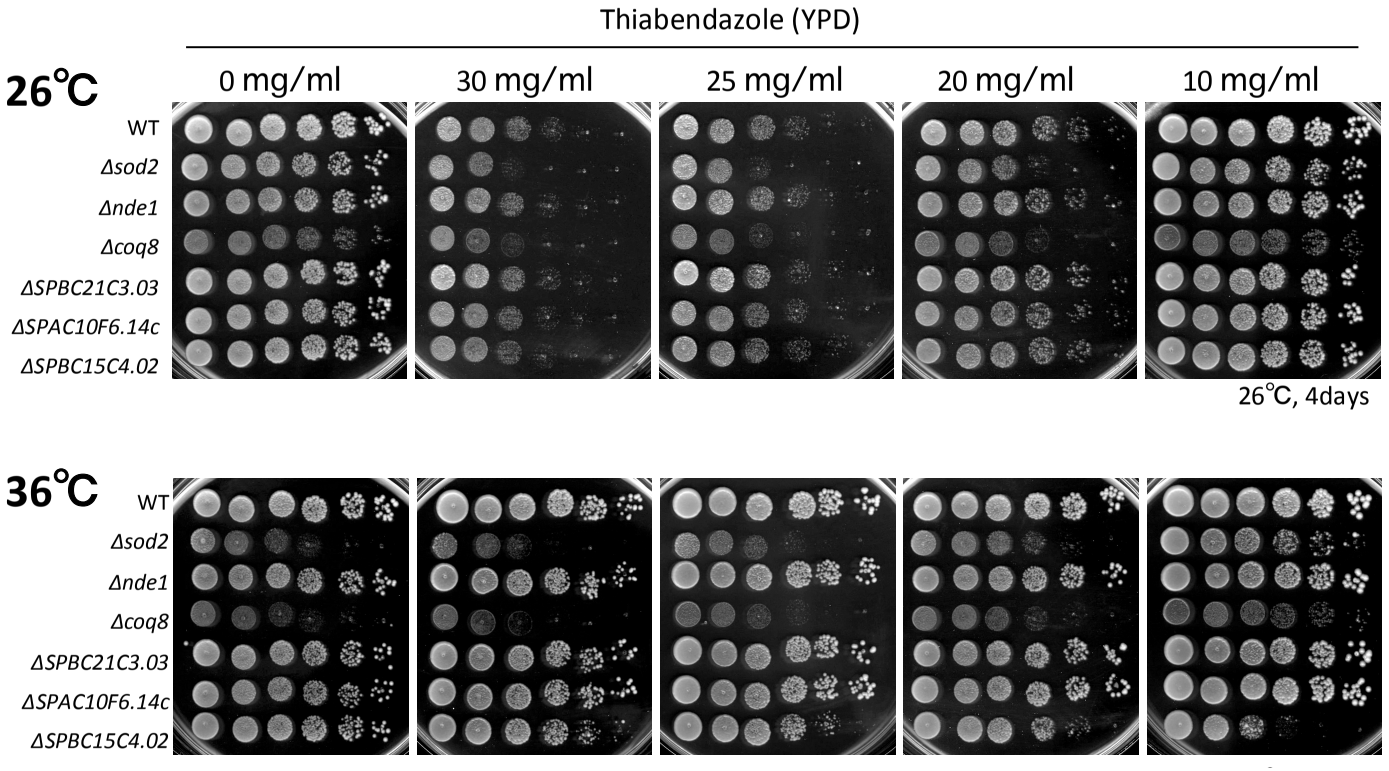

Figure S11 Microtubule inhibitor Thiabendazole screening. Mutant strains showing growth changes on drug-treated YPD agar medium compared to wild type control (WT) are shown: Temperature sensitive (ts) Δ*SPBC15C4.02* (white box), drug resistant Δ*coq8* (red box).

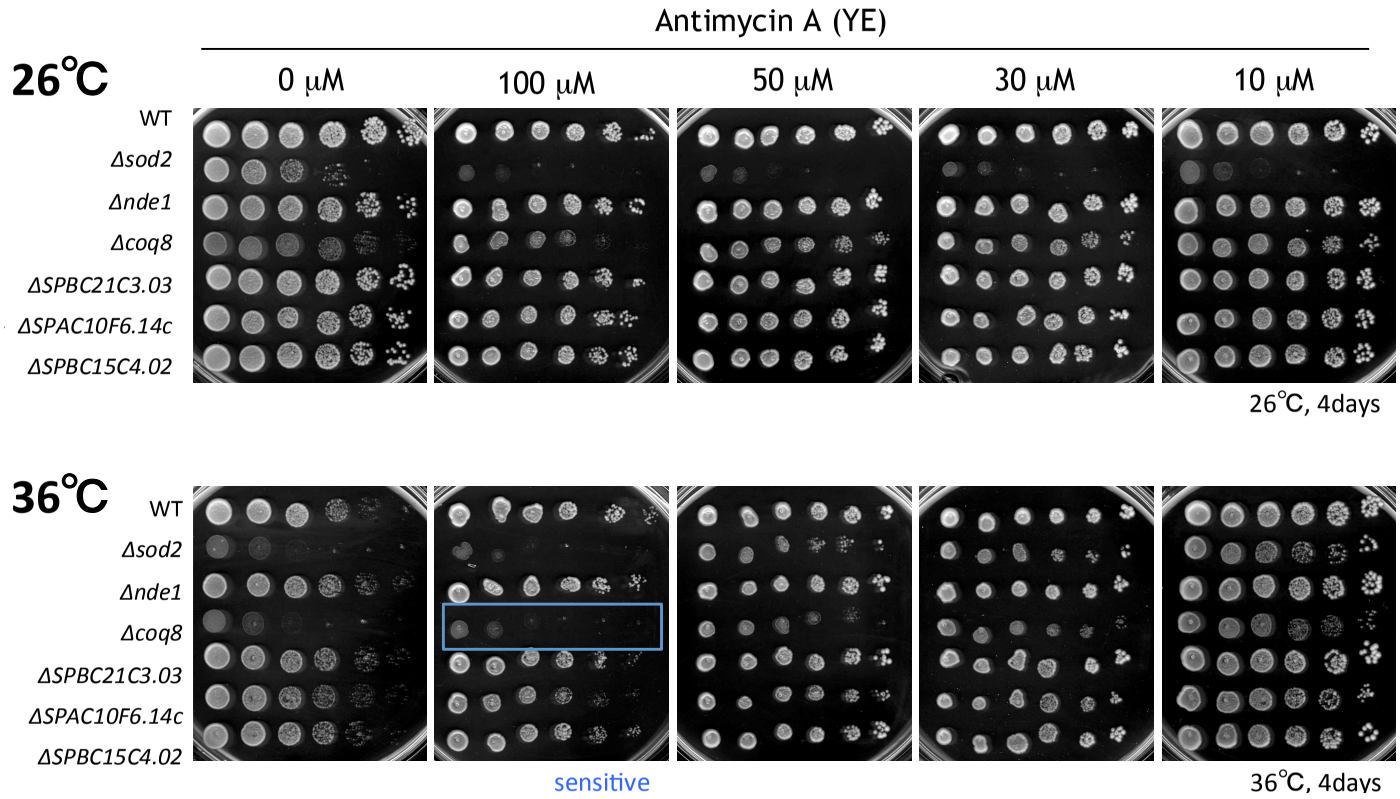

Figure S12 Respiratory complex III inhibiting antimycin A (AA) screening. Mutant strains showing growth changes on drug-treated YE (2 % yeast extract) agar medium compared to wild type control (WT) with AA positive control Δ*sod2* are shown: Drug sensitive Δ*coq8* (blue box).

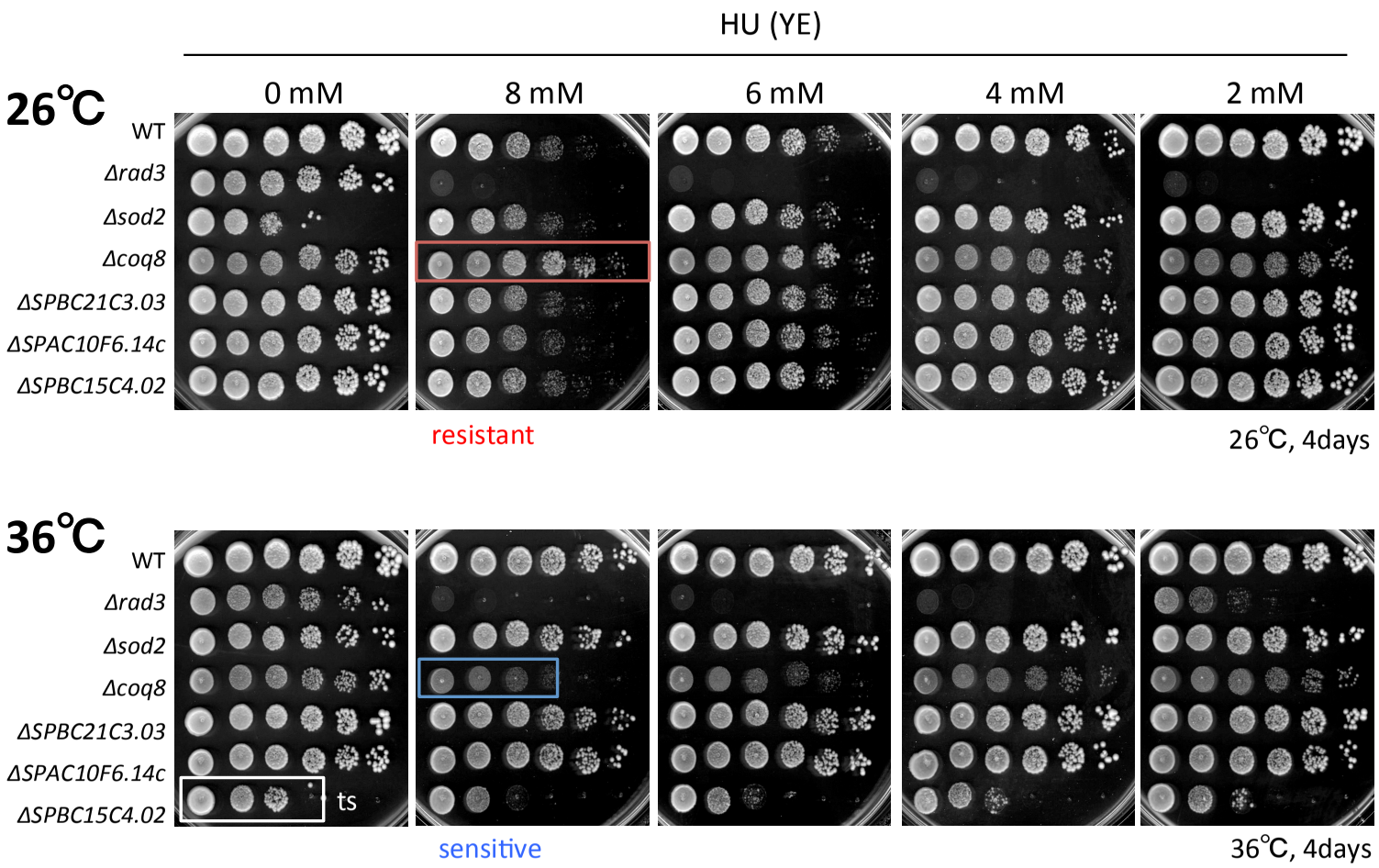

Figure S13 DNA damage inducing hydroxyurea screening. Mutant strains showing growth changes on drug-treated YE (2 % yeast extract) agar medium compared to wild type control (WT) and DNA damage positive Δ*rad3* are shown: Drug-resistant (red box) at 26 but drug sensitive (blue box) at 36 Δ*coq8*. Temperature sensitivity showed up for Δ*SPBC15C4.02*.

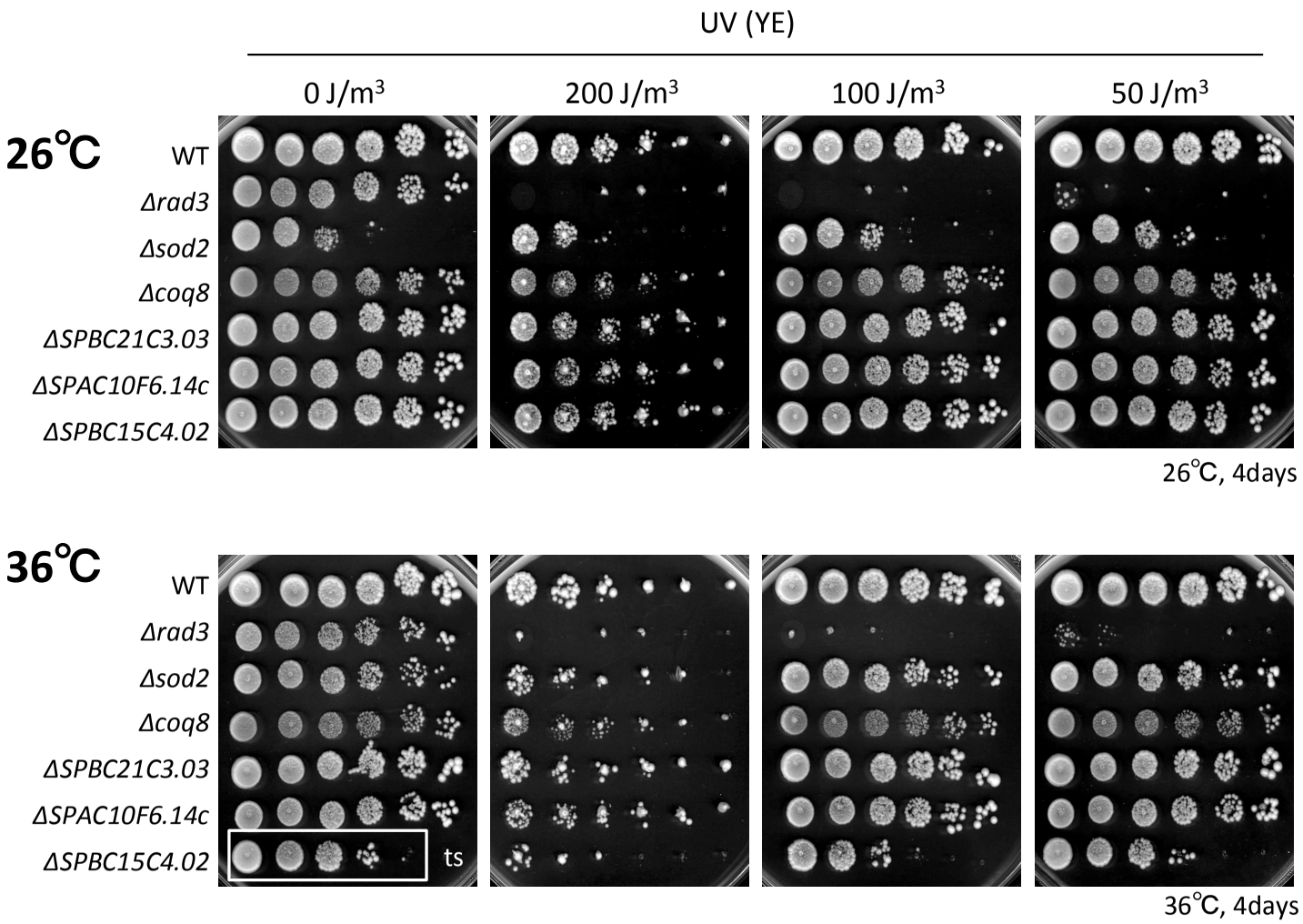

Figure S14 UV irradiation screening. Mutant strains showing growth changes on drug-treated YE (2 % yeast extract) agar medium compared to wild type control (WT) and DNA damage positive control Δ*rad3* are shown: Temperature sensitivity showed up for Δ*SPBC15C4.02*.

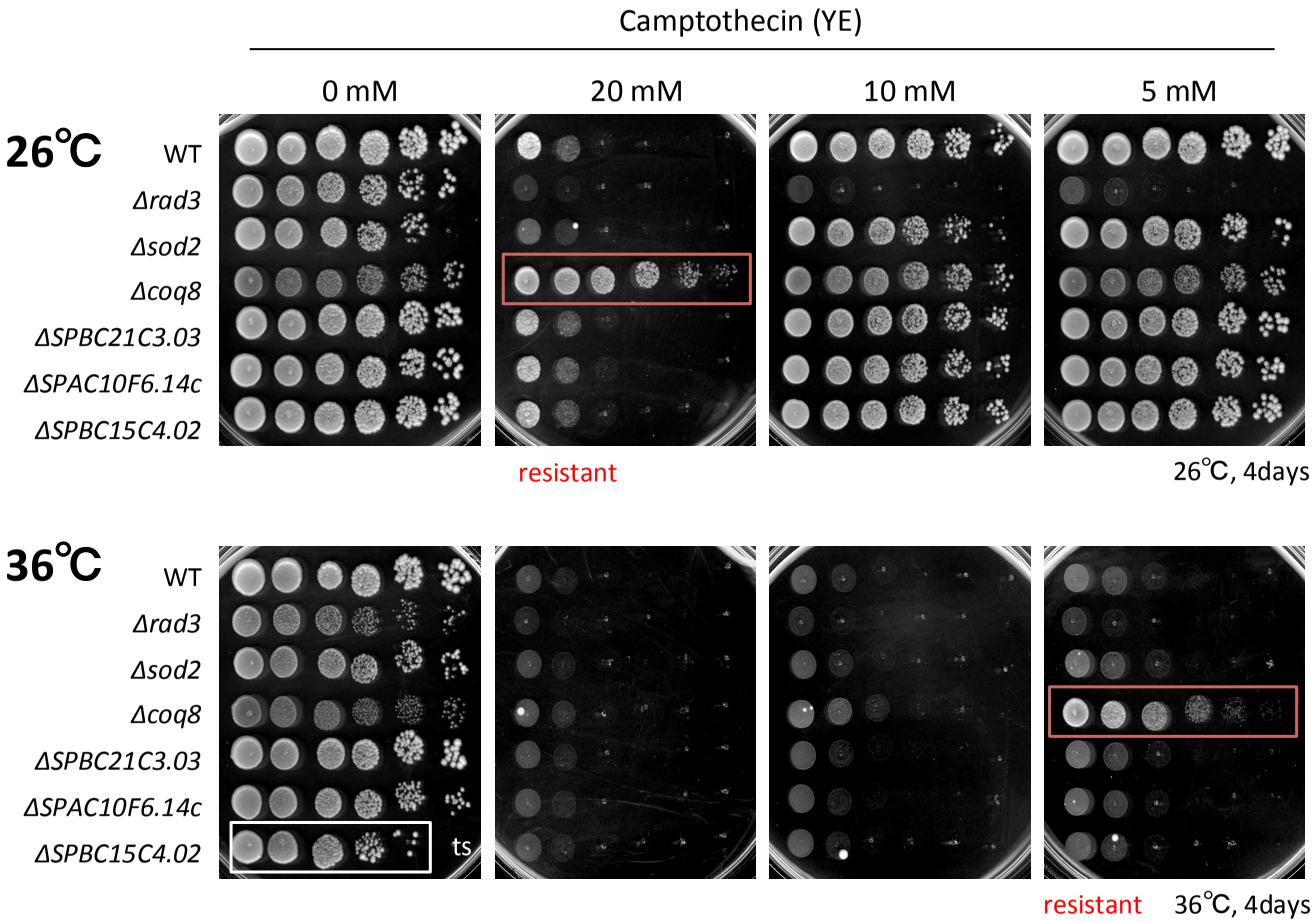

Figure S15 DNA damaging agent screening Camptothecin. Mutant strains showing growth changes on drug-treated YE (2 % yeast extract) agar medium compared to wild type control (WT) and DNA damage positive control Δ*rad3* are shown: Δ*coq8* showed resistance at 26 (red box) Temperature sensitivity showed up for Δ*SPBC15C4.02*.

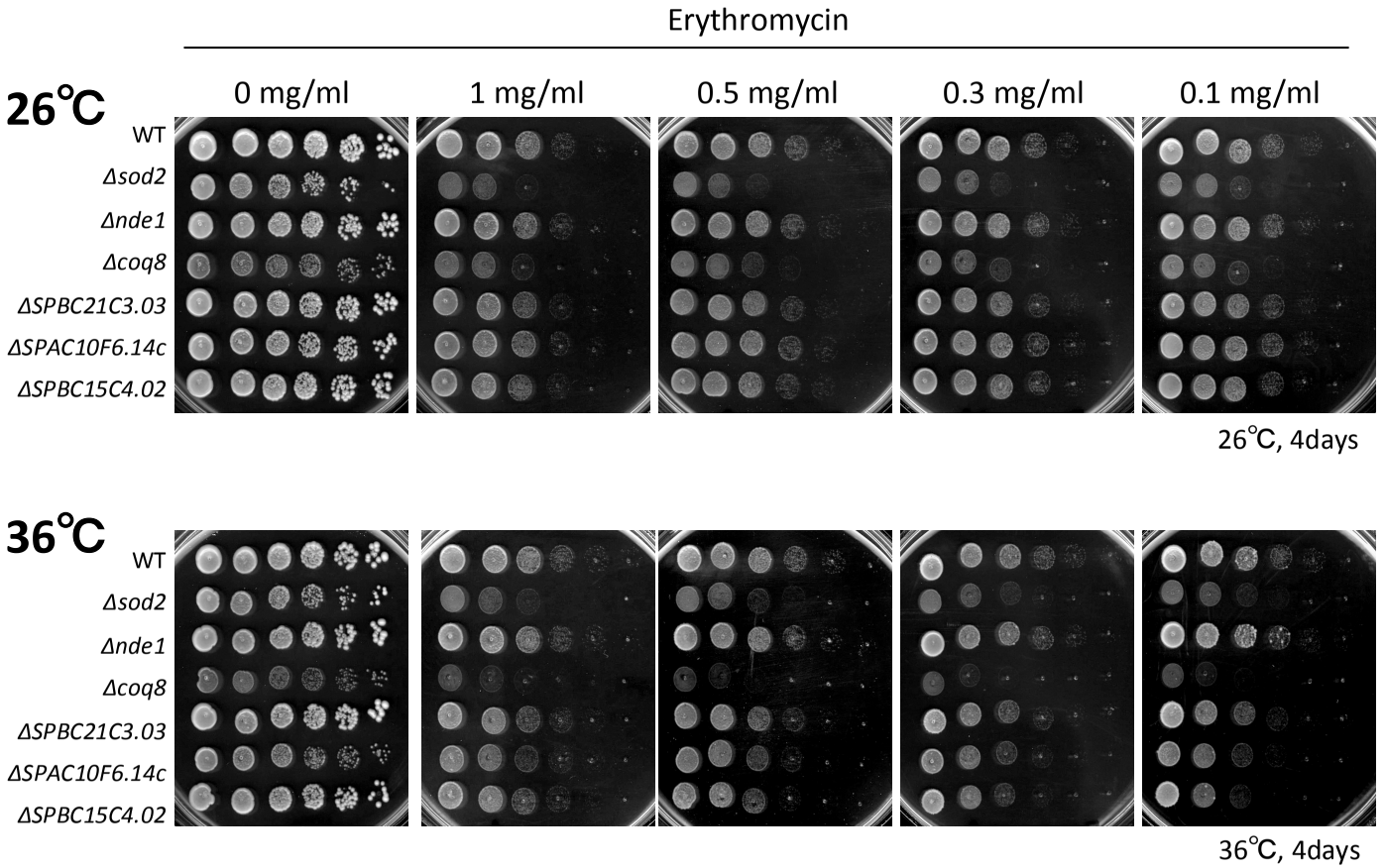

Figure S16 Mitochondrial protein synthesis blocking Erythromycin screening. Mutant strains showing growth changes on drug-treated YE (2 % yeast extract) agar medium compared to wild type control (WT) are shown: Unclear sensitivities may be observed for Δ*sod2*, Δ*SPBC15C4.02*, Δ*SPBC15C4.02* and maybe Δ*coq8*.

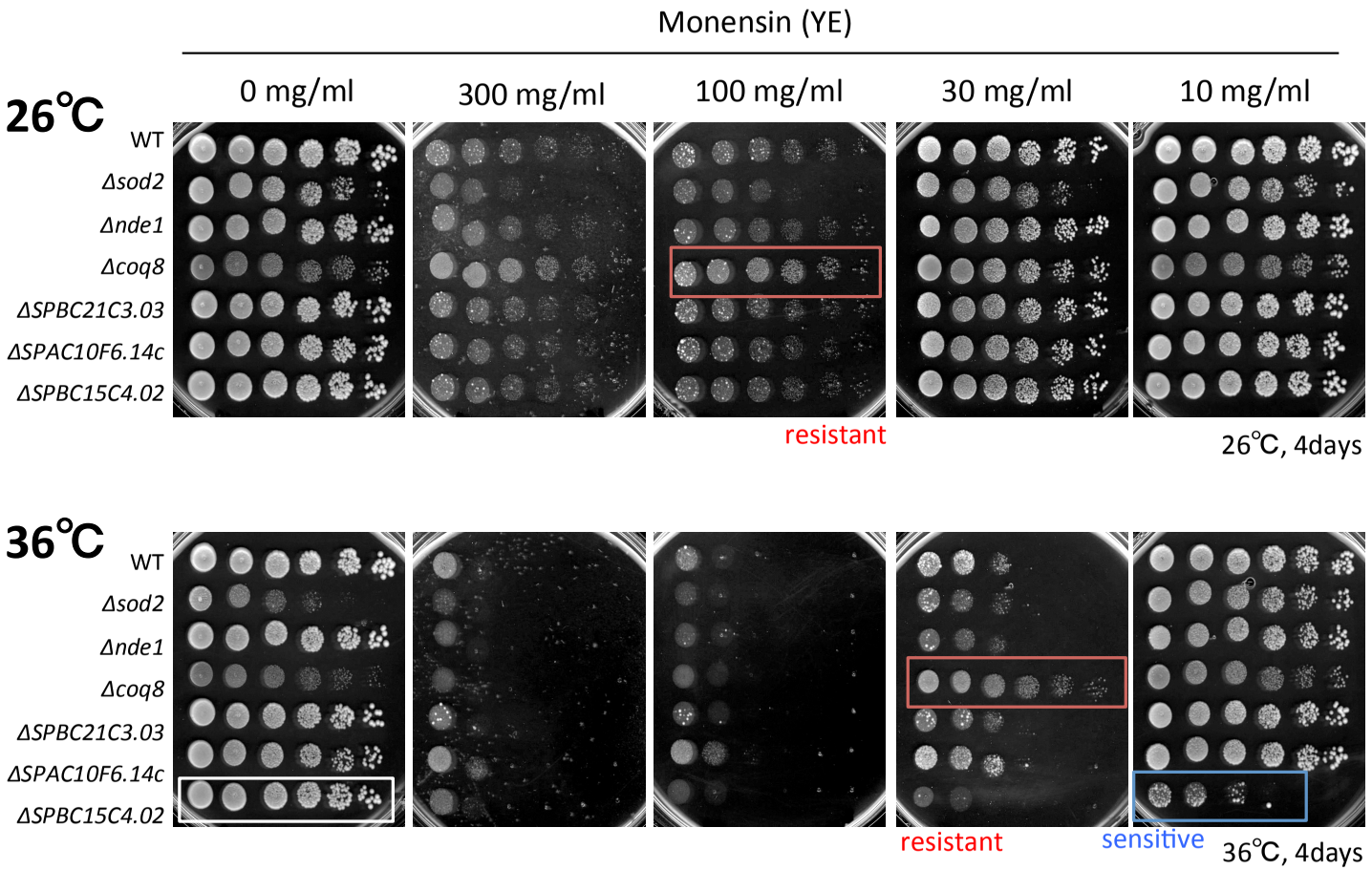

Figure S17 Golgi transport blocking Monensin screening. Mutant strains showing growth changes on drug-treated YE (2 % yeast extract) agar medium compared to wild type control (WT): Δ*coq8* showed resistance (red box) Temperature sensitivity showed up for Δ*SPBC15C4.02* which was sensitive (blue box).

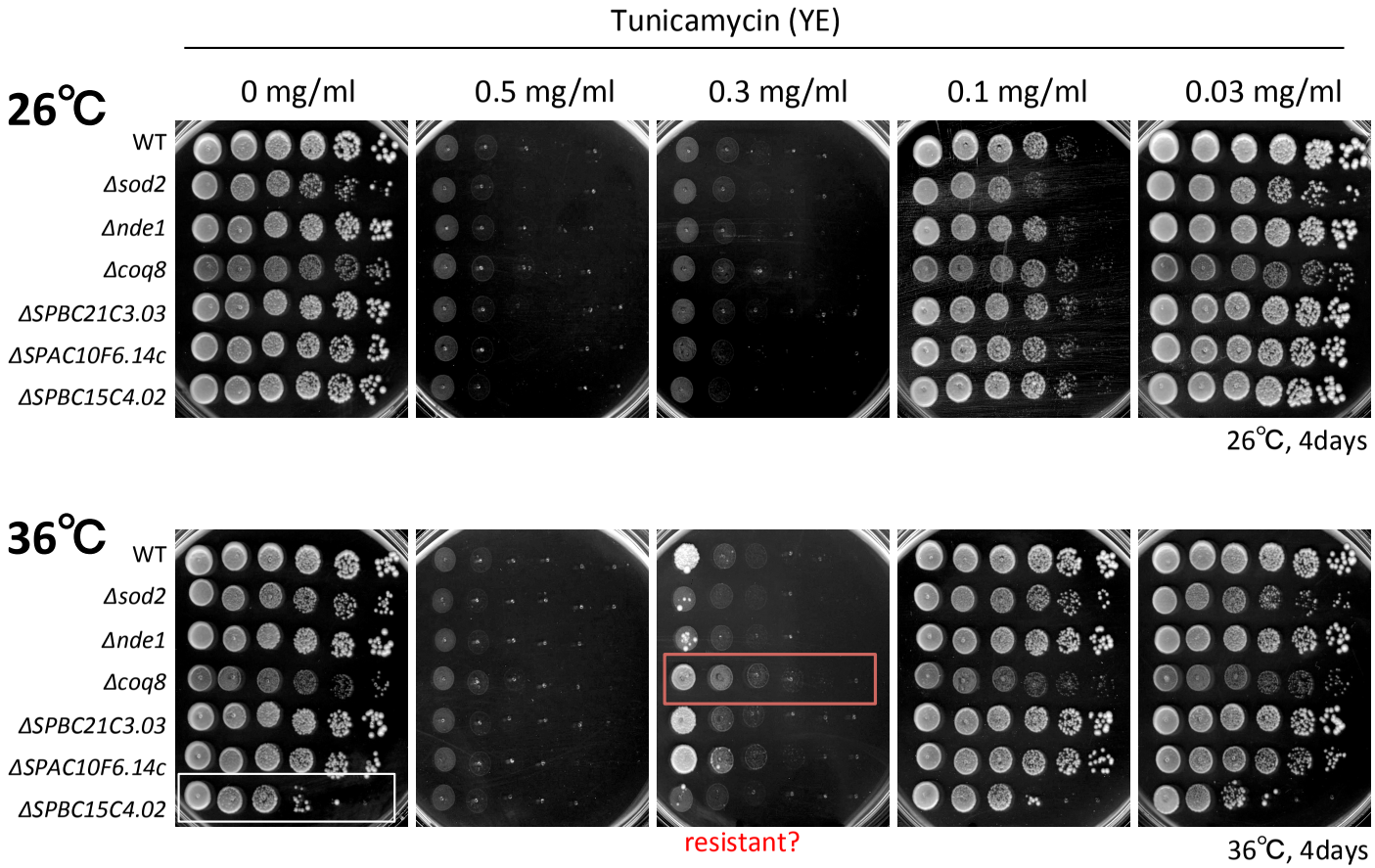

Figure S18 ER blocker Tunicamycin screening. Mutant strains showing growth changes on drug-treated YE (2 % yeast extract) agar medium compared to wild type control (WT): Unclear resistance of Δ*coq8* (red box). Again, temperature sensitivity showed up for Δ*SPBC15C4.02* (white box).

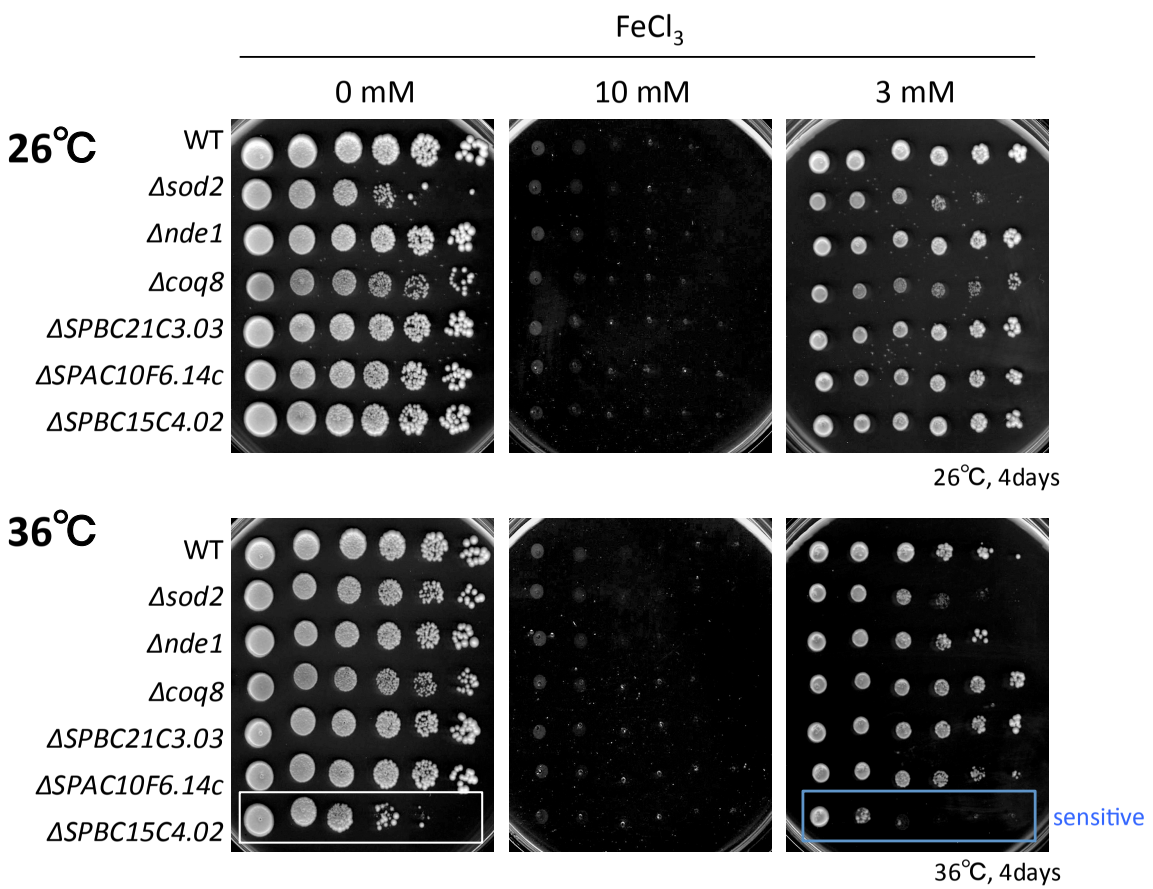

Figure S19 Iron chloride screening. Mutant strains showing growth changes on drug-treated YE (2 % yeast extract) agar medium compared to wild type control (WT): Temperature sensitivity showed up for Δ*SPBC15C4.02* (white box) which was drug sensitive (blue box).

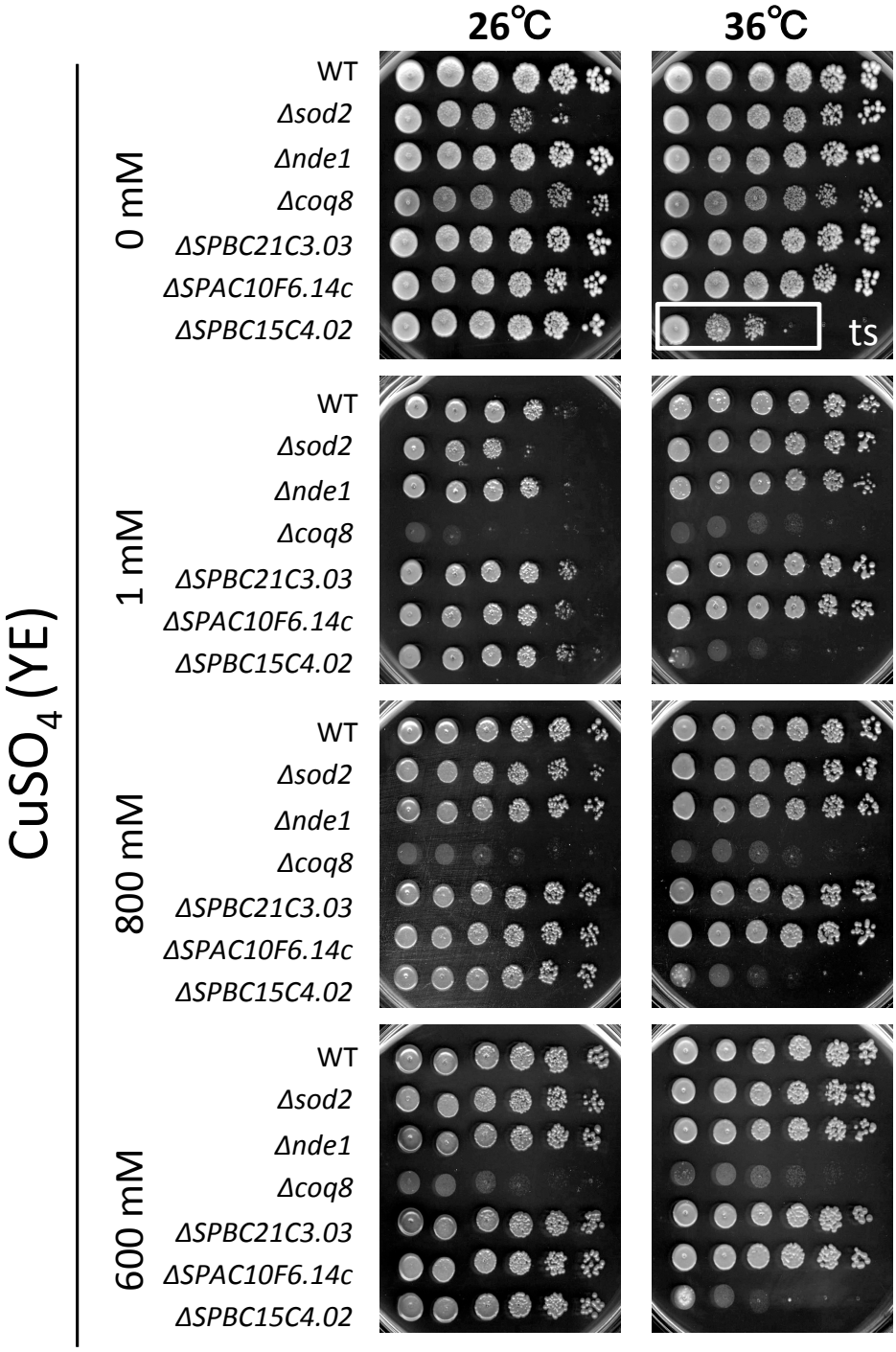

Figure S20 Copper sulfate screening. Mutant strains showing growth changes on drug-treated YE (2 % yeast extract) agar medium compared to wild type control (WT): Unclear resistance of Δ*coq8* (red box). Again, temperature sensitivity showed up for Δ*SPBC15C4.02* (white box) in drug untreated sample.

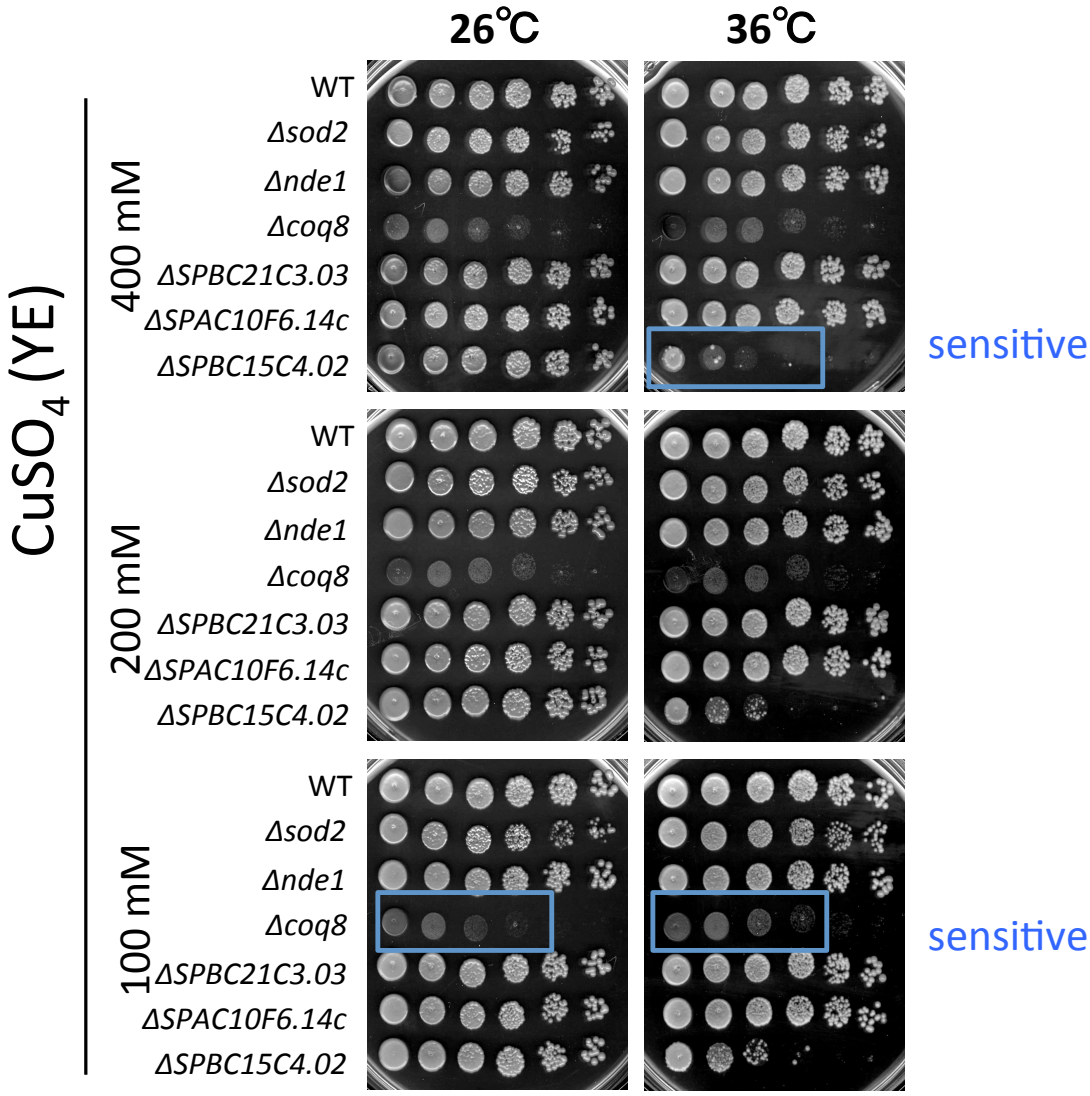

Figure S20 Copper sulfate screening (continued).

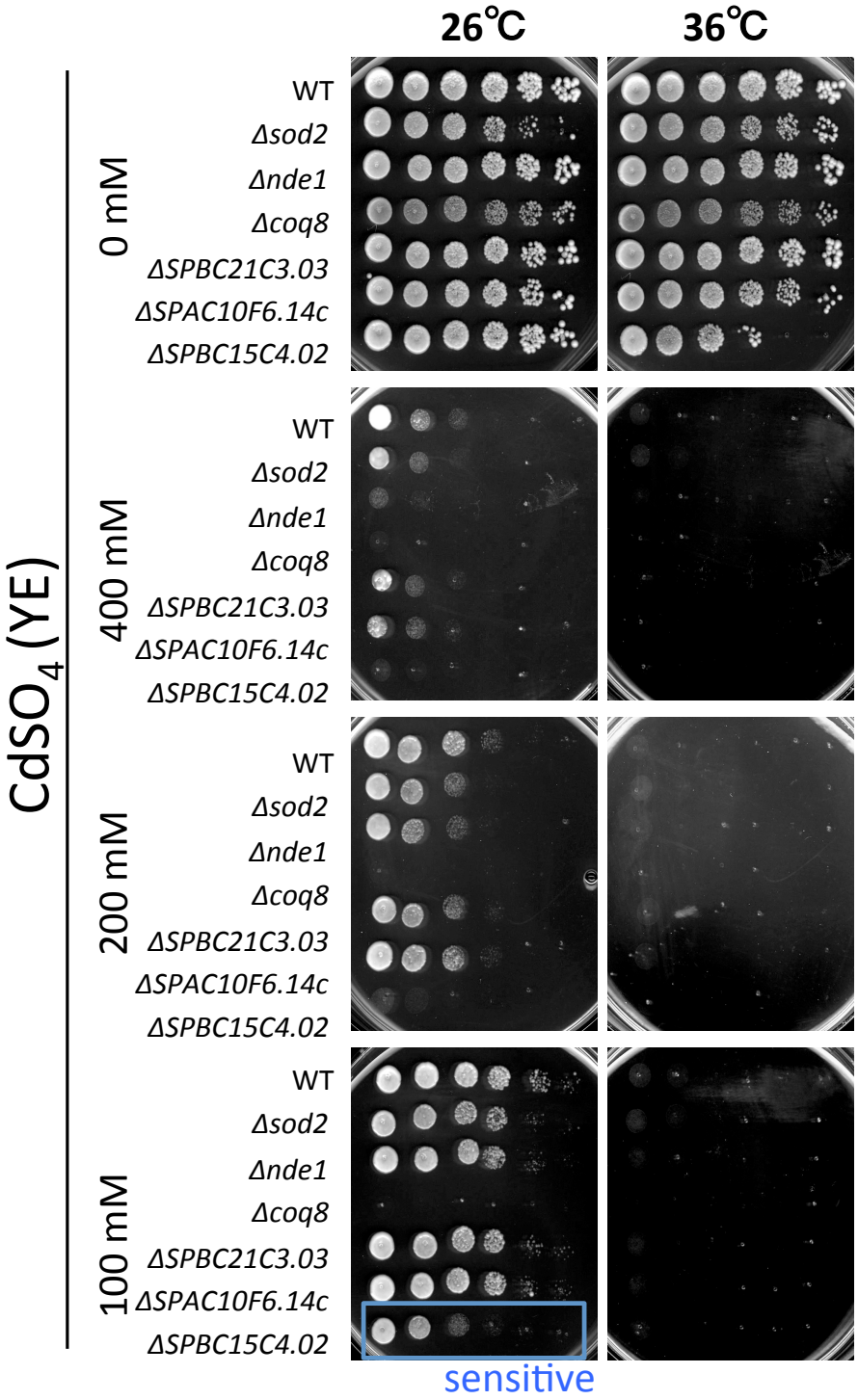

Figure S21 Cadmium sulfate screening. Mutant strains showing growth changes on drug-treated YE (2 % yeast extract) agar medium compared to wild type control (WT): Δ*coq8* and Δ*SPBC15C4.02* showed heavy metal sensitivity (blue box).

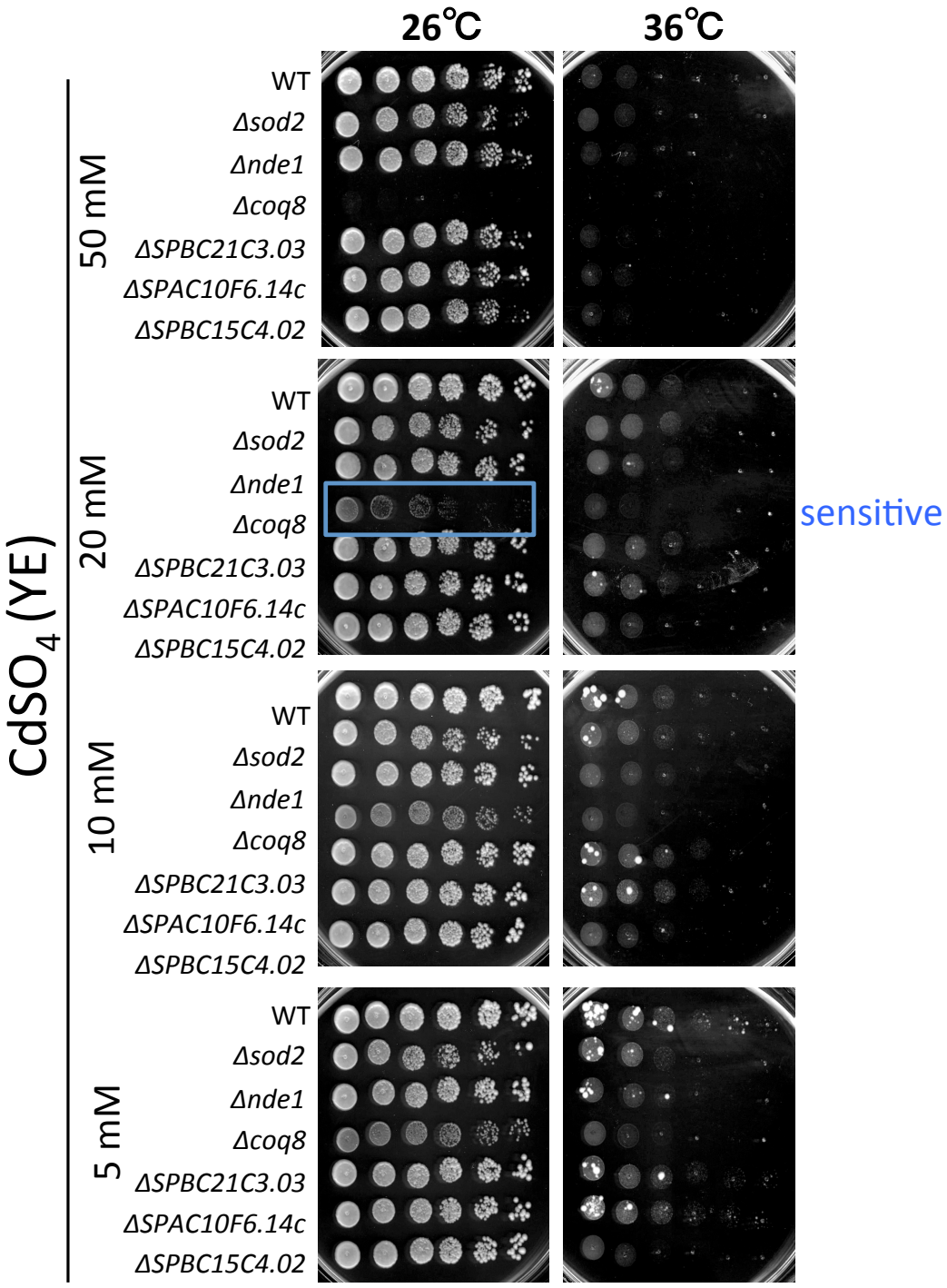

Figure S21 Cadmium sulfate screening (continued).

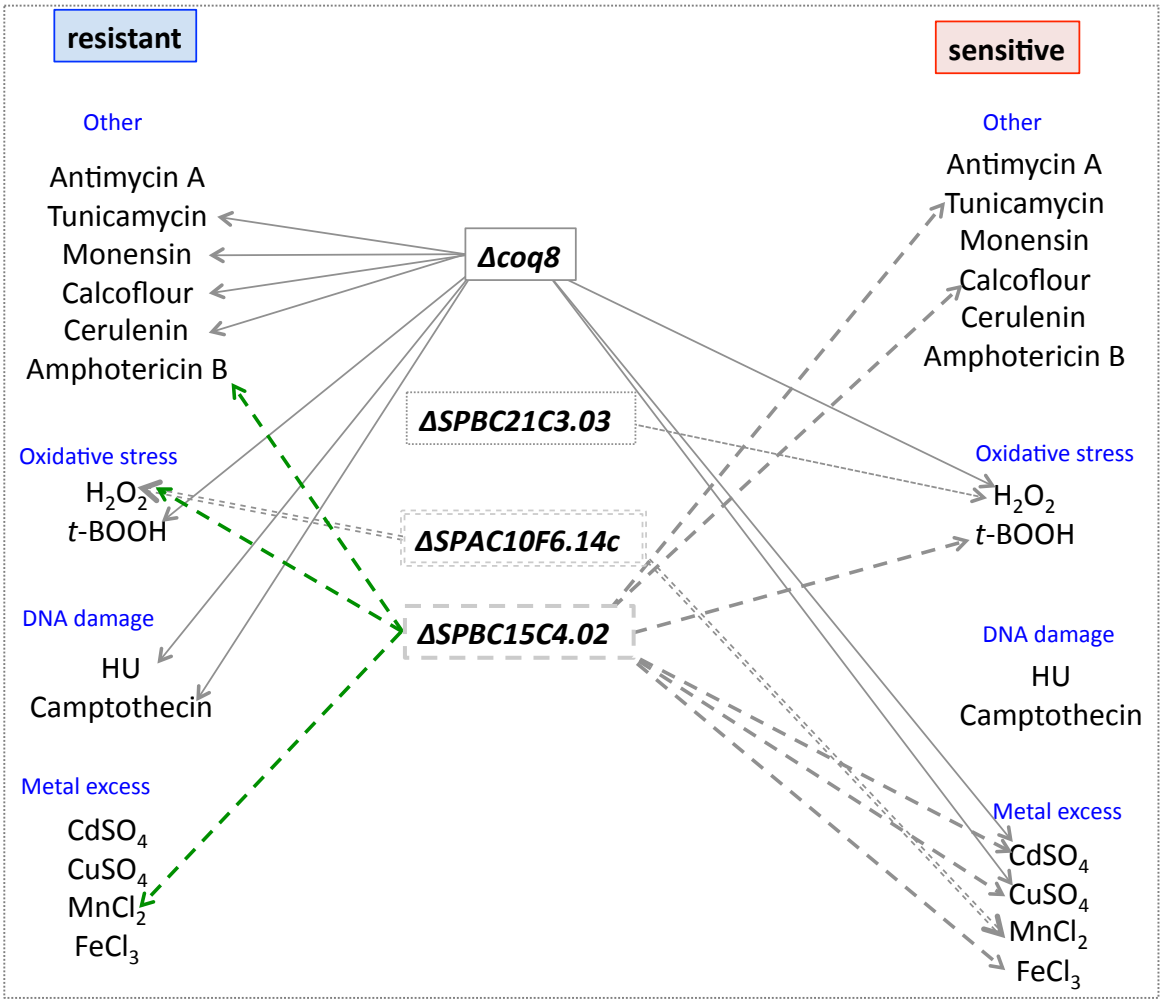

Figure S22 Summary of the drug screenings results. The four UbiB family deletion mutants. Green lines display temperature sensitivity reversal. Δ*SPBC21C3.03* is sensitive to H_2O_2 only. All spot test experiments were done with the help of Ms. Ayaka Mori, a lab technician in the G0 unit. At least two independent repetitions for each drug were performed. Additional results for the manganese excess experiment with $MnCl_2$ were received from the G0 cell unit researcher Dr. Sajiki.

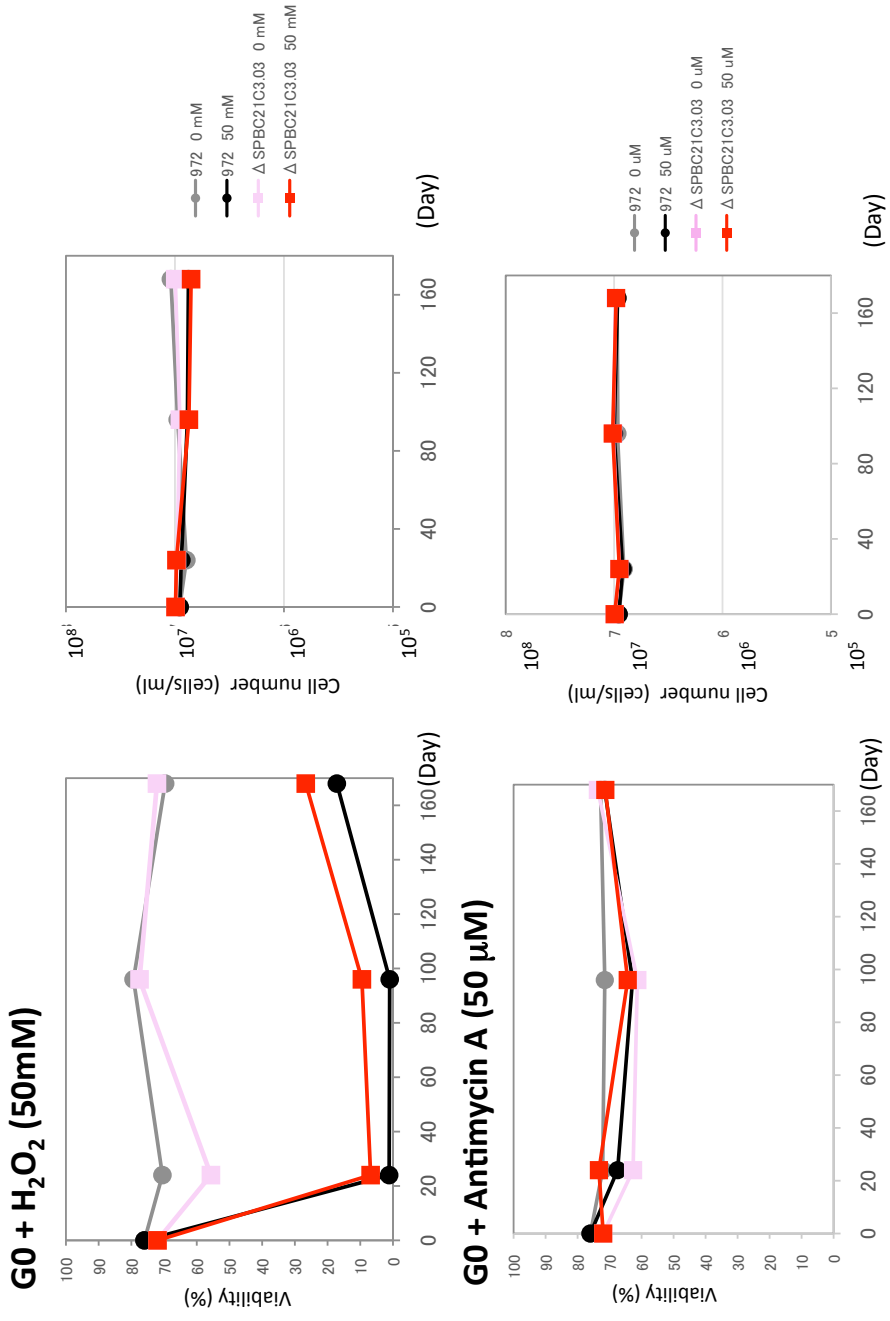

Figure S23 Drug screening under G0 conditions with H_2O_2 and Antimycin A. Oxidative stress inducer H_2O_2 and antimycin A as complex III inhibitor were used to screen for sensitivity in Δ*SPBC21C3.03* and wild type 972h-. No significant change compared to wild type strain was observed.Results were obtained with Ayaka Mori.

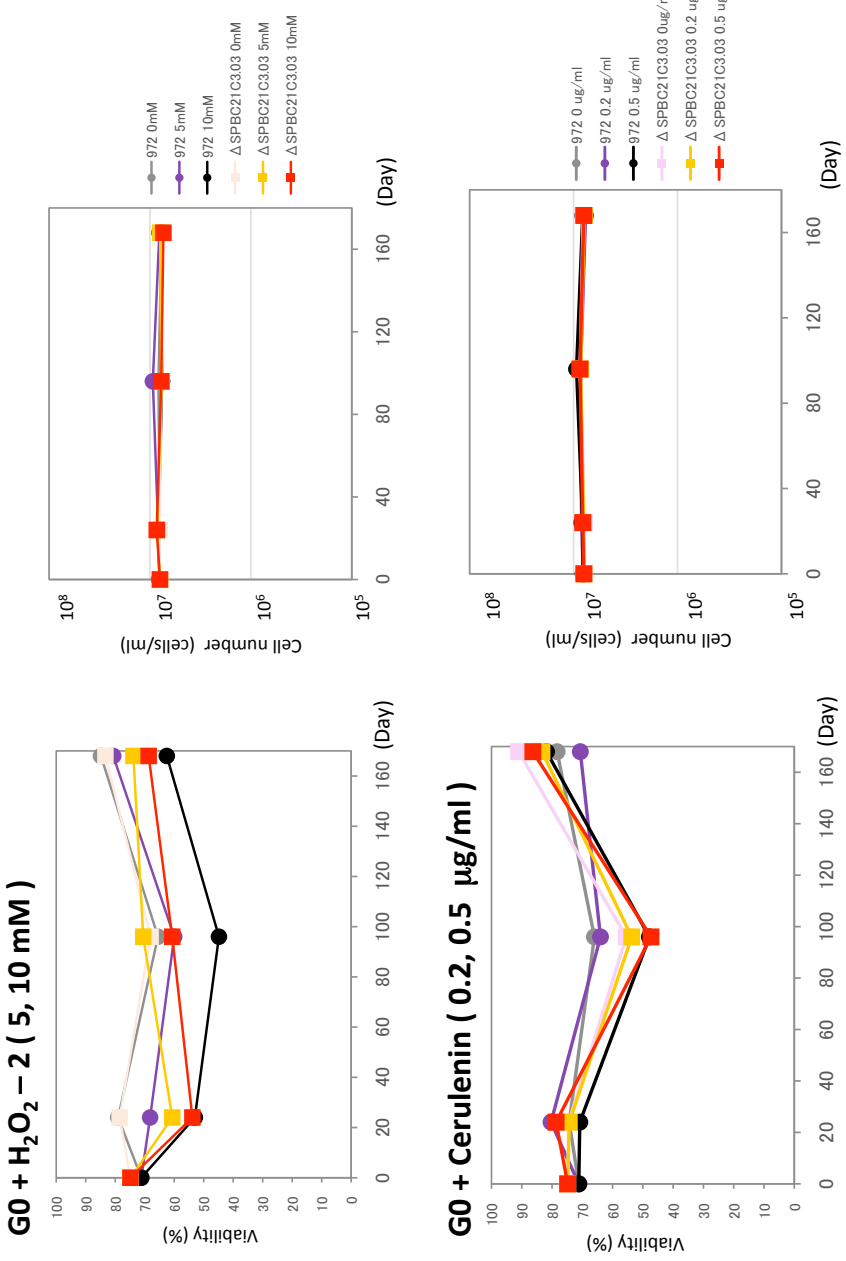

Figure S24 Drug screening under G0 conditions with H_2O_2 and cerulenin. As oxidative stress inducer, H_2O_2 and crulenin, the fatty acid synthase inhibitor, were used to screen for sensitivity in Δ*SPBC21C3.03* and wild type 972h$^-$. No significant change compared to wild type strain was observed. Results were obtained with Ayaka Mori.

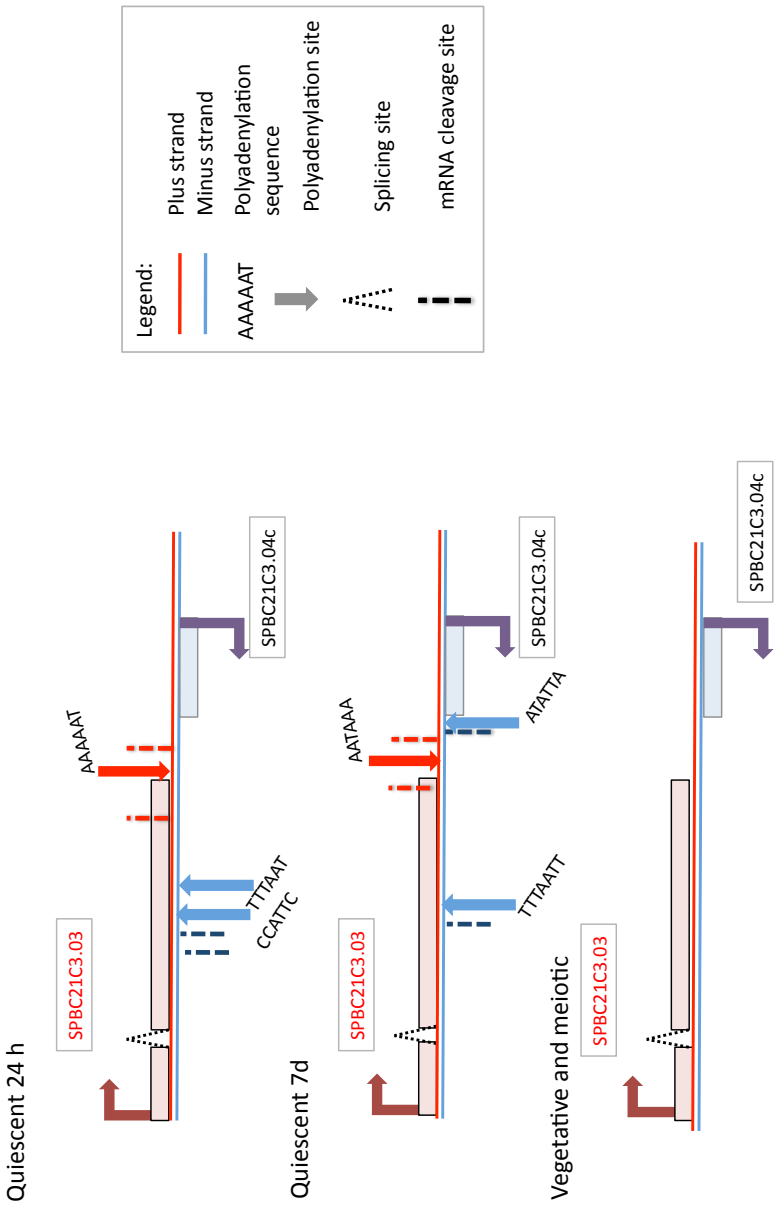

Figure S25 Polyadenylation sites in SPBC21C3.03 ORF. It is likely that *SPBC21C3.03* deletion might affect *SPBC21C3.04c* mRNA stability and therefore might cause negative growth effect. *According to information from pombase.org SPBC21C3.04c* deletion is inviable. Information inferred from Schlackow *et al.*, 2013